

Characterization of the envelope-mediated steps in the life cycle of hepatitis B viruses

Dissertation

zur Erlangung des akademischen Grades eines Doktors der
Naturwissenschaften (Dr. rer. nat.)

am Department Biologie
der Fakultät für Mathematik, Informatik und Naturwissenschaften
an der Universität Hamburg



vorgelegt von

Mouna Mhamdi

Hamburg, im Juni 2007

1. Gutachter: Prof. Dr. Hans Will, Heinrich-Pette-Institut, Hamburg
2. Gutachter: Prof. Dr. Udo Wieland, Universität Hamburg

Tag der Prüfung: 29 Juni 2007

Für
meine Eltern

Danksagung

Mein besonderer Dank gilt Herrn Prof. Dr. Hans Will für die Möglichkeit, in seiner Abteilung meine Dissertation anzufertigen und für sein Vertrauen.

Herrn Prof. Dr. Udo Wienand danke ich für das Interesse an meiner Arbeit und für die Übernahme des Korreferats.

Ganz herzlich bedanken möchte ich mich bei Herrn PD Dr. Hüseyin Sirma für die direkte Betreuung dieser Arbeit, für sein Vertrauen, für die unermüdlichen Diskussionen, für seine tollen Ideen und dafür, dass er immer an mich geglaubt hat und immer ein offenes Ohr für mich hatte. „un GRAND MERCI pour tout ce que tu as fait pour moi“

Danken möchte ich besonders meiner Kollegin Dr. Anneke Funk für das Einführen ins Labor, für ihre grenzenlose Hilfsbereitschaft und für die vielen Korrekturlesungen dieser Arbeit. „Weiterhin viel Glück und viel Erfolg in Australien, ich werde dich vermissen“.

Bei Herrn Dr. Heinz Hohenberg und seiner Arbeitsgruppe möchte ich mich herzlich bedanken für die schöne und erfolgreiche Zusammenarbeit ohne die diese Arbeit sicherlich weniger interessant wäre. Mein Dank gilt Frau Barbara Holsterman für die Präparation der Schnitte für die Elektronenmikroskopie.

Ein großes „Danke schön“ an Dr. Rudolf Reimer „Rudi“ für seine nette Art, für seine ständige Hilfsbereitschaft, für seine hilfreichen Tipps und Tricks bei der konfokalen Mikroskopie und für die Rekonstruktionen der „life cell records“.

Mein weiterer Dank gilt meiner Kollegin und Freundin Nicole Lohrengel für ihre Hilfsbereitschaft und ihre Ermutigung „wenn es mal schlechter lief“, weiterhin bedanke ich mich bei Cynthia Olotu und Li Lin für die schöne Zeit im Labor.

Des Weiteren danke ich der gesamten Abteilung Allgemeine Virologie für die nette Atmosphäre.

Ein besonderer Dank gilt der Studienstiftung des Deutschen Volkes für die umfangreiche finanzielle und geistige Unterstützung.

Der mit Abstand größter Dank gebührt meiner Familie, insbesondere meinen Eltern, die mich immer unterstützt haben, meinen Geschwistern Rasched, Manel und Ahmed für ihre Geduld in den letzten Monaten, meinen Großeltern, meiner Tante Sallouha, und meiner besten Freundin Sourour, die immer an mich geglaubt haben. „Ohne euch wäre ich nie soweit gekommen“.

Diese Arbeit wurde am Heinrich-Pette-Institut für experimentelle Virologie und Immunologie in der Abteilung von Prof. Dr. Hans Will, Abteilung Allgemeine Virologie, durchgeführt und von Herrn PD Dr. Hüseyin Sirma betreut.

Teile der vorliegenden Arbeit wurden bereits veröffentlicht und auf Kongressen präsentiert:

Mhamdi, M., Funk, A., Hohenberg, H., Will, H. and Sirma, H. (2007). **Assembly and budding of a hepatitis B virus is mediated by a novel type of intracellular vesicles.** *Hepatology*. 2007 Jul; 46(1): 95-106.

Mhamdi, M., Funk, A., Hohenberg, H., Will, H. and Sirma, H. (2006). **Biogenesis, Identity and dynamics of morphogenetic centers of duck hepatitis B virus?** The molecular biology of hepatitis B viruses, Vancouver, Canada.

Mhamdi, M., Funk, A., Hohenberg, H., Will, H. and Sirma, H. (2006). **Reorganization of the endomembranes during hepatitis B viral morphogenesis: Virus factories?** Annual Meeting of the German Society for Virology, Munich, Germany.

Mhamdi, M., Funk, A., Hohenberg, H., Will, H. and Sirma, H. (2005). **Reorganization of the endomembranes during hepatitis B viral morphogenesis: Virus factories?** The molecular biology of hepatitis B viruses, Heidelberg, Germany.

Mhamdi, M., Funk, A., Hohenberg, H., Will, H. and Sirma, H. (2005). **Reorganization of the endomembranes during hepatitis B viral morphogenesis: Virus factories?** Retreat of the Heinrich-Pette Institut, Hamburg, Germany.

Mhamdi, M., Hohenberg, H., Funk, A., Lin, L., Will, H. and Sirma, H. (2004). **Budding and secretion of hepatitis B viruses involves an endosome-like compartment.** Annual Meeting of the German Society for Virology, Tübingen, Germany.

INDEX

I. ZUSAMMENFASSUNG / ABSTRACT	1
I.1. ZUSAMMENFASSUNG	1
I.2. Abstract	3
II. Introduction	5
II.1. Hepatitis B viruses	5
II.1.1. Historical background, epidemiology, and pathology	5
II.1.2. Hepadnaviruses	7
II.1.2.1. The liver as a target for hepadnavirus infection	8
II.1.2.2. Duck hepatitis B virus	9
Viral particles.....	9
Virus genome and its organization.....	11
Viral transcripts.....	12
Viral gene expression.....	13
The viral life cycle.....	18
The late steps in the life cycle: assembly, budding, and secretion.....	20
II.2. Assembly and budding of enveloped viruses	21
II.2.1. Subcellular compartments of the secretory pathway as sites for the assembly and budding of enveloped viruses	22
Endoplasmic reticulum.....	23
ER to Golgi intermediate compartment (IC).....	24
The Golgi complex and the trans Golgi network (TGN).....	24
The plasma membrane.....	25
Other subcellular organelles exploited by enveloped viruses during assembly and budding..	25
II.2.2. Assembly and budding of enveloped viruses at “virus factories”	26
II.2.3. Vesicular transport along the secretory pathway	27
II.2.4. Exocytosis	28
II.2.5. Role of the cytoskeleton in the morphogenesis of enveloped viruses	29
Actin filaments or microfilaments.....	29
Microtubules.....	30
II.3. Aim of the study	31
III. Results	32
III.1. Assembly and budding of DHBV	32
III.1.1. Ultrastructural analysis of virus morphogenesis by transmission electron microscopy both <i>in vitro</i> and <i>in vivo</i>	32
III.1.1.1. A new three-dimensional culture system.....	32
III.1.1.2. DHBV morphogenesis is conserved <i>in vitro</i> and <i>in vivo</i>	33
III.1.1.3. Virus particles-containing vesicles are formed by reorganization of endomembranes.....	36
III.1.1.4. Different features of VCVs <i>in vitro</i> and <i>in vivo</i>	40
III.1.1.5. Budding of viral particles at VCVs.....	41
III.1.1.6. DHBV morphogenesis is restricted to hepatocytes <i>in vivo</i> and <i>in vitro</i>	44
III.1.1.7. DHBV morphogenesis in the chicken hepatoma cell line D2 shows similar morphogenetic features as in duck hepatocytes.....	45
III.1.2. Biochemical and cell biological analyses of the assembly and budding sites of DHBV	47
III.1.2.1. Subcellular distribution of the viral structural proteins L and core in PDH cultures...	47
III.1.2.2. Analysis of the subcellular distribution of the viral structural proteins L and core by subcellular fractionation.....	52
III.1.2.3. Immunocapture of VCVs.....	57
III.1.2.4. VCVs are dynamic structures undergoing homo- and heterotypic fusion and fission	60

III.1.2.4. Life cell imaging to visualize the dynamic of VCVs.....	62
III.2. Secretion of DHBV	69
III.2.1. Secretion of DHBV is Golgi-independent	69
III.2.1.1. Viral particles are absent from the Golgi	69
III.2.1.2. Secretion of DHBV is Golgi independent but partially temperature sensitive	73
III.2.2. Viral particles are released via exocytosis	78
III.2.2.1. Ultrastructural evidences for an exocytic release.....	78
III.2.2.2. Biochemical evidences for an exocytic release.....	84
III.2.2.3. Life cell imaging reveals an exocytic release	91
III.2.2.4. Secretion kinetics of DHBV in PDH cultures	94
III.3. Cellular requirements, intracellular transport, and secretion of DHBV	97
III.3.1. BFA strongly inhibits viral secretion	97
III.3.2. Role of the cytoskeleton in DHBV transport and secretion	109
Microtubules are required for DHBV secretion	109
Actin filaments are not required for DHBV secretion	112
III.3.3. Role of cholesterol and sphingolipids in DHBV morphogenesis	116
Depletion of intracellular cholesterol is not critical for viral formation but for viral infectivity..	116
Depletion of cholesterol from the PM is not critical for viral secretion.....	118
Depletion of sphingolipids does not interfere with DHBV secretion	121
IV. Discussion	124
IV.1. Assembly and budding of DHBV	124
IV. 2. Secretion of DHBV	131
IV.3. Cellular requirements for DHBV intracellular transport and secretion.....	136
IV.3.1. BFA strongly inhibits viral secretion	136
IV.3.2. Role of the cytoskeleton in DHBV transport and secretion	139
IV.3.3. Role of cholesterol and sphingolipids in DHBV morphogenesis.....	141
V.MATERIALS & METHODS.....	143
V.1 MATERIAL	143
V.1.1 Chemicals and reagents	143
V.1.2. Bacterial strains	144
V.1.3. Cell culture	144
V.1.4. Antibodies	146
V.1.5. Primers	147
V.1.6. Plasmids	148
V.1.7. Devices	149
V.2. METHODS	151
V.2.1. Cell culture and Treatments	151
V.2.1.1. Preparation of primary duck hepatocytes	151
V.2.1.2. Cultivation of cell lines	151
V.2.1.3. Treatment of cells	152
V.2.1.4. Transient transfections.....	153
V.2.1.5. Secretion kinetic and its quantification.....	154
V.2. 2. Protein biochemistry	154
V.2.2.1. Subcellular fractionation and iodixanol gradient ultracentrifugation	154
V.2.2.2. Immunoprecipitation of virus particles-containing vesicles.....	155
V.2.2.3. Labelling of cell surface proteins with sulfo-NHS-biotin, immunoprecipitation, and detection of biotinylated surface proteins	156
V.2.2.4. SDS-PAGE and Immunoblot.....	157
V.2. 3. Molecular biology techniques	159
V.2.3.1. Detection of viral rcDNA by PCR analysis	159
V.2.3.2. Agarose gel electrophoresis	161
V.2.3.3. Dot Blot hybridization assay	162
V.2.3.5. Cloning	163
V.2.3.6. Amplification and extraction of plasmid DNA.....	165
V.2.3.7. Microscopy	167

VI. REFERENCES.....	170
VII. ABBREVIATIONS.....	180
VIII. FIGURE INDEX.....	183

I. ZUSAMMENFASSUNG / ABSTRACT

I.1. ZUSAMMENFASSUNG

Die Bildung von membranumhüllten Viren erfolgt an zellulären Membranen. Über die späten Schritte des Replikationszyklus der Hepatitis B-Viren (HBV) ist wenig bekannt. Zu diesen gehören der virale Zusammenbau („assembly“), die Knospung („budding“), der intrazelluläre Transport und die Freisetzung der Nachkommensviren.

Das Hauptziel der Dissertationsarbeit war, die zellulären Strukturen, an denen die Morphogenese von HBV erfolgt, am Modell des Enten-Hepatitis B-Virus (DHBV) ultrastrukturell, biochemisch, und zellbiologisch zu charakterisieren.

Es konnte gezeigt werden, dass es im Verlauf einer hepadnaviralen Infektion zu einer massiven Umstrukturierung des Endomembransystems der Hepatozyten kam. Diese äußerte sich in der Umorganisation des rauhen endoplasmatischen Retikulums (rER) und der Bildung zahlreicher intrazellulärer, Virus-enhaltender Vesikel (VCVs) unterschiedlicher Größe. Ein Teil der VCVs leitete sich wahrscheinlich von der äußeren Kernmembran und dem rER ab. In dieser Arbeit konnte erstmals die offene Frage beantwortet werden, ob die für Hepatitis B-Viren typischen subviralen Partikel (SVPs) und Virionen über denselben Morphogeneseweg gebildet werden. Zum ersten Mal wurden frühe und späte Stadien der viralen Knospung an Endomembranen und VCVs abgebildet. Die weiteren ultrastrukturellen Untersuchungen von primären Entenhepatozyten-Kulturen (PDHs), Enten-Leberbiopsien und der DHBV-replizierenden Hühner-Hepatom-Zelllinie D2 zeigten, dass die Morphogenese von DHBV *in vivo* und *in vitro* konserviert ist.

Subzelluläre Fraktionierung von DHBV-infizierten Lebern durch Dichtegradienten-Zentrifugation ergab eine gute Auftrennung von ER und Golgi und zeigte, dass die viralen Partikel in ER-Fractionen angereichert und nicht in Golgi-Fractionen vorhanden waren. Diese Befunde wurden durch Immunisolierung der VCVs mittels L-Antiserum aus Zellhomogenaten bestätigt. Die anschließende biochemische Analyse der Immunpräzipitate zeigte die Anreicherung der ER-Markerproteine Calnexin und MTP (microsomal triglyceride transfer protein), Membrin, ein Marker für das „ER to

Golgi intermediate compartment“ (IC), und Rab5B, ein Marker für frühe Endosomen, an den VCVs. EEA1 („early endosomal antigen 1“), ein Adaptorprotein an frühen Endosomen, war jedoch nicht in VCVs nachzuweisen. Dies deutete auf eine spezifische Rekrutierung und daher besondere Rolle von Rab5B an VCVs hin. Diese Befunde wurden durch Immunfluoreszenzuntersuchungen bestätigt. Diese zeigten deutlich, dass VCVs keine Markerproteine von späten oder von „recycling“ Endosomen enthielten. Weiterhin konnte ausgeschlossen werden, dass es sich bei VCVs um sogenannte „multivesicular bodies“ (MVBs) handelte, obwohl in der Immunfluoreszenzfärbung eine partielle Überlappung der VCVs mit CD-63, einem Marker für MVBs, zu beobachten war.

VCVs sind Virus-induzierte, neue Membranstrukturen mit einzigartiger Identität. Sie enthalten Markerproteine von ER, IC, frühen Endosomen und MVBs. Es sind dynamische Strukturen, deren Form und Größe sowohl durch Fusion als auch Abschnürung reguliert wird, wie mittels Elektronenmikroskopie und Lebendzelldarstellung gezeigt werden konnte.

Der intrazelluläre Transport dieser VCVs benötigte intakte, aber keine dynamischen Mikrotubuli, wobei das Aktinzytoskelett entbehrlich war. Die Freisetzung der Nachkommensviren war weitgehend Golgi-unabhängig und erfolgte über einen alternativen exozytischen Prozess. Ultrastrukturell konnten erstmals das Andocken der VCVs an die Plasmamembran und exozytische Freisetzung des viralen Inhaltes sichtbar gemacht werden. Außerdem konnte gezeigt werden, dass während der Exozytose die in der Vesikelmembran enthaltenen, noch nicht partikularisierten, viralen Hüllproteine an die Zellmembran transferiert wurden.

Die Bestimmung der viralen Ausschleusungskinetik ergab, dass jede einzelne Zelle etwa 40 bis 80 Virionen und etwa 46.000 SVP in einer Stunde freisetzte.

Durch Brefeldin A-Behandlung (BFA) konnte die Sekretion der viralen Partikel stark und reversibel gehemmt werden. Dieser Sekretionsblock führte zur Akkumulation von viralen Partikeln in VCVs, die 4-5-fach größer waren, als die VCVs in unbehandelten Zellen.

Zusätzlich wurde die Rolle der so genannten „lipid rafts“ in der viralen Morphogenese durch pharmakologische Interferenzstudien untersucht. Die Studien zeigten, dass die Zerstörung der „lipid rafts“ die Bildung und Sekretion der Nachkommensviren nicht beeinflusste und diese somit keine Plattform für Zusammenbau, Knospung und Freisetzung der Nachkommensviren darstellten.

Zusammenfassend zeigen die Ergebnisse meiner Dissertationsarbeit, dass die Reorganisation der Endomembranen im Laufe einer DHBV-Infektion zur Bildung neuer Membrankompartimente führt, die als eine zentrale Plattform für den viralen Zusammenbau, Knospung, intrazellulären Transport und die Sekretion dieser Viren fungieren.

I.2. Abstract

Formation of enveloped viruses involves assembly and budding at cellular membranes. Little is known about the late steps of hepatitis B viruses (HBV) infection including assembly, budding, intracellular transport, and secretion of progeny virus.

The aim of this work was to identify and characterize the hepatocellular compartments and pathways exploited during virus morphogenesis using the duck hepatitis B virus (DHBV) and primary duck hepatocytes (PDHs) as a model system.

Ultrastructural analysis showed that the formation of virus progeny initiates at the endoplasmic reticulum (ER) and proceeds via membrane-surrounded vesicles which contain viral particles (virus particles-containing vesicles, VCVs). These VCVs were generated and maintained by reorganization of endomembranes accompanied by a striking disorganisation of the rough ER. VCVs contained both virions and subviral particles (SVPs), indicating a common morphogenetic pathway for both viral particle entities. For the first time, ultrastructural evidence for the early and late features of the budding of both particle types at endomembranes and VCVs was provided. Ultrastructural analysis of DHBV-infected PDH cultures, liver biopsies and the DHBV-transfected chicken hepatoma cell line D2 revealed that DHBV morphogenesis is conserved both *in vitro* and *in vivo*.

Subcellular fractionation of DHBV-infected liver based on iodixanol gradient centrifugation resulted in clear separation of ER from Golgi and showed enrichment of viral particles in ER fractions and their exclusion from Golgi fractions. Native VCVs were immunocaptured from dounce homogenates using L-antiserum as shown by ultrastructural analysis. Biochemical analysis of immunoprecipitates revealed that VCVs contain ER marker proteins such as calnexin and microsomal triglyceride transfer protein (MTP), membrin, a marker for the ER-to-Golgi intermediate compartment (IC), and Rab5B, an early endosome marker. However, the early endosomal antigen 1 (EEA1), another adaptor protein of early endosomes, was

excluded from VCV-membranes, indicating a specific recruitment and role for Rab5 during viral morphogenesis. These findings were confirmed and extended by colocalization studies using a large panel of antibodies against subcellular markers. Overall, these studies showed that VCVs were distinct from late and recycling endosomes. Although part of the VCVs harboured CD63, a tetraspanine protein characteristic for multivesicular bodies (MVBs), they were distinct from these since no overlap with Tsg101, which functions in vacuolar protein sorting, was observed.

VCVs were identified as novel organelles with mixed identity and harboured markers of ER, IC, endosomes, and MVBs. VCVs are dynamic structures and their size and shape are regulated by both fusion and fission as revealed by electron microscopy and live cell imaging.

The intracellular transport of these VCVs required intact but not dynamic microtubules, while actin filaments were dispensable. Virus secretion was mainly Golgi-independent and mediated by an exocytic release mechanism. Docking and fusion of VCVs with the plasma membrane (PM) led to liberation of about 40-80 virions and 46,000 SVPs per hepatocyte and per hour.

Pharmacological interference studies with brefeldin A (BFA), which blocks protein export from the ER and causes disruption of the Golgi complex and subsequent fusion with the ER, resulted in strong, virtually complete inhibition of viral secretion. Under treatment, intracellular viral particles accumulated in large cytoplasmic membrane tubules and these vesicles were 4-5-fold as large as VCVs in non-treated cells. The effects of BFA were presumably due to homotypic fusion of VCVs and to inhibition of exocytosis by blocking the fusion of VCVs with the PM.

Moreover, the role of cholesterol and lipid rafts in viral morphogenesis was investigated by pharmacological interference studies. The results showed that disruption of lipid rafts did not interfere with the formation and secretion of progeny virus. These findings indicated that lipid rafts do not serve as platforms for DHBV assembly, budding, and secretion.

In conclusion, the data obtained offer new insights into the still incomplete “morphogenetic puzzle” of hepadnaviruses. This includes reorganisation of endomembranes during DHBV infection and the biogenesis of novel cellular vesicles which serve as multifunctional platforms for assembly, budding, intracellular transport, and secretion of progeny virus.

II. Introduction

II.1. Hepatitis B viruses

II.1.1. Historical background, epidemiology, and pathology

The first well documented description of a hepatitis virus infection was reported in 1883 in relation to an epidemic of jaundice following smallpox vaccination (1). The identification of the responsible agent followed between 1960 and 1970. In 1952, McCollum showed that the responsible agent was a virus due to its small size as it passed through ultrafiltration membranes with a pore diameter of only 52 nm (2). In 1967, Blumberg et al discovered in the serum of an Australian aborigine an antigen which was first thought to be associated with leukemia and later associated with hepatitis (3). This antigen was called Australia-antigen, and is known today as HBsAg (Hepatitis B surface antigen). In 1968, Prince associated this antigen with acute hepatitis (4). Subsequently, in 1970, Dane described the infectious virion which was called Dane particle and is known as human hepatitis B virus (HBV) (5). Four years after the discovery of the virus, the first vaccination, which was a heat-treated form of the virus, was developed by Blumberg and Millman. In 1981, a second generation of vaccines was developed; it was a plasma-derived vaccine containing neutralising antibodies from patients who had recovered from an HBV infection. The next generation of vaccines was a recombinant vaccine (1986) which did not contain blood products. It consisted of the small surface protein of HBV (HBsAg), expressed in and isolated from yeast.

The problems posed by HBV infection remain considerable despite the existence of safe and efficient vaccination since 1975. According to the most recent World Health Organization (WHO) estimate, more than 2 billion people worldwide have had a transient HBV infection, and 360 millions are chronically infected and at risk for HBV-related liver disease. Approximately, one third of all worldwide cases of liver cirrhosis and half of all cases of hepatocellular carcinoma can be attributed to chronic HBV infection. HBV is estimated to be responsible for 500,000-700,000 deaths each year (6). The global epidemiology of HBV infection has traditionally been described

according to three categories of endemicity: high, intermediate, and low, depending on the proportion of population that is seropositive for HBsAg (Fig. 1).

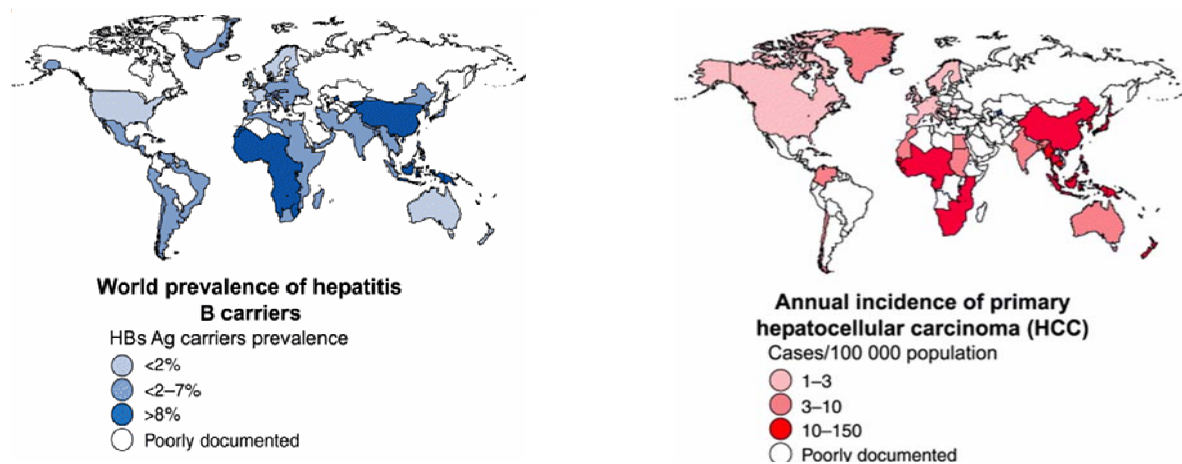


Fig. 1. Geographic distribution of the prevalence of hepatitis B carriers and annual incidence of primary hepatocellular carcinoma (HCC). (Source: www.medscape.com/content/2004/00/47/14/471470).

Approximately 60 % of the world's population lives in areas where HBV infection is highly endemic, including China, Indonesia, Nigeria, and much of the rest of Asia and Africa (6). Southern Europe, the Middle East, and South Asia have an intermediate level of HBV endemicity. Most of Central and South America is considered a region of low HBV endemicity.

Transmission of HBV occurs through several mechanisms. In high prevalence regions, the most common route is perinatal (vertical) from mother to child. In low prevalence area, the HBV infection is usually acquired by horizontal transmission between adults through percutaneous or mucosal exposure to infected blood or unprotected sexual contacts. The highest concentrations of infectious HBV are found in blood and serum. However, other serum-derived body fluids such as semen and saliva are also infectious (7). HBV can cause both acute and chronic infection. For newly infected persons who develop acute hepatitis, the average incubation period is 90 days (8, 9) The likelihood of developing symptoms of hepatitis as a result of HBV infection is age-dependent. Over 90% of perinatal HBV infections are asymptomatic, while the typical manifestations of acute hepatitis are noted in 5-15% of newly infected young children and in 33-50% of older children, adolescents and adults (10). In the case of a self-limiting infection, the immune system clears the virus within 6 months of initial infection, if not, the person is considered to have a chronic HBV

infection. Chronic HBV infection is defined as the presence of HBsAg in the serum for at least 6 months. The probability of developing chronic HBV infection depends on certain factors, especially the age and strength of the immune system. 90% of infants infected at birth develop a chronic infection, the rate falls to about 30% for children infected between the ages of 1 and 5 years, and falls further to about 5% for adults with competent immune systems. Chronic infection is more likely to occur in people with a weakened immune system like immunosuppressed and hemodialysed patients, after chemotherapy and corticosteroid treatments, and HIV-infected persons.

II.1.2. Hepadnaviruses

Hepadnaviruses (Hepatitis-DNA-viruses) are small enveloped DNA viruses that primarily infect the liver. This virus family is subdivided into 2 groups: the mammalian hepadnaviruses also called orthohepadnaviruses of which the prototype is the human hepatitis B virus (HBV), and the avian hepadnaviruses or avihepadnaviruses with the prototype being the duck hepatitis B virus (DHBV). Some other representative members of both families are shown in the table below.

Genus	Virus	Host	Reference
Orthohepadnaviruses	Hepatitis B virus (HBV)	Human	(5)
	Woodchuck-HBV (WHBV)	Woodchuck	(11)
	Ground squirrel-HBV	Ground squirrel	(12)
Avihepadnaviruses	Duck-HBV (DHBV)	Duck	(13)
	Heron-HBV (HHBV)	Heron	(14)
	Stork-HBV (SHBV)	Stork	(15)

All hepadnaviruses contain a small partially double-stranded DNA genome of 3.0-3.3 kb in length and replicate via reverse transcription of the pregenomic RNA (pgRNA) that contains all the genetic information of the virus (16-19). Based on their replication strategy, hepadnaviruses have been classified into the para-retrovirus family.

All hepadnaviruses share a similar genome and structural organization, a similar life cycle and have a narrow host range, e.g. HBV infects only humans and some high primates like chimpanzee. DHBV infects only distinct duck and geese species but

neither Muscovy ducks nor chickens (20). Although many features of hepadnaviruses have been discovered in DHBV infection and then confirmed for HBV, there are differences between both. The mode of transmission for example is not identical. DHBV is presumably exclusively transmitted vertically from mother to the foetus *in ovo* whereas HBV is transmitted either vertically or horizontally between individuals. Another main difference is that chronic HBV infection is associated with the development of hepatocellular carcinoma (HCC) whereas chronic DHBV infection is not. Furthermore, major differences exist in sequence, posttranslational modifications and structure of the surface proteins from both viruses: wild-type HBV has 3 in part N-glycosylated surface proteins whereas those of DHBV are not N-glycosylated. Besides these and other differences, DHBV is still the best characterised virus model to study the different aspects of the life cycle of hepadnaviruses.

II.1.2.1. The liver as a target for hepadnavirus infection

The liver is composed of different types of cells (Fig. 2), hepatocytes represent the main cell population (about 60% of the liver), followed by liver sinusoidal cells (about 30% of all liver cells), bile epithelium, and Kupffer cells (liver macrophages). Most of the functional activity of the liver resides in hepatocytes.

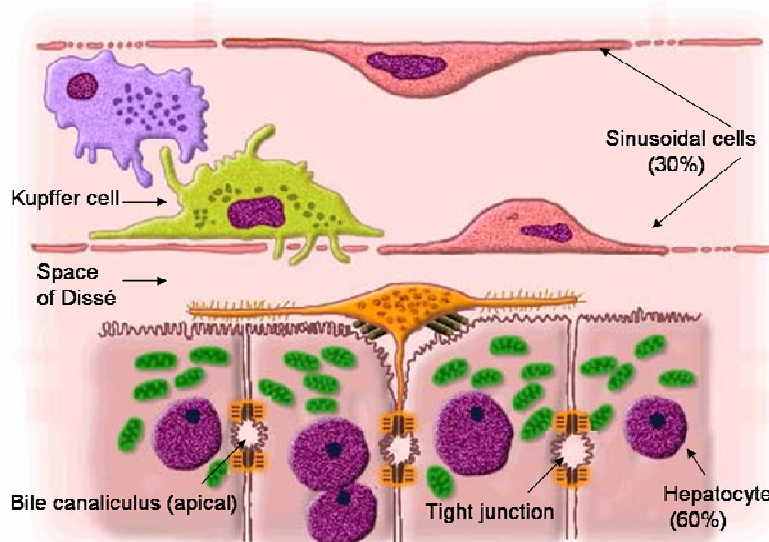


Fig. 2. Cellular composition of the liver. The liver is composed of different cell types. These mainly are hepatocytes (60% of the total liver cells), liver sinusoidal cells (30%), and other cells like Kupffer

cells, natural killer cells, and fat storing cells called Ito cell, shown in yellow). (Adapted and modified from www.bmu.unimelb.edu.au/showcase/bilesalts40.html)

The replication of hepadnaviruses is largely restricted to hepatocytes. However, bile duct epithelial cells may also be a target of infection, as may be also a subset of non-hepatic cells in the pancreas, kidney, and lymphoid system (21-23).

II.1.2.2. Duck hepatitis B virus

An HBV-related virus was for the first time discovered by Summers et al in duck sera from China (13). In 1980, Mason et al. reported about an HBV-related virus, in 10% of Pekin ducks (*Anas platyrhynchos forma domestica*) from two different sources in the USA (13) and designated it duck HBV (DHBV). Many fundamental discoveries have first been made with DHBV, such as hepadnavirus replication by reverse transcription (RT) (16) and the pathway leading to cccDNA formation (24). This and the establishment of primary duck hepatocyte cultures permissive for reproducible DHBV infections made the DHBV an invaluable model system for studies on hepadnaviruses. If not otherwise indicated, the remaining part of the introduction describes the molecular and cellular biology of DHBV.

Viral particles

DHBV-infected cells produce two types of spherical viral particles: virions and subviral particles (SVPs). Virions are the infectious virus particles with a diameter between 40 and 60 nm (Fig. 3A). The virion is formed by a core particle containing the partially double stranded, relaxed-circular-DNA (rcDNA). This nucleocapsid (27-35 nm in diameter) is surrounded by a lipid bilayer envelope, which is presumably derived from the endoplasmic reticulum (ER), in which the surface proteins L and S are inserted.

Subviral particles (SVPs) are empty particles lacking the nucleocapsid and are thus not infectious. These particles with varying diameters (30 and 60 nm) have an identical envelope to that of virions (Fig. 3B). SVPs, whose secretion by infected cells is a unique feature of hepadnaviruses, are secreted in 1,000 to 10,000-fold excess compared to virions. The biological relevance of these particles during virus infection

is still not clear. It has been shown that SVPs interfere with the infection by competing viral binding (25) and that SVPs enhance infection at low multiplicity of infection (MOI) (26).

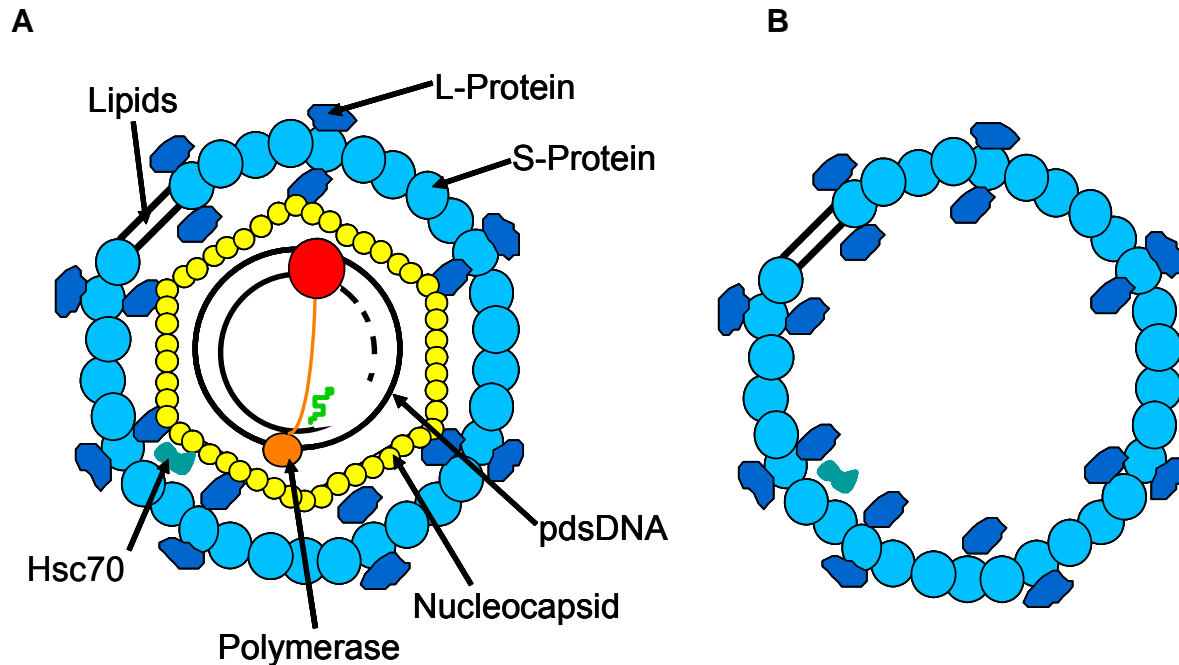


Fig. 3 Structure of duck hepatitis B viral particles. The DHB virion (A) consists of an envelope surrounding the nucleocapsid which harbours the viral rcDNA and the viral polymerase. SVPs (B) are formed only by the envelope. Pds: partially double stranded DNA.

The envelope of hepatitis B viruses is remarkable for the following reasons: unlike the envelope of other viruses with a lipid composition resembling the lipid composition of the host membrane where the virus is formed, the envelope of HBV, has a lipid composition different from that of the ER where the virus assembles and buds. For circulating HBsAg (serum derived) it has been shown that 60% of all lipids are phosphatidylcholine and 30% cholesterol (27). This indicates that during viral assembly and/or budding, a rearrangement of the ER lipids must occur in the way that specific lipid species are selected or excluded from the viral envelope. In addition, the envelope is presumably organized as a discontinuous rigid bilayer of lipids interacting with protein aggregates of surface proteins since the ratio between protein and lipids within the membrane is unconventionally high (4 to 1) (28).

Virus genome and its organization

The viral genome consists of a partially double stranded and circular, relaxed DNA (rcDNA) of about 3 kb (Fig. 4). The circularity of the genome is achieved by overlapping cohesive 5' ends (29). The negative strand (minus-strand) is full length and its 5'-terminal nucleotide is covalently linked to the viral polymerase (P). The positive strand (plus-strand) is incomplete in length and this results in a variously sized single stranded region of the viral genome, designated the "gap region". Its 5'-end is linked to a short ribonucleotide which is a remnant of the pgRNA (17). The 5' terminal structures of both DNA strands function as primers during viral replication. In addition, the genome has two direct repeats (DR1 and DR2) of 11 base pairs (bp) which are essential for genome replication.

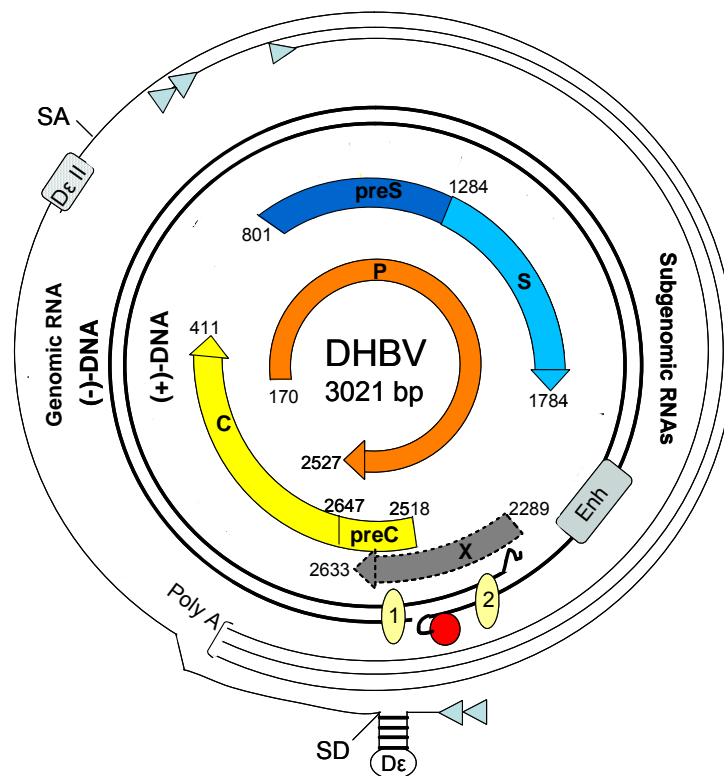


Fig. 4. Genome organization of duck hepatitis B virus. The partially double stranded viral DNA (thick lines) with the covalently attached polymerase (red circle) is shown. The various transcripts are depicted in thin lines with the small arrow heads indicating the start sites. The positions of the direct repeats DR1 and DR2 (numbered circles 1 and 2) as well as the enhancer domain (Enh) are represented. The ORFs encoding core (C), polymerase (P), the surface proteins (preS and S), and the cryptic X-like ORF are symbolized by thick arrows. Epsilon (D ϵ) is the stem loop structure on the pgRNA which acts as an encapsidation signal and replication origin. The second encapsidation

element D ϵ II is unique to avian hepatitis B viruses. SD and SA represent the major splice donor and acceptor sites, respectively.

A typical feature of all hepadnaviruses is the compact genome organisation, every nucleotide (nt) has a coding function in at least one of the 4 ORFs (open reading frames). In addition, all regulatory elements such as promoters and enhancers and various other cis-elements overlap with coding information. The first ORF encodes the surface proteins L and S, the second codes for the capsid protein and the e-antigen (early antigen), the third for the polymerase, and a cryptic fourth for the X-like protein.

Viral transcripts

The template for viral transcription is the so called cccDNA (circular covalently closed DNA). This DNA results from the conversion of the incoming rcDNA (relaxed circular) by the cellular machinery. This conversion implies removal of the 5' structures (protein and RNA), repair of the gap and finally covalent ligation of both strands. The cccDNA remains as an episome in the nucleus and serves as a template for all viral transcripts. The transcription is mediated by cellular RNA polymerase II (30) and results in two classes of transcripts: the genomic and the subgenomic RNAs. All transcripts are capped and are 3'-terminally identical in sequence (31). They have the same 3'-end due to a single processing/polyadenylation site within the viral genome, but have different 5'-ends as the result of heterogenous transcription initiations driven by different promoters. The subgenomic transcripts function exclusively as messenger RNA (mRNA) for translation of the surface proteins L and S. The genomic RNAs are more than full length with heterogenous 5'-ends upstream the precore ATG, frequently designated preC mRNAs, or with 5'-ends between the precore and the core ATG start codon, designated C-mRNA/pgRNA. The preC mRNAs serve as mRNA for synthesis of the precursor protein of e-antigen and are not encapsidated into core particles, except when the preC start codon is mutated. The C-mRNA/pgRNA serves both as a template for synthesis of the viral core protein and the polymerase and is encapsidated into core particles where it is reverse transcribed into the viral DNA minus-strand. Whether a separate mRNA for the X protein exists is so far unknown. Following synthesis of the RNAs by transcription, they are exported to the cytoplasm where protein translation takes place. A fraction

of the more than genome length RNAs is spliced and used as mRNA for L protein synthesis (32).

Viral gene expression

Polymerase and replication

The polymerase (P) is a multifunctional protein of 90 kDa, and is divided into 4 different functional domains (Fig. 5): (i) the terminal protein domain (TP) which functions as primer of DNA synthesis and which contains a conserved tyrosine residue (Tyr 96) to which the viral DNA is covalently linked during synthesis (33), (ii) the spacer domain with no known function as several insertions and deletions tested did not interfere with any of the P-functions, (iii) the reverse transcriptase/DNA polymerase domain which contains both polymerase activities required for DNA synthesis. Mutations in a highly conserved motif (YMDD) of the RT domain lead to nucleoside analogue resistance and can impair synthesis of both DNA strands (34), and (iv) the RNaseH domain which contains the RNaseH activity which degrades the viral RNA from the RNA-DNA hybrid during reverse transcription (35).



Fig. 5. Domain organization of the polymerase. The 4 domains of the P-protein, the position of the amino acid Tyr 96 that primes DNA synthesis, and the YMDD motif which is essential for RT activity are indicated. Numbers stand for amino acid positions.

The polymerase participates in several steps of the viral life cycle. Following transcription of the pgRNA from the cccDNA by cellular RNA polymerase II, the pgRNA is exported to the cytoplasm where it interacts with P and core protein dimers. P recognizes a specific RNA structure, designated encapsidation signal (ϵ) on the pgRNA. This reaction depends on host factors including the heat shock protein Hsp90 and leads to the formation of a ribonucleoprotein complex (RNP). Within this complex, the reverse transcription of the first 4 nucleotides of the pgRNA takes place starting with the first nucleotide linked covalently to Tyr 96 located within the TP domain of P. The DNA oligonucleotide linked to the P protein is then translocated to

the 3'-proximal direct repeat (DR1), often referred to as the first template switch and this occurs either concomitantly with formation of the core particle or shortly thereafter within the core particles. Next, the DNA primer is extended until the 5'-end of the pgRNA is reached resulting in a more than full-length minus-strand DNA with a short terminal redundancy. During DNA synthesis, the pgRNA, except for a short 5'-terminal oligonucleotide with the 5'-copy of DR1 at its 3'-end, is degraded by the RNaseH activity of P protein. For DNA plus-strand synthesis, this oligonucleotide is transferred to the DR2 (second template switch) located upstream of DR1 where it serves as primer. The synthesis proceeds to the 5'-end of the DNA minus-strand generating a short DNA-plus strand-fragment equivalent to a strong stop plus-strand DNA in the retroviral life cycle. Continuation of DNA plus-strand synthesis is then accomplished by circularization of DNA and strand exchange. To a low degree, the transfer of the RNA oligonucleotide to DR2 is unsuccessful and this can lead to the elongation of the plus-strand from the primer still bound to its 5' proximal position. This process is called *in situ* priming and gives rise to a linear double stranded DNA leading to a dead end for viral replication. However, this process is suppressed by a small hairpin structure that favours transfer of the RNA primer to DR2 (36).

Core protein and e-antigen

The viral nucleocapsid is a protective container harbouring the viral DNA. It is made of dimeric subunits of a single core protein species. The core protein (DHBc) of most DHBV isolates has 262 aa with a predicted molecular weight of 32 kDa. DHBc self-assembles into a nucleocapsid in a concentration-dependent manner.

DHBc is composed of two domains: the N-terminal domain which assures the assembly capability of the protein (37), and a C-terminal domain, an Arg-rich region, which is required for the binding of nucleic acid (38) and facilitating reverse transcription. In addition, a nuclear localization sequence (NLS, aa 214-218) is present and essential for nuclear pore association of the nucleocapsid and thus delivery of the viral DNA into the nucleus during infection. Furthermore, DHBc has activities which indicate a nuclear export signal, presumably counterbalancing the NLS function in the productive state of the infection and thereby preventing nucleoplasmic accumulation of nucleocapsids (39). Moreover, the core protein has 6 highly conserved phosphorylation sites, including 4 sites (T239, S245, S257, and S259) that were previously (40) and 2 sites (S230 and S232) recently identified (41).

The core protein plays important and opposing roles during the viral life cycle. During virus entry, the nucleocapsid must disassemble and release the viral DNA in order to initiate infection, while during progeny formation it must bind DNA and encapsidate the viral genome to form new virus particles. This multifunction of core is regulated by (i) its subcellular localization, (ii) its quaternary structure, and (iii) posttranslational modifications like phosphorylation. DHBc has been shown to be both in the nucleus and cytoplasm. In the nucleus, DHBc is concentrated in distinct nuclear bodies called nuclear core bodies (NCBs) (42). These NCBs were shown to colocalize with foci of pgRNA suggesting a possible role for the nuclear core in the synthesis and/or maturation of the pgRNA. In the cytoplasm, core was found either free (cytosolic) or attached to membrane compartments. The association with membranes depends on the maturation status of the nucleocapsid (43). Only mature core particles, consisting of hypophosphorylated core proteins and containing the rcDNA, are able to interact with cellular membranes independently of the presence or absence of the surface proteins. This subpopulation of nucleocapsids is destined to be enveloped, secreted and appears to resemble nucleocapsids present in the secreted virus particle. The immature nucleocapsids (with hyperphosphorylated core proteins and immature nucleic acid) lack this intrinsic membrane-binding affinity (42). The phosphorylation status of core is not only important during viral morphogenesis, but also for nucleocapsid binding to the nuclear pore during infection (44). Besides DHBc, a second protein called precore, the precursor protein of e-antigen (DHBe) is translated from the same ORF. The precore protein differs from DHBc by an additional signal peptide sequence at its N-terminus. This sequence motif directs the precore protein into the ER where the signal sequence is cleaved off (45). The protein is then directed to the cellular secretory pathway. During secretion, the Arg-rich region is proteolytically removed resulting in a C-terminally truncated protein, designated DHBe. This protein is usually detectable in the serum of infected ducks as a glycosylated and non-glycosylated protein which is not viral particle associated. The function of DHBe is still unknown but it seems not to be essential for viral replication, morphogenesis, or infectivity (46) but appears to exhibit immunomodulatory functions (47).

Envelope proteins

The DHBV surface proteins are encoded by a single ORF consisting of the preS and S regions. The differential transcription of the ORF results in 2 mRNAs (2.35 and 2.13 kb) from which the surface proteins L and S are translated, respectively. Both proteins share an identical C-terminus (167 aa) representing the S domain, whereas L has an N-terminal extension of about 161 aa corresponding to the preS domain of the protein (48) (Fig.5).

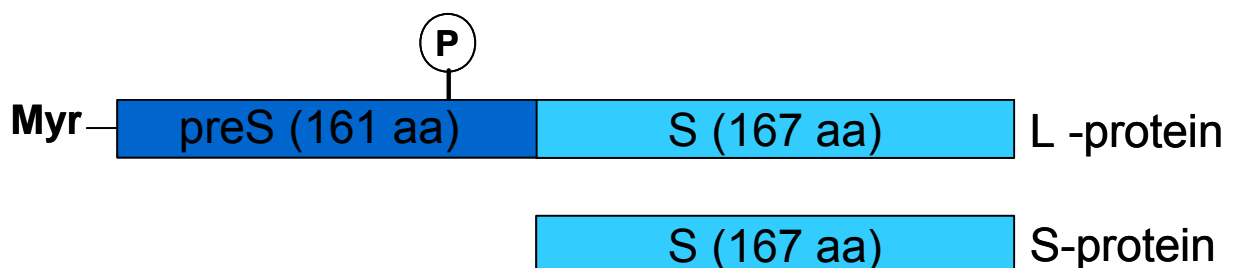


Fig. 6. Structural organization of the envelope proteins S and L. Both proteins share a common C-terminus (167 aa), while the L protein is N-terminally extended by 161 aa. In addition, L is phosphorylated at Serine 118 in the preS domain and myristoylated (Myr).

The S protein has a molecular weight of 18 kDa and represents about 80% of the envelope proteins incorporated into the particle, the L protein is 36 kDa and represents 20%. This ratio of 4:1 between S and L is found in the envelope of virions as well as in that of SVPs (48, 49). Unlike the HBV surface proteins, the envelope proteins of DHBV are not N-glycosylated (48) despite the presence of consensus sequences for glycosylation. Both surface proteins are synthesized in the ER and co-translationally inserted into the ER membranes.

The envelope proteins L and S have a spontaneous and very efficient budding activity. In the absence of other viral components (e.g. nucleocapsid), they are able to assemble and bud to form SVPs. The basis of this property is not known, however it is assumed that both proteins assemble into microdomains in the ER membrane, and spontaneously bud into the lumen when a critical density is reached. Furthermore, each protein, when expressed alone, is able to form SVPs in yeast (25). The L protein is post-translationally modified by myristoylation at its N-terminus (50) and by phosphorylation at Serine 118 in the preS domain (51, 52) (Fig.6). The phosphorylated and non-phosphorylated forms of L are designated p35 and p36, respectively. Phosphorylation does not play a role in envelope assembly and

infectivity (53) while myristoylation is required for infectivity but not for DHBV assembly (54). Another major L species consistently found in the liver is a protein of 28 kDa (p28) identified as a proteolytic product of the L protein.

L and S are multispanning transmembrane proteins with 4 transmembrane domains (TM1 to TM4) predicted to form α -helices and serving as anchors for the proteins in the membranes. Furthermore, TM1 was shown to be important for the assembly process, the 2 charged residues K24 and E27 are essential determinants for L translocation and particle assembly (55). The S protein as the major species in the envelope determines envelope curvature and drives the budding and secretion of virions and SVPs. The role of S in viral secretion was demonstrated by overexpressing L alone which results in the formation of SVPs which were retained within the cell. This retention was overcome when S was coexpressed (56). While the function of the minor processed L species p28 is unknown, full-length L protein plays important functions in viral entry, replication, and assembly. This multifunctionality of L is achieved by an unusual dual topology. After synthesis and co-translational insertion into the ER membrane, half of the L molecules is post-translationally translocated across the ER membrane by an unknown mechanism, resulting in 50% of L with an N-terminus oriented to the luminal side of the ER and 50% with an N-terminus directed to the cytosolic side of the ER membrane (57, 58). This dual topology enables L to exert two functions (Fig.7): the proteins with the N-terminus showing to the cytosol interact with the nucleocapsid leading to the envelopment of the virions (59) while the proteins with the N-terminus oriented to the inside of the ER are later found on the surface of viral particles and mediate the interaction with the cellular receptor(s) (25, 60).

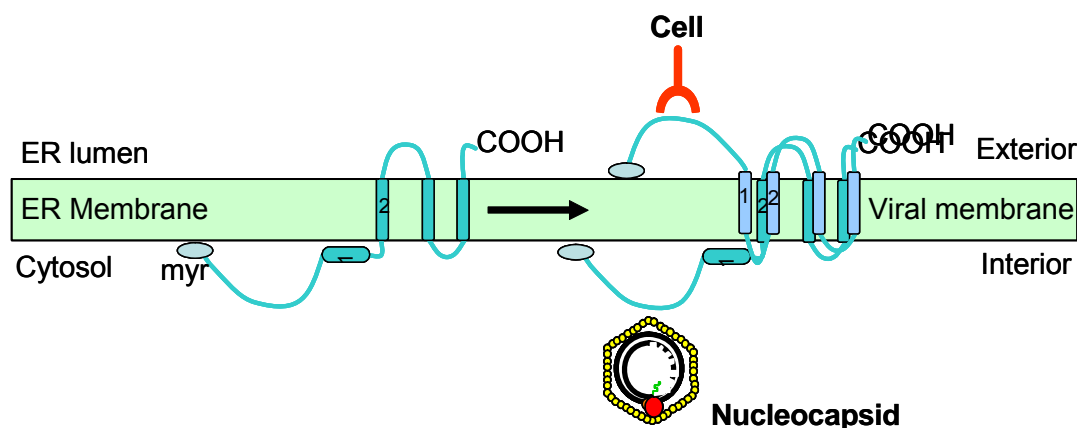


Fig. 7. Dual topology of the surface protein L. The dual topology of L reflects its dual function in the early steps of infection by binding to the receptor and in the late steps of the life cycle by interacting with the nucleocapsid to form virions. (By courtesy Dr. Funk, Heinrich Pette Institute, Hamburg).

Besides these two functions, L exercises other roles like cccDNA regulation (for more details see viral life cycle) (61, 62) and seems to exclude superinfection of infected hepatocytes (63).

The X protein

It was believed for a long time, that unlike mammalian hepadnaviruses, DHBV lacks the X ORF which encodes a regulatory protein believed to contribute to the development of hepatocellular carcinoma. In 2001, Chang et al demonstrated the presence of a hidden ORF from which the DHBx is expressed both *in vitro* and *in vivo* (64). Like HBx, DHBx is a transcriptional regulator and modulates cellular signalling in *in vitro* assays. However, it has recently been reported that DHBV harbouring a knockout mutation in the putative X ORF shows comparable infectivity as the wild type virus *in vivo* (65). This raises the question whether DHBx plays any physiological role during infection.

The viral life cycle

The life cycle of hepadnaviruses is not completely elucidated. While the early and the late steps are still largely unknown, the replication of these viruses was well studied. A representative model for the life cycle of DHBV is shown in Figure 8. The replicative cycle of DHBV starts by binding of the virus to a still unknown receptor or receptor complex at the surface of hepatocytes. This binding is mediated by the viral large envelope protein L. Following binding, the virus enters the cell via receptor-mediated endocytosis (66, 67). Within the endosomes, the surface proteins are proteolytically processed leading to the activation of translocation motifs (TLMs) within the L proteins. This results in the translocation of the virus through the endosomal membrane and its delivery into the cytosol (68). The nucleocapsid is then transported to the nucleus in a microtubule-dependent step (69). At the nuclear pore, the core protein is presumably phosphorylated leading to the exposure of a nuclear localization signal. Via interaction with nuclear factors like importins, the capsid is presumably taken up into the nucleus (44). Once arrived in the nucleus, the rcDNA is

converted into the cccDNA, the transcripts are made and exported to the cytoplasm where the viral proteins are translated.

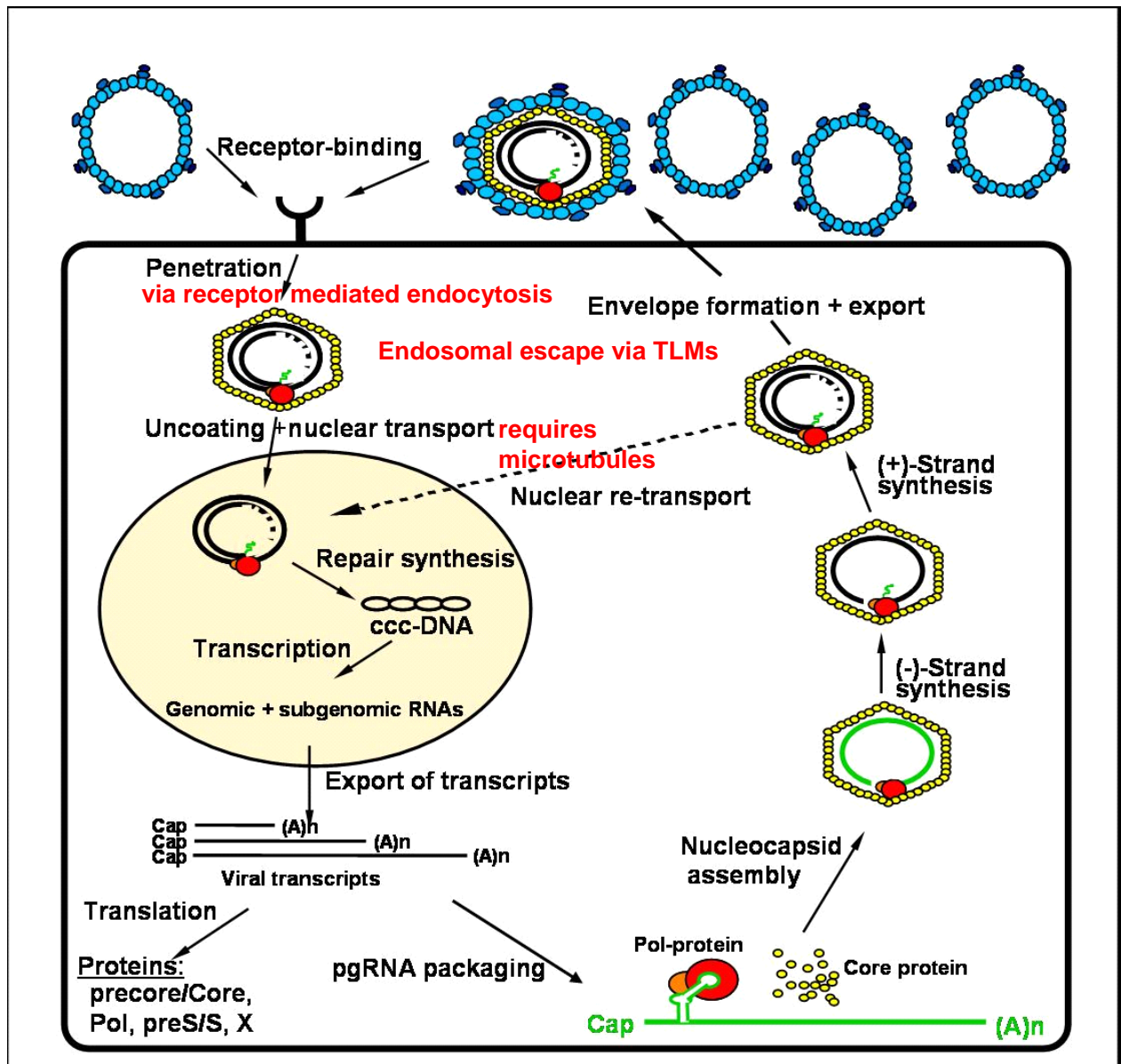


Fig. 8. Illustration of the viral life cycle. The principles and well known steps of the viral life cycle are illustrated, whereas the very early steps (binding and entry) as well as the very late steps (envelopment and export) are still largely unknown.

The surface proteins L and S are synthesised at the ER and are co-translationally inserted into the ER membranes. There, the surface proteins either bud spontaneously to form SVPs or interact with the nucleocapsid. In the cytoplasm, the packaging of the pgRNA starts with the interaction of the P protein with an RNA stem-loop structure called $D\epsilon$ which also serves as replication origin for the reverse

transcription (RT). This interaction is mediated by the specific chaperone complex Hsp90-p23 (heat shock protein 90 and its partner p23) (70) and is indispensable for initiation of DNA synthesis (71, 72). The pgRNA-P complex then interacts with the self-assembled core dimers to form a ribonucleoprotein complex. Prior to packaging, the core proteins are phosphorylated (73). Whether initiation of RT precedes assembly of the capsid is not known, however, the bulk of DNA synthesis occurs within the nucleocapsid. At the end of this process, the core protein is dephosphorylated and the resulting nucleocapsid is mature. The nucleocapsid can then follow two different fates: either it re-infects the nucleus to increase the pool of cccDNA pool or it interacts with the surface protein L via the cytoplasmically exposed preS domain leading to the envelopment and budding of virions. Whether the nucleocapsid follows one or the other pathway is regulated by the abundance of the L protein. At the beginning of an infection, when the level of L is low, the re-infection of the nucleus is favoured. Later, when the infection is established and the L protein is expressed at high concentrations, the envelopment and export of virions is preferred.

The late steps in the life cycle: assembly, budding, and secretion

The first details about the morphogenesis of hepatitis B viruses were described by using liver biopsies from patients with chronic hepatitis. Electron microscopic analysis of liver biopsies showed the presence of core particles within the nucleus and cytoplasm of infected hepatocytes (74-76) and the presence of numerous 20 to 30 nm tubular and circular structures in the cisternae of the ER (77). Further studies in the duck model system using liver specimens from DHBV-infected ducklings showed similar findings as viral particles were described within hypertrophied cisternae of the ER. Furthermore, the authors observed core particles within the nuclei, free in the cytoplasm and near or on the cisternal membrane of the ER (78). Based on these observations, it has been assumed that viral particles are formed by protrusion of the core particles through the ER and by simultaneous encapsidation with a coat derived from this compartment (78). Later, the morphogenesis was investigated in *in vitro* systems namely in stably or transiently HBV-transfected hepatoma cell lines, mouse fibroblasts, or other cell lines such as CHO (Chinese hamster ovary cells). These systems contributed a lot to our current understanding of the hepatitis B

morphogenesis although some contradictory results were reported. Many groups reported that the assembly of HBsAg particles occurs in the ER as they observed the presence of HBsAg cylindrical and spherical particles within dilated cisternae of the rER (79). Others reported that HBsAg assembles in a post-ER, pre-Golgi compartment (80) and that enveloped virions are secreted via the constitutive secretory pathway.

Besides this quite detailed view of the morphogenetic puzzle, many pieces are still missing. This is due to some limitations of the *in vitro* systems like the inefficient production of viral particles, especially of virions. *In vitro*, like in the natural HBV infection, about 1 to 10 virions are released per single hepatocyte and per day (81) making the understanding of many processes associated with the formation of virions very difficult. Until now for example, the direct observation of viral budding or the processes of viral release were not possible in these systems. In contrast to the HBV *in vitro* systems, the DHBV and primary duck hepatocytes (PDHs) offer a convenient and suitable model system to investigate such questions for many reasons: (i) The virus production rate of DHBV *in vitro* is higher than for HBV (82) and thus the frequency of the morphogenetic steps is higher, making the probability to visualize such events more likely. (ii) Using congenitally DHBV-infected PDHs (prepared from embryos which were infected *in ovo*) is closer to the natural infection making the results more authentic to the *in vivo* situation. (iii) A direct correlation between *in vitro* and *in vivo* data is possible due the availability of both PDHs and liver samples from DHBV-infected ducks. Understanding the morphogenesis of hepatitis B viruses is not only a major step to complete our still fragmented picture of the life cycle of these viruses but also to understand the requirements for the formation of progeny viruses in order to try to interfere with these steps to prevent spreading of the virus in the whole liver.

II.2. Assembly and budding of enveloped viruses

Virus assembly is a key step in the replicative cycle of any virus. This process involves interactions between different types of virus components and a large subset of cellular factors in order to generate new progeny viruses. This implies that the different viral components and the cellular factors required must be concentrated at the assembly site and thus must be transported along different transport pathways to

reach this point. Moreover, enveloped viruses have to acquire their envelope, this occurs by budding at cellular membranes containing the viral envelope proteins. A diversity of strategies is employed by different viruses in order to achieve this goal and to ensure an efficient production of offspring. Some viruses take advantage of pre-existing intracellular compartments of the secretory pathway in order to assure the production and exit of progeny viruses. Others induce the recruitment of organelles to a specific site, usually the perinuclear area, to build new structures that function in viral replication, assembly, and budding, these structures are known as “viral factories” (83).

In the following parts, the focus will be on enveloped viruses and their site of assembly and envelopment, the assembly in the nucleus will not be discussed since hepatitis B viruses are known to assemble and bud in the cytoplasm.

II.2.1. Subcellular compartments of the secretory pathway as sites for the assembly and budding of enveloped viruses

All proteins destined to be incorporated into subcellular organelles like the ER, the Golgi, later secretory pathway organelles, and the plasma membrane, or to be secreted from the cell travel along a highly conserved route known as the secretory pathway (Fig. 9). The transport from one compartment to another is mediated by the formation of coated membrane vesicles that travel to and fuse with the target organelle. Viruses exploit the different organelles along this pathway for their assembly, to bud and acquire their envelope, and to travel within transport vesicles to exit the host cell.

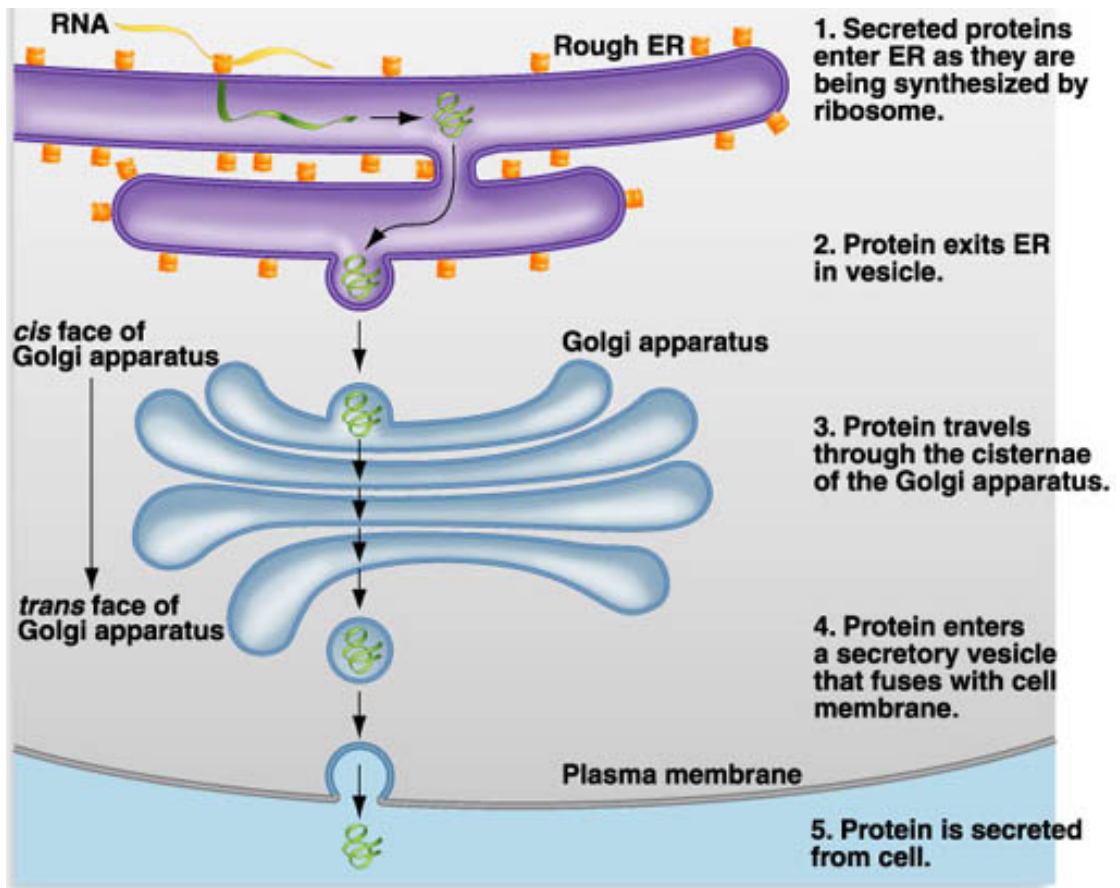


Fig. 9. Subcellular compartments of the secretory pathway. The subcellular compartments as well the pathway followed by a protein to be secreted are depicted and described. (Adapted from <http://fig.cox.miami.edu/~cmallery/150/cells/organelle.htm>)

Endoplasmic reticulum

Flaviviruses, a genus of small enveloped RNA viruses within the family of Flaviviridae, assemble and bud into the endoplasmic reticulum (ER). The ER is the starting point in the exocytic pathway and is a network of membrane tubules or flat saccules, called cisternae. This system is divided into 3 distinct specialized regions, (i) the rough ER (rER), which is studded with ribosomes on its cytoplasmic face, and which is specialized in protein synthesis and folding. (ii) The transitional elements are the sites from which transport vesicles with cargo for the Golgi bud, and (iii) the smooth ER (sER), composed of tubular elements like the rER but lacking the ribosomes.

Flaviviruses were detected by electron microscopy within the lumen of both rough and smooth ER (84, 85). Subsequent maturation of the virus occurs within the secretory pathway (86). Moreover, rotaviruses which contain double-stranded RNA, were shown to bud into the lumen of the ER. This virus replicates and assembles its

capsid at cytoplasmic inclusion bodies, called viroplasms, which are then transported to the ER where they are enveloped (87).

ER to Golgi intermediate compartment (IC)

The second step along the secretory route is the ER to Golgi intermediate compartment (IC). This compartment is formed by small vesicles (60-80 nm in diameter) and elongated membrane tubules which assure the transport of cargo from the ER to the Golgi and back from the Golgi to the ER (retrograde transport). This compartment is used by coronaviruses for their budding (88). These viruses generate a replication complex derived from ER membranes where the replication of viral RNA and the assembly of the nucleocapsid occur. Later on, the viral nucleocapsid is transported to the IC where the viral glycoproteins accumulate and particle formation occurs (89).

The Golgi complex and the trans Golgi network (TGN)

The Golgi is also a site for assembly and budding of many viruses like bunyaviruses (90). After cotranslational cleavage from a precursor protein, the 2 viral glycoproteins are transported as heterodimers from the ER to the Golgi where they accumulate. Afterwards, the nucleocapsid proteins and the genomic RNA accumulate in the Golgi region where they presumably interact with the spike proteins and bud into the Golgi lumen to form virus particles (91). Furthermore, rubella virus, which is the sole member of the genus Rubivirus within the family of togaviruses, buds also at the Golgi. The surface proteins are transported as heterodimers to the Golgi where they are retained and consequently direct the budding process into this compartment (92). Many viruses which assemble and bud in the ER or IC are transported through the Golgi to be modified and to mature. Within the Golgi, many of the incoming proteins undergo further modifications like remodelling of the N-linked oligosaccharides acquired in the ER, addition of O-linked saccharides and proteolytic processing of precursor proteins.

For HBV for example, it is believed that after assembly and budding into a post-ER and pre-Golgi compartment (80), the virus transits the Golgi and is secreted through the secretory pathway (93).

Cargo proteins or viruses coming from the ER and IC enter the Golgi from its cis-side, move through the medial-Golgi and exit from the trans-side of the Golgi arriving in the

trans-Golgi network (TGN). The TGN has been identified as the site for re-envelopment of herpes simplex virus type-1 before travelling to the plasma membrane for its extracellular release (94). The TGN is an interconnected network of membranous tubules and associated vesicles located adjacent to the trans-most cisterna of the Golgi. It is recognised as a distinct compartment by its content of residual proteins. The TGN is the sorting station for proteins where they are packaged and sent to their final destination.

The plasma membrane

Many viruses have been shown to bud at the plasma membrane (PM). These include alphaviruses (95), orthomyxoviruses (96), paramyxoviruses (97), retroviruses (98), and rhabdoviruses (99). For all these viruses, their glycoproteins traversed the entire secretory pathway to be delivered to the PM. In addition, the other viral components (e.g. nucleocapsid, matrix proteins) also have to be transported to this assembly and budding site. Once the assembly occurred, the viral particle buds through the PM to acquire its envelope, and to be directly released into the extracellular space.

Other subcellular organelles exploited by enveloped viruses during assembly and budding

Beside the organelles of the secretory pathway, other cellular compartments are exploited by viruses for their assembly and budding. This is the case for the human immunodeficiency virus type 1 (HIV-1) which has been shown to assemble in multivesicular late endosomes in primary macrophages (100).

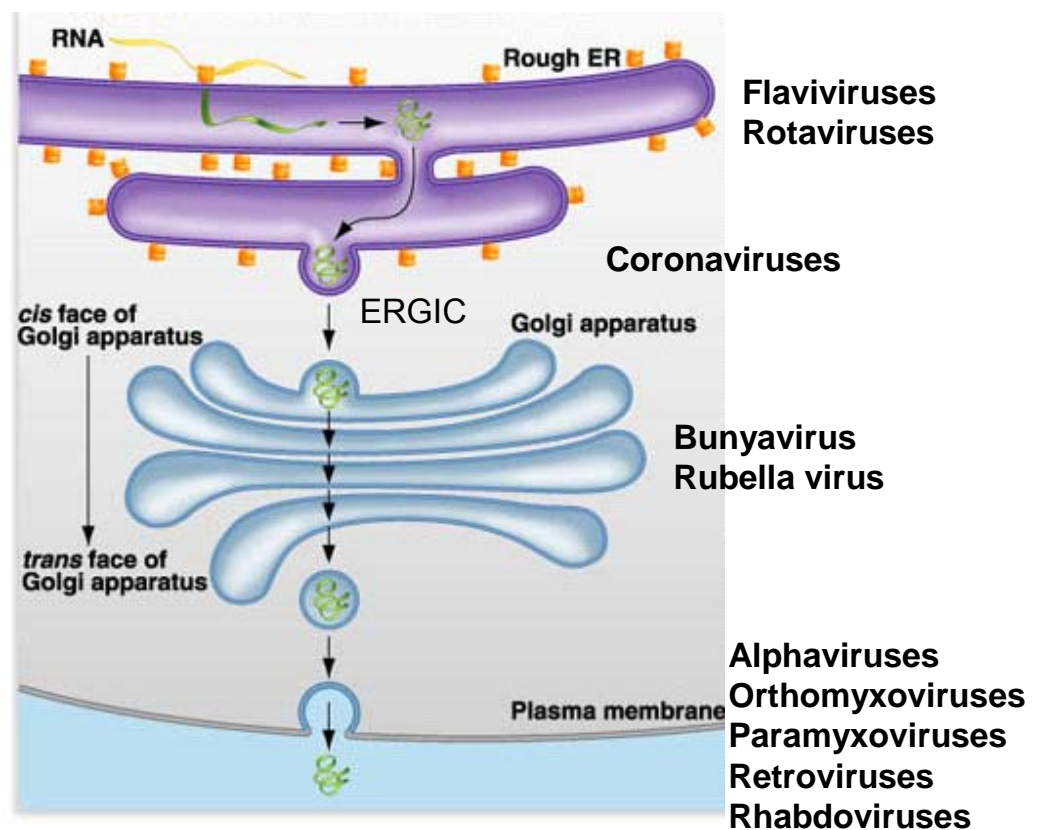


Fig. 10. Viral assembly and/or budding at cellular membranes. Schematic representation showing the intracellular locations at which enveloped virus assembly takes place.

II.2.2. Assembly and budding of enveloped viruses at “virus factories”

For a number of viruses, the formation of “factories” has been described. These factories consist of perinuclear or cytoplasmic foci that dramatically alter large areas of the infected cells. These factories are generated by excluding host proteins and organelles and recruiting specific organelles to build a unique structure where replication, assembly or both take place. Mitochondria, cytoplasmic membranes and the cytoskeleton participate in the formation of such structures (83).

Vaccinia virus, a representative member of Poxviridae which are large DNA viruses, build factories resembling aggresomes. Early in infection, cellular proteins and organelles are excluded from an area close to the nucleus where large amounts of viral structural proteins and viral DNA accumulate in addition to mitochondria, cytoskeletal filaments, and different types of membranous structures. Some of these

membranes are required for viral replication while others are modified to produce the viral envelope. These factories are very dynamic structures where viral and cellular factors move in and out. During virus replication, the factory is surrounded by rER membranes, when assembly initiates, these membranes dissociate from the replication site and new structures are observed in those areas.

Togaviruses, which contain single-stranded RNA, use endosomes and lysosomes as sites for viral replication (101). They modify these structures to form cytopathic vacuoles. Similar virus-induced vesicles have been reported as replication complexes for flaviviruses and picornaviruses (102, 103). However, the replication complexes of these viruses are derived from the ER rather than from endosomal compartments.

II.2.3. Vesicular transport along the secretory pathway

Membrane vesicles and tubules assure the communication between organelles and the maintenance of the identity of each cellular compartment. When two transport vesicles with the same identity encounter each other, they undergo homotypic fusion. This occurs to build larger vesicular-tubular structures that are transported en bloc. In contrast, heterotypic fusion involves interaction of membranes with different composition.

The intracellular transport flow can be interrupted using pharmacological inhibitors which interfere specifically with distinct steps along the secretory pathway. This can be useful in order to distinguish which pathway or which proteins are required for the virus to exit the cell. The macrocyclic lactone brefeldin A (BFA) for example has been extensively used to study the dynamics of the transport machinery. BFA inhibits the protein transport between ER and Golgi and induces the tubulation of the Golgi and its rapid collapse into the ER. These effects are due to the inhibition of small GTPases required for the formation of coated vesicles. However, BFA has pleiotropic effects since it also causes the tubulation of endosomes and TGN (104, 105). In addition to chemical inhibitors, it is possible to interfere with the transport of proteins from the TGN to the PM for example, by incubating cells at 20°C (106). At this temperature, the proteins accumulate in the TGN and only reach the PM when cells are warmed to 37°C.

II.2.4. Exocytosis

Exocytosis is defined as the fusion of an intracellular trafficking vesicle with the plasma membrane. Two different kinds of exocytosis are known: constitutive and regulated exocytosis. Constitutive exocytosis includes all fusion events in which vesicles are generated from the TGN, transported, and fuse with the PM continuously without being subject to a short-time regulation. This constitutive pathway operates in all cells. Regulated exocytosis requires that precursor membranes are stored in specialized intracellular pools from which they are mobilized upon activation of signalling cascades. This allows the controlled delivery of secretory products such as proteins, hormones, neurotransmitters, or the controlled incorporation of PM components such as transporters, enzymes, and channels. This kind of exocytosis occurs in specialized cells such as neurons as well as endocrine and exocrine cells.

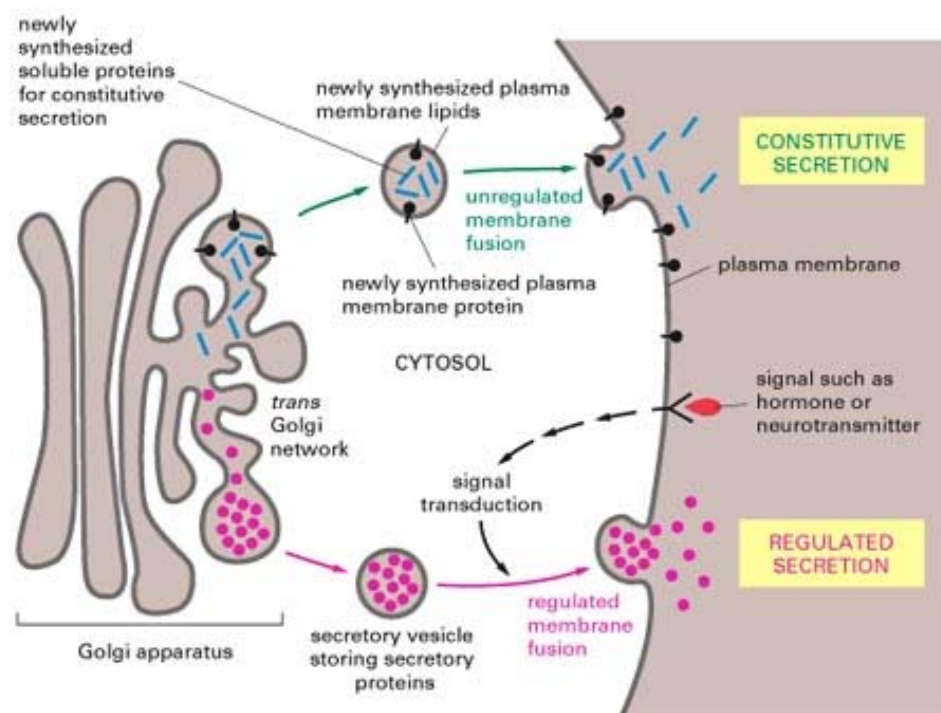


Fig. 11. In secretory cells, regulated and constitutive pathways of exocytosis diverge in the TGN. Many soluble proteins are continually secreted from the cell by the constitutive secretory pathway, which operates in all cells. This pathway also continually supplies the PM with newly synthesized lipids and proteins. Specialized secretory cells have, in addition, a regulated exocytosis pathway by which selected proteins in the TGN are diverted into secretory vesicles, where the proteins are concentrated and stored until an extracellular signal stimulates their secretion. (Adapted from *Essential Cell Biology, Second Edition*, published by Garland Science in 2004.)

Exocytosis consists of 4 steps:

(i) Vesicular trafficking. Certain vesicles have to be transported over a long distance, which can be achieved by the help of the cytoskeleton (actin or tubulin) and motor proteins. Once arrived at the PM, the vesicle comes in contact with tethering factors.

(ii) Vesicle tethering. This step involves links over long distance (more than 25 nm) between the vesicle and the PM.

(iii) Vesicle docking. This refers to the tight interaction of two membranes. It is a tight and close association which involves molecular interactions and rearrangements required to trigger bilayer fusion.

(iv) Vesicle fusion. This step is driven by SNARE (soluble NSF attachment protein receptor, where NSF stands for N-ethylmaleimide-sensitive fusion protein) proteins, a v-SNARE at the vesicle and a t-SNARE at the PM leading to the merging of the vesicular membrane with the PM. This fusion leads to (i) an increase of the PM surface which is important for the regulation of cell size during cell growth, (ii) release of the substances within the vesicle, and (iii) delivery of proteins which were embedded in the vesicular membrane to the PM.

There are 2 well described mechanisms for exocytic release. The first is known as “kiss-and-fuse” which involves the complete fusion of the vesicle with the PM, the second is the “kiss-and-run” mechanism which occurs in more specialized cases such as regulated exocytosis. This mechanism involves the formation of a transient fusion pore that allows release of a limited amount of the vesicle content, followed by re-sealing of the pore and dissociation of the vesicle from the PM. The vesicle can undergo re-exocytosis at the same site or at a new site until the content is completely released.

II.2.5. Role of the cytoskeleton in the morphogenesis of enveloped viruses

Cytoskeletal filaments are not only indispensable for many cellular processes but they also play important roles at different steps of the life cycle of many viruses.

Actin filaments or microfilaments

They are thin filaments of about 7 nm in diameter, mostly concentrated beneath the PM giving the cell mechanical strength, link transmembrane proteins to cytoplasmic proteins and allow locomotion of cells. Actin filaments were shown to play several

roles in regulated exocytosis such as the capture and transport of secretory granules (107, 108) and synaptic vesicles close to the PM (109). In contrast, actin plays no role in constitutive exocytosis as the depolymerization of filamentous actin with Cytochalasin D had no significant inhibiting effect on transport, docking, and fusion of vesicles. In contrast, depolymerization of the actin cortex facilitates the fusion process (110). Moreover, intact actin microfilaments are required for the maturation of measles virus. In the presence of the actin disrupting agent Cytochalasin B, the release of this virus was drastically decreased (111). Furthermore, retroviral Gag proteins were shown to interact with actin filaments, when actin was stabilized by phalloidin, the production of virions was reduced, however when actin was depolymerised briefly, virion secretion was enhanced (112).

Microtubules

They are cylinders of about 25 nm in diameter, which participate in a wide variety of cell activities such as transport of vesicles and organelles via motor proteins like kinesins and dyneins which hydrolyse ATP. Microtubules were shown to play important roles in constitutive exocytosis: (i) they determine the morphology of the vesicle since a tubular shape is a consequence of the attachment of the vesicle to the microtubule at multiple points. (ii) The transport of vesicles not only to the cell periphery but also to the fusion site at the plasma membrane is microtubule-dependent. (iii) Vesicles stay associated with microtubules until the initiation of the fusion process (110). Microtubules are exploited by many viruses. For instance, entry and egress of herpes simplex virus are both microtubule-dependent processes (113) (114). Vaccinia virus also uses microtubules at 2 distinct steps during assembly and budding, first for the transport of the intracellular mature virions from the assembly site to the envelopment site (Golgi-derived membranes) (115) and second for transport of the intracellular enveloped virions to the PM (116). These transport processes are inhibited by the microtubule-disrupting agent Nocodazole.

II.3. Aim of the study

The aim of this study was to identify and characterize the cellular compartments and factors exploited or modified during the morphogenesis of hepatitis B viruses. Using the duck hepatitis B virus (DHBV) as a model system, the following questions have been specifically addressed:

(i) Which cellular compartments and pathways are exploited by DHBV for assembly, budding, and secretion? (ii) Do virions and SVPs exploit the same morphogenetic pathway? (iii) What is the mode and kinetics of viral secretion? (iv) By which mechanism do viral particles exit the host cell?

These questions have been addressed using DHBV because it is a well characterized animal model for hepatitis B viruses, in which *in vivo* and *in vitro* infection is possible (infected Pecking ducks and PDHs). The use of an authentic infectable cell culture system in this study is a major advantage compared to previously published studies.

To characterize the cellular sites at which the assembly and budding take place, a combination of the following approaches was used: (i) ultrastructural analysis of primary duck hepatocyte cultures, liver biopsies, and a hepatoma cell line stably transfected with the DHBV genome; (ii) colocalisation studies by immunofluorescence microscopy; (iii) subcellular fractionation of DHBV-infected liver; (iv) immunoprecipitation experiments, and (v) live cell imaging.

Using pharmacological inhibitors interfering with specific cellular transport pathways and cytoskeletal elements, the role of intracellular transport in viral formation and release were tested.

Moreover, the still unanswered question of a common or rather a divergent morphogenetic pathway for virions and SVPs, a characteristic feature of hepadnaviruses, was addressed by ultrastructural and by interference studies.

Furthermore, the mechanism of viral secretion was investigated by electron microscopy, live cell imaging and by determination of the viral secretion kinetics. Thus, first correlative *in vitro* and *in vivo* quantitative information on assembly and secretion of virions and SVPs should be obtained.

III. Results

III.1. Assembly and budding of DHBV

At the late steps of viral replication enveloped viruses assemble and acquire their envelope through budding at cellular membranes. For hepadnaviruses, the exact nature of the compartment at which these assembly and budding steps occur is still poorly characterized. In order to identify and characterize these compartments, a combination of ultrastructural and biochemical approaches was used.

III.1.1. Ultrastructural analysis of virus morphogenesis by transmission electron microscopy both *in vitro* and *in vivo*

III.1.1.1. A new three-dimensional culture system

As a first step towards the characterization of the hepadnaviral assembly and budding sites, ultrastructural analysis by transmission electron microscopy (TEM) in a relevant model culture system was performed.

Primary duck hepatocytes (PDHs) were cultured in a 3D-cell culture system (Fig.12) consisting of a special microtube. The capillary wall is semi-permeable, transparent and has a molecular cut-off of 5 kDa (117-119). The advantage of this system is the 3-dimensional organization of the cells within the tube which is closer to the liver structure than the currently 2-dimensional culture methods. A further advantage is the possibility to fix and prepare the cells for TEM analysis within the tube and without further manipulations in contrast to conventional preparation methods where cells have to be scraped from the support, pelleted by centrifugation and embedded. Within the microtube, the cells were viable as shown by the green staining of hepatocytes by fluorescein diacetate (FDA), this substance is converted by a specific lipase within the hepatocytes resulting in green fluorescence (Fig. 12B, middle panel). Furthermore, the hepatocytes and the non-parenchymal cells were organized in a fashion that a layer of non-parenchymal cells forming a carpet for the hepatocytes which are organized in trabecules, thus forming a kind of liver organoid (Fig. 12B lower panel).

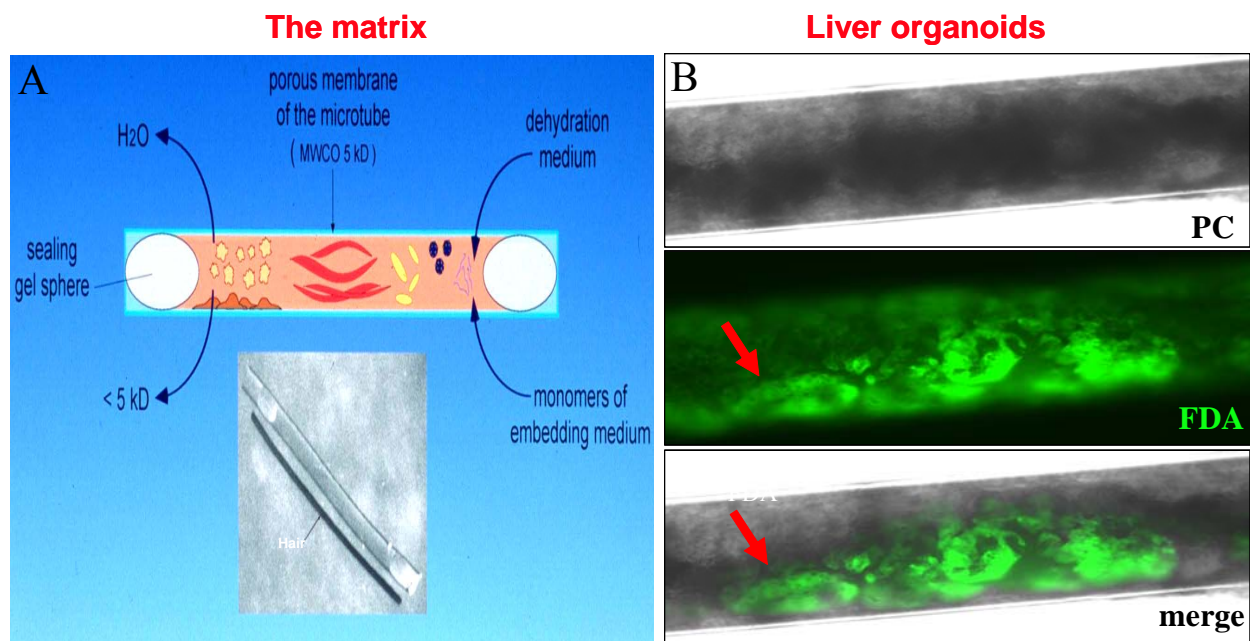


Fig. 12. Primary duck hepatocytes were cultured in a 3D-cell culture system. (A) Scheme of the microtube which is represented in comparison to a hair in the lower panel. (B) PDH cultures within the microtube, upper panel phase contrast (PC) of the cells, middle panel staining with FDA which stains preferentially living hepatocytes, lower panel shows the merge between PC and FDA stain showing the 3D organization of the culture as non-parenchymal cells are attached to the membrane of the microtube forming a layer to which the hepatocytes attach.

III.1.1.2. DHBV morphogenesis is conserved *in vitro* and *in vivo*

Congenitally DHBV-infected PDHs grown in microtubes for 7 days and liver biopsies from adult DHBV-infected ducks were fixed in 2.5% glutaraldehyde for 20 min at room temperature (RT) and processed as described in section Material and Methods. The ultra thin sections were examined by TEM.

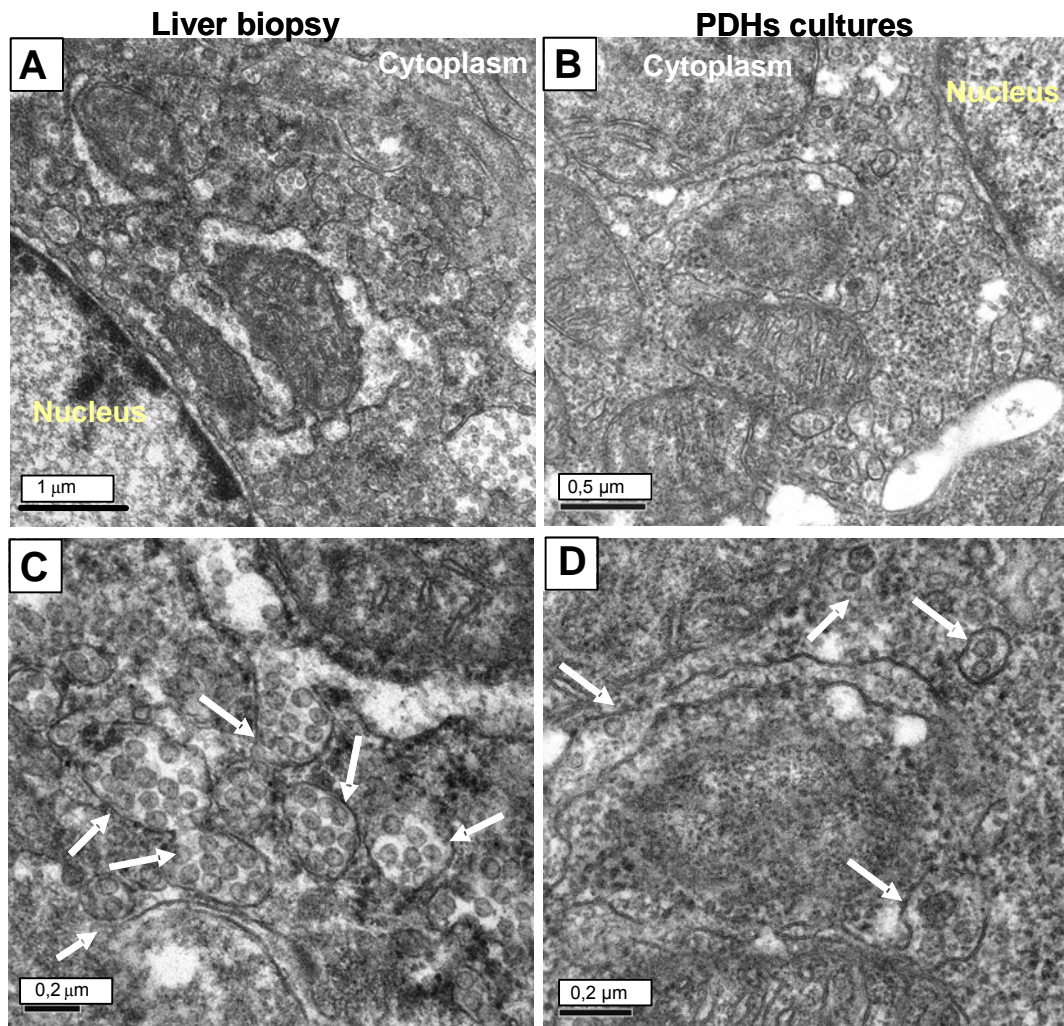


Fig. 13. The principal morphogenetic features of DHBV are conserved both *in vitro* and *in vivo*. The cytoplasm of DHBV-infected hepatocytes from both liver samples (A) and PDH cultures (B) contains vesicular structures. (C and D) The vesicles contain viral particles (arrows). The black bars indicate the size.

The cytoplasm of DHBV-infected hepatocytes from PDH cultures as well as from liver biopsies was filled with vesicles of different size and shape (Fig. 13A-D). Higher magnification revealed that the lumen of these vesicles contained spheroid-shaped particles corresponding from their size and morphology to DHBV viral particles as described earlier (78, 120).

To confirm the viral nature of the particles observed within the vesicles, immunogold staining of paraformaldehyde-fixed ultrathin sections of DHBV-infected PDHs using an L- and core protein-specific antiserum were performed (Fig. 14). Immunogold staining, of glutaraldehyde fixed sections was not successful due presumably to the loss of antigenicity of L and core. Using paraformaldehyde, the antigenicity was

preserved, however under these conditions the membrane structures as well as the viral particles were less well preserved. L staining was seen associated with intracytoplasmic vesicles and showed strong labelling of viral particles in the lumen of these structures (Fig. 14A and B). The pattern of anti-core labelling was different from that of L and was often seen in the cytosol or close to the limiting membrane of VCVs and less frequently inside the vesicles (Fig. 14C and D). These results confirmed the identity of the particles observed in native TEM as viral particles.

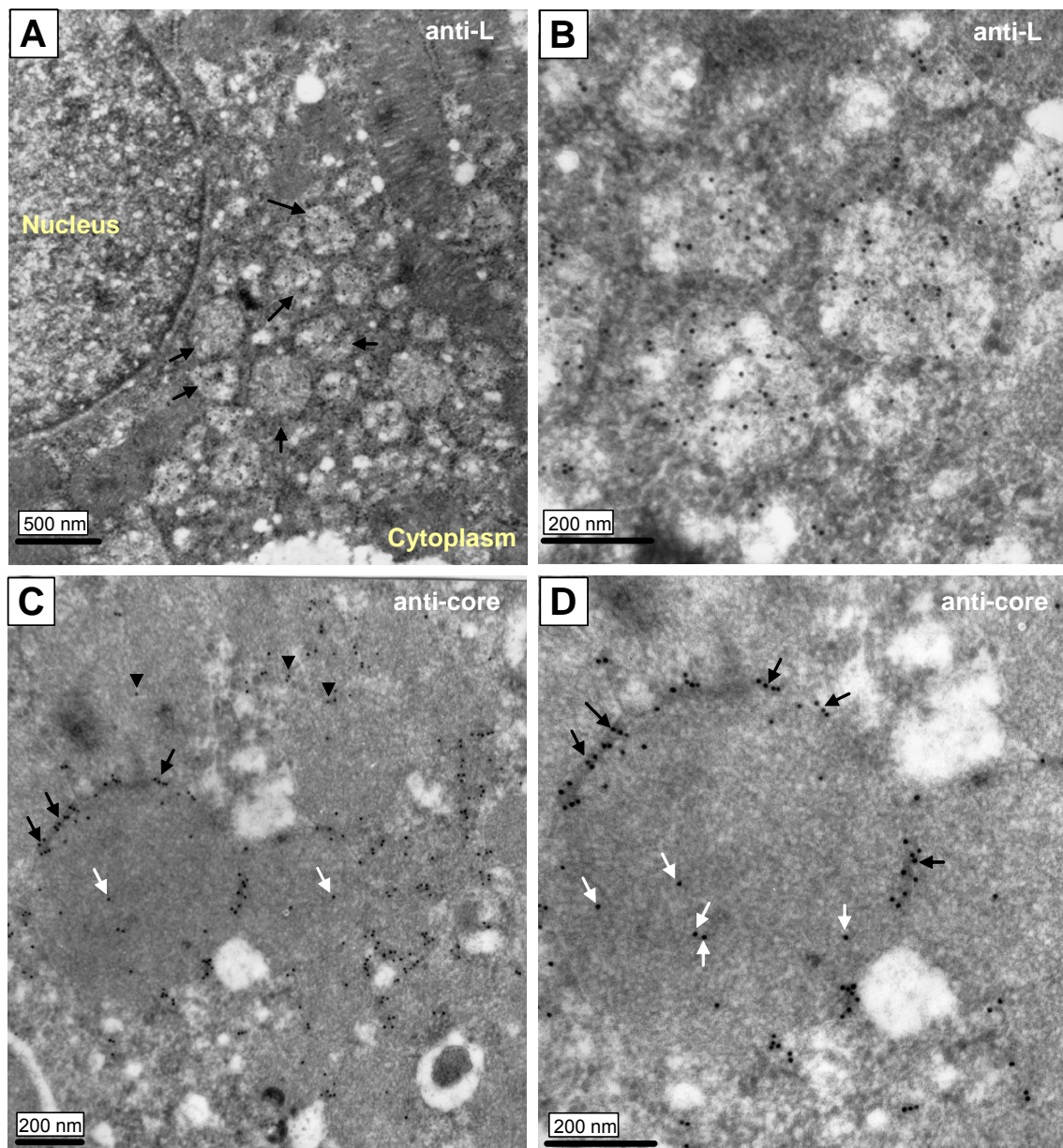


Fig. 14. Transmission electron microscopy of immunogold-labelled congenitally DHBV-infected duck hepatocytes. Sections of hepatocytes were stained for viral L (A and B) and core protein (C and D). Panel A shows that L staining was virtually restricted to VCVs which were distributed throughout

the cytoplasm (arrows). (B) Immunogold staining was mainly found on the viral particles residing in the lumen of VCVs. (C and D) Immunogold particles were predominantly scattered in the cytosol (arrow heads) and at the limiting membrane of VCVs (black arrows), and rarely found inside the vesicles (white arrows). The black bars indicate the size.

III.1.1.3. Virus particles-containing vesicles are formed by reorganization of endomembranes

The assembly and budding of enveloped viruses can occur at two different intracellular membrane systems: at pre-existing organelles or at virus-induced novel endomembranes. To test whether the observed vesicles belong to the first or to the second group, a comparative analysis between non-infected and congenitally DHBV-infected PDHs cultured in microtubes was performed.

Figure 15A shows a section of the cytoplasm of a non-infected hepatocyte, where the extensive tubulo-reticular ER network was the most prominent organelle (Fig. 15A and 15B, arrows). The strong decoration of these endomembranes with ribosomes identifies them as rough ER (rER) (Fig. 15B, inlet). In contrast, the cytoplasm of DHBV-infected hepatocytes lacked the impressive rER network and was instead full of vesicular structures (Fig. 15C and D, arrows). The lumen of these vesicles contained spheroid-shaped particles corresponding in their size and morphology to viral particles as described earlier (78). These vesicles were absent in non-infected hepatocytes (Fig. 15A and B) indicating that they were generated during DHBV infection. In the following, I will refer to these vesicles as virus particles-containing vesicles (VCVs).

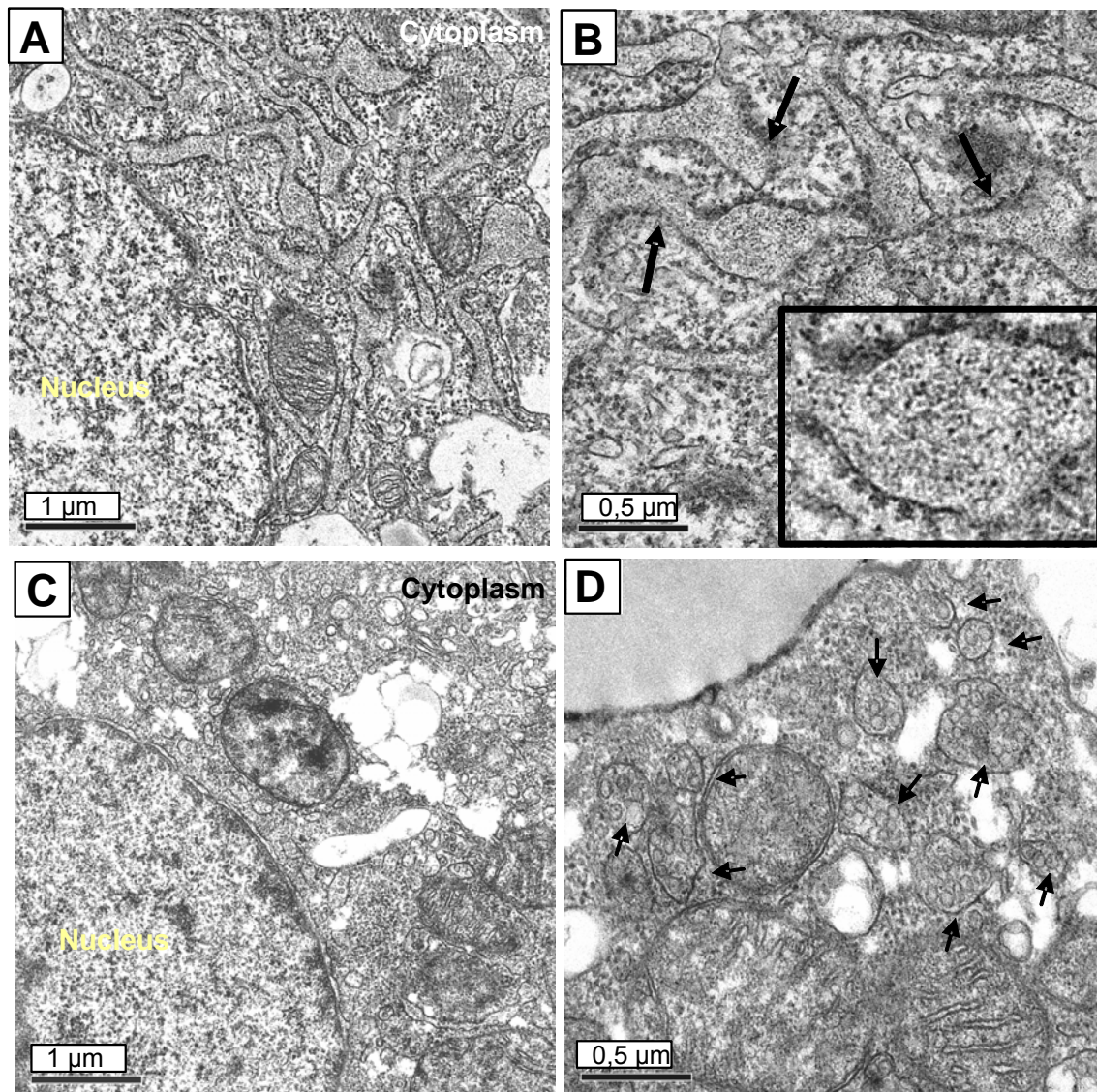


Fig. 15. Disorganisation of the rough ER network during DHBV infection. Non-infected hepatocytes show the typical distribution of ER membranes throughout the cytoplasm. (B) rER structures (arrows) in the cytoplasm of non-infected hepatocytes. The inset shows a magnification to visualize ribosomal structures on the cytosolic surface of the rER membrane. (C) The cytoplasm of infected hepatocytes lacks the typical rER structures and is instead full of vesicular structures. (D) The numerous vesicular structures (arrows) in infected hepatocytes contain viral particles. The black bars indicate the size.

Closer examination of the cytoplasm of DHBV-infected hepatocytes showed the presence of tubular smooth (sER) and rough ER (rER) cisternae located in close proximity to the nucleus (Fig. 16A and C, respectively). Viral particles were found within the lumen. Vesicles containing viral particles segregated from the sER and rER

(Fig. 16B and D white arrows). These findings clearly show that VCVs are formed by segregation from both sER and rER. This process leads to the disorganization and disappearance of the reticular ER network as shown in Fig. 15A and C.

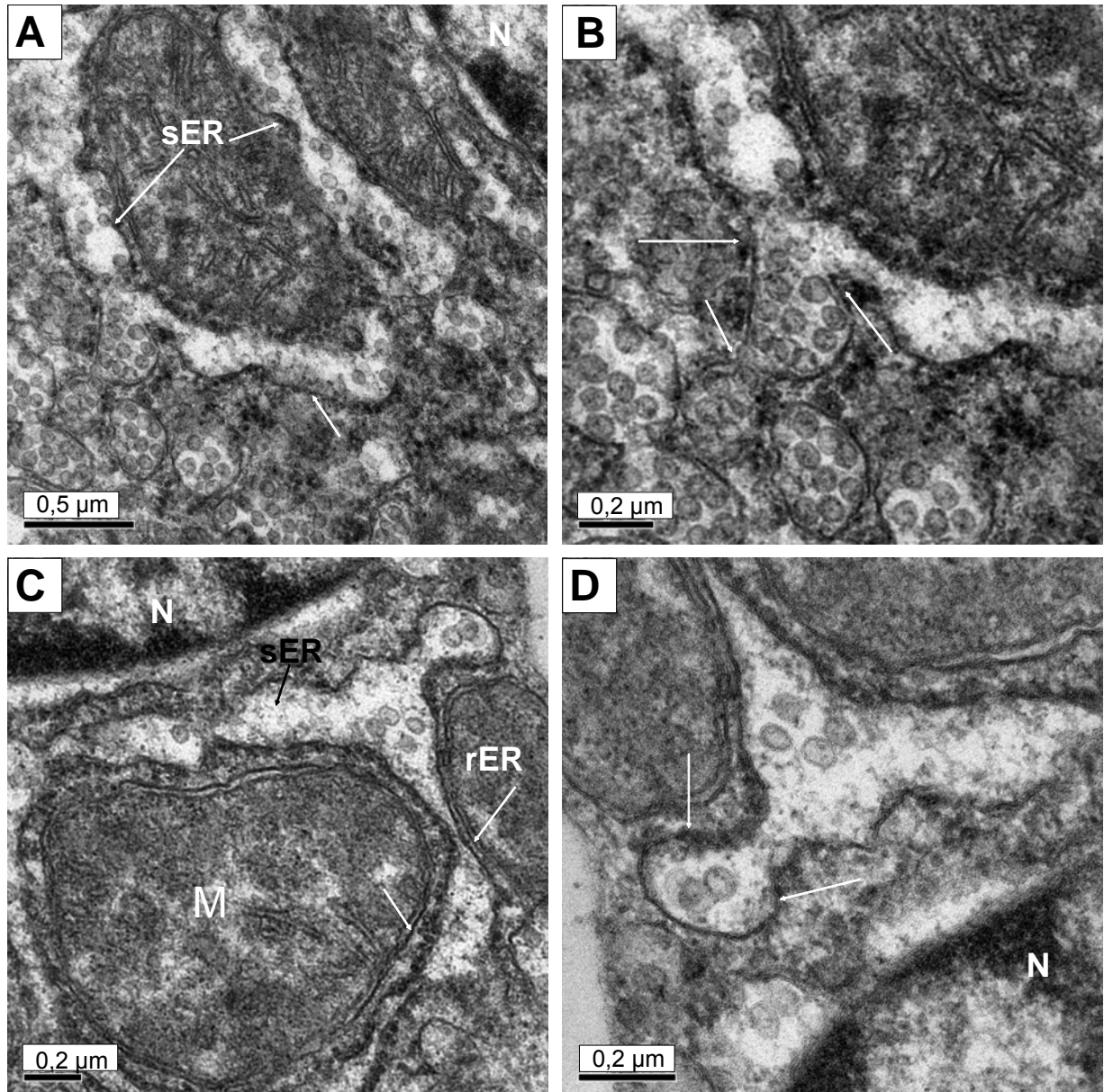


Fig. 16. VCVs are generated through segregation from the smooth ER and rough ER. (A and C) Tubular sER (black arrows) and rER (white arrows) located near the nucleus (N) contain viral particles (B and D). Vesicles segregate from the sER and rER forming VCVs (white arrows). M, mitochondrion. The black bars indicate the size.

Further examination revealed membrane dilatations of different extent at the outer nuclear membrane (ONM) of infected hepatocytes (Fig. 17A-D). In the perinuclear space one (Fig. 17A and B) or few viral particles (Fig. 17C) were frequently observed.

It is conceivable that after reaching a certain critical size, the membranous sacs extend into the cytoplasm and finally segregate from the outer nuclear membrane forming VCVs. An intermediate and a late state of this process are shown in figure 17C and 17D, respectively. As the outer nuclear membrane is part of the ER, the observed dilatations suggest that the VCVs originate at least in part from this compartment.

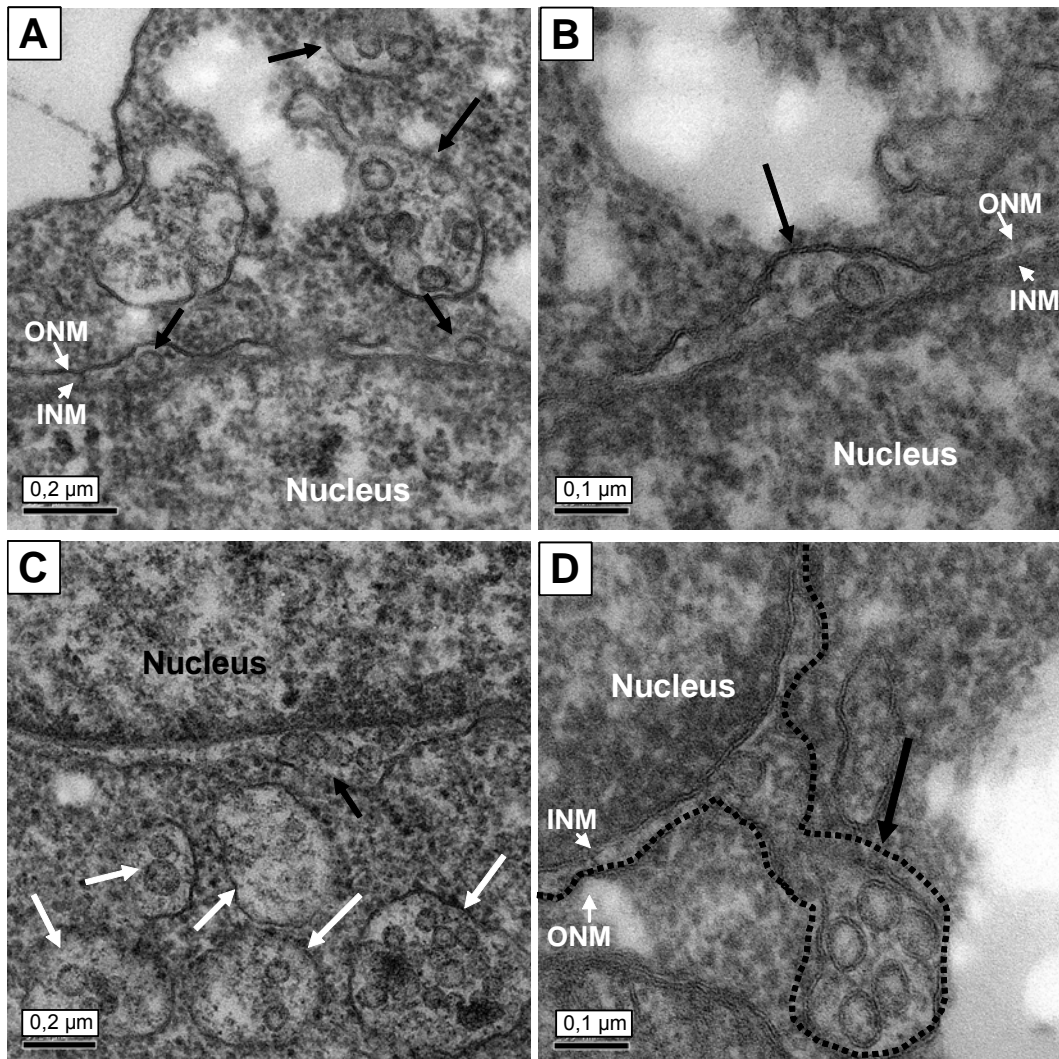


Fig. 17. VCVs segregate from the outer nuclear membrane. (A) The outer nuclear membrane (ONM) of infected hepatocytes shows two dilatations, each containing one viral particle in the perinuclear space (black arrows). In the cytoplasm near the nucleus VCVs can be observed (yellow arrows). (B) A higher magnification of the ONM dilatation (red arrow). (C) A more extended dilatation of the ONM (black arrow) containing 4 viral particles in the perinuclear space. (D) A VCV (black arrow) is segregating from the ONM (the punctuated line underlines the contour of the ONM). INM, inner nuclear membrane. The black bars indicate the size.

III.1.1.4. Different features of VCVs *in vitro* and *in vivo*

VCVs were heterogeneous in size and shape (Fig. 18 A-E). They appeared as tubules, spherical vesicles or as undefined shaped structures ranging between 100 and 800 nm in diameter.

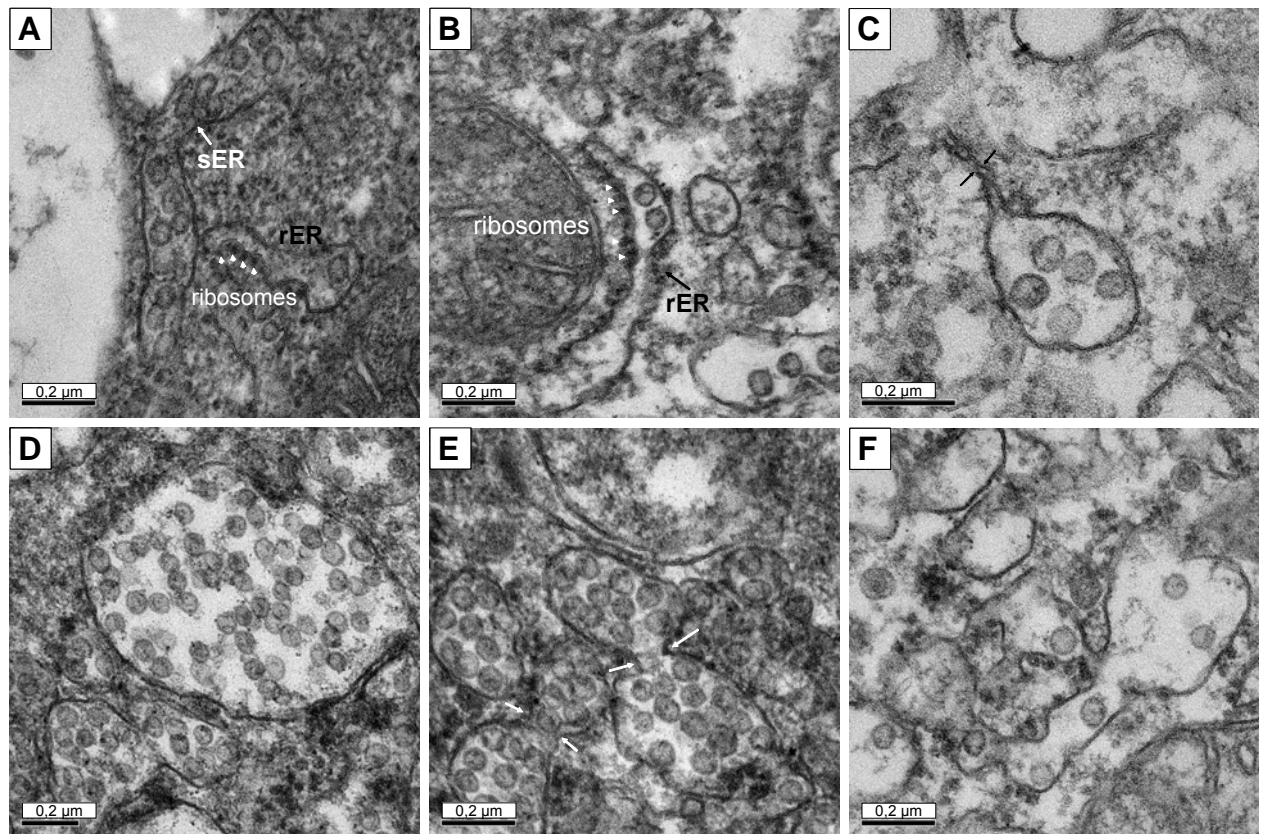


Fig. 18. Different features of VCVs. (A and B) Viral particles were found in the lumen of rER (black arrows) decorated with ribosomes (white arrowheads) and smooth ER (sER, white arrow) structures indicating that VCVs originated from these compartments. (C) VCV still connected through a membrane appendix (black arrows) to the organelle from which it had probably segregated. (D) VCVs are variable in size and shape. (E and F) VCVs probably segregate to form smaller vesicles (red arrows). Bars indicate the size.

VCVs were seen as tubular structures with smooth membranes probably derived from the sER (Fig. 18A, white arrow) or as tubules and vesicles associated with ribosomes indicating that they originated from the rER (Fig. 18A and B, black arrows). Furthermore, VCVs were found either free in the cytosol without any membrane connections (Fig. 18D) or still linked to the endomembranes from which they have

probably segregated (Fig. 18C, black arrows). One other interesting aspect was that these VCVs can further segregate to form smaller vesicles or fuse together to form bigger ones (Fig. 18E and F, white arrows).

III.1.1.5. Budding of viral particles at VCVs

Closer examination of the vesicular content revealed 2 types of particle entities (Fig. 19A and 20 B-D). The vast majority of viral particles consist of membrane-surrounded “empty” spheroids with a mean diameter of about 50 nm representing subviral particles (SVPs). A few vesicles contained in addition ‘filled’ particles with an electron dense nucleocapsid corresponding to virions with a mean diameter of about 60 nm (Fig. 19A and 20 B-D, black arrows). The majority of these vesicles contained only SVPs, whereas only few contained both particles. Pleomorphic filamentous and/or tubular particles characteristic for HBV were not observed. Also, free viral particles in the cytoplasm outside the VCVs were not observed. The overall ultrastructure of the intracellular viral particles is similar, if not identical, to extracellular progeny as reported previously (121). Furthermore, concurrence of both particle types in the same compartment is strongly suggestive for a common morphogenetic pathway.

Ultrastructural analysis of VCVs revealed that not all were spherical in shape. Some vesicles showed slight (Fig. 19A and B, red arrows) or strong inward indentations (Fig. 19C and D, red arrows). These different invaginations presumably represent early, intermediate, and late stages of SVP budding. The later steps of budding such as pinch-off and release of viral particles into the lumen of VCVs were rarely observed (Fig. 19C and D, red arrows), probably due to the fact that they are very fast processes.

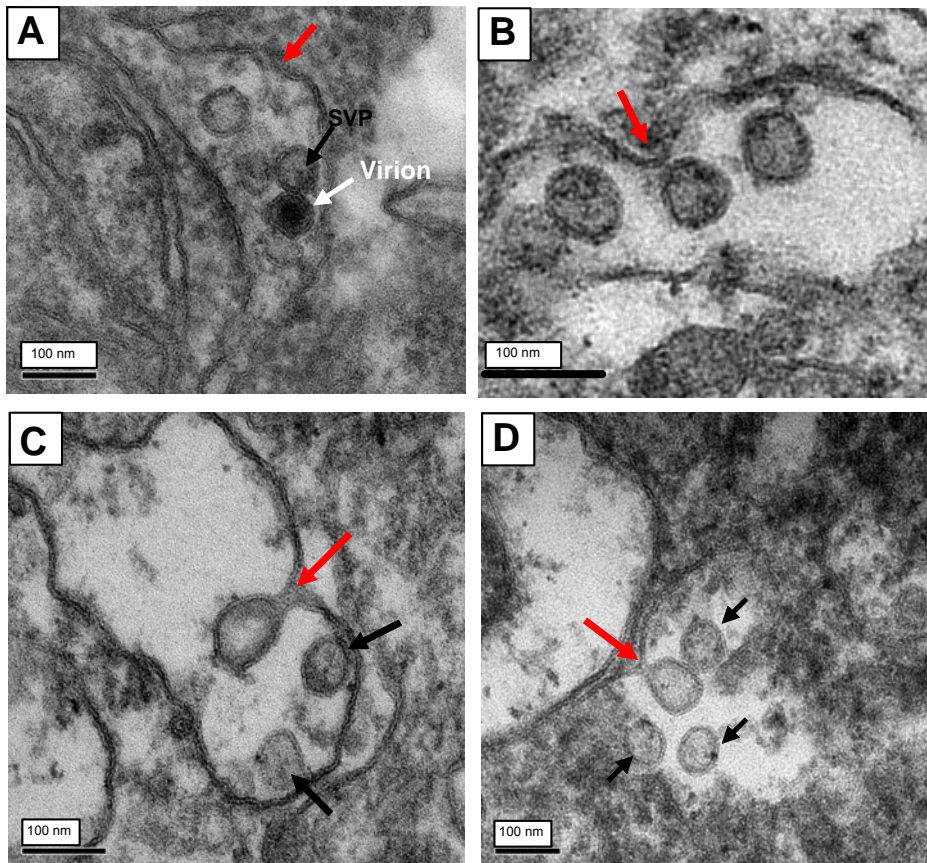


Fig. 19. Ultrastructural features of the budding steps of SVPs. (A) A VCV showing slight membrane indentations (red arrow) as an early step of viral budding. The black arrow indicates a SVP, the white arrow a virion. (B) Advanced membrane indentation (red arrow) indicating an intermediate step of viral morphogenesis/budding. (C and D) Strong membrane indentations (red arrows) in VCVs already containing viral particles (black arrows). Bars indicate the size.

Formation of virions requires maturation of nucleocapsids and their interaction with endomembranes containing envelope proteins. Maturation of nucleocapsids involves reverse transcription of the pgRNA into rcDNA, which results in mature capsids, which presumably are electron denser than immature ones and have an intrinsic membrane affinity (43).

Figure 20 A and B shows particles of different densities measuring 22-27 nm in diameter in the cytoplasm located near VCVs (arrowheads). These particles were identified as nucleocapsids based on their morphology and size compared to those within the virions in the lumen of the VCVs (Fig. 20C and D). These capsids were either distributed randomly in the cytoplasm (Fig 20A, arrowheads) or arranged in ordered structures (Fig. 20B, arrowheads).

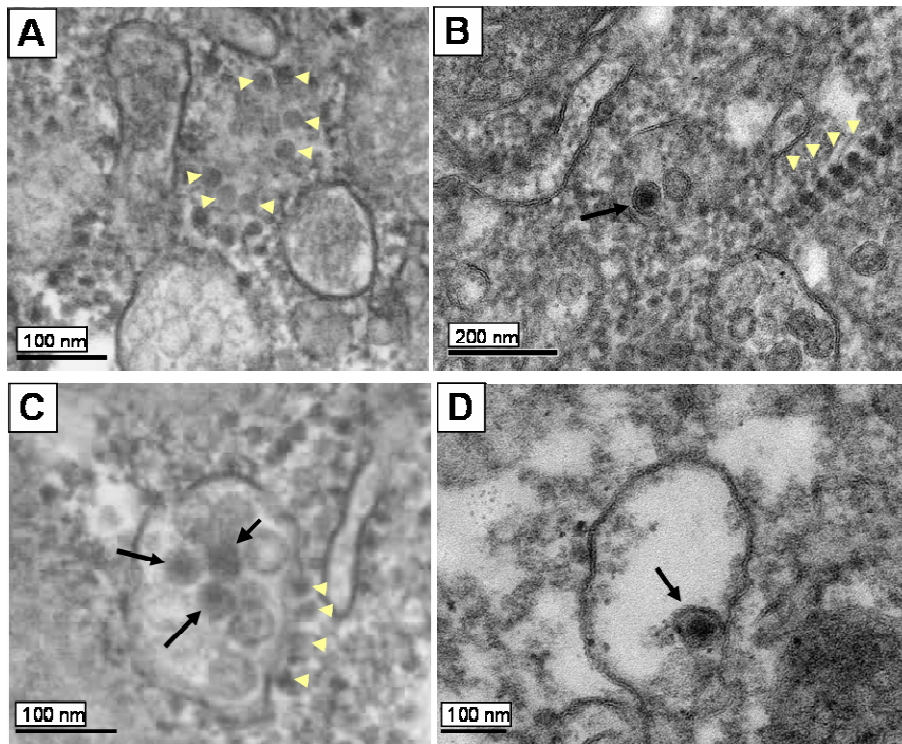


Fig. 20. Ultrastructural features of the budding steps of virions. (A and B) Nucleocapsids with different electron densities (arrowheads) can be observed in close proximity to VCVs. (C) Interaction of nucleocapsids (arrowheads) with VCVs on a vesicle already containing virions (black arrows). (D) A virion in the lumen of a VCV that presumably just budded. Bars indicate the size.

The nucleocapsids were observed both in close proximity and tethered to the membrane of VCVs (Fig. 20C, arrowheads). The interaction of nucleocapsids with vesicular membranes was exclusively observed at membrane indentations and presumably represents the earliest step of virion budding (Fig. 20C, arrowheads). Unfortunately, the later steps of virion budding into the vesicles were not observed under our experimental conditions, although the virion depicted in figure 20 D seems to just budded as it is still in close contact with the vesicular membrane.

Taken together, the data shown above indicate that VCVs are generated via reorganization of endomembranes such as the sER and rER and by segregation from the outer nuclear membrane leading to the formation of vesicles with variable size and shape. These vesicles are platforms for the assembly and budding of both SVPs and virions.

III.1.1.6. DHBV morphogenesis is restricted to hepatocytes *in vivo* and *in vitro*

As already mentioned in the introduction, the liver is composed of different cell types, with hepatocytes being the major cell type (60%). The rest is composed by liver sinusoidal cells, bile ductile epithelial, liver macrophages (Kupffer cells), and others. The morphogenesis of hepatitis B viruses is believed to be restricted to hepatocytes, but there is no ultrastructural evidence for this assumption. To test this in both duck liver biopsies and duck liver cell cultures, non-parenchymal cells were investigated for the presence of viral particles.

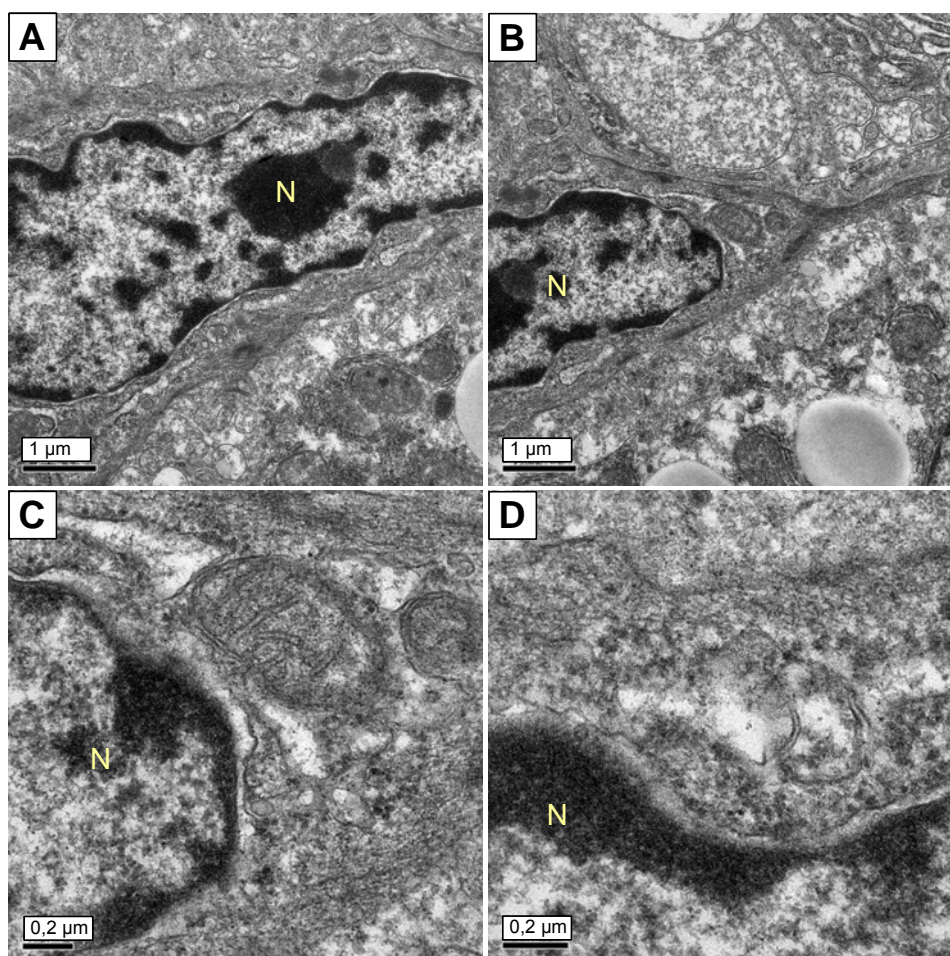


Fig. 21. VCVs are absent in non-parenchymal cells. (A-D) Different magnifications of a non-parenchymal cell, presumably a liver sinusoidal cell, showing the absence of VCVs in this cell type. N, nucleus, bars indicate the size.

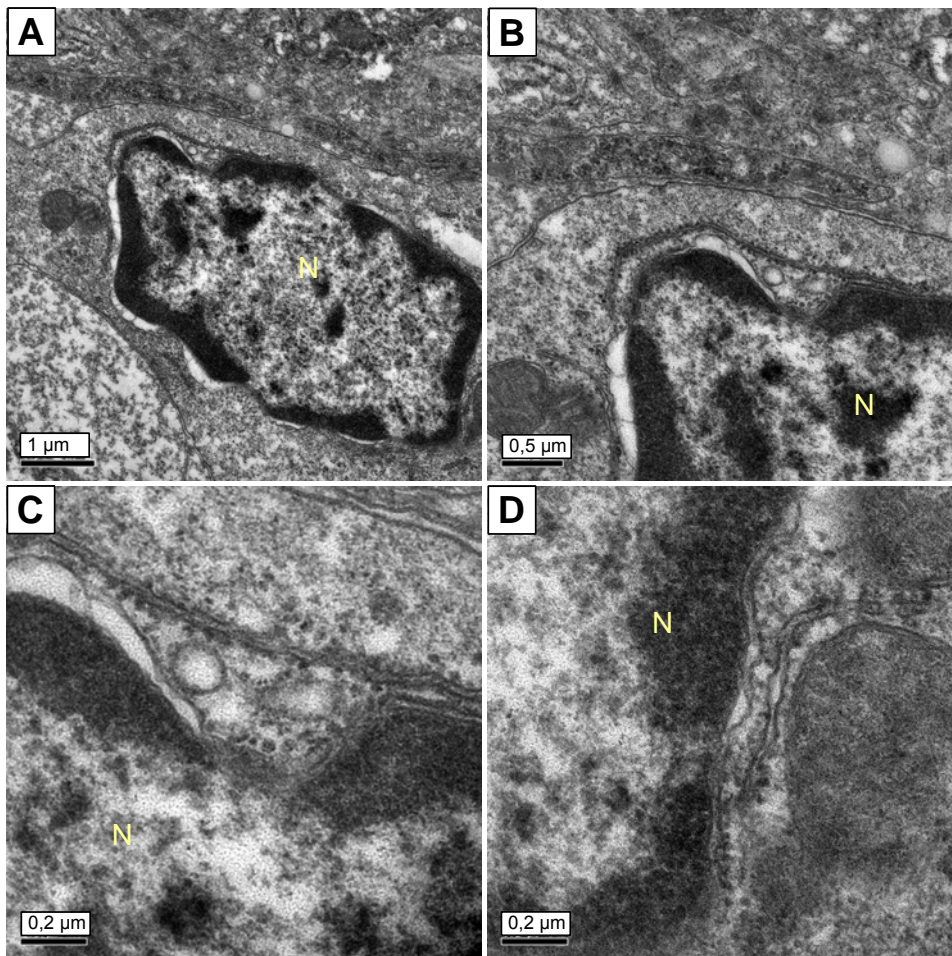


Fig. 22. VCVs are absent in non-parenchymal cells. (A-D) Different magnifications of another non-parenchymal cell, presumably a liver macrophage, showing again the absence of VCVs in this cell type. N, nucleus, bars indicate the size.

Figures 21 and 22 are representative pictures and show two non-parenchymal cells, the first one presumably being a liver sinusoidal endothelial cell, and the second one probably being a liver macrophage as identified by the shape of the nucleus (Fig 21 and 22, respectively). The examination of both cells at higher magnifications revealed the absence of VCVs and any viral particles in these cells indicating that the DHBV morphogenesis is restricted to hepatocytes.

III.1.1.7. DHBV morphogenesis in the chicken hepatoma cell line D2 shows similar morphogenetic features as in duck hepatocytes.

The chicken hepatoma cell line D2 is stably transfected with the complete DHBV genome and produces high amounts of viral particles from chromosomally integrated

overlength DHBV genome and DHBV cccDNA (122). I tested whether the morphogenetic features of DHBV are conserved in this non-permissive cell line which replicates the genome and for which no ultrastructural information is available, and whether the assembly and budding are similar to that observed in PDHs.

Examination of ultrathin sections of D2 cells cultured in the 3D culture system shows similar morphogenetic features as observed in duck hepatocytes *in vitro* and *in vivo*. As shown in figure 23 A and B, the cytoplasm of a D2 cell is filled by a large VCV containing viral particles. The empty spheres are SVPs while the filled ones are virions. At the cytoplasmic face of this VCV, nucleocapsids are tethering to the membrane, which represent probably the early budding event of virions. Remarkable was the presence of few, but very large VCVs in D2 compared to hepatocytes.

Taken together, the principal morphogenetic features of DHBV in D2 cells were similar to those found in hepatocytes *in vitro* and *in vivo*.

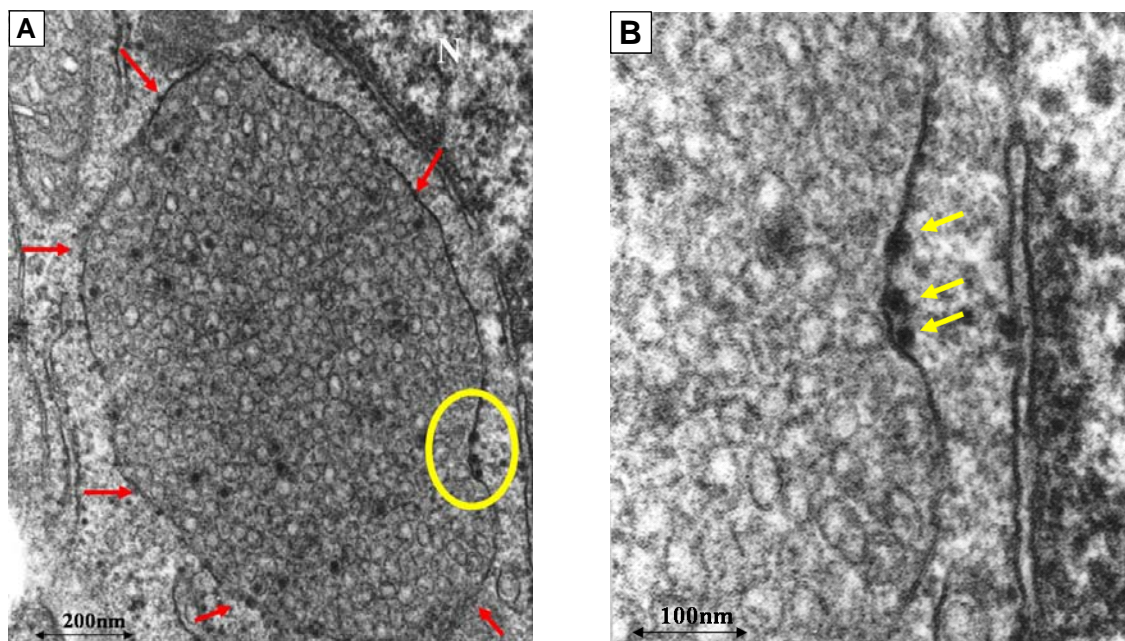


Fig. 23. Ultrastructural features of the chicken hepatoma cells D2. (A) A cytoplasmic section of D2 cells containing a large VCV (red arrows) filled with both SVPs (empty spheres) and virions (full spheres). The oval indicates the magnified area in panel B. (B) Nucleocapsids are tethered to the vesicular membrane. Black arrows indicate the size.

III.1.2. Biochemical and cell biological analyses of the assembly and budding sites of DHBV

III.1.2.1. Subcellular distribution of the viral structural proteins L and core in PDH cultures

The origin and nature of VCVs were characterized by extensive double-immunofluorescence staining analyses of DHBV-infected PDHs using antibodies against marker proteins of different cellular compartments. The staining of L revealed three easily distinguishable patterns: a reticular one which most likely corresponds to non-particulated surface proteins, a vesicular one of different sizes, and a PM-associated one as shown by the visible contour of the cell (Fig. 24A). Core protein was detected as a fine punctuate cytoplasmic staining (Fig. 24B) where it partially colocalized with the L protein (Fig. 24C). A nuclear dot-like staining for core protein was also observed (Fig. 24B) and presumably corresponds to nuclear core bodies previously reported (42).

In the following experiments, the intracellular distribution of L was used as an indicator for virions and SVPs since both viral particle entities were co-compartmentalising to a high degree.

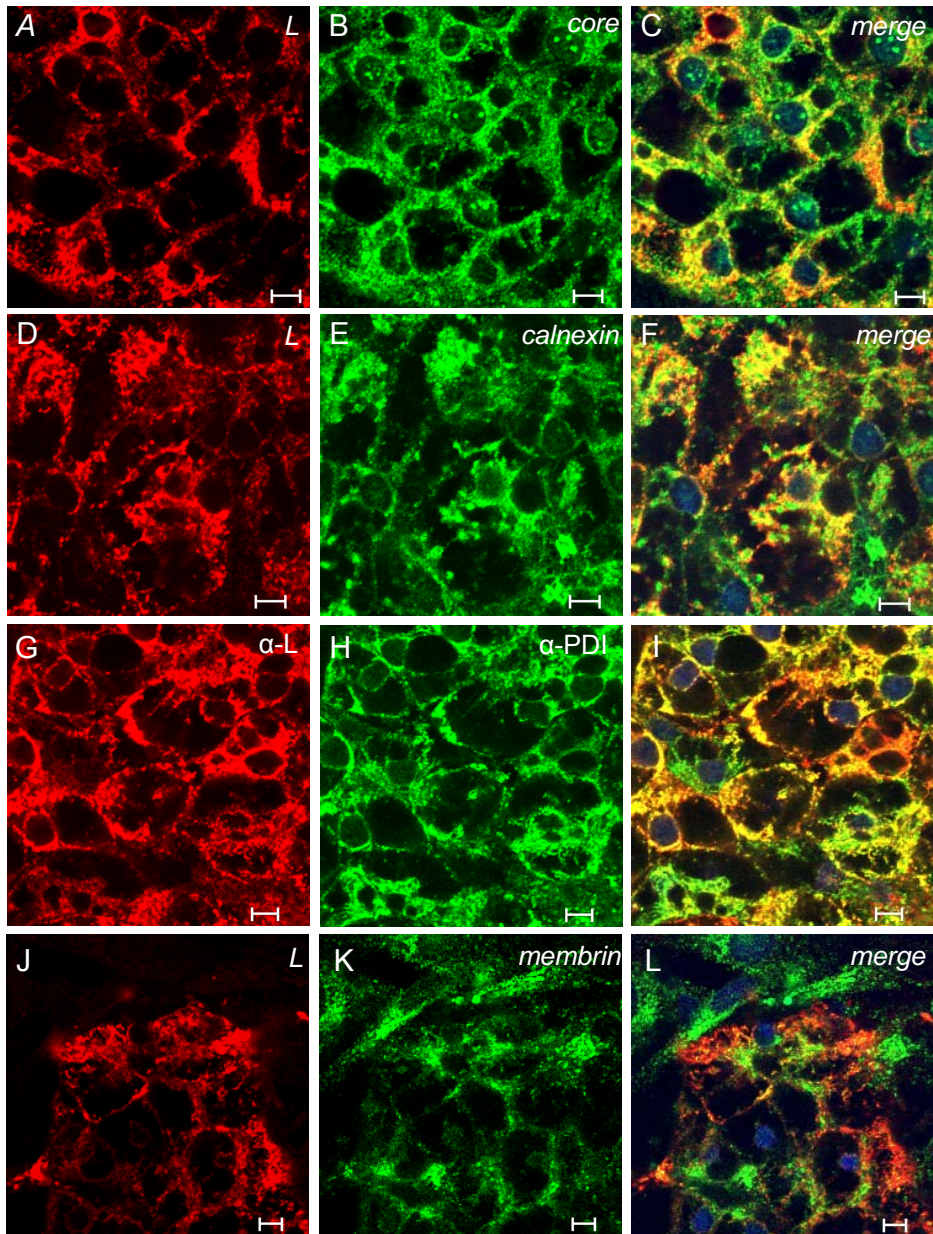


Fig. 24. Intracellular distribution of the viral envelope protein L in correlation to protein markers of organelles in infected PDHs. Cells were indirectly co-immunostained for L (panels A, D, G, J) and the following marker proteins: viral core protein (panel B), calnexin and PDI (panel E and H, respectively) as ER markers, membrin as a marker for the IC (panel K). Merged signals of L and marker proteins together with the counterstained nuclei are shown in the right column. Bars correspond to 5 μ m.

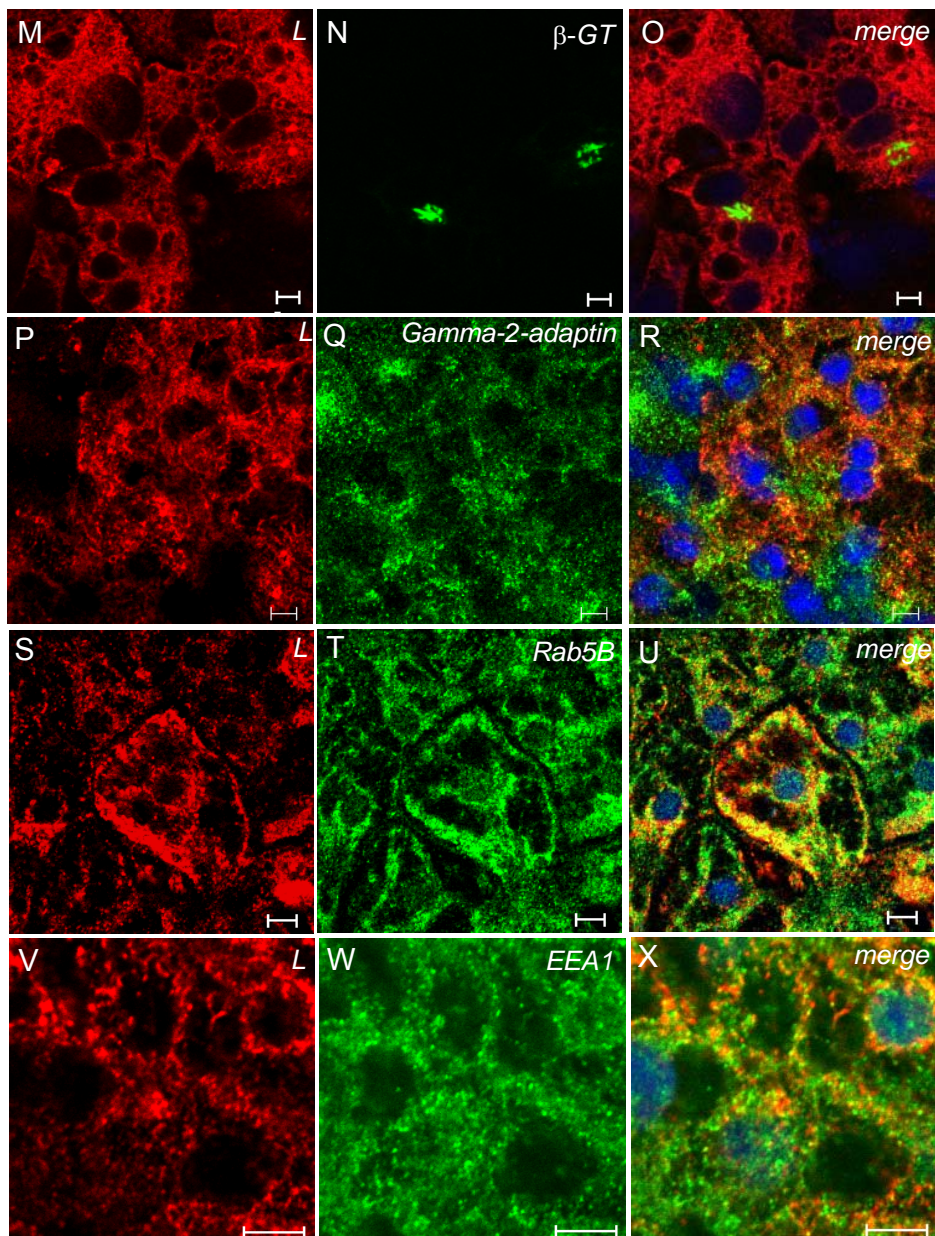


Fig. 24. Intracellular distribution of the viral envelope protein L in correlation to protein markers of organelles in infected PDHs. Cells were indirectly co-immunostained for L (panels M, P S and V) and the following marker proteins: ectopically expressed β -galactosyltransferase (β -GT) and gamma-2-adaptin as markers for the Golgi compartment (panel N and Q, respectively), Rab5B and EEA1 as early endosome markers (panel T and W, respectively). Merged signals of L and marker proteins together with the counterstained nuclei are shown in the right column. Bars correspond to 5 μ m.

Anti-calnexin and anti-protein disulfide isomerase (PDI) antibodies were used to detect marker proteins of the ER. As judged from the immunofluorescence staining, the distribution of L overlapped almost completely with that of the ER (Fig. 24F and I). Membrin, an ER-to-Golgi SNARE which mediates the transport between both compartments, is mainly located in the IC and to a minor extent in the cis-Golgi (123).

This marker protein was found in variously sized and shaped cytoplasmic foci indicative of peripheral, vesicular, and tubular clusters of the IC (Fig. 24K). The membrin staining overlapped only to a minor extent with that of L in infected cells (Fig. 24L). These data imply that VCVs partially overlap with the IC.

The ectopically expressed Golgi marker protein yellow fluorescent protein (YFP)- β -galactosyltransferase, which showed a typical juxtannuclear Golgi distribution (Fig. 24N), did not colocalize with L-positive vesicles (Fig. 24O). To confirm this, a second Golgi marker gamma-2-adaptin (Fig. 24Q) was used. This marker showed two different staining patterns in hepatocytes and non-parenchymal cells. In hepatocytes (cells showing the L stain), it exhibit a vesicular pattern which does mainly not overlap with that of the L protein (Fig. 24R) while in the non-parenchymal cells (cells which are stained for gamma-2-adaptin, but lack the L stain), it showed a typical juxtannuclear Golgi and a vesicular staining. The different pattern of gamma-2-adaptin staining in hepatocytes and non-parenchymal cells could reflect its cell-type specific distribution.

Immunofluorescence analysis of Rab5B (Fig. 24T), a marker protein for early endosomes, revealed a partial colocalization of Rab5B with L-positive vesicles although part of Rab5B-positive structures was devoid of L (Fig. 24U). However, the staining pattern for the early endosomal adaptor protein EEA1 (Fig. 24 W) showed only a minor overlap with L (Fig. 24X). This indicates that L is not enriched in early endosomes, but that a subpopulation of Rab5B is presumably recruited to VCV membranes.

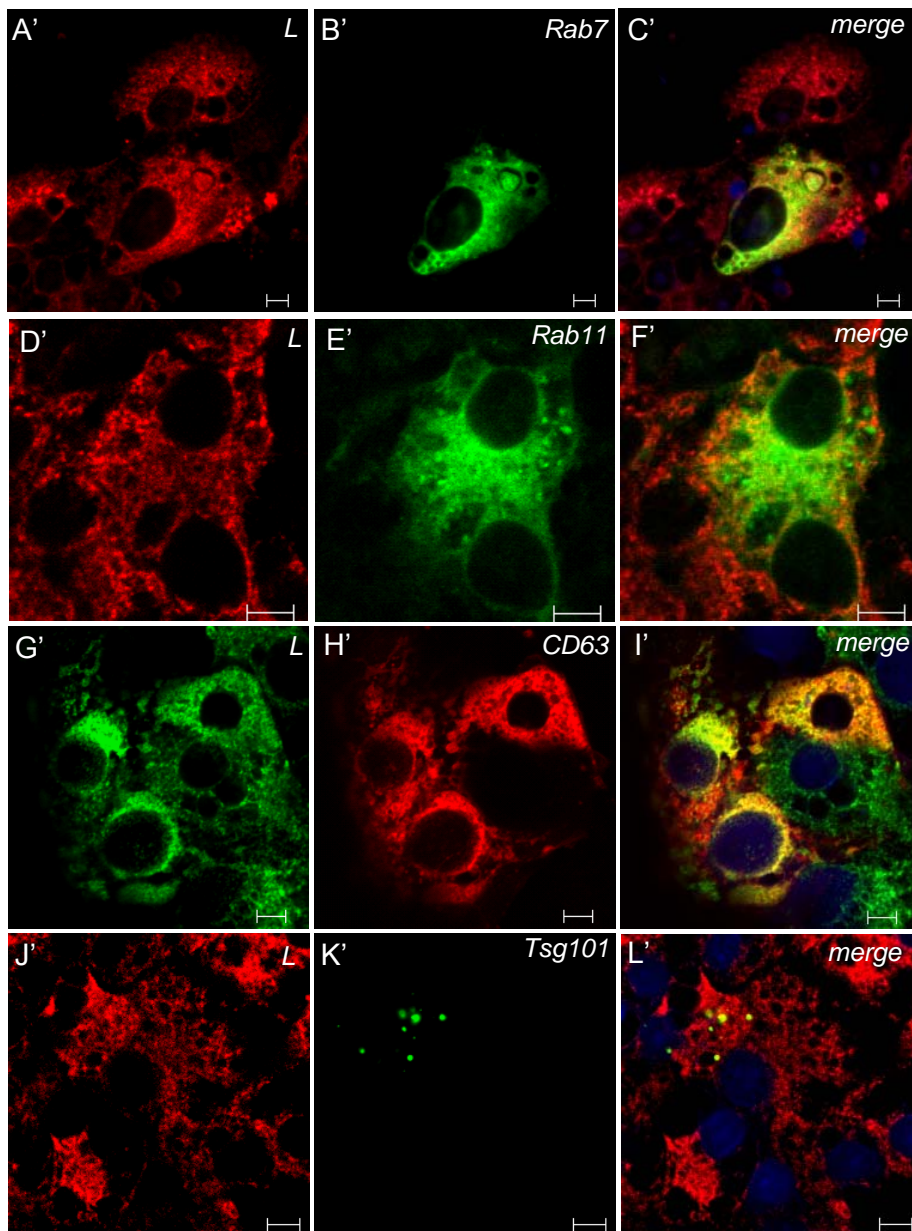


Fig. 24. Intracellular distribution of the viral envelope protein L in correlation to protein markers of organelles in infected PDHs. Cells were transfected with expressions vectors encoding cellular marker proteins tagged with either green fluorescent protein (GFP) or red fluorescent protein (RFP). Three days post-transfection, cells were fixed and indirectly immunostained for L (panels A', D', G', and J'). The following marker proteins were visualized: Rab7-GFP (panel B') as marker for late endosomes, Rab11-GFP (panel E') as marker for recycling endosomes and TGN, CD63-RFP (panel H') as multivesicular bodies (MVBs) marker and finally Tsg101-GFP as a late endosomes/MVBs marker. Merged signals of L and marker proteins together with the counterstained nuclei are shown in the right column. Bars correspond to 5 μ m.

These colocalization studies were supplemented by overexpression of fluorescently tagged compartment-specific marker proteins in DHBV-infected PDHs. To test

whether DHBV exploits endosomal compartment for its budding, colocalization analysis of VCVs with Rab7 (Fig. 24B'), a marker for late endosomes (124), and Rab11 (Fig. 23E'), a marker for both recycling endosomes and TGN, was performed (125). L did not colocalize with any of these marker proteins (Fig.24C' and F'). This indicates that VCVs are distinct from late and recycling endosomes. In addition, Rab7 and Rab11 are not recruited to L-positive cellular compartments. To test whether DHBV assembly involves MVBs, we overexpressed CD63/lamp-3 (Fig. 24H'), a tetraspannin found in late endosomes and MVBs (126, 127), and Tsg101 (Fig. 24K'), a member of the vacuolar protein sorting (VPS) machinery which is known to play an essential role in formation and sorting of cargo into MVBs/late endosomes in a wide range of eukaryotic cells (128, 129). A partial colocalization of L-positive vesicles with CD63, but not with Tsg101-positive compartments (Fig. 24I' and K', respectively), was observed. This indicates that VCVs are distinct from MVBs and that DHBV probably recruits proteins like CD63 of the multivesicular machinery to its assembly and budding sites.

In conclusion, these data show that the majority of L protein in infected cells is located in cytoplasmic vesicular structures positive for the ER marker proteins calnexin and PDI. Only a small fraction of L protein colocalized with the IC and the early endosome marker Rab5B. In addition, VCVs containing L are clearly distinct from late endosomes and more importantly do not colocalize with any of the Golgi marker proteins tested so far. Besides, some cellular proteins like Rab5B and CD63 seem to be specifically recruited to VCVs.

III.1.2.2. Analysis of the subcellular distribution of the viral structural proteins L and core by subcellular fractionation

To confirm and extend the results obtained from the colocalization studies, an independent biochemical approach was used. Therefore, subcellular fractionation assays using a 0-26% iodixanol-based, linear density gradient were performed. These membrane floating experiments involved dounce-homogenates of non-infected and congenitally DHBV-infected livers.

To determine the subcellular distribution of DHBV structural proteins core and L as well as viral DNA, fractions were first analysed by immunoblot and PCR, respectively. L protein was detected in fractions 6-14 with a major peak in fractions 9-11, while

core protein was found in the same fractions with a peak in fractions 7-8 (Fig. 25). PCR analysis of the same fractions showed enrichment of the viral DNA in fractions 6-11 (Fig. 25). Considering the coincidence of the viral structural proteins with viral DNA in the same fractions, we concluded that VCVs harbouring viral cargo were mainly present in fractions 6-12.

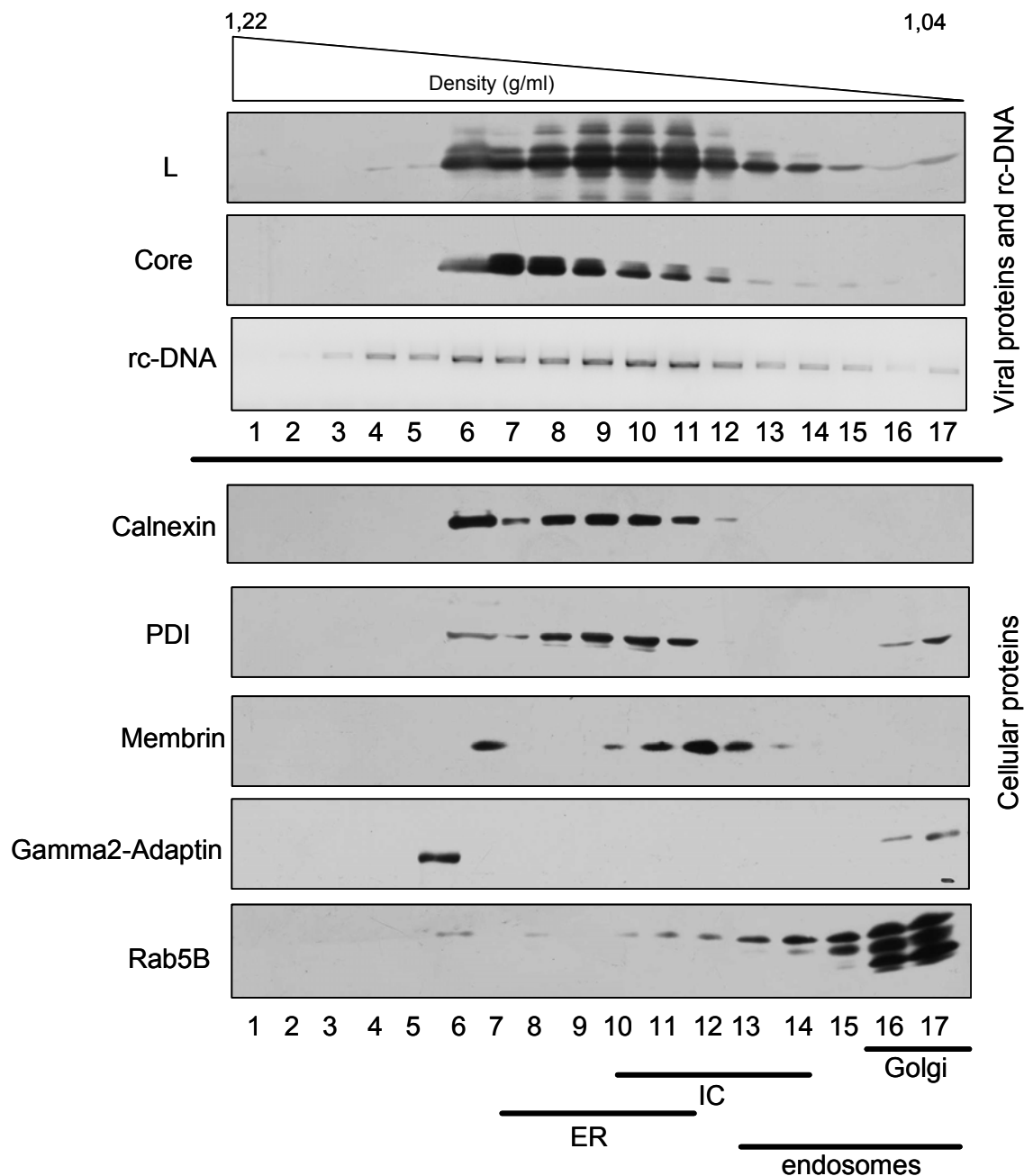


Fig. 25. Analysis of subcellular fractions from DHBV-infected liver for viral and cellular markers. Homogenates of congenitally DHBV-infected PDHs were subfractionated using a 0-26% iodixanol-based linear density gradient and 17 fractions were recovered from bottom to top. Aliquots of each

fraction were separated by 5-20% gradient SDS-PAGE and analyzed for viral L, core protein, and organelle marker proteins calnexin and PDI (ER), membrin (IC), gamma-2-adaptin (TGN), and Rab5B (early endosomes). Viral rcDNA in the same fractions was analyzed by PCR.

Immunoblot analysis of the same fractions for ER marker proteins calnexin and PDI showed that ER was mostly enriched in fractions 6-11, although a small amount of PDI was also observed in the last two fractions 16-17 (Fig. 25). Thus, the ER fractions strongly overlapped with fractions containing viral markers confirming the colocalization studies described above.

Immunoblot analysis of the same fractions for the IC and Golgi marker proteins membrin and gamma-2-adaptin showed that fractions 6 and 10-14 contained the IC as indicated by enrichment of membrin, whereas gamma-2-adaptin and thus the Golgi was present in fractions 6 and 16-17 (Fig. 25). The presence of the Golgi marker in fractions 16 and 17 explained the result that also PDI was present in these last fractions. PDI is known to form a complex with the microsomal triglyceride transfer protein (MTP) mainly in the ER. But in addition, the PDI/MTP complex mediates transfer of membrane triglycerides to nascent apolipoproteins in the ER and then shuttles them to the Golgi, where the assembly of the apolipoprotein particle is completed (130). Thus, PDI in fractions 16 and 17 corresponds to the Golgi-associated protein fraction. Immunoblotting of the subcellular fractions for the early endosomal marker protein Rab5B showed that endosomes were mainly present in the lighter fractions of the gradient (fractions 14-17) (Fig. 25). But a small fraction of Rab5B was also detectable in fractions 6, 8, and 10-13 where it overlapped with that of L. This subpopulation of Rab5B presumably corresponds to the fraction which colocalized with VCVs in the immunofluorescence analysis (Fig. 24U). Fraction 6 was positive for all tested cellular and viral proteins and most likely contains aggregated and thus inseparable material.

Taken together, VCVs were highly and partially enriched in fractions containing ER (microsomes) and the IC, respectively. Furthermore, they were excluded from fractions containing Golgi membranes as shown in figure 26.

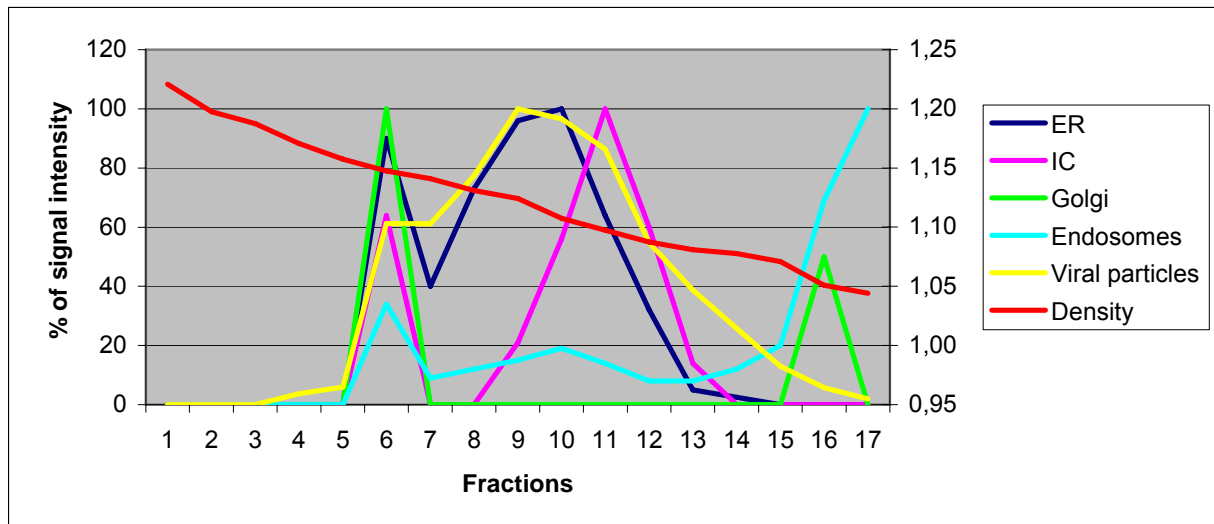


Fig. 26. Distribution of viral and cellular proteins from a congenitally DHBV-infected liver in a linear 0-26% iodixanol gradient. Viral marker proteins (yellow) highly co-fractionated with ER fractions (blue) and partially with fractions containing the IC (pink), but not with Golgi fractions (green). Endosomes (light blue) were partially present in the same fractions as viral particles. The red line shows the density of the gradient in the different fractions. The left axis represent the percentage of signal intensity as quantified by a multiimager. The right axis represents the density (g/ml) of the fractions.

The strong reorganization of the endomembranes in DHBV-infected hepatocytes observed in the ultrastructural analyses compared to non-infected cells (chapter III.1.1.3) may result in a shift of cellular marker proteins in this assay. To test this, a non-infected liver was fractionated parallel to that of a congenitally DHBV-infected liver. The fractions were subjected to immunoblot analysis for the same cellular marker proteins shown above.

The ER marker proteins calnexin and PDI showed a nearly similar distribution in fractions from non-infected liver (fractions 6-11) (Fig. 27) compared to that of DHBV-infected liver (fractions 6-12), with one fraction shift to the lighter fractions in the infected cells. The amount of calnexin in DHBV-infected and non infected cells varied in the different fractions. In non-infected cells, PDI was also detected in fractions 6-11, however the small fraction of PDI found in the lighter fractions (Fig 25, fractions 16 and 17) in infected cells was shifted to the fractions 15-17.

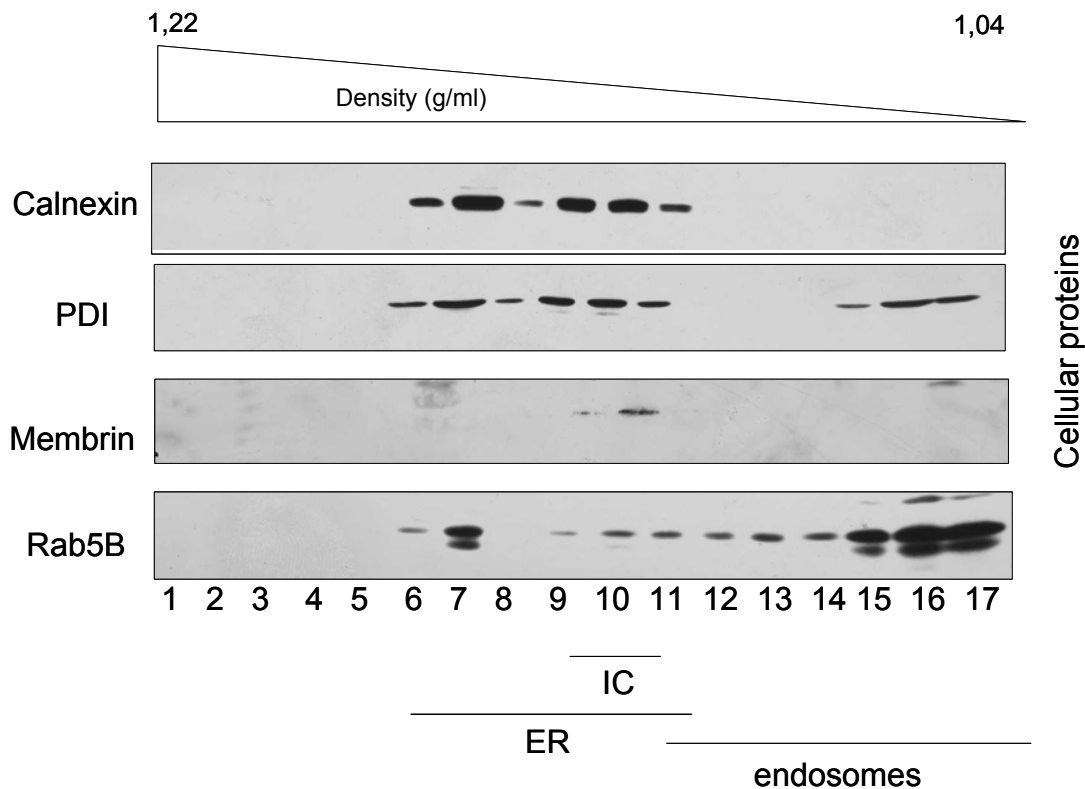


Fig. 27. Analysis of subcellular fractions from non-infected liver for cellular markers. Homogenates of a non-infected liver were subfractionated using a 0-26% iodixanol-based linear density gradient and 17 fractions were recovered from bottom to top. Aliquots of each fraction were separated by 5-20% gradient SDS-PAGE and analyzed for organelle marker proteins calnexin and PDI (ER), membrin (IC), and Rab5B (early endosomes).

In contrast to calnexin and PDI, the IC marker membrin showed a different distribution between infected and non-infected cells. It was found only in fractions 10 and 11 in the non-infected cells while membrin was present in fractions 6 and 10-14 in the infected cells. In addition, membrin was less abundant in the non-infected cells. This could be explained by either lower total protein level in the non-infected liver and thus less membrin. However, this is unlikely since the other marker proteins showed comparable levels between infected and non-infected cells. Alternatively, this may be due to an upregulation of membrin in infected cells induced by DHBV.

The early endosomes marker Rab5B showed a similar distribution in both gradients, with the exception that Rab5b was more enriched in fraction 7 in the non-infected cells.

Unexpectedly, the distribution of the ER in non-infected and DHBV-infected fractions was very similar. This is presumably due to the fact that during dounce

homogenization of non-infected liver, the ER cisternae are fragmented into small vesicles and these fractionate in the same fractions as the ER-derived small vesicles created during the virus assembly and budding processes in the infected cells.

Taken together, these data show that the overall distribution of cellular compartment markers within the gradient are similar between non-infected and DHBV-infected livers with one fraction shift for ER markers (calnexin and PDI) and a less abundance of membrin in non-infected livers.

III.1.2.3. Immunocapture of VCVs

Enrichment of VCVs in microsomal and IC fractions, as shown by the subcellular fractionation, is indicative for an association of VCVs with or their derivation from these cellular compartments. To show a direct association of VCVs with the above mentioned endomembranes, native VCVs were immuno-isolated from the cytoplasm of infected hepatocytes. This assay was based on the assumption that VCVs contain yet non-particulated viral surface proteins in their membranes. If this is true, it should be possible to immunocapture VCVs from dounce homogenates of infected hepatocytes using an envelope-specific antiserum.

To test whether the hypothesis was true, material was immunoprecipitated with anti-L antibodies from a pool of the subcellular fractions 8, 9, 10, and 11 derived from the gradient above and the pellet was examined. To exclude a significant alteration of VCV integrity which may occur during homogenisation, fractionation, and immunoprecipitation procedure, material bound to the protein A-beads was first analysed by TEM.

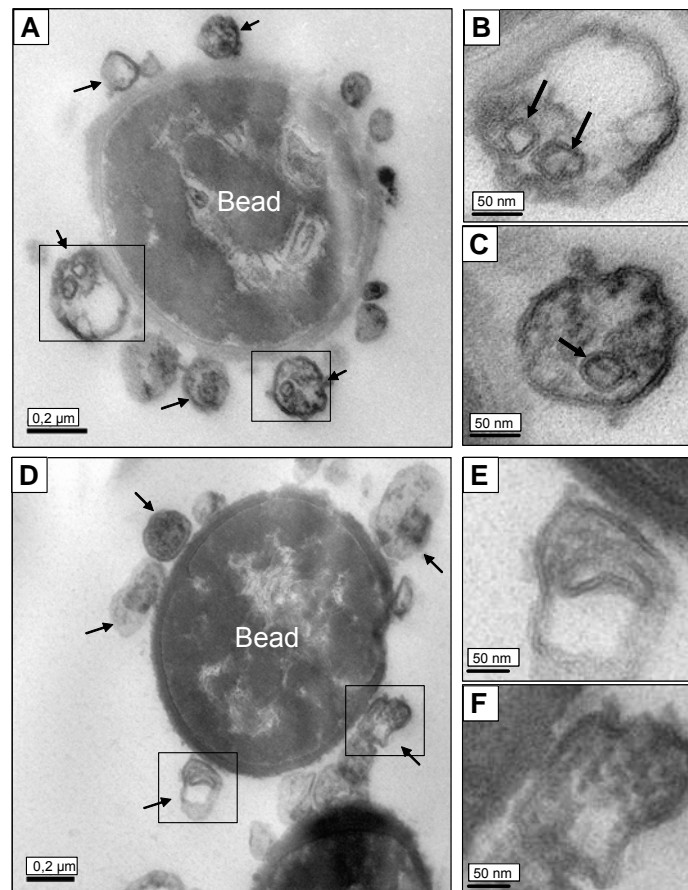


Fig. 28. Ultrastructural analysis of immunoprecipitated VCVs. L-containing cellular vesicles and membranes were immunocaptured from a pool of fractions 8, 9, 10, and 11 after subcellular fractionation of DHBV-infected (A-C) and non-infected (D-E) livers shown above. Samples were fixed by glutaraldehyde and subjected to transmission electron microscopical analysis. (A) Pansorbin bead decorated with vesicular structures (black arrows). (B and C) Higher magnification of VCVs harboring SVPs (black arrows). (D) Pansorbin bead associated with vesicles (black arrows). (E and F) Higher magnification of these vesicles devoid of SVPs. Bars indicate the size.

As shown in figure 28A, it was feasible to isolate native and intact vesicles of different size from the fraction pool (8, 9, 10, 11) (arrows). As expected, VCVs harboured viral particles (Fig. 28B and C, arrows). Such vesicles were not immunoprecipitated from the same fraction pool (8, 9, 10 and 11) of non-infected cells although a non specific binding of few vesicles to the bead was also observed indicating that either the antibody or the beads have a non-specific binding affinity for some cellular vesicles. These data also imply that VCV membranes indeed contain non-particulated, cytosolically accessible envelope proteins allowing their immuno-isolation.

After showing that the isolation of VCVs with an anti-L antibody was possible, a second assay was performed. This time, DHBV-infected PDHs were used,

homogenized by dounce homogenization, and the homogenates were subjected to immunoprecipitation using anti-L or a control antibody (rabbit anti mouse IgG). Then the immunoprecipitates (IP) were analysed for the presence of cellular marker proteins such as calnexin, membrin, Rab5B, and others by immunoblotting.

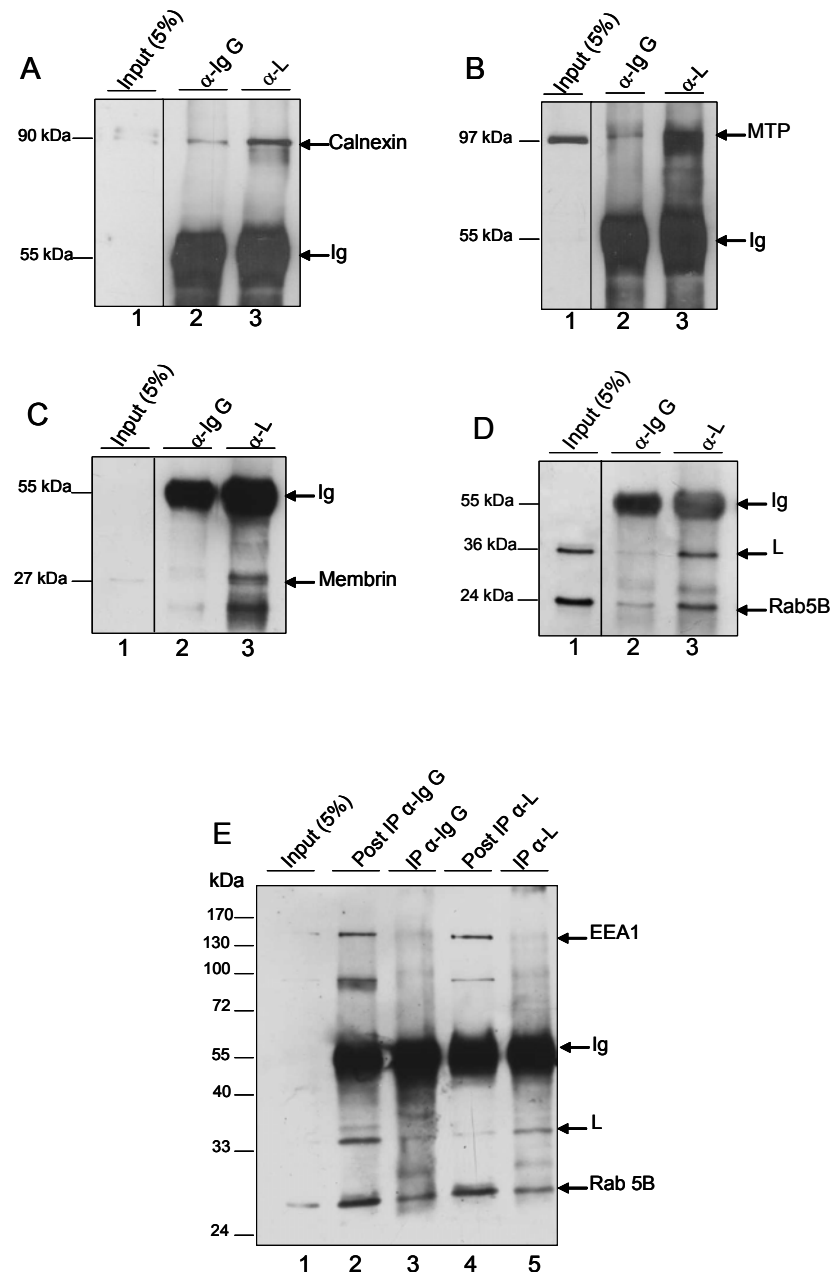


Fig. 29. Immunocapture of VCVs. (A-E) VCVs have mixed properties of ER, IC, and early endosomes. VCVs were immunocaptured from cell homogenates of infected PDHs using an L-specific antiserum (α -L) or non-related antiserum (α -IgG). The subsequent immunoblot analysis identified calnexin, MTP, membrin, and Rab5B (D-G, lane 3) as with viral L protein co-immunoprecipitating cellular proteins in comparison to the controls (D-G, lane 2). (F) EEA1 was not co-immoprecipitated

with Rab5B and viral L protein (F, lane 5), it remains in the post immunoprecipitated supernatant (post IP) (F, lane 4).

The IP was enriched for calnexin, MTP, membrin, and Rab5B (Fig. 29 D-G, lane 3) compared to the IgG control (Fig. 29 D-G, lane 2). To test whether the association of VCVs with Rab5B was specific and significant, we analysed whether EEA1 was also associated with VCVs. As predicted from the immunofluorescence experiments, EEA1 was absent in the IP and was exclusively detected in the post-IP supernatant (Fig. 29E). This underscores the specificity and selectivity of Rab5B recruitment to VCV membranes.

In summary, VCVs were isolated from cell homogenates of infected hepatocytes by IP using an L-specific antiserum. These IPs were enriched for calnexin, MTP, membrin, and Rab5B, but not for EEA1. The heterogeneous mixture of proteins, which are known to be marker proteins for different subcellular compartments, indicates that VCVs are generated during virus replication through the reorganization of ER membranes and recruitment of specific cellular proteins.

III.1.2.4. VCVs are dynamic structures undergoing homo- and heterotypic fusion and fission

VCVs have a size of 100-800 nm in diameter and harbour mixed properties of ER, IC, and endosomes (early and MVBs). The size heterogeneity could be the result of homo- and heterotypic fusion between VCVs or between VCVs and other membrane compartments leading to the formation of bigger vesicles. On the other hand it could also be the result of fission events of big VCVs which form smaller ones. The heterogeneity in composition could be explained by the heterotypic fusion of VCVs with other cellular vesicles leading to the formation of such mixed structures. An alternative explanation would be the specific recruitment of certain proteins to VCVs.

Ultrastructural evidences for homo- and heterotypic fusion and fission

To confirm or reject the above proposed hypotheses, a careful examination of VCVs for any sign of fusion and segregation was performed.

As shown in figure 30 A-D, different features suggestive for fusion and fission events were observed. Some VCVs were found in close contact with other VCVs or other

vesicles (Fig. 30A and B). Other VCVs were seen in a state that could either be interpreted as an ongoing fusion or fission (Fig. 30C and D). Moreover, VCVs were observed in a state which could represent the early step of a fusion or a late step of a segregation event (Fig. 30E and F).

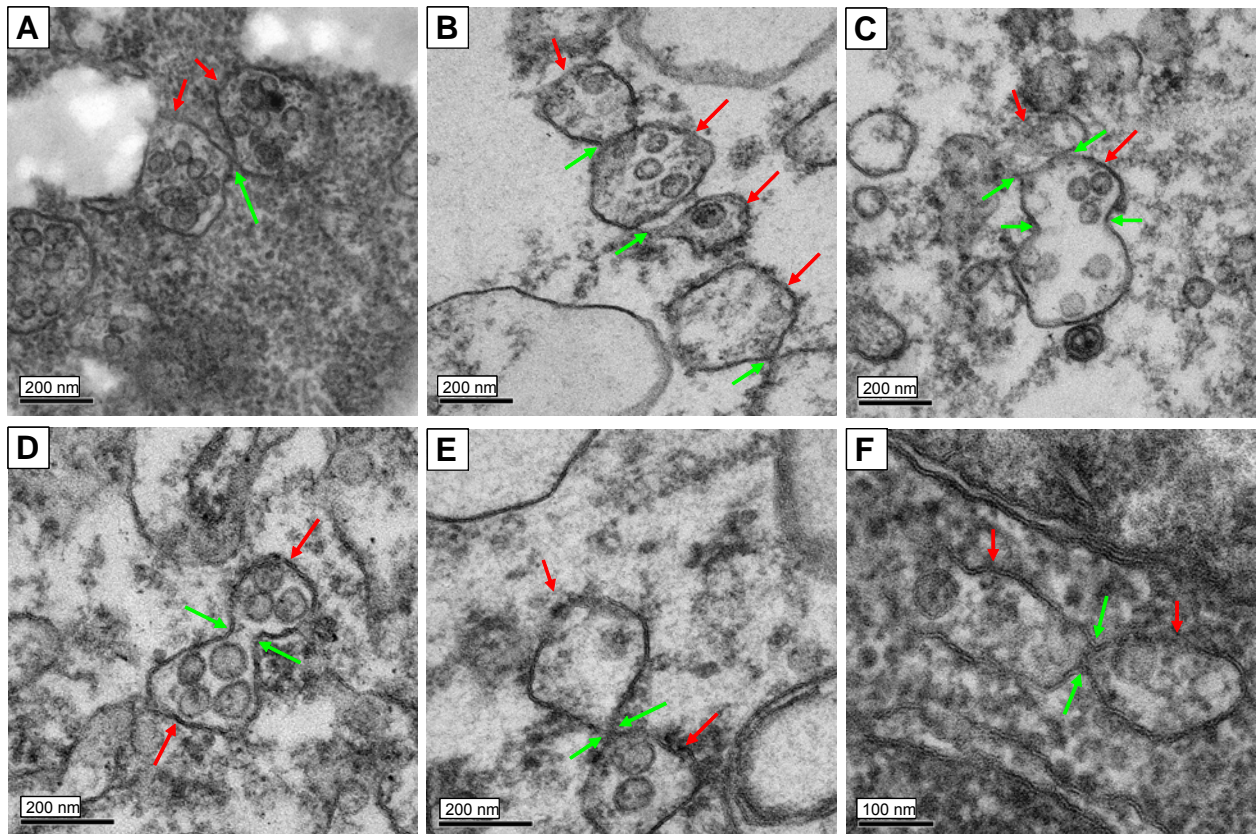


Fig. 30. VCVs undergo homo- and/or heterotypic fusion as well as fission. (A and B) VCVs (red arrows) are in close contact to other VCVs or vesicles (green arrows). (C and D) show VCVs (red arrows) that are either fusing to form a bigger vesicle or to segregate to form smaller ones (green arrows). (E and F) show either the fusion or the fission between a VCV and another vesicle (green arrows). Bars indicate the size.

The ultrastructural analysis provided clear evidence for possible fusion and fission between VCVs and other vesicles indicating that they are dynamic structures interacting with each other or with other cellular membrane compartments. However, it was not possible to discriminate between both events, since the EM pictures only the steady state, while fusion and fission are very dynamic events. In order to overcome the limitation of the EM, a second approach involving life cell imaging was used.

III.1.2.4. Life cell imaging to visualize the dynamic of VCVs

Life cell imaging offers the advantage to visualize the dynamics of cellular processes. A prerequisite for such analysis is a fluorescent reporter that marks the protein or compartment of interest. Commonly used for such investigation are fluorescent proteins, like GFP, which are fused to the protein of interest. The GFP-tag is specific, sensitive, relative photostable and in many cases does not perturb the normal trafficking and the function of the protein.

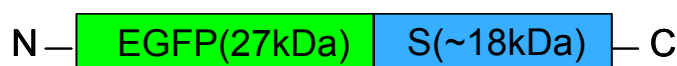
Cloning and characterization of the GFP-labelled reporter protein constructs

To visualize the dynamic of VCVs, the small surface protein of DHBV was fused to GFP. The S protein was chosen because this protein is an essential and abundant constituent of the viral envelope as compared to the large protein L (80 and 20%, respectively). Thus, the probability that GFP-tagged S proteins will be incorporated into the viral envelope is higher. Furthermore, the L protein has a dual topology, in about 50% of the molecules, the preS-domain of the L-protein is exposed to the inside of the virus and 50% outside of the virus. Thus, N-terminal fusion of GFP to L could interfere with the virus envelopment due to sterical hinderance. For the S protein, it is not known whether it also exhibits a dual topology. To reduce any problems related to this, the GFP was fused either to the N- or C-terminus of S in order to see which form will be compatible to the envelopment and which protein exhibits a more authentic subcellular localization compared with the wild type S protein.

Constructs encoding EGFP-S and S-EGFP are schematically shown in figure 31.



S-EGFP~45 kDa



EGFP-S~45 kDa

Fig. 31. Schematic representation of S-EGFP-fusion constructs. Upper and lower panels show the fusion proteins S-EGFP and EGFP-S, respectively, formed by the viral surface protein S (18 kDa) which is in frame with the EGFP (27 kDa) resulting in a fusion protein of about 45 kDa. N and C indicate the N- and C- termini of the proteins, respectively.

Both fusion constructs were transiently expressed in the chicken hepatoma cell line LMH. Cells were harvested 3 days later and analysed by immunoblotting using GFP- and S-specific antisera. As shown in figure 32, the EGFP-S and S-EGFP were expressed as about 45-kDa protein as predicted for the fusion protein.

However, in addition to the 45-kDa protein, a further protein was expressed by the S-EGFP construct as shown by the GFP-specific immunoblot (Fig 32 lane 1). A tiny band corresponding to the fusion protein (upper band) and a stronger band corresponding to EGFP as compared to the EGFP protein in EGFP-transfected control cells (Fig. 32, lane 6). This could be due to a preferential translation initiation at the EGFP start codon rather than at the S start codon leading to the synthesis of EGFP.

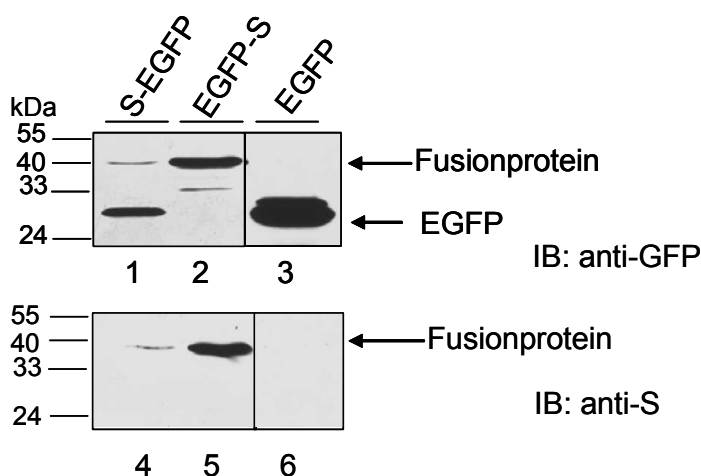


Fig. 32. The fusion proteins EGFP-S and EGFP-S are both expressed in LMH cells. LMH cells were transfected with vectors encoding either S-EGFP, EGFP-S or with EGFP alone. Cells were lysed 3 days later and subjected to immunoblot analysis using anti-GFP or anti-S antibodies (upper and lower panel, respectively). IB means immunoblot.

Next, the subcellular distribution of both fusion proteins were compared to that of the wild type S protein. Therefore, LMH cells were transfected with plasmids encoding S-EGFP, EGFP-S or with a construct expressing the duck surface protein S (pcDNA3-

duck S). Two days post transfection, cells were fixed and stained for S by indirect immunofluorescence staining. As shown in figure 33, the S protein was distributed throughout the cytoplasm in small punctuate structures (Fig. 33 panel A), the S-EGFP yielded big “dots” in the perinuclear region (Fig. 33, panel B), presumably corresponding to aggregates of mis-folded S-EGFP destined for degradation rather than free EGFP which normally shows a diffuse pattern. The EGFP-S protein was found in different sized punctuate structures distributed throughout the cytoplasm (Fig. 33, panel C).

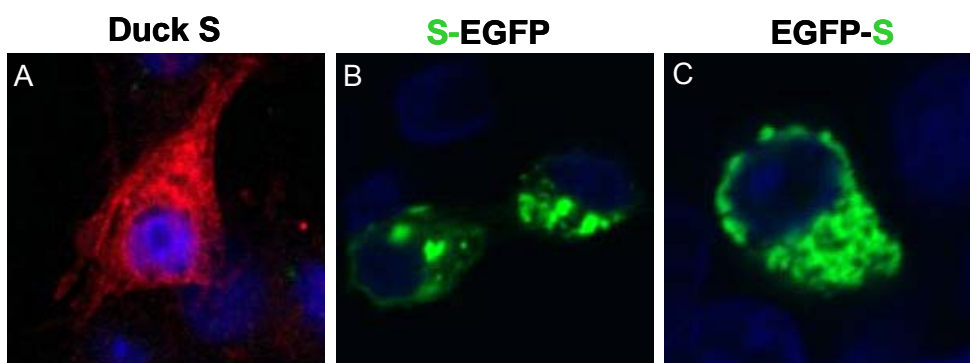


Fig. 33. EGFP-S shows a subcellular distribution similar to the wild type S protein. LMH cells were transfected with constructs expressing S-EGFP, EGFP-S or duck S-protein. Cells were fixed 2 days later with ice-cold methanol-aceton (1:1) for 10 min. Cells transfected with the duck-S construct were stained for S by indirect immunofluorescence.

From the immunoblot and immunofluorescence analyses above, it was concluded that the EGFP-S construct encodes a fusion protein which behaves more authentic as compared to the wild type duck S protein and thus was used in all further experiments.

EGFP-S as reporter for VCVs

Since the goal of this approach was to follow the dynamics of VCVs using the EGFP-S protein as a reporter for viral particles and VCVs, the next step was to test whether EGFP-S authentically reports the assembly and budding sites of DHBV. Therefore, LMH cells were co-transfected with EGFP-S and pGEM-D10G, a construct coding for non tagged surface proteins L and S. This construct allows the formation of viral

particles and induces the generation of VCVs. Two days post transfection, cells were fixed and stained for the surface protein L to visualize the VCVs.

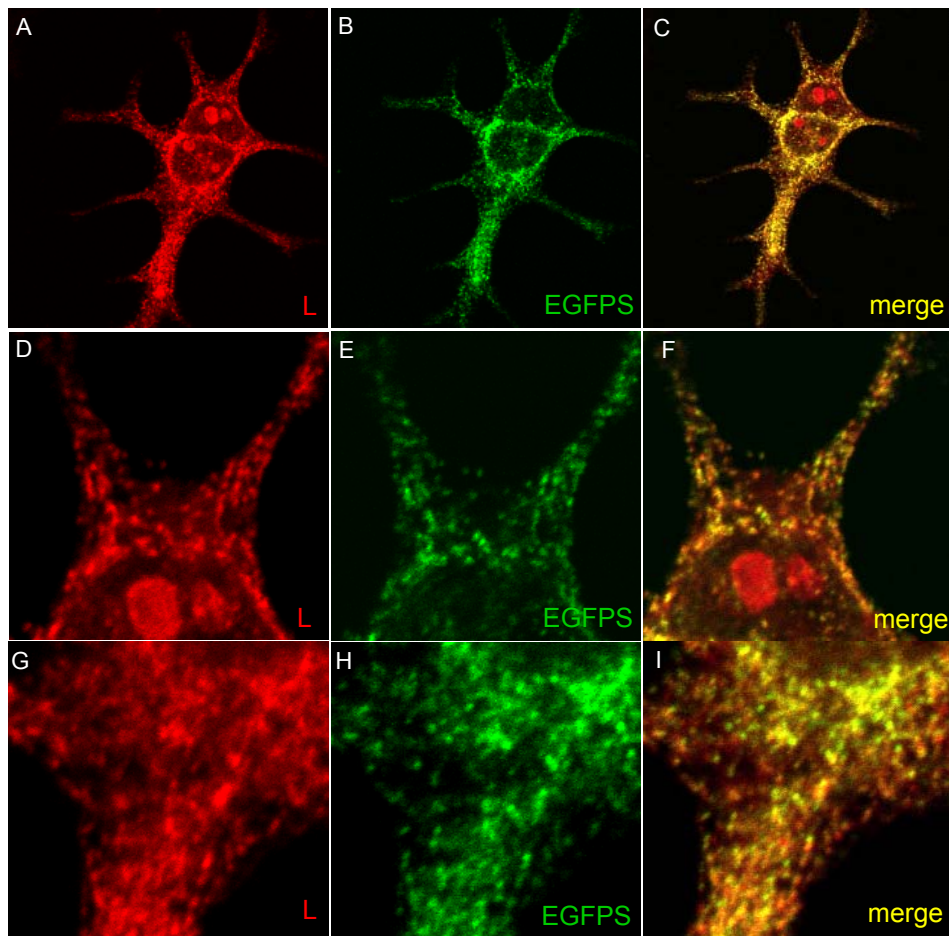


Fig. 34. A large fraction of EGFP-S colocalizes with VCVs. LMH cells were co-transfected with EGFP-S and pGEM-D10G which encodes both wild type proteins S and L. Cells were fixed 2 d post transfection with ice-cold methanol-acetone (1:1) for 10 min and stained for the surface protein L (red signals).

As shown in figure 34, both EGFP-S fluorescence (panels A, D, and G) and the L stain (panels B, E, and H) strongly colocalize and were detected in vesicular structures of different size, distributed throughout the cytoplasm (panels C, F, and I). A small fraction of VCVs was devoid of EGFP-S protein and vice versa. This strong colocalization of EGFP-S with L indicates that the fusion protein EGFP-S could be used as a reporter for life cell imaging of VCVs.

Live cell imaging and 3-dimensional (3D) reconstructions

To analyse the dynamics of VCVs in live cells, EGFP-S and surface proteins S and L were co-expressed in LMH cells. In addition, a construct coding for CD82-tagged to red fluorescent protein (RFP), a tetraspannin known to localize to internal vesicles and to the PM, was cotransfected in order to label the cell surface. Two days post transfection, cells were analysed by CLSM. Z-stacks records were performed every 30 sec over 30 min, the 3D reconstructions and the orthogonal projections were made using “Imaris v.4.1.3”.

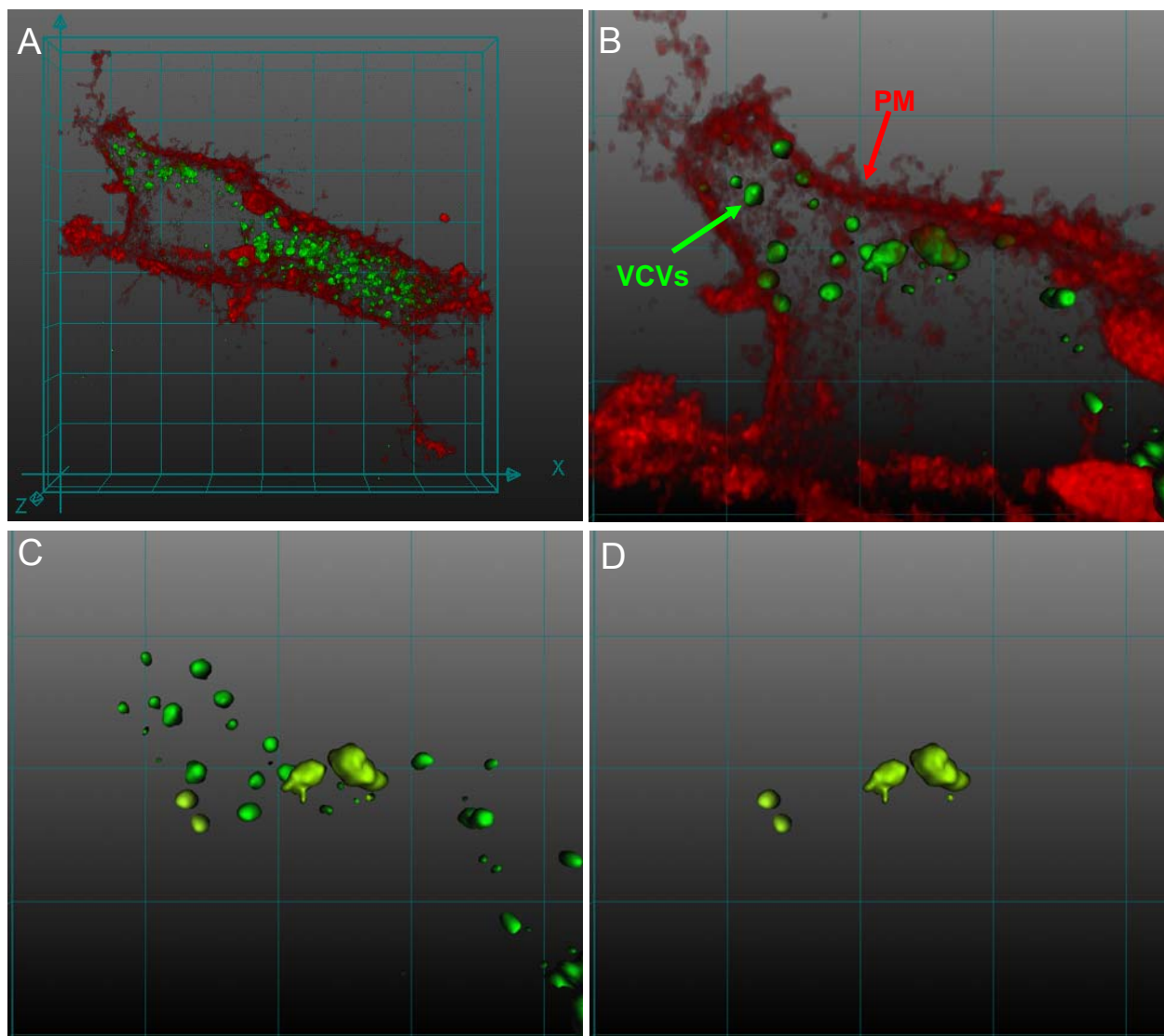


Fig. 35. 3D reconstructions of VCVs in live cells. EGFP-S, wild type surface proteins S and L and CD82-RFP were expressed in LMH cells. Two days later, cells were analysed by confocal microscopy and (3D) records over time were acquired. The 3D records were reconstructed using Imaris software. Panel A shows such a 3D reconstruction of a cell, in red is the plasma membrane shown, in green are

the VCVs visualized via the fusion protein EGFP-S. B shows a magnification of a part of the cell shown in (A). (C) Shows VCVs after subtraction of the red signals to better visualize the vesicles. (D) Only selected VCVs are shown. Distance between the ticks in the grid corresponds to 5 μm .

Figure 35 A shows such a reconstruction, the PM is labelled in red and EGFP-S positive membranes are shown in green. The labelled membranes were different in size and shape and heterogeneously distributed all over the cytoplasm (Fig. 35 panel A and B). Near the nucleus, big and compact structures were concentrated corresponding presumably to the ER where the protein is synthesised. Towards the periphery of the cell, the EGFP-S positive membranes become smaller and less compact. These are the ones which colocalize with L-positive vesicles, as shown above in figure 34 and thus will be the reporters for VCVs.

In order to reduce the complexity and concentrate on individual VCVs, the PM staining as well as some of the VCVs were digitally subtracted using Imaris software (Fig. 35 panel C and D). The next figure shows the 3D reconstruction of individual VCVs recorded over 25min 30 sec.

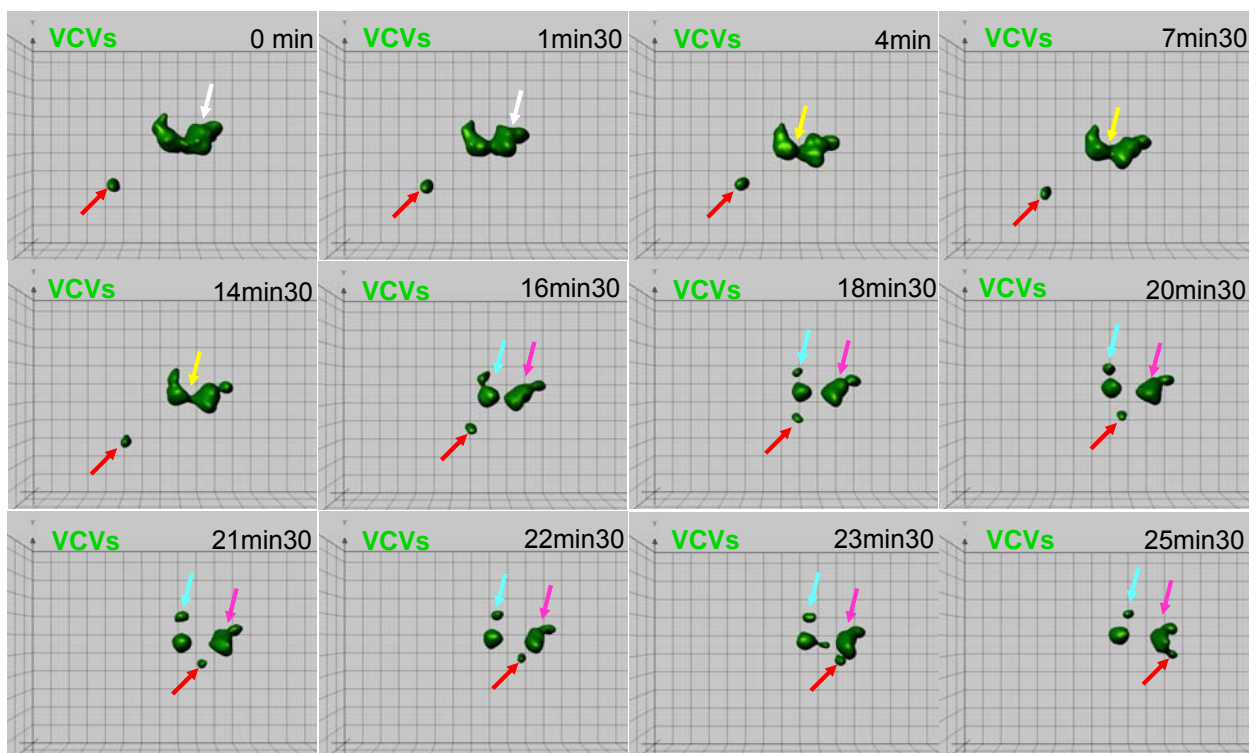


Fig.36. VCVs are dynamic structures undergoing homotypic fusion and fission as revealed by life cell imaging. 3D reconstructions show that VCVs can fuse with each other and that small VCVs can be generated by fission from bigger VCVs. Distance between the ticks in the grid corresponds to 1 μm .

At time point 0 min (corresponding to the beginning of the records), 2 VCVs are observed, a small one indicated by the red arrow and a bigger one indicated by the white arrow. 4 min later and up to 14 min 30, the shape of this VCV changes and shows constrictions in the middle (indicated by the yellow arrow) indicative for a segregation, 2 min later the fission occurred and two VCVs are generated from the previous one (indicated now by the blue and pink arrows). The VCV indicated by the blue arrow further segregate at time point 18 min 30 into 2 vesicles and no further dynamics of these vesicles was observed until the end of the records.

The VCV indicated by the red arrow started to move at time point 16 min 30 towards the VCV indicated in pink with an approximate speed of 35 nm/s, reaches this vesicle at time point 23 min 30 as shown by the close contact of both and fuse with it 2 min later. This analysis clearly shows that VCVs are dynamic structures moving, fusing with and segregating from each other.

In conclusion, the live cell imaging data revealed that VCVs are indeed dynamic structures of different size and shape that are presumably regulated by homotypic fusion and fission between VCVs. These data clearly corroborate the aforementioned ultrastructural findings.

III.2. Secretion of DHBV

III.2.1. Secretion of DHBV is Golgi-independent

The Golgi apparatus and the trans-Golgi network (TGN) play central role in the control of constitutive and regulated secretion. Cellular proteins destined to be secreted or to be incorporated into either the plasma membrane or other subcellular organelles, pass through the Golgi, are modified and reach the TGN where they are sorted and then delivered to their final destination via transport vesicles.

Many viruses which assemble and bud at membranes of the secretory pathway pass through the Golgi to be modified into mature and infectious particles. For hepatitis B viruses it is assumed that the progeny virus is secreted through the Golgi (93). However, there are no clear data on this issue. To test the involvement of the Golgi in DHBV secretion, ultrastructural as well as biochemical investigations were performed.

III.2.1.1. Viral particles are absent from the Golgi

VCVs were identified as the assembly and budding sites of DHBV as described in section III.1, and viral particles were found to be largely excluded from the Golgi apparatus as shown by both colocalization studies and subcellular fractionation. To further confirm these findings, concerning the potential non-involvement in DHBV morphogenesis, ultrathin sections from DHBV-infected PDHs cultures and liver biopsies were carefully analysed for the presence of viral particles in the Golgi apparatus.

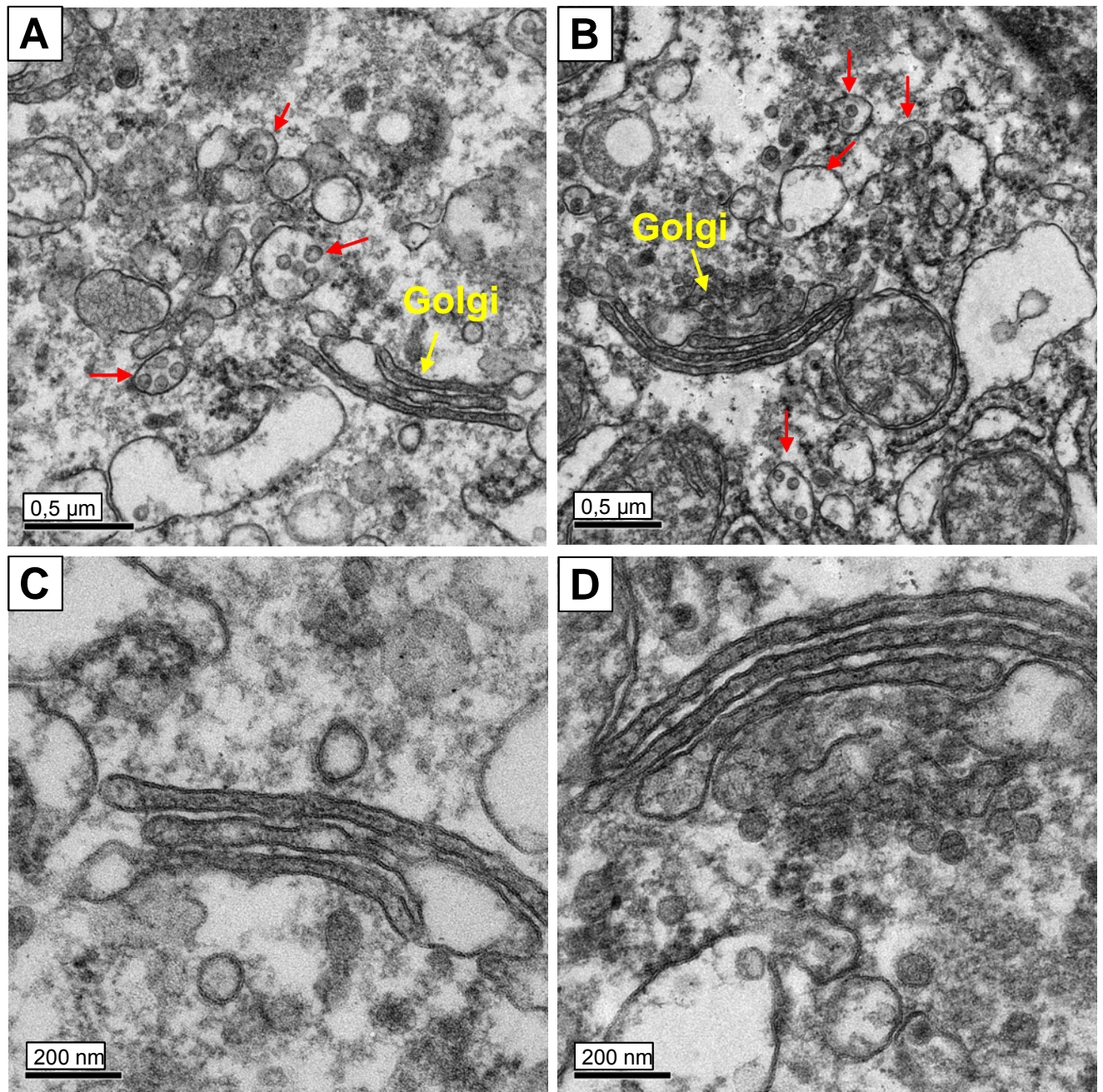


Fig. 37. Viral particles were absent from the Golgi. (A and B) A section of the cytoplasm of 2 different DHBV-infected hepatocytes showing VCVs (red arrows) in proximity of the Golgi (yellow arrow). (C and D) Magnifications from A and B, respectively, showing the Golgi and transport vesicles. No viral particles were found within the Golgi nor were VCVs seen to bud from the Golgi. Bars indicate the size.

VCVs were often seen in close proximity to the Golgi (Fig. 37 and 38). The localization of VCVs near the Golgi reflects presumably the minor overlap between L-positive vesicles and the ectopically expressed Golgi marker YFP-β-

galactosyltransferase observed by immunofluorescence microscopy (Fig. 24 panel N). However, no VCVs were seen budding from or connected to the Golgi stacks. The examination of the lumen of the Golgi itself at high magnifications (Fig. 37 C and D) revealed no viral particles within this organelle. Consistent with this finding, the overall ultrastructural appearance of the Golgi apparatus in infected hepatocytes was comparable to that in non-infected hepatocytes indicating that the Golgi is not reorganized during virus morphogenesis in contrast to the ER.

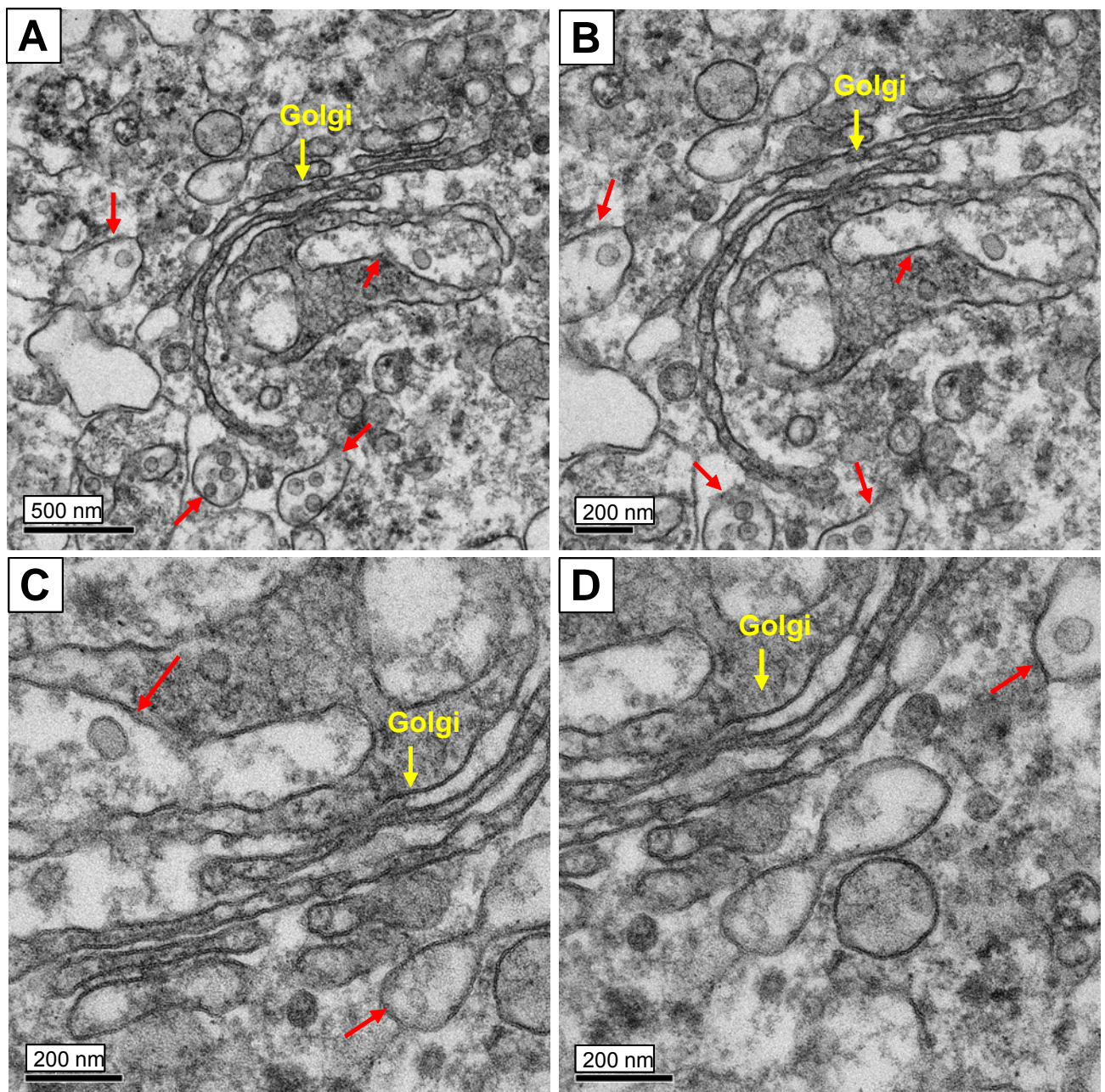


Fig. 38. VCVs were located in close proximity to the Golgi but no viral particles were found within the Golgi. (A-D) The Golgi apparatus from one DHBV-infected hepatocyte is shown at different

magnifications showing the presence of VCVs (red arrows) in close proximity to the Golgi (yellow arrows). Bars indicate the size.

Examination of the Golgi apparatus from 7 different DHBV-infected hepatocytes for a sign of viral morphogenesis or passage of viral particles through this compartment was negative. Golgi with dilated cisternae and budding of vesicles of different sizes were often seen, but none of them contained viral particles (Fig. 39 A-D, white arrows).

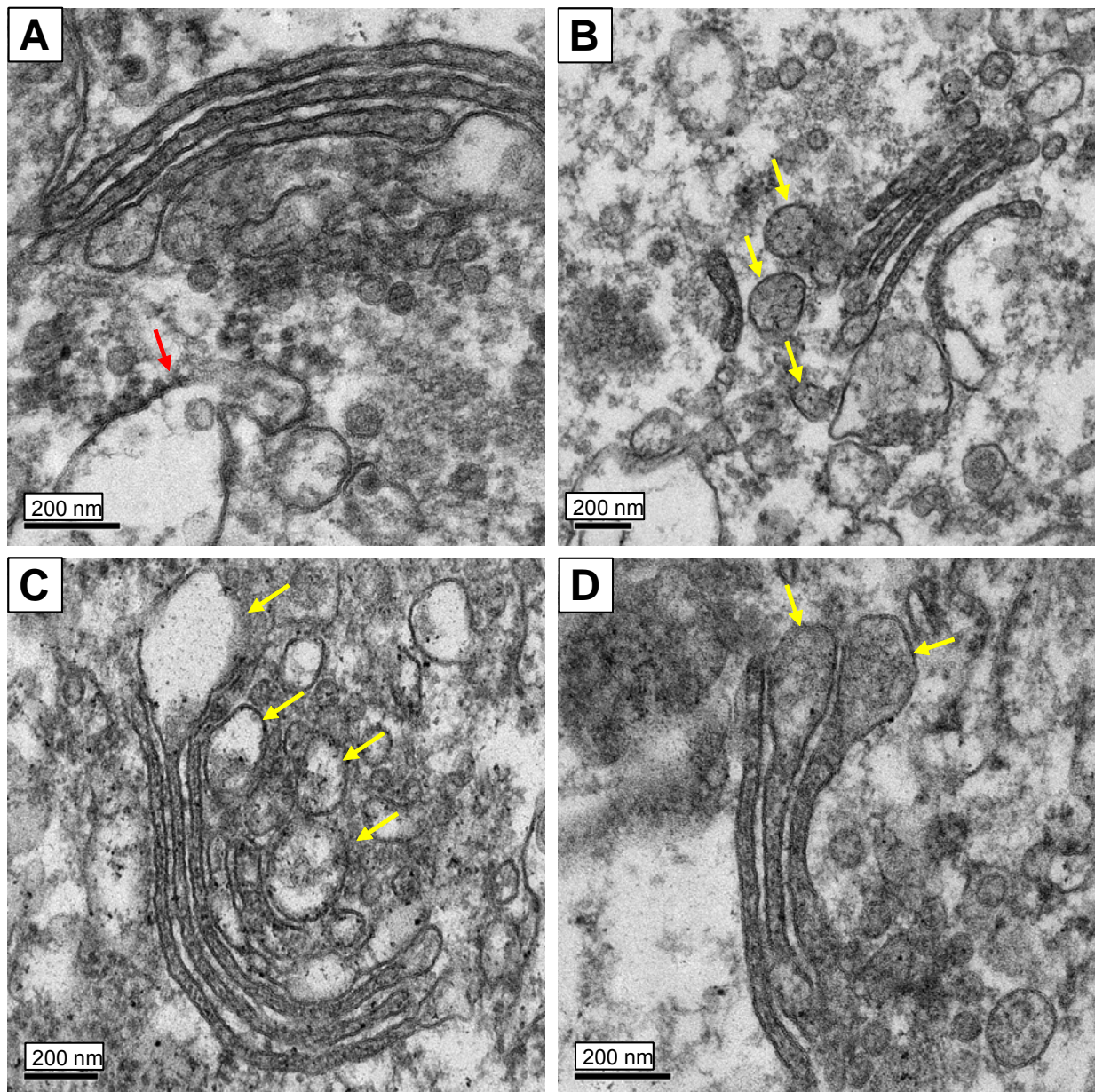


Fig. 39. The Golgi apparatus seems not to be involved in DHBV morphogenesis. (A-D) The Golgi apparatus from 4 different DHBV-infected hepatocytes at high magnifications show dilated cisternae

and budding of different sized vesicles devoid of viral particles (white arrows), the red arrow in panel A indicates a VCV located in proximity to the Golgi. Bars indicate the size.

In summary, the overall morphological appearance of the Golgi and careful analysis of the stacks for the presence of viral particles or budding of VCVs provided no evidences for its involvement in DHBV morphogenesis.

However, it is not possible to completely exclude that a minor subpopulation of VCVs is transported to and through the Golgi, since such vesicles were observed in close proximity. These findings corroborate the data from the subcellular fractionation and the colocalization studies shown in section III.1.2.2 indicating that viral particles are largely excluded from Golgi fractions while a minor overlap of L protein and Golgi were observed in the immunofluorescence studies.

In order to further analyse a possible non-involvement of the Golgi in DHBV secretion an independent experiment was performed.

III.2.1.2. Secretion of DHBV is Golgi independent but, partially temperature sensitive

In mammalian cells, there are specific, low-temperature-sensitive transport steps along both the endocytic and the exocytic pathways. Exocytosis of both secretory and membrane proteins is inhibited by reducing the culture temperature to 15-20°C (131). Transport of viral glycoproteins from the TGN to the PM is reversibly arrested at these temperatures (132, 133). To test whether DHBV secretion is temperature sensitive and whether viral particles accumulate in the Golgi at 20°C, congenitally DHBV-infected PDHs were incubated for 16 h either at 37°C or at 20°C. Thereafter, supernatants were harvested and analysed for viral L protein and DNA by immunoblotting and PCR, respectively.

To control the efficacy of the temperature block, D2 cells were transfected with the glycoprotein of vesicular stomatitis virus tagged to GFP (VSV-G-GFP) and incubated in parallel to the PDHs. D2 cells were used in this experiment, since the transfection efficiency of PDHs is very low and thus the visualization of the effects of the temperature block on the distribution of VSV-G-GFP is easier to monitor in D2 cells. Next day, D2 cells were fixed with 3.7% paraformaldehyde and analysed by CLSM.

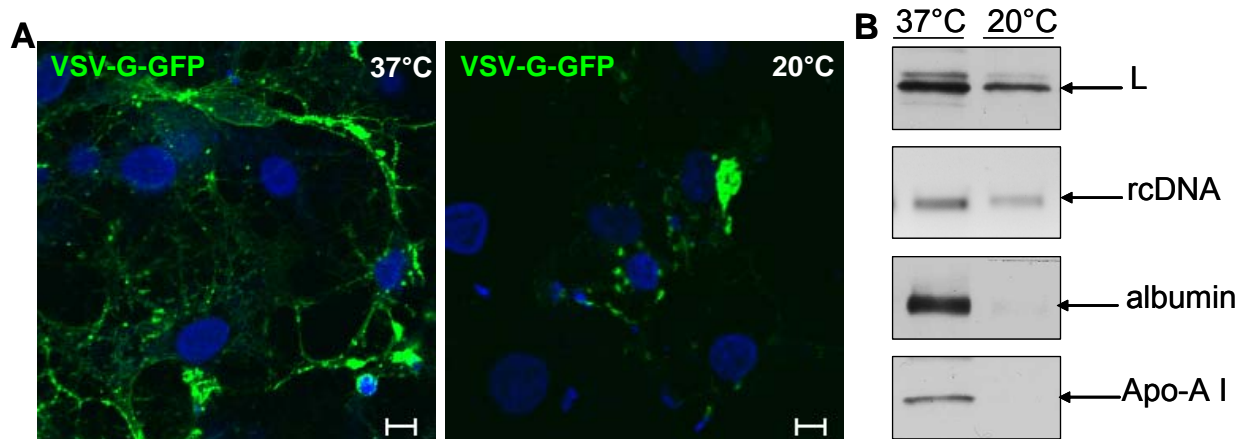


Fig.40. DHBV secretion is only moderately affected at 20°C. VSV-G-GFP transfected D2 cells and congenitally DHBV-infected PDHs were incubated over night either at 37°C or at 20°C. Next day, D2 cells were fixed in 3.7% PF for immunofluorescence analysis while the supernatants of PDHs were analysed for viral L and for 2 secretory cellular proteins albumin and apolipoprotein A I as well as for viral DNA by immunoblotting and PCR, respectively.

At 37°C, VSV-G-GFP was found to be located intracellularly in different sized vesicles corresponding presumably to the ER, to the Golgi and to transport vesicles carrying this protein. In addition VSV-G-GFP was found at the PM (Fig. 40 panel A). At 20°C, VSV-G-GFP was seen to accumulate in a compact structure corresponding probably to the Golgi and TGN as previously reported (106). Moreover, PM staining was lost indicating that the transport of this protein from the TGN to the cell surface was efficiently inhibited.

Incubation of congenitally infected PDHs at 20°C, reduces slightly the secretion of SVPs and virions as demonstrated by the L blot and the PCR, respectively (Fig. 40, panel B). The amount of the 2 cellular proteins albumin and apolipoprotein A I secreted into the medium was strongly reduced as compared to viral particles (Fig. 40, panel B). To see whether this slight reduction leads to the accumulation of viral particles within the Golgi, D2 cells transfected with VSV-G-GFP incubate either at 37°C or at 20°C were fixed and stained for L.

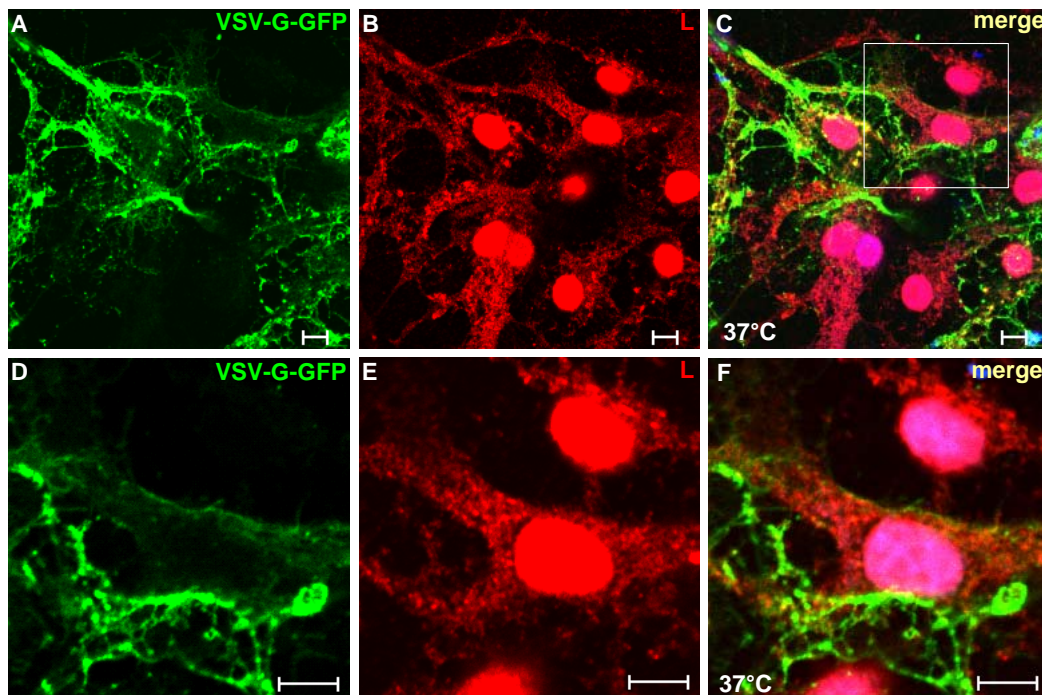


Fig. 41. The viral surface protein L and VSV-G-GFP do not colocalize at 37°C. VSV-G-GFP transfected D2 cells were incubated over night at 37°C, next day cells were fixed and stained for L (red signals) and analysed by CLSM. The square in panel C is magnified in D-F. Nuclei are shown by the big red dots. Bars correspond to 5 μm .

CLSM, showed that at 37°C VSV-G-GFP (Fig. 41, panels A and D) was found in vesicular structures of different size which were distinct from VCVs stained by the L antibody (Fig. 41, panel B and E). Only a minor colocalization of both proteins near the nucleus was observed (Fig. 41, panels C and F). This corresponds presumably to VSV-G-GFP and L within the ER where they are synthesized. However, it seems that both proteins follow 2 distinct pathways since no significant colocalization was observed between them, with the exception of the ER at 37°C.

When cells were incubated over night at 20°C, the subcellular distribution of VSV-G-GFP was drastically changed, it was no longer found in small vesicles but was concentrated within one compact structure presumably the Golgi (Fig. 42, panels A and D). Under these conditions, the pattern of L was unchanged, VCVs were still seen as vesicles of different size distributed throughout the cytoplasm. There was no overlap with VSV-G-GFP positive structure (Fig. 42, panels B and E). This indicates that unlike VSV-G-GFP the L protein does not pass through the Golgi since it is not arrested within this compartment at low temperature.

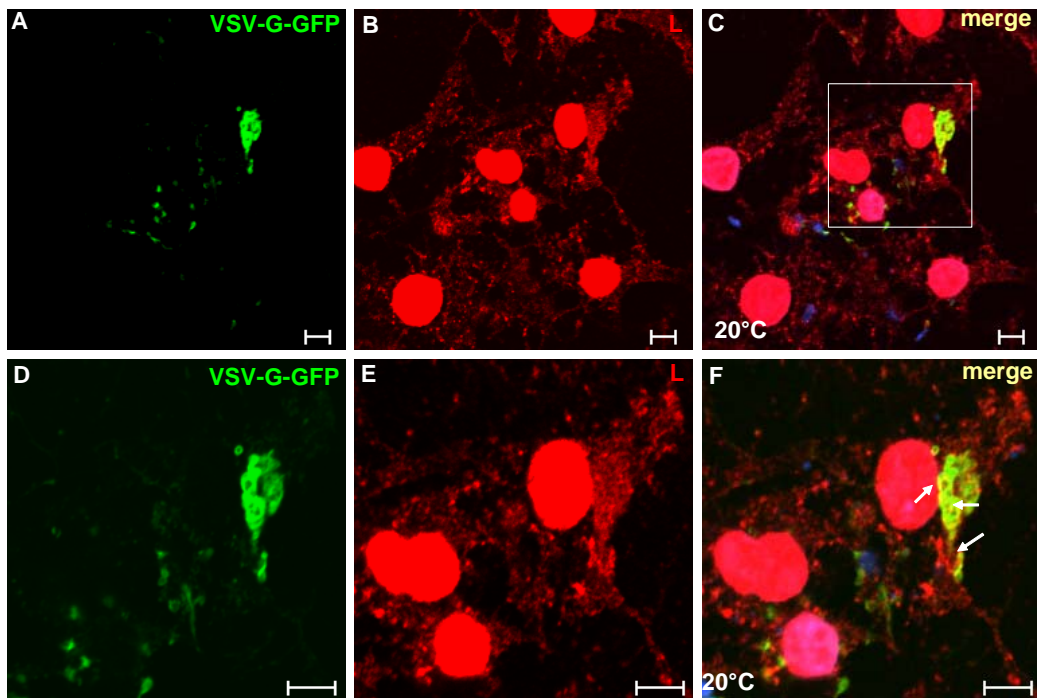


Fig. 42. The viral surface protein L and VSV-G-GFP do not colocalize at 20°C. VSV-G-GFP transfected D2 cells were incubated over night at 20°C, next day cells were fixed and stained for L (red signals). Nuclei are shown by the big red dots. Bars correspond to 5 μ m.

Nevertheless, a very small fraction of L protein was found to colocalize with VSV-G-GFP near the compact structure (Fig. 42, panel F, white arrows).

For closer examination of the minor colocalization of VSV-G-GFP and L, z-stacks of the above shown cell were performed and presented as 3D maximum intensity projection (MIP). A series of such analysis is shown in figure 43.

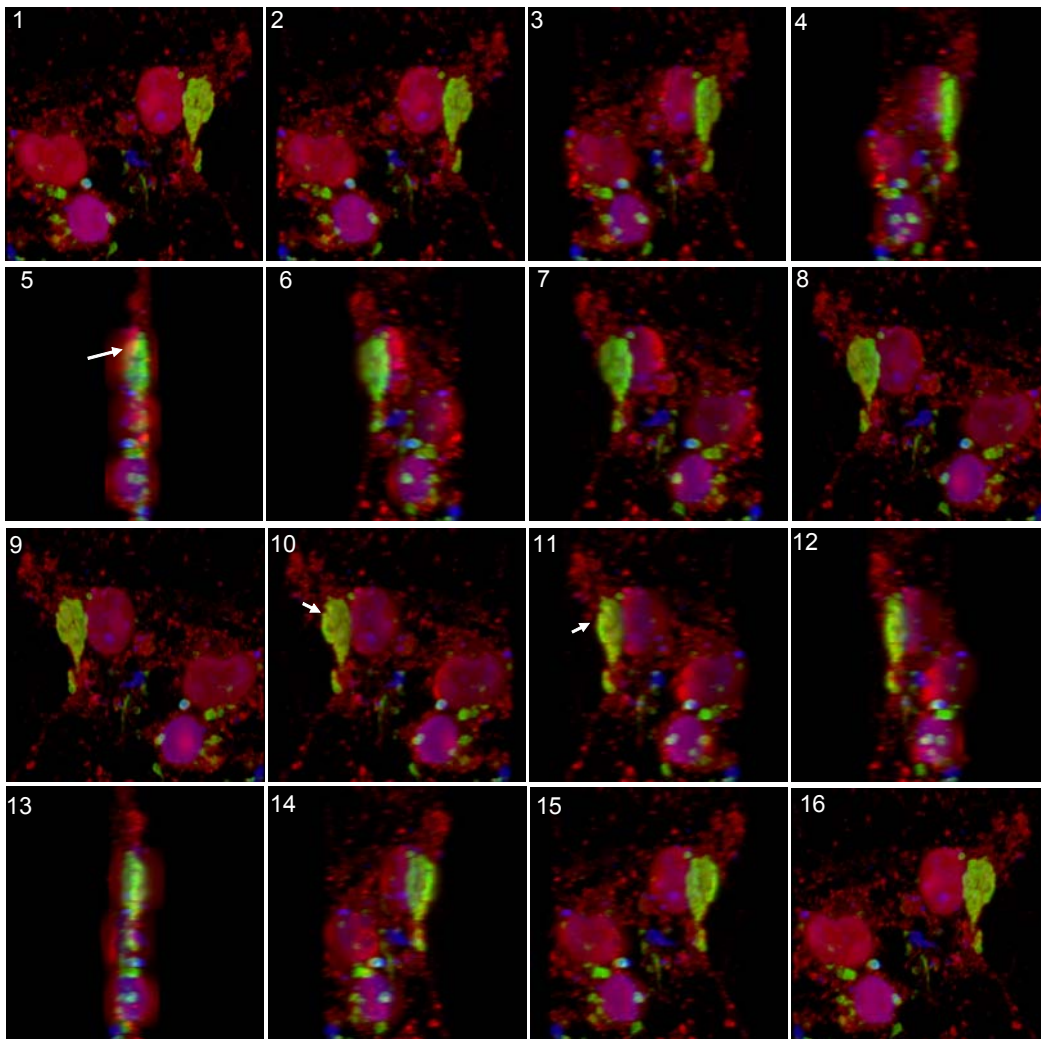


Fig. 43. Only a minor fraction of L was colocalized with VSV-G-GFP. Z-stacks from the cells in figure 42 were performed and show as MIP. VSV-G-GFP is seen in green, L is shown in red. The colocalization between both proteins is indicated by the white arrows.

The projection revealed that a small fraction of L was localized in close contact to the compact structure visualized by VSV-G-GFP, rather than being within this structure.

Taken together, the data shown above indicate that the secretion of DHBV was Golgi independent since the distribution of L was not affected at low temperature and L does not colocalize with VSV-G-GFP which accumulate within the Golgi at 20°C. Nevertheless a very small fraction of the L protein was seen in close contact to the Golgi. Viral secretion was slightly reduced at 20°C. This could be due to the requirements of cellular factors and proteins, which are temperature sensitive and thus indirectly influence DHBV secretion.

III.2.2. Viral particles are released via exocytosis

III.2.2.1. Ultrastructural evidences for an exocytic release

Our group has previously shown that the spread of DHBV infection occurs via extracellular viruses and that the VCVs harbouring these particles are presumably primarily located near the basolateral membrane of hepatocytes (82).

The observation of the compartmentalisation of preformed viral particles in membraneous vesicles led to the speculation that the mode of DHBV secretion involves an exocytic process occurring by the fusion of VCVs with the PM. To test this idea, membrane regions of infected hepatocytes were analysed for ultrastructural features proving, suggesting or rejecting an exocytic release mechanism.

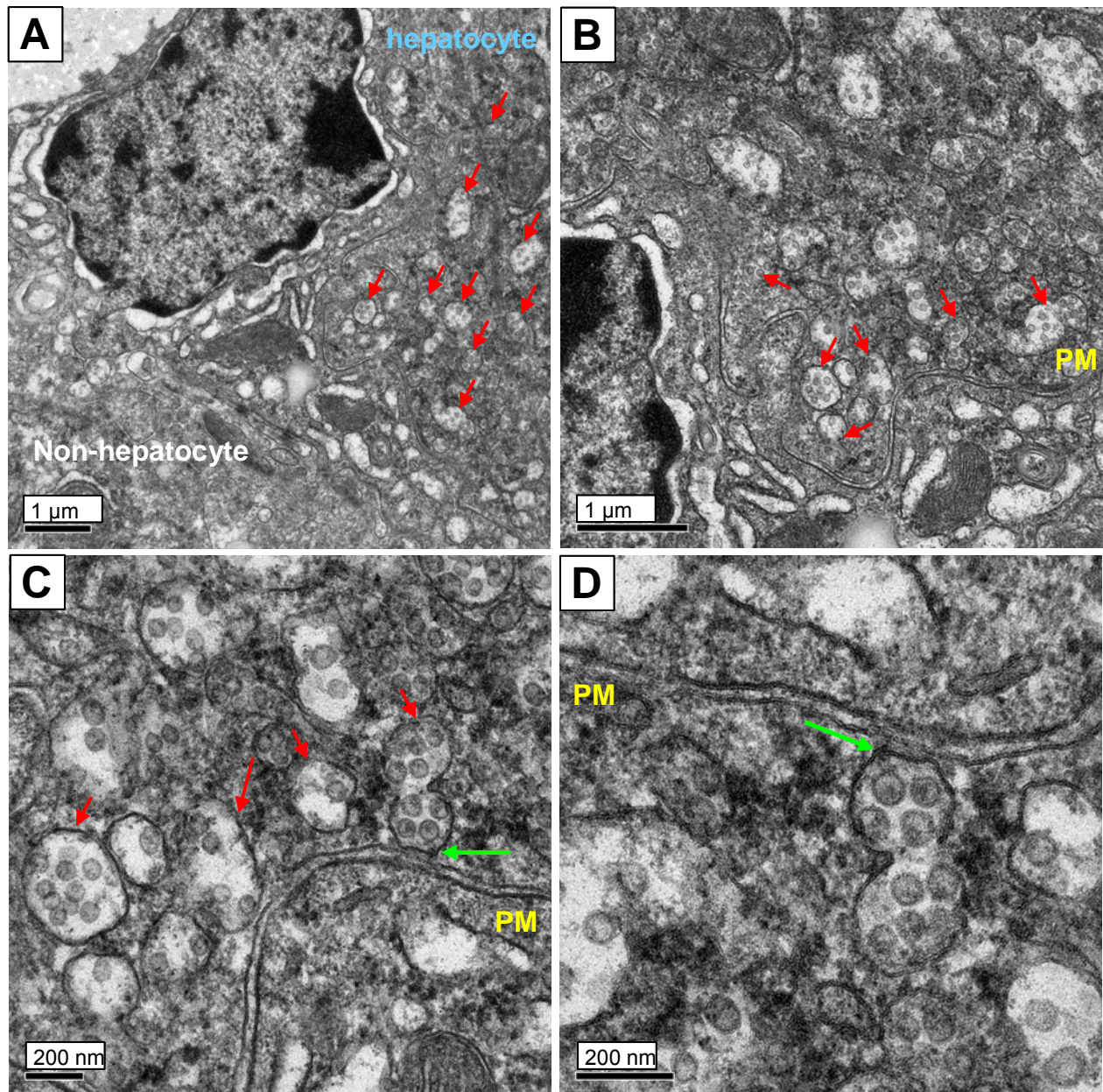


Fig. 44. VCVs are located in close proximity to the PM. (A) Part of the cytoplasm of a hepatocyte and a non-parenchymal cell are shown. Many VCVs (red arrows) are located near the PM of the hepatocyte. (B) Shows a magnification of the area between both cells. (C and D) Further magnifications of the same area reveal the close contact of some VCVs to the PM (green arrow). Bars indicate the size.

Numerous VCVs were found in close proximity to the PM of a hepatocyte located adjacent to a non-parenchymal cell, probably a sinusoidal endothelial cell (Fig. 44A, red arrows). The magnification of this area showed variously sized VCVs containing different numbers of viral particles located along the PM, some of these VCVs were in very close contact with the cell surface (Fig. 44C and D, green arrows). These

VCVs were similar to those observed intracellularly in proximity to the nucleus indicating that the same VCVs are anterogradely transported to the PM. Moreover, VCVs were often seen located beneath the PM of hepatocytes near the extracellular space (ECS) as shown in figure 44 A-D (red arrows). Some VCVs were subcortically located with a distance of less than 20 nm to the cell surface. The PM exhibit membrane activities like clathrin-mediated endocytosis (Fig. 45 A-D light blue arrow) indicating active exchanges between the intra- and extracellular space.

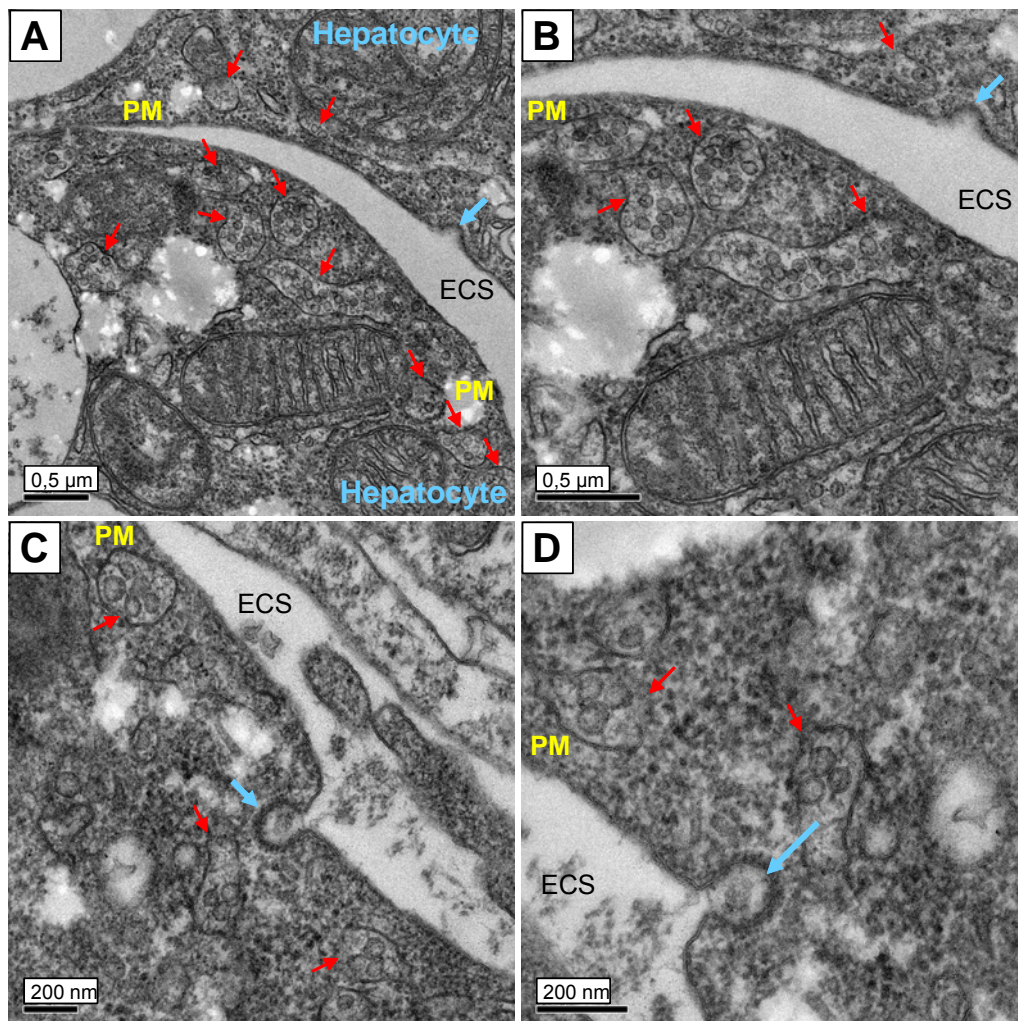


Fig. 45. VCVs are located beneath the PM of 2 adjacent hepatocytes. (A) Parts of the cytoplasm of 2 adjacent hepatocytes separated by the extracellular space (ECS). In both cells, VCVs (red arrows) are located close to the PM. The upper cell shows a membrane invagination probably corresponding to clathrin-mediated endocytosis (light blue arrow). (B-D) Magnifications of the PM area to visualize the close contact of VCVs to the cell surface. Bars indicate the size.

Some VCVs were seen in direct contact with the PM (Fig. 46A and B, green arrows). This observation is compatible with the first step of an exocytic fusion process between the membrane of VCVs and that of the PM.

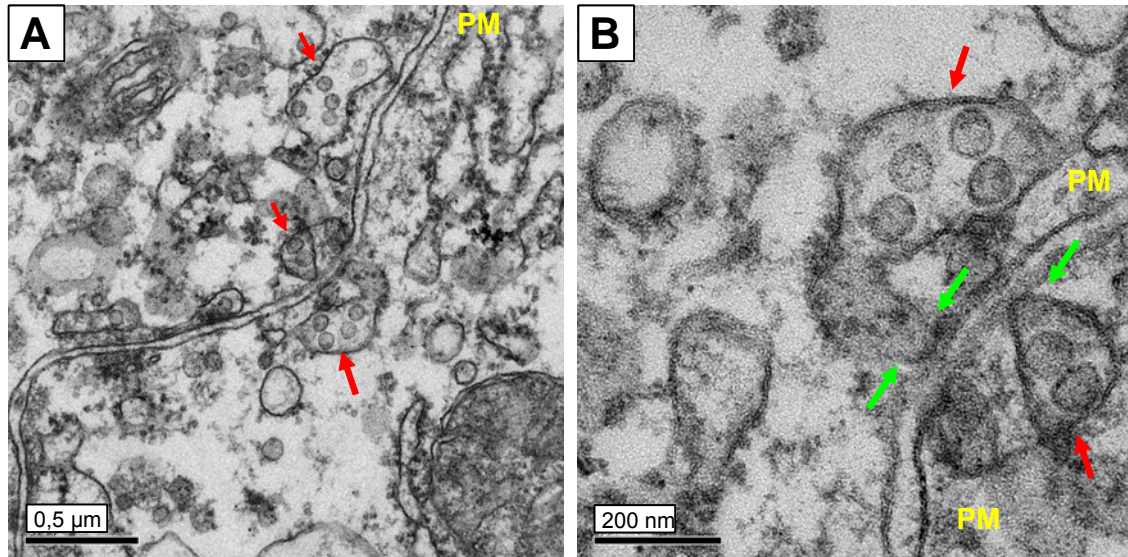


Fig. 46. VCVs were seen in close contact with the PM. A and B show VCVs (red arrows) which are in direct contact with the cell surface (green arrows). Bars indicate the size.

Beside the VCVs, which were located at or in close contact with the PM, released viral particles were often seen in the extracellular space as shown in figure 47 and 48.

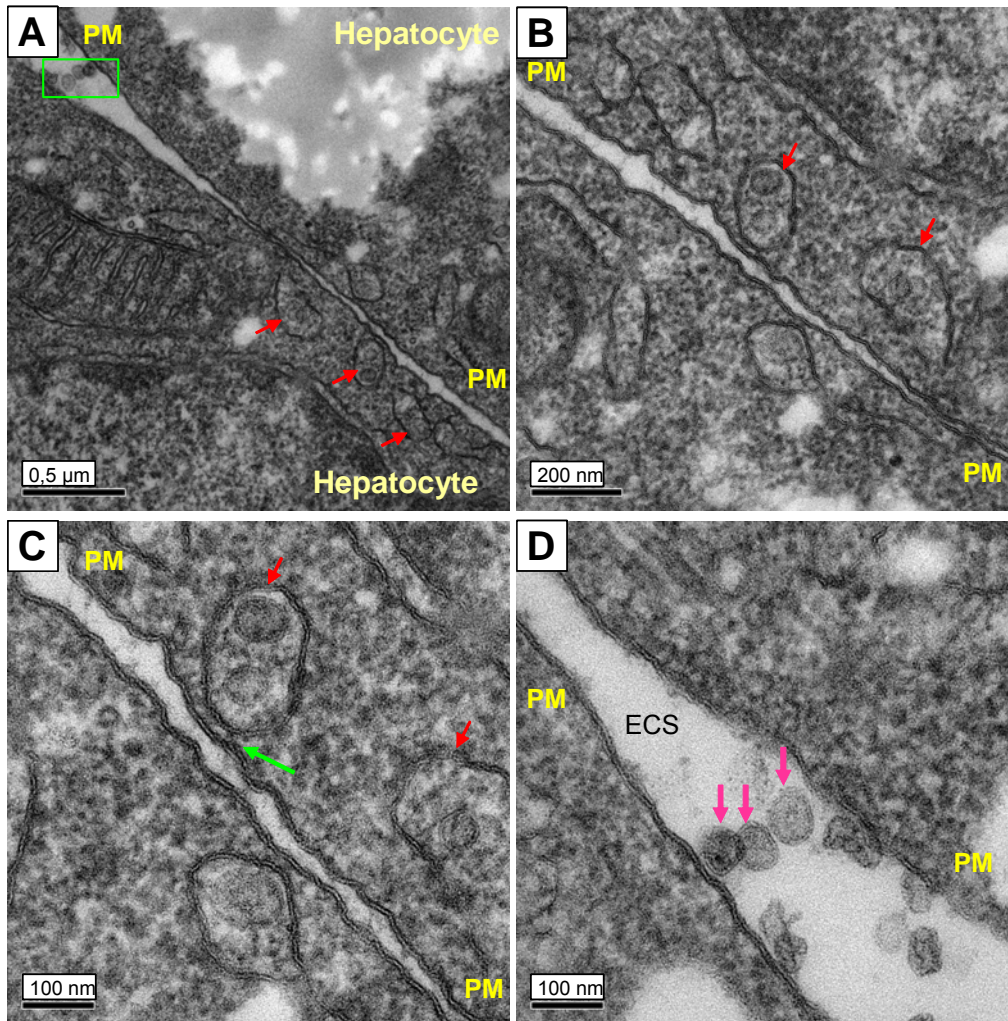


Fig. 47. Viral particles are found in the extracellular space between two hepatocytes. (A) Section of the cytoplasm of 2 hepatocytes with VCVs (red arrows) located near the PM. The green rectangle shows viral particles in the extracellular space (ECS). (B and C) Magnifications of VCVs at the PM, the green arrow shows the close location of the VCV to the PM. (D) Magnification of the area within the green rectangle in (A). It clearly shows viral particles that have been secreted into the ECS. Bars indicate the size.

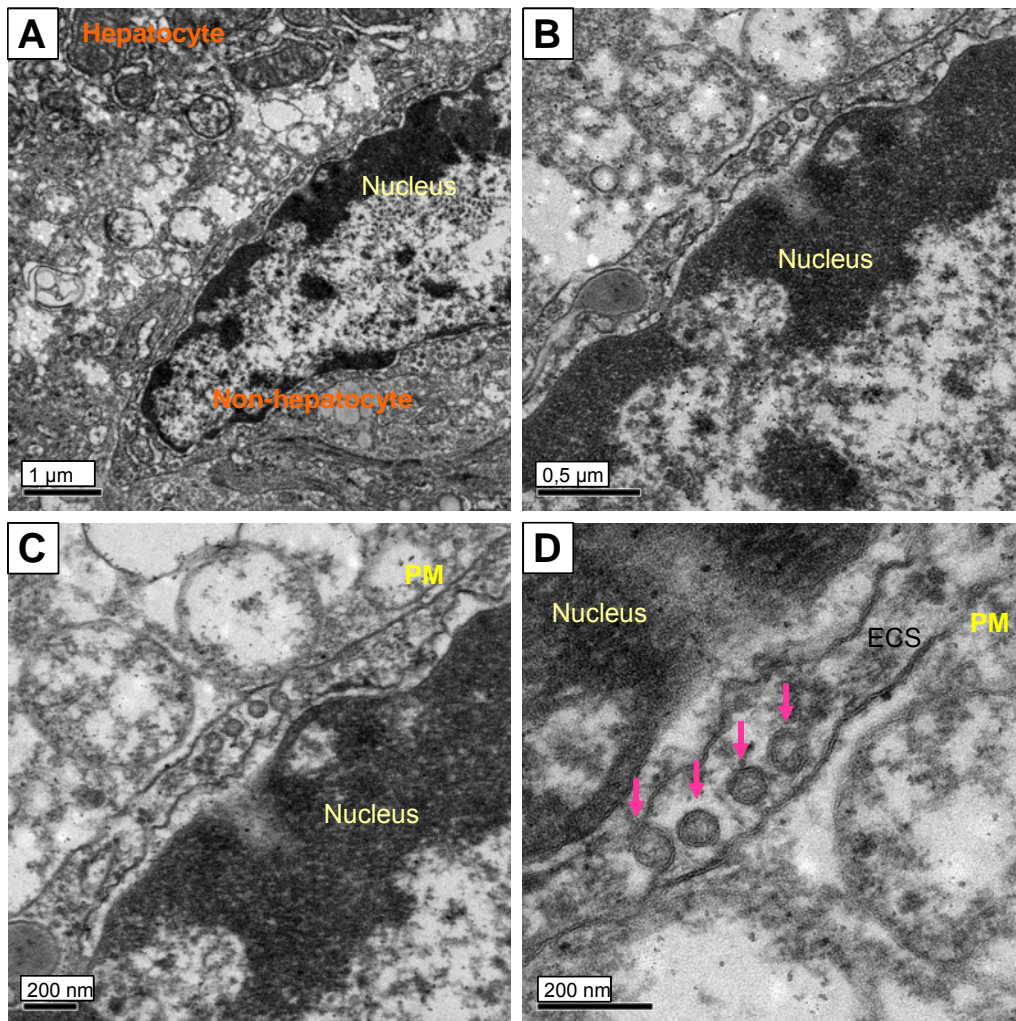


Fig. 48. Viral particles are found in the extracellular space between hepatocytes and non-parenchymal cells. (A) Section of the cytoplasm of a hepatocyte and a non-parenchymal cell, probably a liver sinusoidal cell. (B-D) Magnification of the extracellular space between both cells. The arrows point to viral particles in the intercellular space which have been secreted. Bars indicate the size.

Viral particles were found in the extracellular space between adjacent hepatocytes indicated by the pink arrows (Fig. 47), while in figure 48, viral particles are found in the intercellular space between hepatocytes and non-parenchymal cells (arrows).

All ultrastructural data shown above are strongly suggestive for an exocytic release of viral particles from the VCVs. However, the direct fusion and the exocytosis itself were rarely seen. The screening of several sections provided finally the direct ultrastructural evidence for such a release mechanism as shown in figure 49.

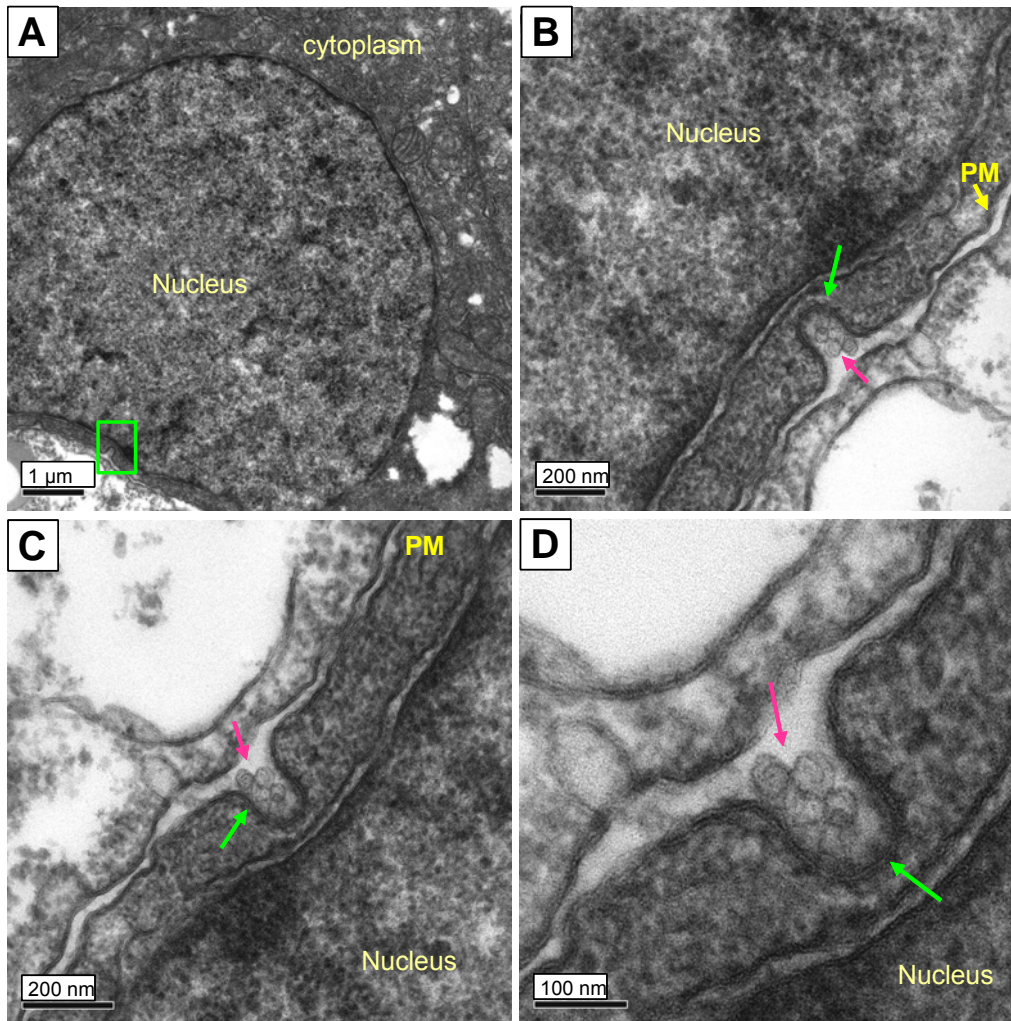


Fig. 49. Viral particles are released via exocytosis. (A) A hepatocyte with a big nucleus and parts of the cytoplasm are shown. The rectangle marks the region of interest. (B-D) Different magnifications of the rectangle in (A) showing an invagination of the PM (arrows) containing viral particles (arrows), which are secreted into the extracellular space. Bars indicate the size.

In figure 49 A, a section of a hepatocyte with a big nucleus is shown. The area within the rectangle is magnified in figure 49 B-D. The magnifications show the invagination of the plasma membrane forming a basket (arrows) containing viral particles (arrows). Presumably, this picture finally provides the direct evidence for exocytic release as the mechanism for viral secretion. However, it is important to stress that such exocytic events were rarely observed suggesting that this process is very fast and could not be efficiently captured under the experimental conditions used.

III.2.2.2. Biochemical evidences for an exocytic release

The membranes of VCVs harbour non-particulated envelope proteins as it was shown by (i) the immunogold staining (Fig. 14), (ii) by immunocapture of native VCVs by envelope specific antisera from dounce homogenates (Fig. 28). Beside release of the viral cargo, a further consequence of the exocytic fusion of the VCV with the PM would be the transfer of non-particulated envelope proteins to the cell surface. If this is true the PM should harbour envelope proteins.

L localizes to the PM as shown by immunofluorescence analysis

Immunofluorescence analysis of L in infected hepatocytes always revealed a staining pattern reminiscent of the PM, since the contour of the cells was easily recognisable as shown in the colocalization studies in figure 24.

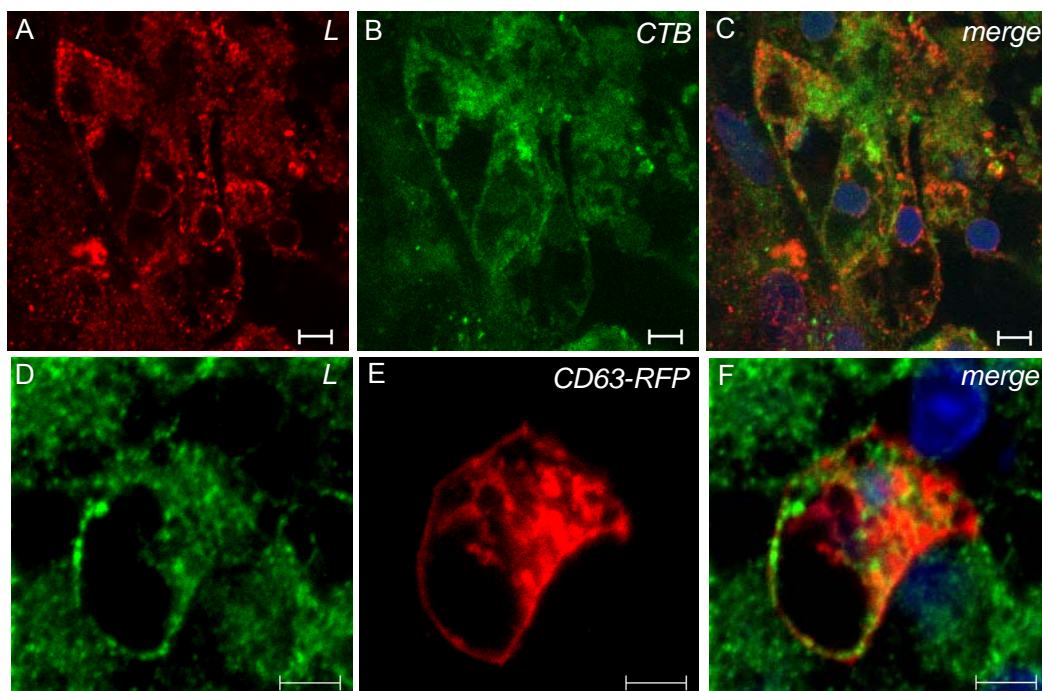


Fig. 50. The viral surface protein L is localized to the PM. (A-C) Congenitally DHBV-infected PDHs were incubated for 1h with 5 $\mu\text{g/ml}$ cholera toxin subunit B (CTB)-FITC (panel B) at 37°C. Cells were washed with PBS, fixed with 3.7% paraformaldehyde for 10 min and permeabilized with 0.1% Triton X-100. Subsequently, cells were stained for L (panel A). The merge and counterstained nuclei are shown in panel C. (D-F) Congenitally DHBV-infected PDHs were transfected with 3 μg DNA encoding CD63-RFP (panel E) at 1 day post plating and fixed 3 days later with ice cold methanol-acetone (1:1). Cells were then stained for L (panel D). The merge and the counterstained nuclei are shown in panel F. bars correspond to 5 μm .

Co-staining of DHBV-infected hepatocytes for L and the PM using either FITC-labelled cholera toxin subunit B, which binds to its receptor, the ganglioside M1 at the cell surface or with ectopically expressed CD63-RFP, a tetraspannin localizing to MVBs and the PM, revealed that both markers stain the same membrane as labelled using anti-L antibody indicating that L was indeed present at the PM (Fig. 50C and F). However, this PM staining by L could be due to the attachment of secreted progeny viruses to the hepatocellular membranes.

An argument against this hypothesis is (i) no viral particles were seen to be homogeneously distributed along the cell surface as shown by electron microscopy, (ii) inhibition of viral secretion by BFA resulted in loss of L staining at the PM. A detailed study about the effects of this substance will be presented in the next section. Here, the focus will be on the effect of this substance on the PM-association of L.

Since BFA strongly inhibits the secretion of DHBV (section III.3.1), it can be assumed that PM-associated L will also be reduced because no fusion of VCVs with the PM will occur and thus no L protein will be transferred to the cell surface. To test this, congenitally DHBV-infected PDHs were treated or not for 24 h with 10 µg/ml BFA followed by 30 min incubation with CTB-FITC, subsequently fixed and stained for L. The results show that BFA treatment led to a loss of L-staining of the PM. L was found in big dots located in the cytoplasm and near the cell surface (Fig. 51, compare panels B and E). This indicates that inhibition of virus secretion also reduced the transfer of L protein to the cell surface.

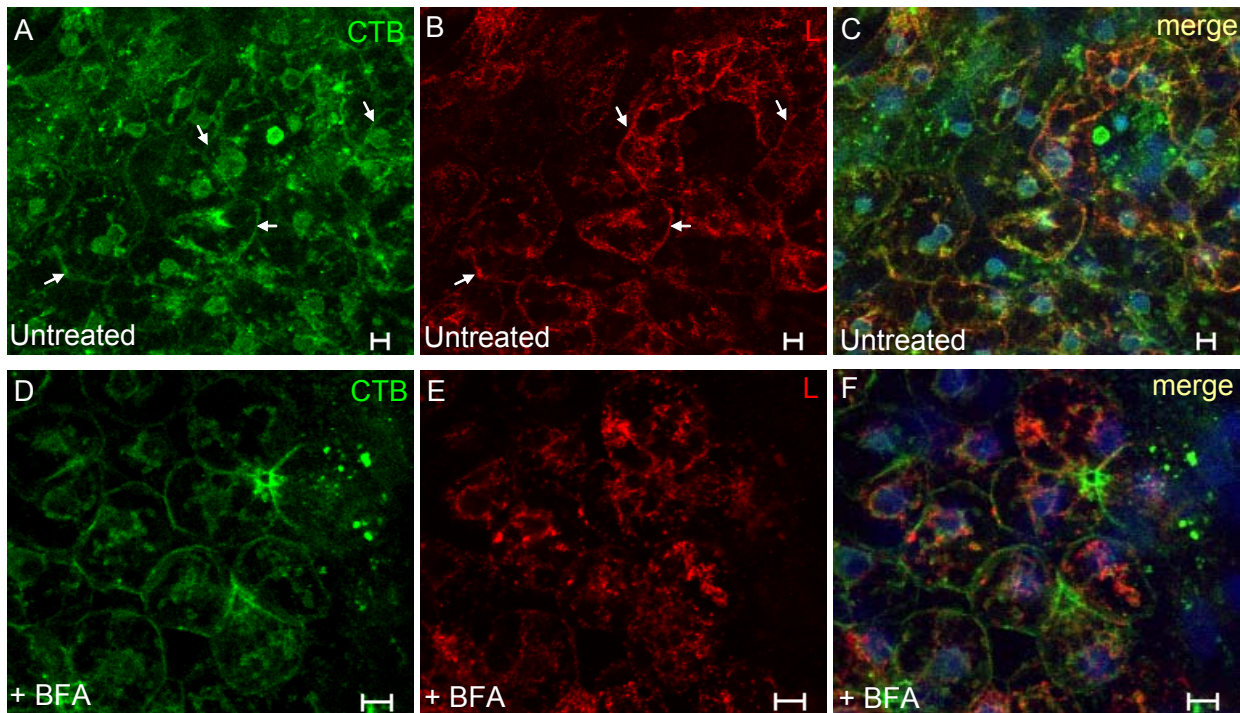


Fig. 51. Following BFA treatment, the L-associated membrane staining was lost. Congenitally DHBV-infected PDHs were treated (D-F) or not (A-C) for 24 h with 10 $\mu\text{g/ml}$ BFA, then incubated for 1 h with 5 $\mu\text{g/ml}$ CTB and subsequently fixed with 3.7% paraformaldehyde. Cells were immunostained for the viral surface protein L. Nuclei were counterstained with DRAQ5. Bars correspond to 5 μm .

The surface protein L is located at the PM as shown by a biotinylation assay.

Surface biotinylation was used as a strategy to specifically label proteins present on the cell surface and to investigate whether the surface protein L was really present at the PM as shown above by the immunofluorescence analysis (Fig. 50). Cells were labelled with membrane-impermeant, non-cleavable biotin (sulfo-NHS-biotin) for 1 h at 4°C. After biotinylation of cell surface proteins, cells were lysed, and subjected to immunoprecipitation using streptavidin-coated microspheres. Immunoblotting of the input sample and the immunoprecipitates (IPs) using horseradish peroxidase (HRP)-conjugated to streptavidin labels all biotinylated proteins as shown in figure 52. The efficiency of biotinylation was comparable between non-infected and DHBV-infected cells (Fig. 52 lane 1 and 2, respectively). The amount of biotinylated proteins was strongly reduced in cells harvested with trypsin in comparison to the control cells (Fig. 52 lanes 3 and 2, respectively) indicating that the signals were indeed due to labelled proteins.

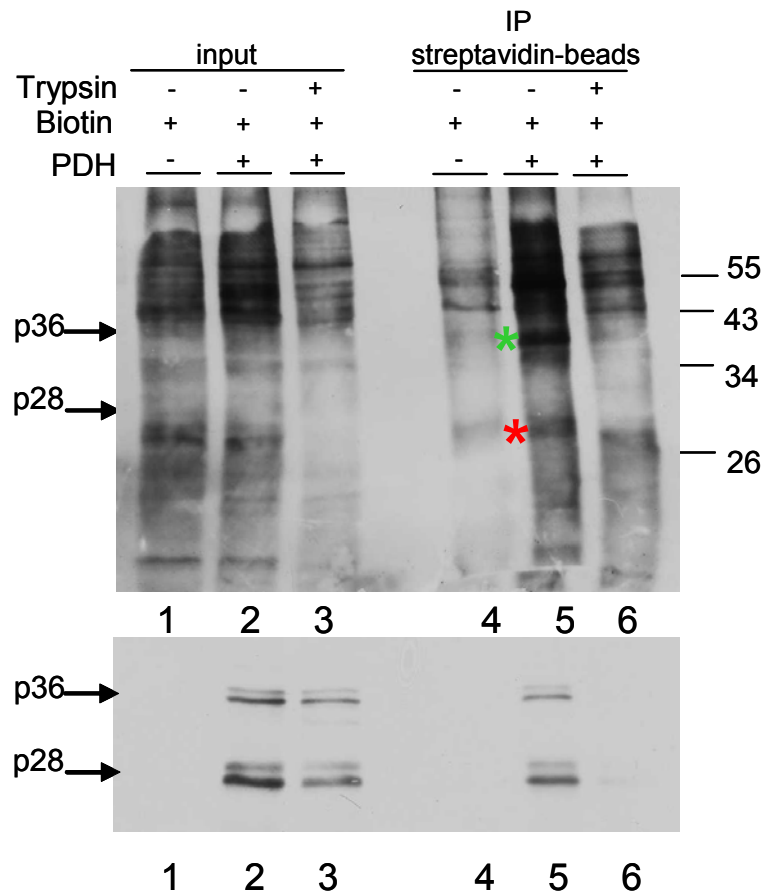


Fig. 52. The viral surface protein L is localised to the PM. Non-infected and congenitally DHBV-infected primary duck hepatocytes were incubated with 100 µg/ml NHS-biotin for 2 h at 4°C. Cells were lysed and subjected to immunoprecipitation (IP) using streptavidin-coated beads. IPs were analysed by immunoblotting for biotinylated proteins with streptavidin-HRP and subsequently for the viral surface protein.

The IP from DHBV-infected cells showed two bands of molecular mass 28 and 36 kDa (Fig. 52, lane 5, indicated by the red and green asterisk, respectively) which were absent in the non-infected cells (Fig. 52, lane 4) and could efficiently be removed by trypsin (Fig. 52, lane 6). Then the same immunoblot was probed with a DHBV-preS specific antiserum after inactivation of HRP-activity by sodium azide. The immunoblot for L (Fig. 52, lower panel) showed 2 double bands (Fig. 52, lanes 2, 3 and 5), one running at about 36 kDa (p36) corresponding to the hyper- and hypophosphorylated forms of L (upper and lower bands, respectively) and one band running at about 28 kDa corresponding to the hyper- and hypophosphorylated forms of p28, a cleavage product of p36.

The amount of L in the input sample was reduced in cells harvested with trypsin (Fig. 52, lanes 2 and 3) compared to cells harvested without trypsin, indicating that a fraction of L was trypsin-sensitive and the remaining fraction of L corresponded to the intracellular fraction which is trypsin resistant.

The most important result from this experiment was that L was only precipitated from cell lysates harvested without trypsin, but not from those harvested with trypsin. (Fig. 52, lanes 5 and 6). This indicates that only L which is at the cell surface and has been biotinylated could be immunoprecipitated using streptavidin-coated beads, but not the non-biotinylated L (corresponding to the intracellular L fraction). This shows the specificity of the immunoprecipitation using streptavidin-coated beads for biotinylated surface proteins. These results clearly show that a fraction of the surface protein L was located at the PM and accessible for biotinylation.

To further confirm these findings the reverse experiment was performed. A second biotinylation assay as described above was done, and the cell lysate were first subjected to immunoprecipitation using a DHBV-L-specific antibody. Immunoblots were then inversely probed with HRP-streptavidin (Fig. 53, upper panel).

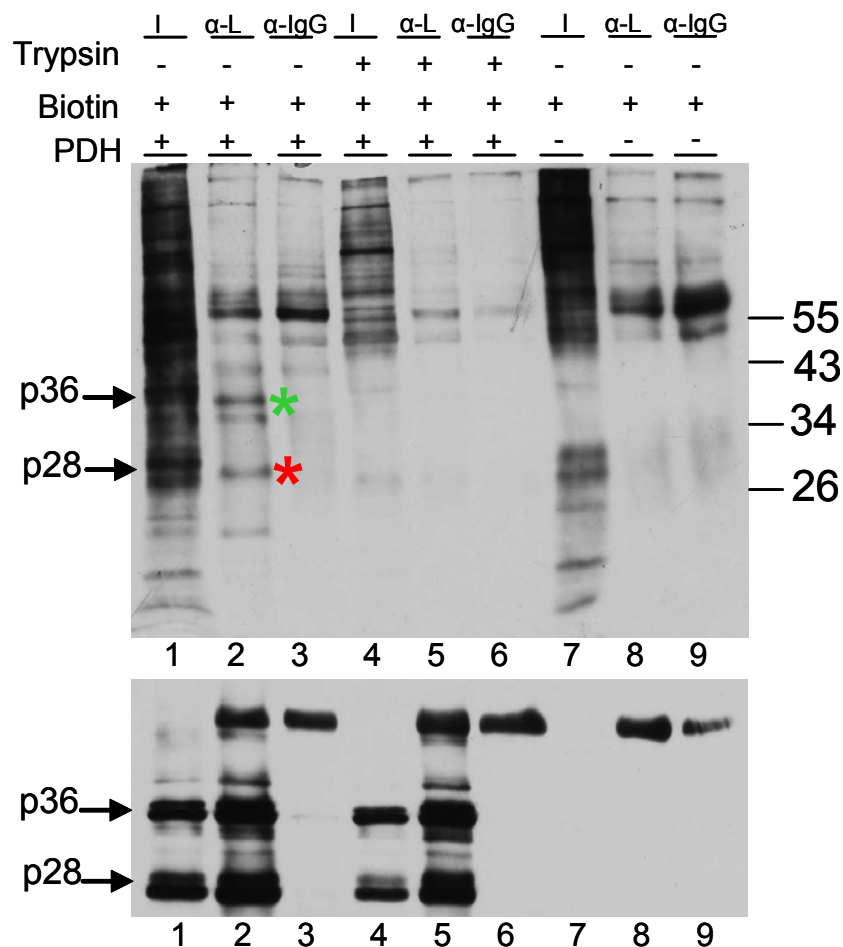


Fig. 53. The viral surface protein L is localised to the PM. Non infected and congenitally DHBV-infected PDHs were incubated with 100 μ g/ml NHS-biotin for 2 h at 4°C. Cells were lysed and subjected to IP with anti-L or a non-specific antibody. IPs were analysed by immunoblotting for the detection of biotinylated proteins with streptavidin-HRP and subsequently for the viral surface proteins.

Two bands of 28 and 36 kDa were specifically immunoprecipitated with anti-L, but not with the control antibody from DHBV-infected lysates (Fig. 53, lanes 2 and 3, red and green asterisk, respectively). These bands are strongly reduced when cells were harvested with trypsin (lane 5) indicating that they are cell surface-associated. The bands were absent in the anti-L IP from non-infected cells (lane 8) showing that they are not cellular proteins which are non-specifically immunoprecipitated with the L-antibody. The same membrane was probed with anti-L after inactivation of the HRP-activity with sodium azide.

As shown in the lower panel of figure 53, L was specifically immunoprecipitated (lane 2), since no L was immunoprecipitated with the control antibody (lane 3). Treatment of cells with trypsin prior to their harvest, reduce both the total amounts and the

immunoprecipitated fractions of L were slightly reduced (Fig. 53, lower panel, lanes 4 and 5, respectively) indicating that a small fraction of L was trypsin-sensitive and presumably reflects the fraction at the PM. In conclusion, this assay shows clearly that the observed bands running at about 36 and 28 kDa as shown by streptavidin-HRP immunoblot correspond to the biotinylated viral proteins p36 and p28.

Taken together, the data from these 2 independent complementary experiments clearly show that the fraction of the non-particulated viral surface protein L is accessible to biotinylation. These findings further support the immunofluorescence studies shown in figure 50 and indicate that during secretion of viral particles, a fraction of envelope proteins embedded in VCV membranes is transferred to the PM. This transfer occurs during the VCV membrane-PM interaction.

III.2.2.3. Life cell imaging reveals an exocytic release

Both the ultrastructural and biochemical analysis revealed that DHBV secretion is mediated by an exocytic mechanism. However, it was not possible to efficiently visualize this rare process by electron microscopy. This was presumably due to the experimental limitations of this method since exocytosis is a very fast process and thus could not be fixed and captured by conventional chemical fixation methods and EM, respectively.

To overcome these experimental restrictions, life cell imaging was performed. In principle, the same assay as presented in section III.1.2.4 was used. This time the focus was on the VCVs located near and at the cell surface in order to visualize the events leading to the secretion of viral particles. Briefly, LMH cells were transfected with EGFP-S, surface proteins S and L and CD82-RFP. Two days post transfection, cells were analysed by CLSM. Z-stacks records were acquired every 30 sec over a time period of 30 min. The 3D reconstructions and the orthogonal projections were performed with “Imaris v.4.1.3”. Figure 54 A shows a confocal image from these records where VCVs were found to localize in close proximity to the cell surface and to tether to the PM. These findings are compatible with the ultrastructural data showed in figures 44-47 where VCVs were often seen near and in contact with the PM. In figure 54 B, is shown a 3D reconstruction of the records is shown and revealed the distribution of VCVs throughout the cytoplasm.

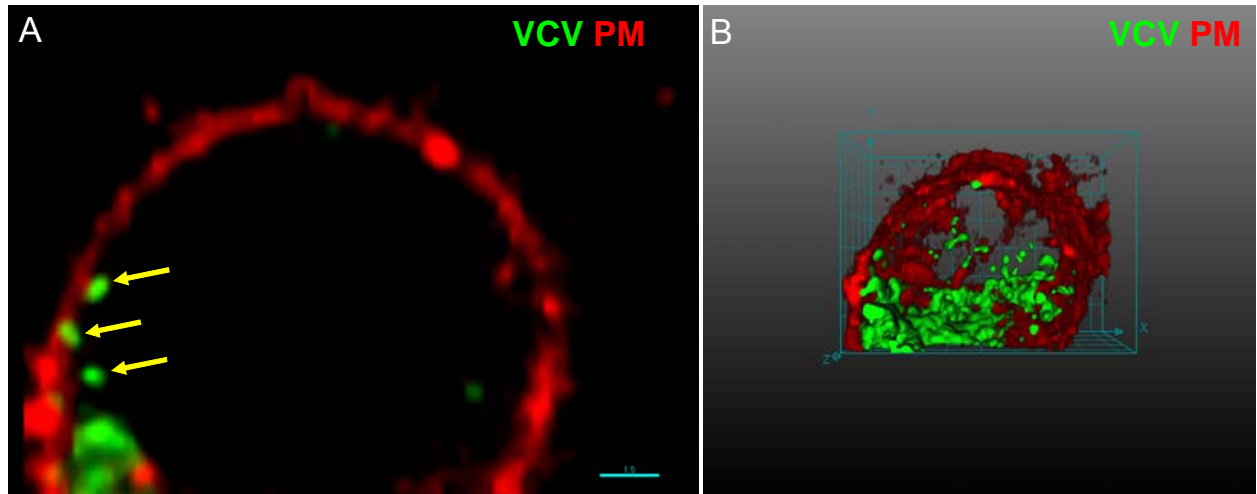


Fig. 54. VCVs were located to and interacting with the PM. EGFP-S, wild type surface proteins S and L and CD82-RFP were expressed in LMH cells. Two days later, cells were analysed by confocal microscopy (panel A) and (3D) records over time were acquired. The 3D records were reconstructed using Imaris software (panel B). The 3D projections show the localization of VCVs within the cell and near the cells surface and their interaction with the PM. The yellow arrows point to VCVs which tether the PM. Distance between the ticks in the grid correspond to 5 μ m.

In order to reduce the complexity and concentrate on individual VCVs at the PM, a region of interest from the 3D reconstruction in figure 54 B was cropped out digitally using Imaris software and represented in figure 55.

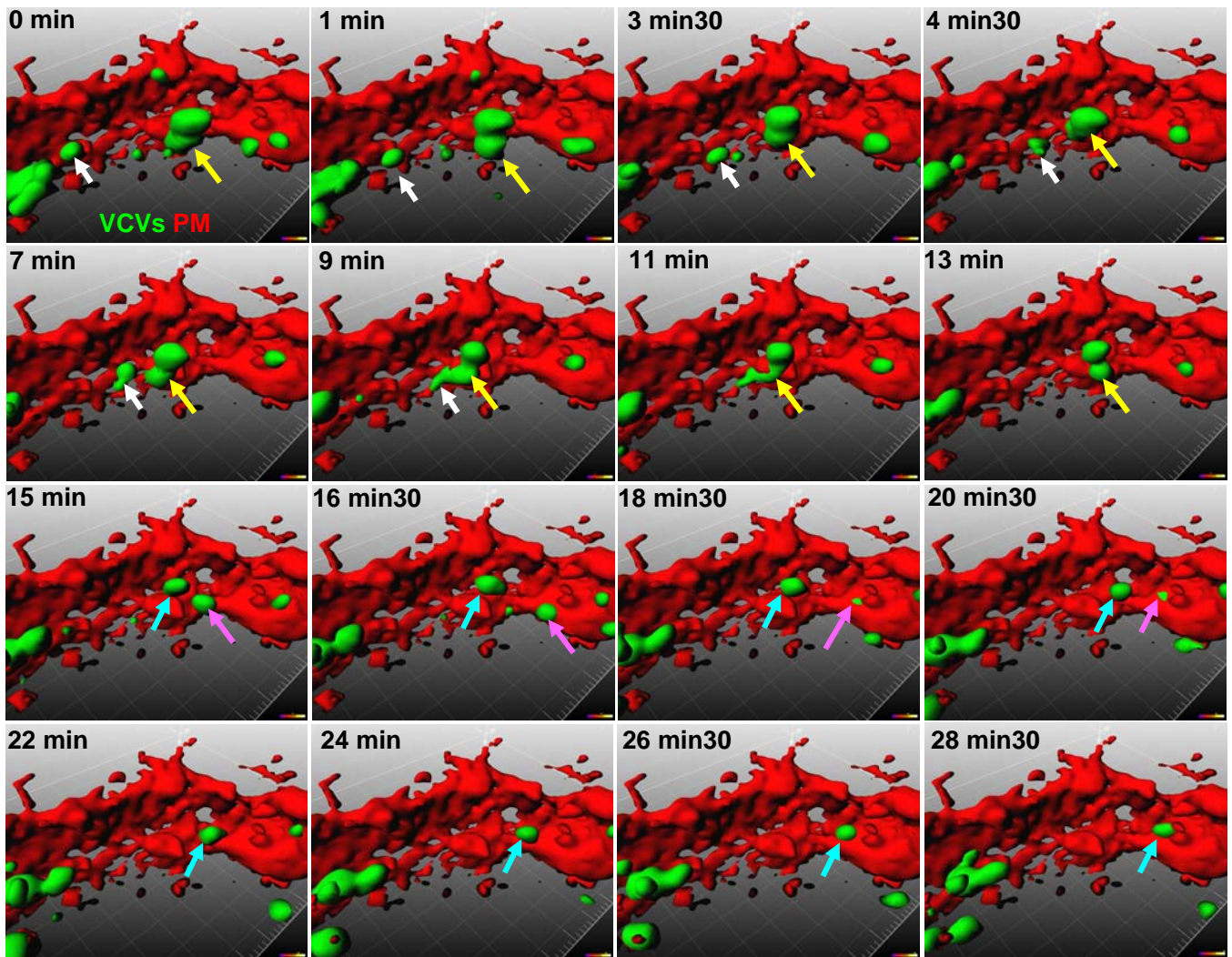


Fig. 55. VCVs are located near and interact with the PM. A region of interest was cropped out digitally from the 3D reconstruction shown in figure 54 B. The 3D projections show the localization of VCVs near the cell surface and their interaction with the PM. The white arrow points to a VCV which fuses with another, the yellow arrow to a VCV from which a smaller VCV is segregating (blue arrow). Distance between the ticks in the grid corresponds to 1 μm .

In figure 55, a part of the PM area is represented. VCVs of different sizes were found near the cell surface and tethering the PM recapitulating the observations made by TEM analysis (Fig. 44-47). Moreover, these VCVs were seen to move along the cell surface and to disappear, such a VCV is indicated by the yellow arrow. At time point 0 sec, the VCV is seen as a big vesicle which fuses at time point 9 min with a smaller VCV (indicated by the white arrow). The VCV starts to segregate at time point 13 min into 2 distinct vesicles as clearly shown at time point 15 min (the new segregated vesicles are indicated by the blue and pink arrows). At time points 16 min 30 sec and

18 min 30 sec, the VCV indicated by the pink arrow moves towards the PM and disappears at time point 22 min. This later event could presumably represent the exocytic event. The tentative fusion event was fast, below the time resolution of the microscope used. It is unlikely that the disappearance of VCVs was caused by bleaching since weaker intensities VCVs in the vicinity remained bright and many of these VCVs were observed until the end of the records.

Taken together, life cell imaging confirmed and extended the following findings already suggested by TEM analysis: (i) VCVs were located near the cell surface (for correlation see Fig. 47), (ii) they tether the PM (correlative Fig. 46), (iii) and presumably fuse with it (correlation is shown in Fig. 49). Moreover, life cell imaging shows the movement of VCVs towards and along the PM and their dynamics seen as fusion and fission near the cell surface (for correlation see Fig. 44).

III.2.2.4. Secretion kinetics of DHBV in PDH cultures

The secretion kinetics of viruses can give hints about their release mechanism. Thus, the release kinetics of single viral particles is different from that of bulk liberation of viruses. To characterize the kinetics of DHBV release, cell-culture supernatants of congenitally DHBV-infected PDHs were collected every hour in triplicates and the amount of virions was determined by DNA-dot blot analysis. Serial dilutions of a DHBV-viremic serum with known genome equivalents (GE) were included for quantification purposes. Aliquots of the samples were also analysed by L-immunoblot.

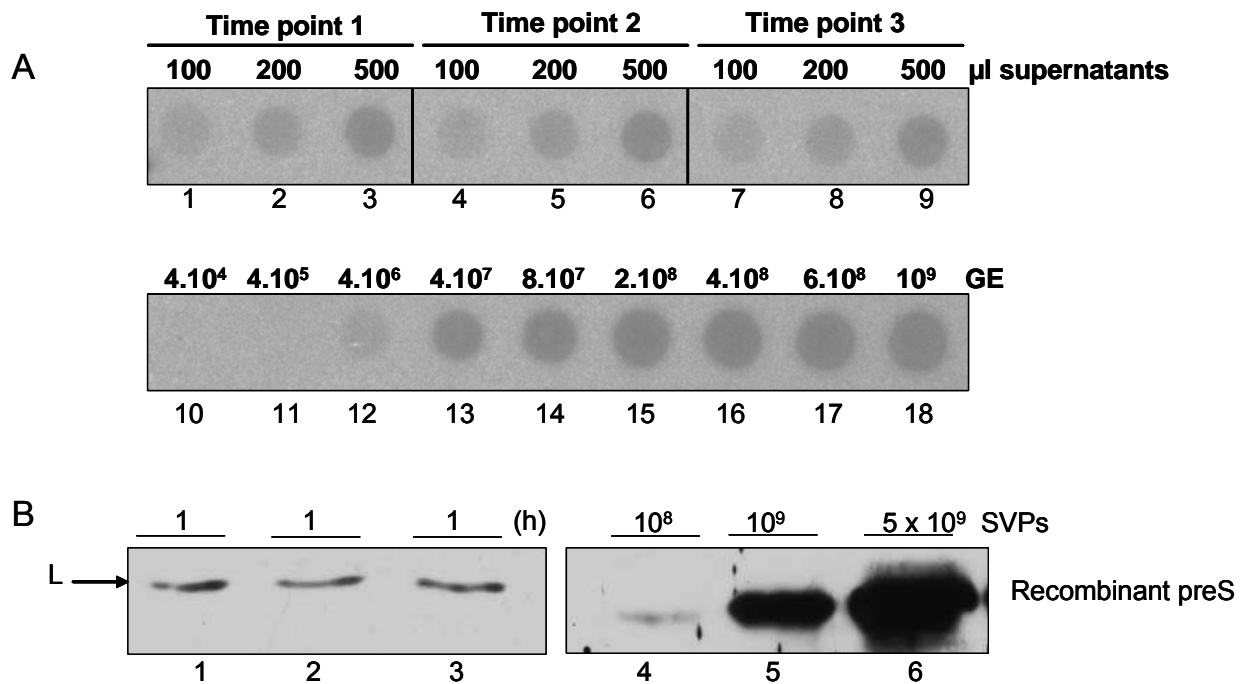


Fig. 56. About 40-80 virions and 46,000 SVPs are secreted per hepatocyte and per hour. (A) Supernatants of congenitally DHBV-infected PDHs were harvested every 1 h for 3 times, and subjected to DNA-dot blot analysis for quantification of virions. 100, 200, and 500 μl of the supernatants were loaded, in addition, serial dilutions with known GE were included. (B) For quantification of SVPs, supernatants were analysed for the surface protein L by immunoblot analysis. Dilutions of recombinant preS were included as standards. The signals were acquired with a Bioluminescence Imager and quantified.

The dot blot membrane was probed with a radioactively labelled DHBV DNA and the signals were analysed by phosphorimaging (Fig. 55A). The standards included revealed a sensitivity of 4×10^6 genome equivalents (GE) and linearity between 4×10^6 and 2×10^8 GE. Based on these standards, the quantification revealed that an average of 40-80 virions were secreted per hour and per hepatocyte.

There are no published data concerning the amounts of secreted SVPs. In order to determine the average number of secreted SVPs and its ratio to virions, aliquots of the supernatants used above were subjected to semi-quantitative immunoblot analysis for L protein. Serial dilutions of a recombinant duck preS proteins used as standards revealed a sensitivity of about 10^8 SVPs and linearity between 10^8 and 10^{10} SVPs. Based on this standardisation quantification of the signals obtained revealed that about 46,000 SVPs were secreted per hepatocyte and per hour (Fig. 55B). These results indicate that the ratio between DHBV virions and SVPs in

supernatants of PDHs cultures was about 1 to 1000, respectively. These are the first quantitative data showing the secretion kinetic and the ratio between both viral particle entities.

These results imply that the secretion of DHBV is likely to occur in bulk rather than as single particles. Since a huge number of viral particles (about 7600) was liberated per minute, it is more likely that this presumably occur via quantal exocytosis. This secretion kinetics is compatible with the exocytic mechanism suggested by figure 36 showing that many viruses are liberated at once from the VCVs.

III.3. Cellular requirements, intracellular transport, and secretion of DHBV

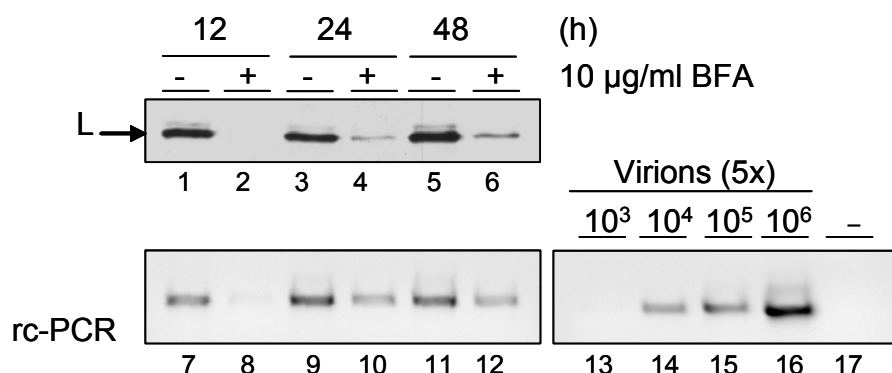
The cellular requirements and the pathway exploited by hepatitis B viruses to exit the host cell are largely unknown. In order to get insights into these final steps of the viral morphogenesis, pharmacological interference studies were performed.

III.3.1. BFA strongly inhibits viral secretion

To investigate whether the Golgi and TGN are involved in the transport of preformed viral particles to the cell surface, substances known to interfere with intracellular transport along the secretory pathway were used.

Brefeldin A (BFA), a fungal lactone, has multiple effects on the organelles of the secretory pathway such as inhibition of protein trafficking between ER and Golgi, tubulation of the Golgi and its redistribution to the ER resulting in the disappearance of the Golgi. Moreover, BFA is also known to exhibit different effects on intracellular membrane fusion events and interferes with endosomal transport and sorting processes (105, 134, 135).

Congenitally DHBV-infected PDHs were treated with 10 $\mu\text{g/ml}$ BFA for 12, 24, and 48 h. Thereafter, supernatants and cells were harvested and subjected to immunoblot and PCR analysis for viral L protein and DNA, respectively.



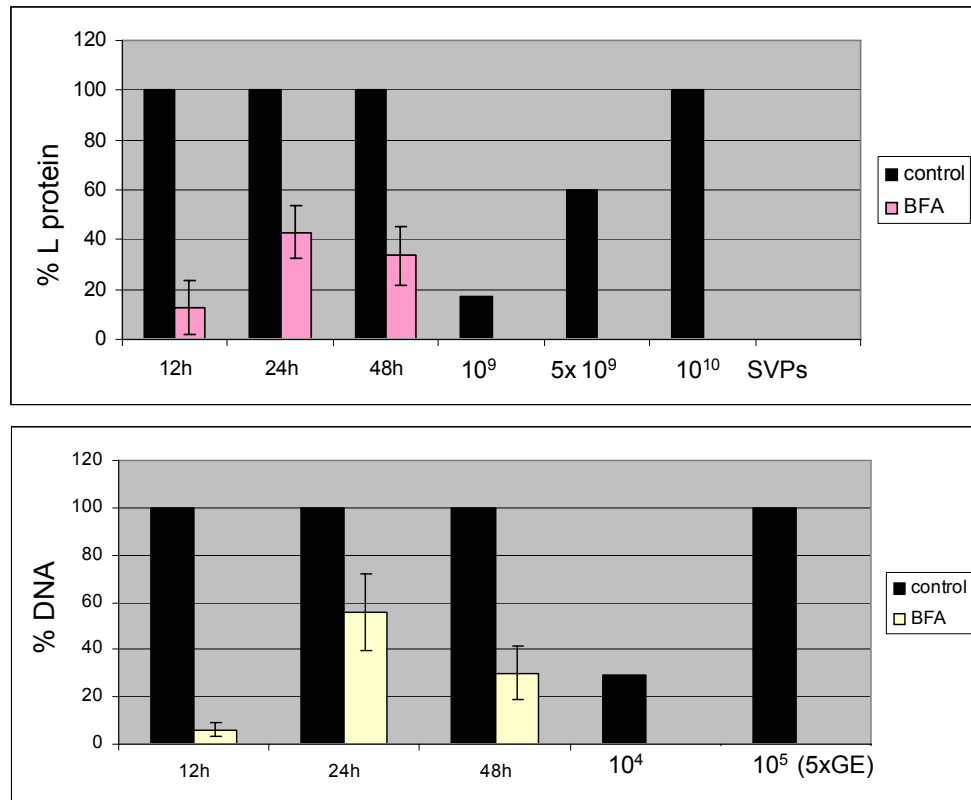


Fig. 57. BFA strongly inhibits the secretion of both SVPs and virions. Congenitally DHBV-infected PDHs were treated with 10 μ g/ml BFA for different time periods (12, 24, and 48 h). Supernatants were harvested and subjected to immunoblot and PCR analysis for detection of viral surface protein L and rcDNA, respectively. Signals were acquired by bioimaging and the quantification was performed from 3 independent experiments. Bars show the standard deviation.

BFA treatment of DHBV-infected PDHs up to 48 h strongly inhibits the secretion of both SVPs and virions as shown in figure 57 by the immunoblot and PCR analysis of cell culture supernatants, respectively. The strongest effect was seen after 12 h treatment (compare lane 1 with 2 and 7 with 8), the secretion of both SVPs and virions was strongly, if not completely inhibited. The quantification of the L and DNA signals from the semi-quantitative L-immunoblot and PCR for viral DNA revealed a reduction of more than 95% in signal intensity for both. This reduction reflects a more than 50-fold and 30-fold decrease in the amounts of virions and SVPs, respectively, based on the comparison with the included standards. The reduction factor varied slightly between experiments, but was always more than 90% in signal intensity as shown by the quantification of 3 independent experiments (Fig. 57, graph).

At time point 24 h post treatment, the inhibitory effect of BFA was less pronounced compared to time point 12 h (compare lanes 3 with 4 and 9 with 10) indicating that

the BFA effect was partially reversible presumably due to a metabolic inactivation of the drug during the experimental incubation period. Nevertheless, at this time point, an inhibitory effect of about 50% in signal intensity was still observed corresponding to a 5-fold reduction in the amount of secreted SVPs and virions. When cells were then treated again with BFA, and supernatants were harvested 24 h later (total treatment period 48 h), the extent of the block for of both viral particles was comparable to that of time point 24 h (compare lines 5 with 6 and 11 with 12). These results indicate that BFA drastically inhibits the secretion of both SVPs and virions.

To exclude a possible cytotoxic effect of BFA on cells during these long treatments, a viability test using trypan blue and FDA was performed. This test showed no signs of cytotoxicity between BFA-treated and control cells (Fig. 58).

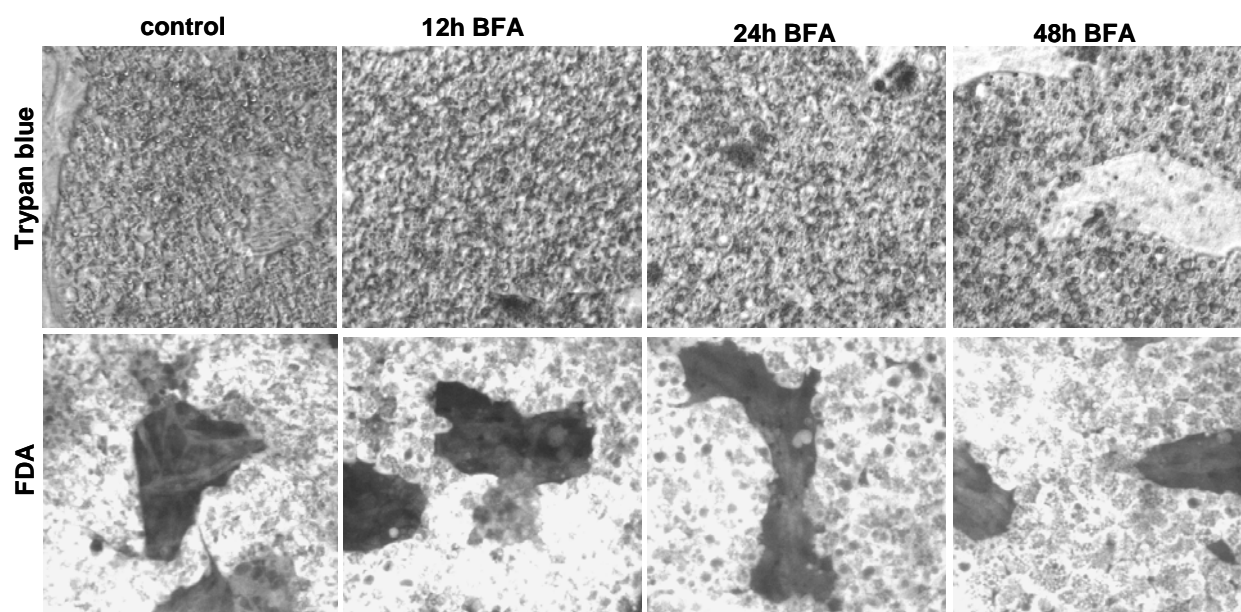


Fig. 58. Treatment of BFA for 12, 24, and 48 h showed no cytotoxic effects. Congenitally DHBV-infected PDHs were treated with 10 $\mu\text{g/ml}$ BFA for the indicated time periods. Subsequently, a cytotoxicity test was performed using trypan blue and FDA. Trypan blue stains only dead cells, while FDA stains only living hepatocytes within the culture.

To show that the BFA effect is reversible and cells recover from a 12 h treatment, I performed a washout assay. DHBV-infected PDHs were treated with 10 $\mu\text{g/ml}$ BFA for 12 h, the next day supernatants were harvested (corresponding to time point 0 h washout) and cells were washed twice with PBS. Fresh medium was added and cells were further incubated at 37°C for the indicated time periods. Supernatants were

harvested and analysed for viral particles by immunoblotting for L protein and PCR for viral DNA.

The strong inhibitory effect of BFA on virus secretion starts to become reversible at 5 h after removal of the substance (compare time points 0 and 5 h washout), was re-established to about 80% of the controls 8 h after washout and was completely reversible at 24 h washout. At this time point, the secretion was even enhanced by about 20% compared to the control cultures (Fig. 59). This washout kinetic indicates that (i) BFA was not toxic, (ii) the strong inhibitory effect was reversible, and (iii) the secretion of viral particles gradually returned to the control levels. These findings were unexpected since removal of the substance results in rapid structural and functional reestablishment of the Golgi (104).

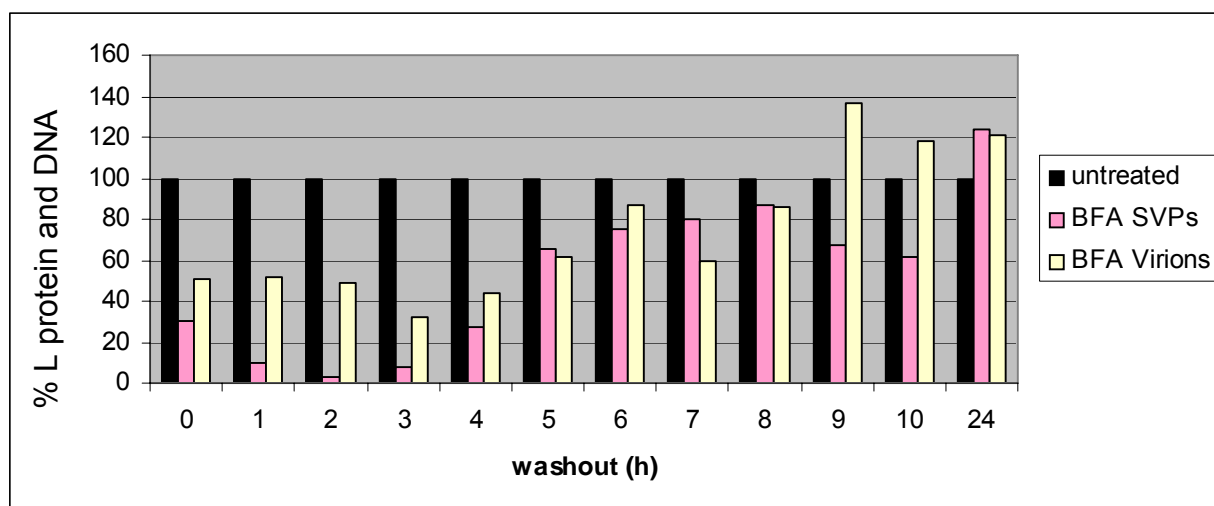


Fig. 59. The secretion block induced by BFA is reversible. Congenitally DHBV-infected PDHs were treated with 10 μ g/ml BFA over night. Next day, cells were washed twice with PBS and fresh medium was added. Supernatants were collected at the indicated time points and analysed for L and viral DNA. The signals were quantified in a bioimager.

The observed prolonged secretion block could have many reasons: (i) BFA could inhibit viral protein synthesis and consequently less viral particles are secreted; (ii) it could interfere with virus assembly and/or a budding step; (iii) BFA could interfere with the transport of VCVs to the PM; and (iv) BFA could inhibit the fusion of VCVs with the PM. In order to discriminate between these different possibilities, the intracellular levels of viral proteins as well as viral DNA were investigated in the corresponding cell lysates from the aforementioned experiment.

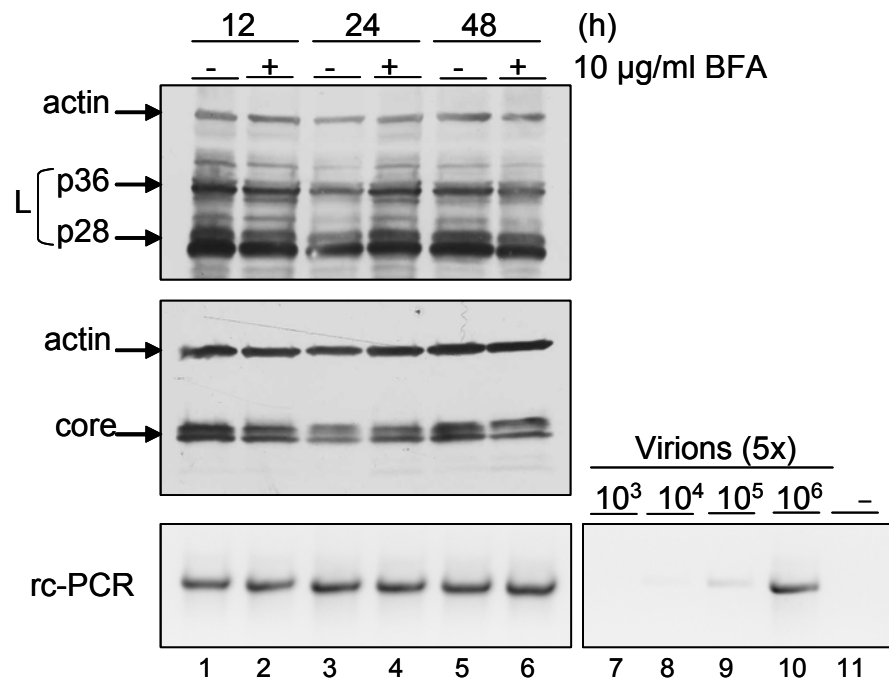


Fig. 60. Intracellular L, core, and rcDNA were not affected by BFA treatment. Cells from the previously shown experiment were harvested in SDS-loading buffer or PCR lysis buffer for immunoblot and PCR analysis, respectively. Prior to PCR, cell lysates were digested with proteinase K.

The intracellular levels of viral protein L and core as well as viral rcDNA were comparable between BFA treated and non-treated cells (Fig. 60, compare the lanes – and + at each time point) indicating that the viral protein biosynthesis was not affected by BFA treatment and thereby could not account for the strong inhibitory effect of BFA on viral secretion.

To investigate whether BFA affects the assembly and budding steps, congenitally DHBV-infected PDHs were treated with 10 µg/ml BFA for 24 h and subjected to TEM. The ultrastructural analysis revealed large membranes sacs full of viral particles located near the nucleus and the periphery of the cells (Fig. 61, red arrows). Remarkable was the large size of these vesicles and the absence of the typical small and intermediate sized VCVs as compared to the non-treated cells (section 1 and 2).

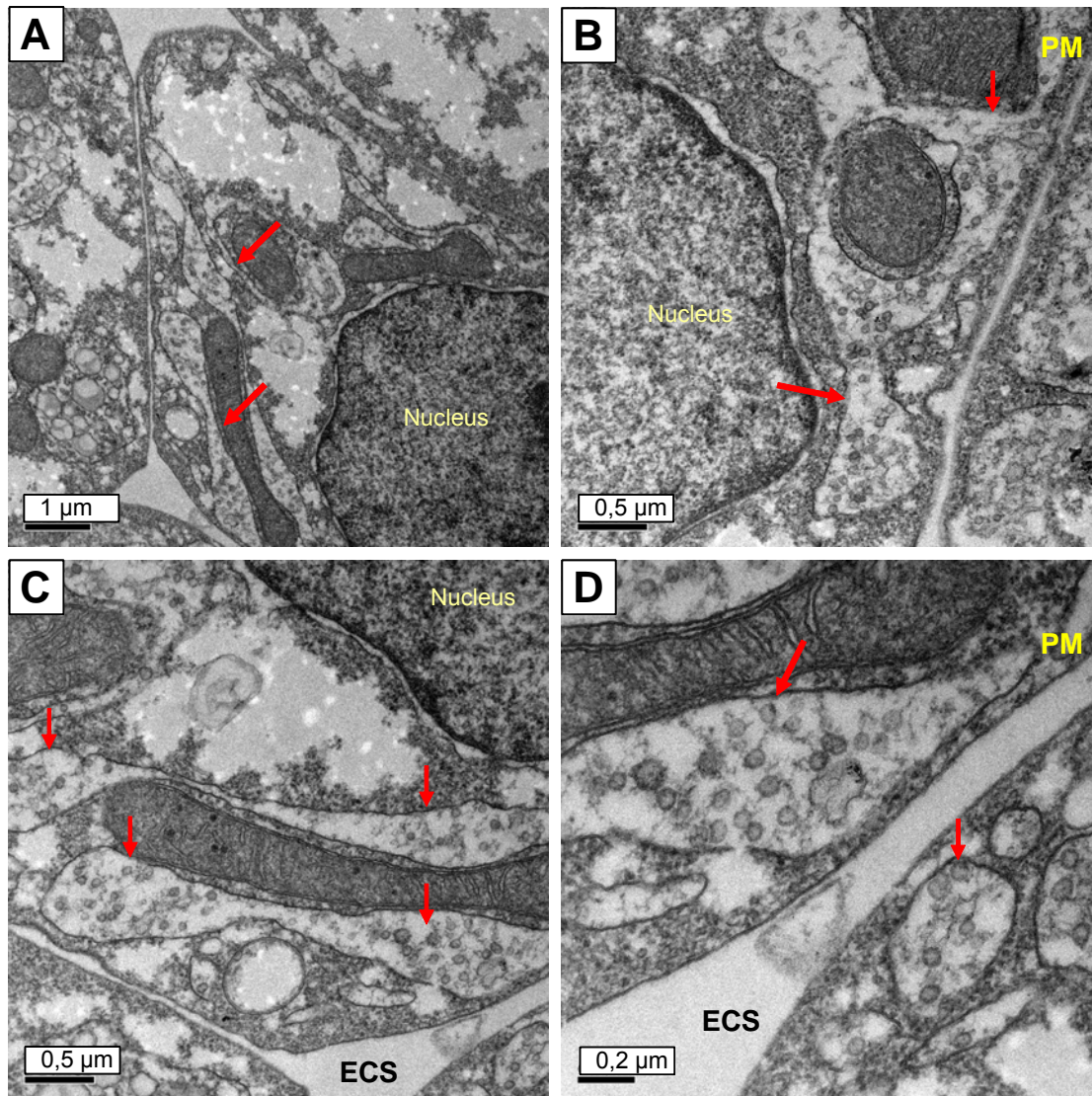


Fig. 61. BFA treatment leads to the formation of large VCVs. Congenitally DHBV-infected PDHs were treated with 10 µg/ml BFA for 24 h and analysed by TEM. A-D show large membrane sacs (red arrows) full with viral particles. Bars indicate the size.

These findings clearly show that intracellular viral particles were easily detectable and thus the secretion block could not be explained. However, it seems that BFA leads to the disappearance of the typical small and intermediated sized VCVs (100-800 nm) in favour of few but large membrane sacs (1-4 µm in diameter). These big VCVs were presumably the result of homotypic fusions induced by BFA, which is known to induce such effects, or to the non-segregation of small VCVs as previously shown by TEM (Fig. 30) and live cell imaging (Fig. 35).

To test whether the formation of such big membrane vesicles is a general effect of BFA on cellular endomembranes or whether it is specific for VCVs, non-infected PDHs treated for 24 h with BFA in parallel to the infected cells were analysed by TEM.

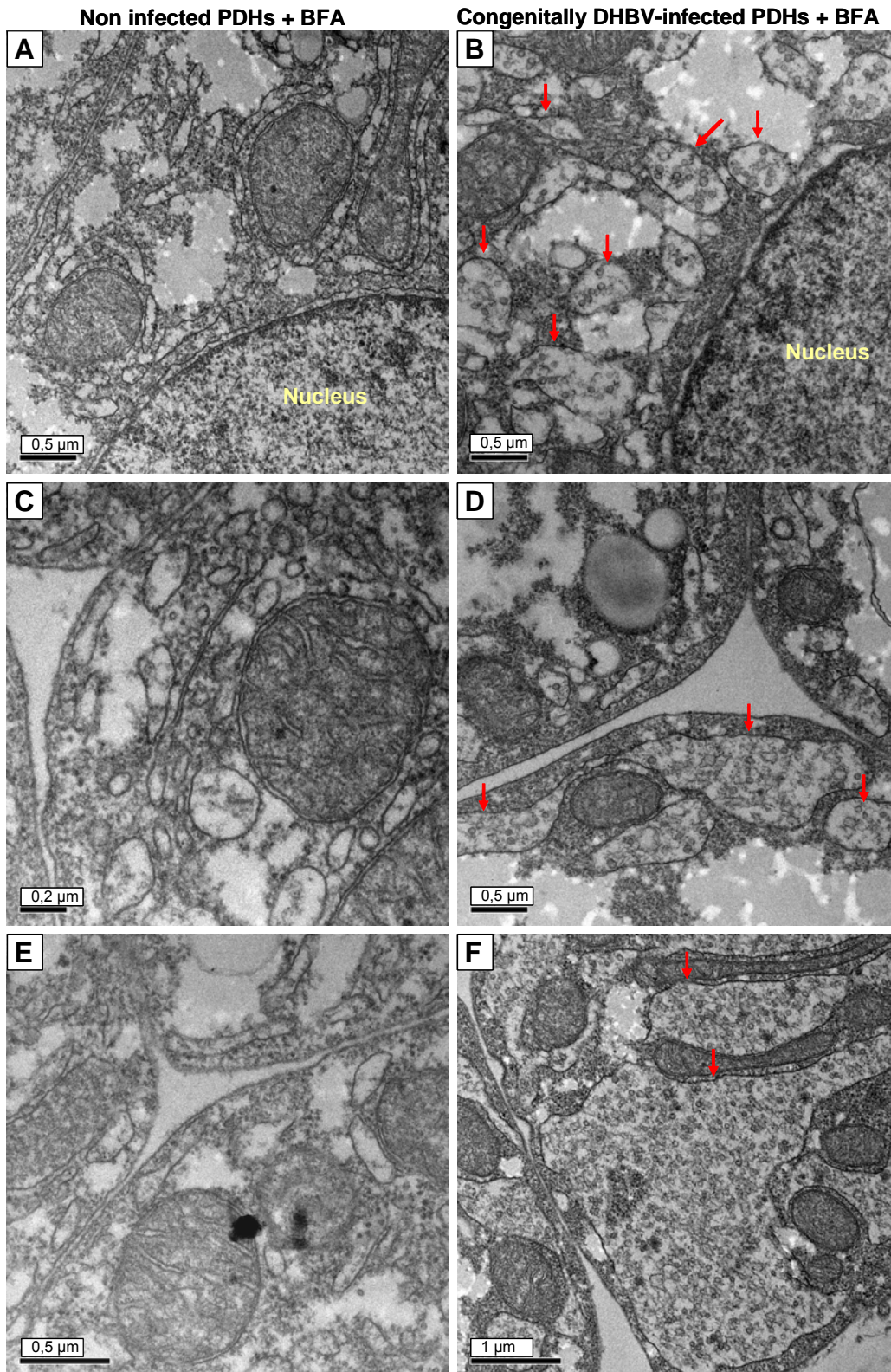


Fig. 62. BFA induces the formation of large membrane sacs only in DHBV-infected but not in non-infected cells. A, C, and E are sections from non-infected PDHs, B, D, and F section from congenitally DHBV-infected PDHs both treated with 10 µg/ml BFA for 24 h.

Under BFA treatment, non-infected cells showed neither large membrane sacs near the nucleus nor large vesicles located near the PM (Fig. 62A, C, and E). Only DHBV-infected cells showed immense membrane structures containing viral particles (Fig. 62B, D, and F). This indicates that the formation of large membrane vesicles was a specific feature of infected cells. These large VCVs are presumably formed by the fusion of the small and intermediate sized VCVs leading to large ones or alternatively, they are the result of the non-segregation of VCVs from their donor membranes. However, it is clear that the observed BFA effect is not due to a general effect on cellular membranes since this happens only in DHBV-infected, but not in the non-infected cells.

Since the strong secretion block of progeny viruses by BFA was neither the result of inhibition of viral protein synthesis nor assembly and budding, an alternative explanation would be that the intracellular transport of VCVs to the PM is altered and thus the secretion is inhibited. To test this possibility, the PM of DHBV-infected cells was screened for the presence of VCVs in the proximity of cell surface.

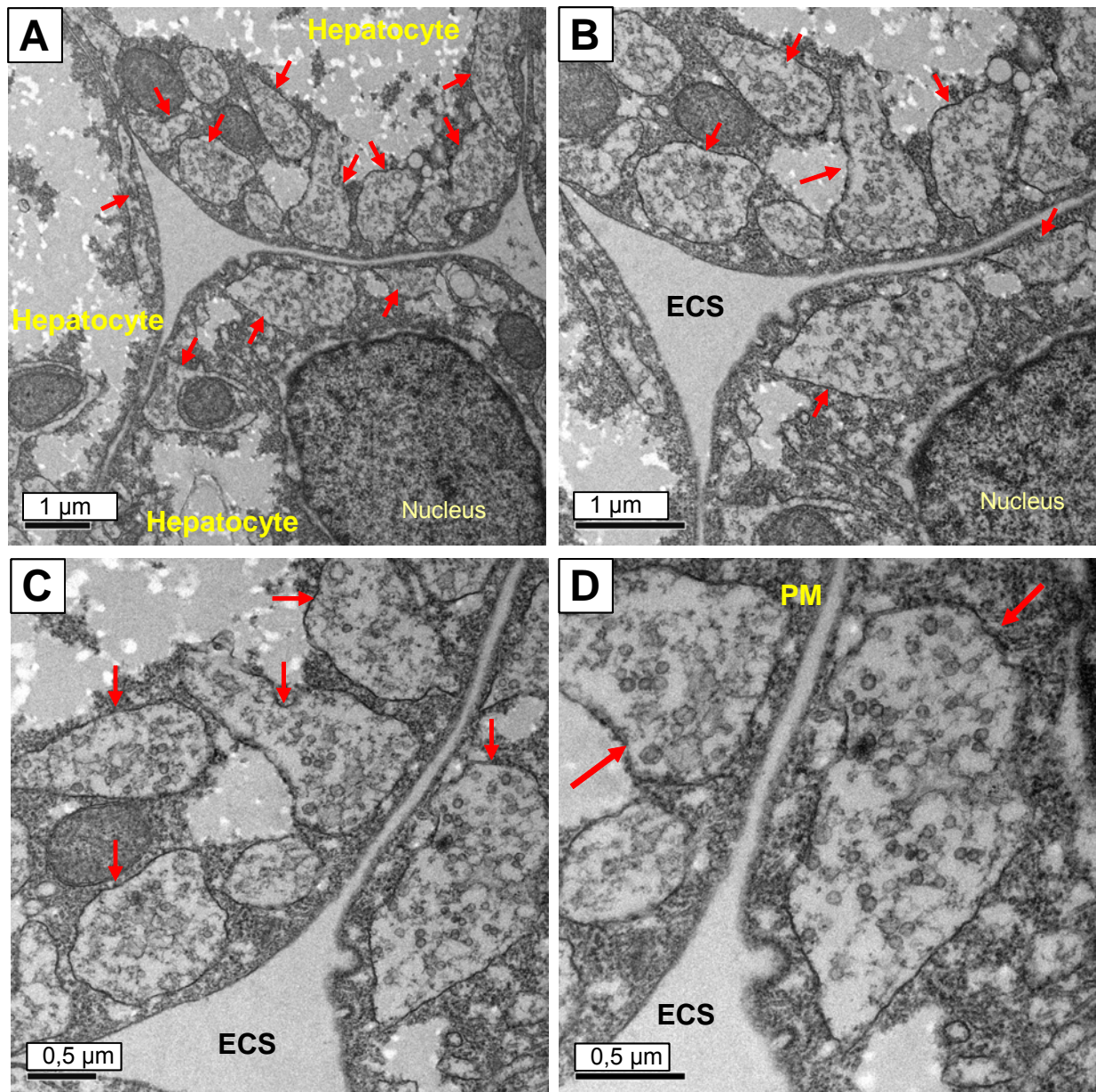


Fig. 63. BFA leads to the accumulation of large VCVs beneath the PM. A and B show sections of 3 hepatocytes with large VCVs (red arrows) located near the PM. C and D are magnifications of the areas. ECS, extracellular space. Bars indicate the size.

As shown in figure 63, large VCVs (red arrows) reaching more than 2 μm in diameter were located near the PM indicating that the anterograde transport of these vesicles was not affected by BFA. Thus the hypothesis that BFA affects the intracellular transport of VCVs to the PM was rejected. Beside the concentration of large numbers of huge vesicles beneath the cell surface, none of these VCVs was observed in close contact with the PM suggesting that BFA somehow inhibits either the tethering of VCVs to the PM or their fusion with the cell surface.

The disappearance of the envelope protein L from the PM upon BFA treatment as already shown in figure 51 is in favour of this hypothesis. Upon BFA treatment (Fig. 64, panels B and D), the cell contour of L-stained cells was no longer recognisable compared to the untreated cells (panel A and C). This indicates that the transfer of L proteins during the fusion of VCVs with the PM was inhibited.

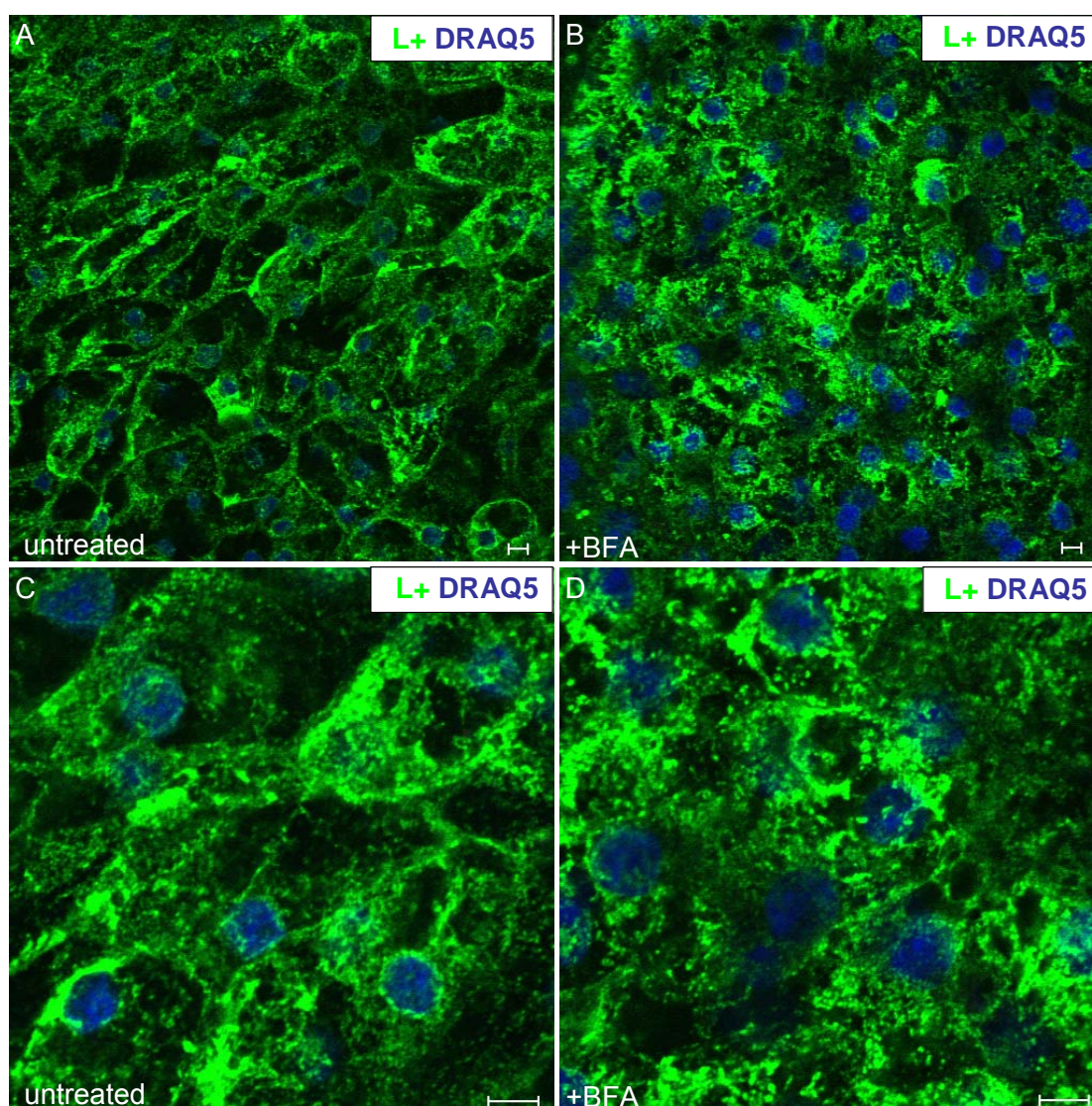


Fig. 64. L protein disappears from the PM upon BFA treatment. CLSM images of congenitally DHBV-infected PDHs treated (A and C) or not (B and D) with 10 $\mu\text{g/ml}$ BFA for 24 h and fixed for 10 min with ice-cold methanol/acetone (1:1). Subsequently, cells were stained for the envelope protein L (green signals), nuclei were counterstained with DRAQ5 (blue signals). Bars correspond to 5 μm .

To better visualize the presence or absence of L protein at the PM, z-stacks from the L-stained cells were performed and represented as 3D projections.

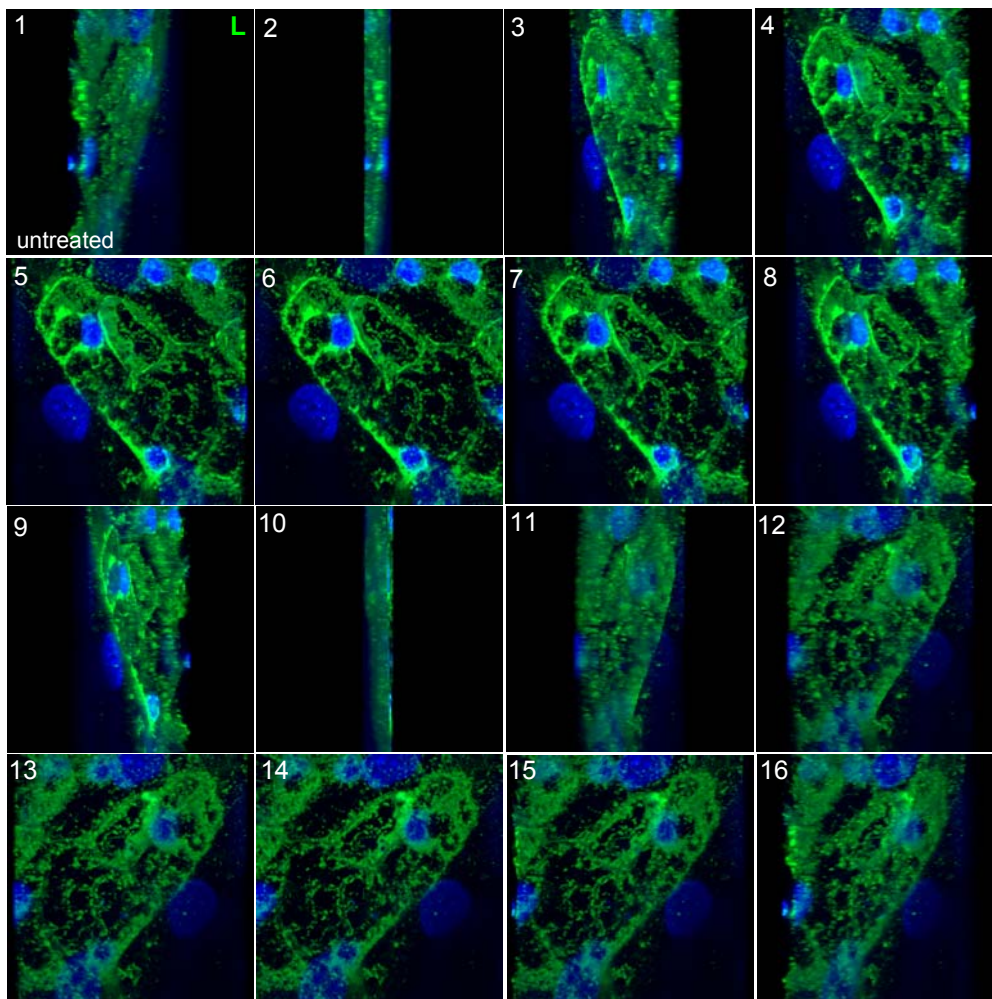


Fig. 65. L protein is associated with the PM. Z-stacks of CLSM images from congenitally DHBV-infected PDHs stained for L (green signals) were performed. Subsequently, the z-stacks were projected and represented as a series. Nuclei were counterstained with DRAQ5 (blue signals).

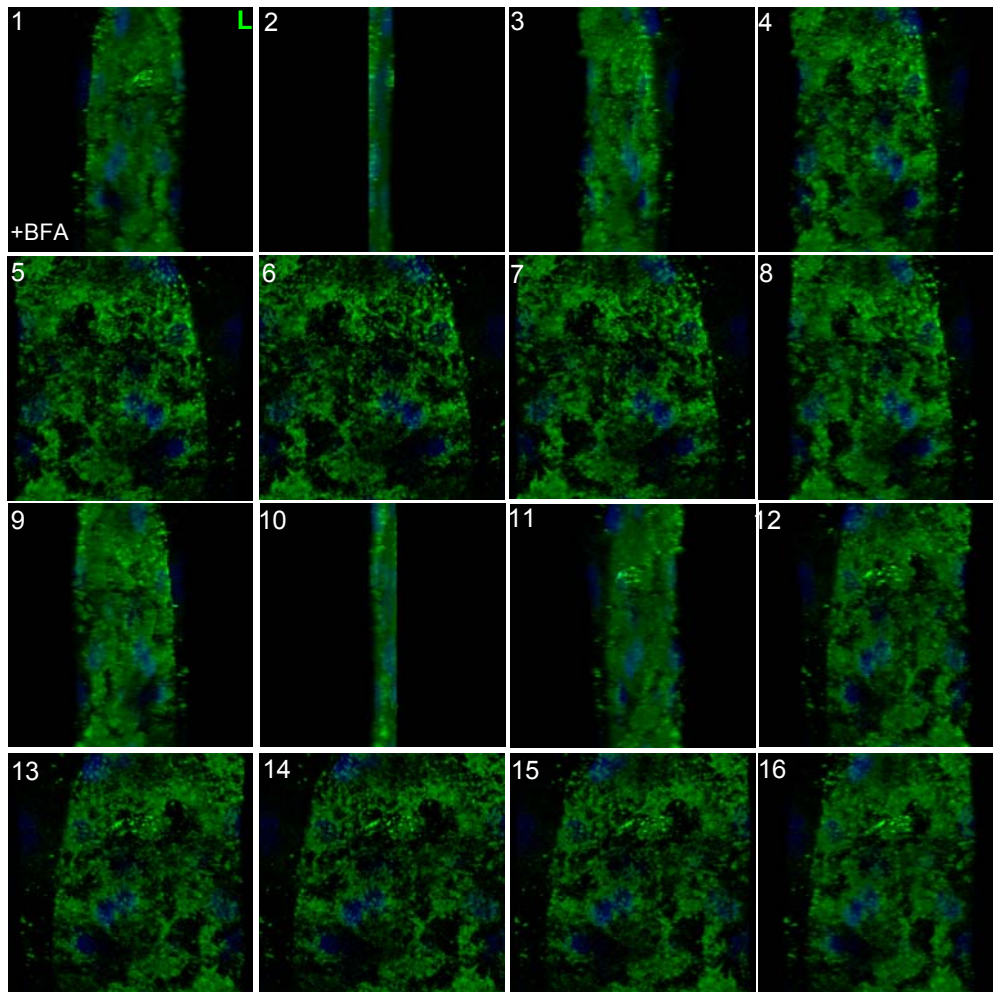


Fig. 66. PM-association of L is inhibited by BFA. Z-stacks of CLSM images from congenitally DHBV-infected PDHs treated with 10 $\mu\text{g/ml}$ BFA for 24 h and stained for L (green signals) were performed. Subsequently, the z-stacks were projected and represented as series. Nuclei were counterstained with DRAQ5 (blue signals).

The 3D projections of untreated cells (Fig. 65) clearly show the PM-association of the envelope protein L since the contour of single hepatocytes as well as the entire hepatocyte-island was easily recognisable. In BFA treated cells, these contours were no longer visible (Fig. 66). These findings clearly show that the L-associated PM staining was lost upon BFA treatment. Thus BFA inhibits the transfer of L proteins to the cell surface by preventing the fusion of VCVs with the PM.

Taken together, BFA strongly inhibits viral secretion by interfering with the fusion of VCVs with the PM, leading to the accumulation of viral particles within large membranes compartments.

III.3.2. Role of the cytoskeleton in DHBV transport and secretion

To be secreted, viruses must be transported from their assembly and budding sites to the cell surface where they are liberated. For this transport, they are dependent on the host cytoskeleton. For DHBV, it is not known whether and if yes which cytoskeletal elements are required.

Microtubules are required for DHBV secretion

To test whether microtubules (MTs) are required for the intracellular transport and thus the secretion of DHBV, congenitally DHBV-infected PDHs were treated with 2 substances known to interfere with the function of MTs. Nocodazole (Noco) depolymerises the MTs while Paclitaxel stabilizes them by inhibiting their dynamic turn over.

To show that the substances used were active, PDHs were treated or not over night with Noco, fixed, and stained for α -tubulin. As shown in figure 66, the MTs were efficiently depolymerised by Noco in comparison to the mock-treated cells.

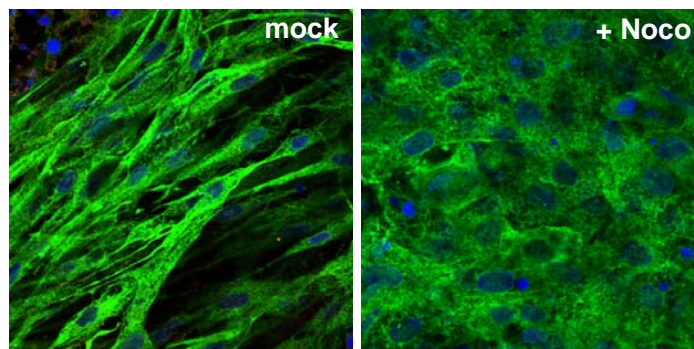


Fig. 67. MTs are efficiently depolymerised by Nocodazole treatment. Congenitally DHBV-infected PDHs were mock- or Nocodazole-treated over night. Next day, cells were fixed with 3.7% paraformaldehyde and immunostained for α -tubulin to visualize the MTs (green signals). Nuclei were counterstained with DRAQ5 (blue signals).

Next, the cytotoxicity of these substances was tested by trypan blue and FDA staining. The used concentrations as well as the duration of the treatments were not toxic for the PDHs as shown in figure 68.

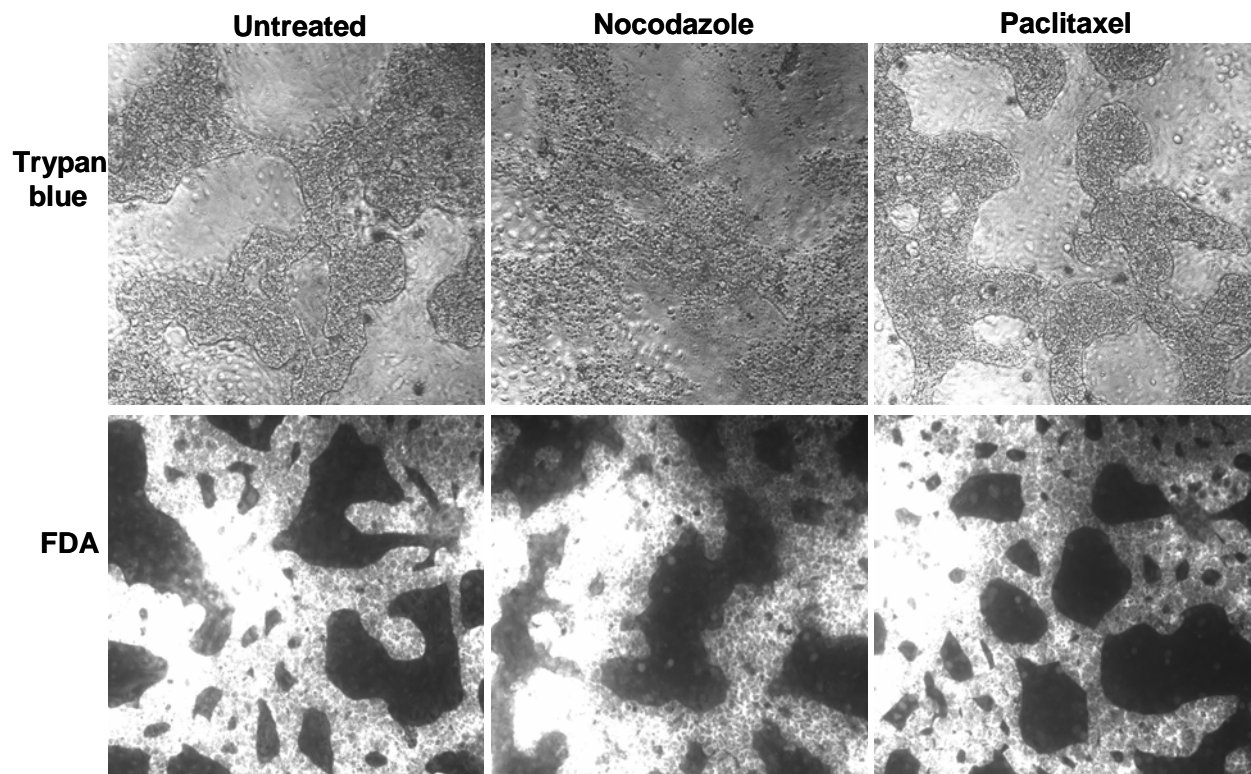


Fig. 68. Nocodazole and Paclitaxel have no cytotoxic effects on PDHs. Congenitally DHBV-infected PDHs were treated over night with Nocodazole or Paclitaxel. Subsequently, the viability test with trypan blue and FDA was performed.

Under the same experimental conditions as described above, DHBV-infected PDHs were treated either with Nocodazole or with Paclitaxel over night. Mock-treated cells were included as a control. Next day, supernatants were harvested and subjected to immunoblot and PCR analysis for viral envelope protein L and DNA, respectively. In figure 69, a representative immunoblot and PCR with the quantifications of the signals from 3 independent experiments are shown. The results show that Nocodazole treatment inhibits the secretion of both SVPs and virions by about 54 and 70%, respectively, while Paclitaxel has nearly no effects on the amount of secreted SVPs (only 10% reduction) and only a moderate effect (40% reduction) on the secretion of virions.

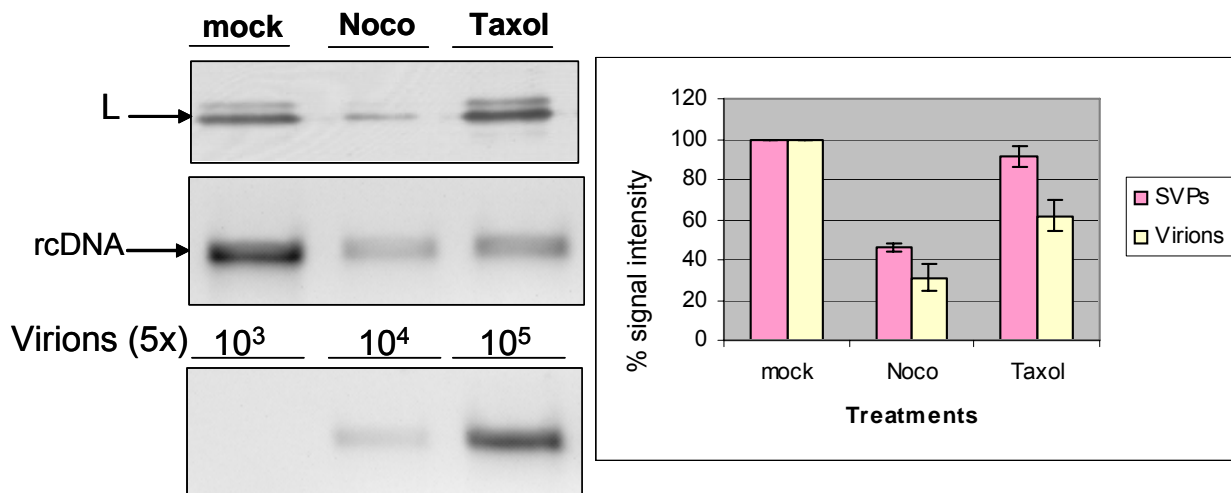


Fig. 69. Intact but not dynamic MTs facilitate DHBV secretion. Congenitally DHBV-infected PDHs were treated over night either with Nocodazole (Noco) or with Paclitaxel. Mock-treated cells were included as controls. Next day, supernatants were harvested and subjected to immunoblot and PCR analysis for viral L protein and rcDNA, respectively. L and DNA signals were quantified using a bioimager. The shown quantifications were from 3 independent experiments. Bars indicate the standard deviations.

These results indicate that intact but not dynamic MTs are required for efficient viral secretion. They are not completely indispensable, since viral secretion was only partially abrogated in cells with depolymerised MTs.

The inhibitory effect of Nocodazole persisted until 24 h after removal of the substance and was completely reversible at 48 h after washout (Fig. 70).

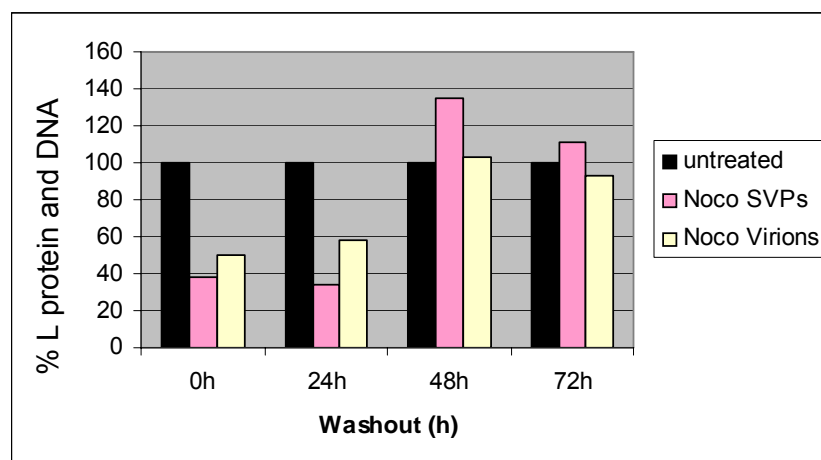


Fig. 70. The inhibitory effect of Nocodazole is reversible 48 h after washout. Congenitally DHBV-infected PDHs were treated over night with Nocodazole. Untreated cells were included as controls.

Next day, cell culture supernatants were harvested (corresponding to time point 0 h washout) and cells were washed twice with PBS. Fresh medium was added to the cells and supernatants were harvest at the indicated time points (24, 48, and 72 h after washout). Immunoblot and PCR analysis were performed and the signals were quantified by bioimaging.

The pharmacological data showing the dependence of DHBV secretion on MTs together with ultrastructural analysis showing the localization of VCVs next to MTs (Fig. 71) strongly suggest the involvement of the MT cytoskeleton in virus secretion.

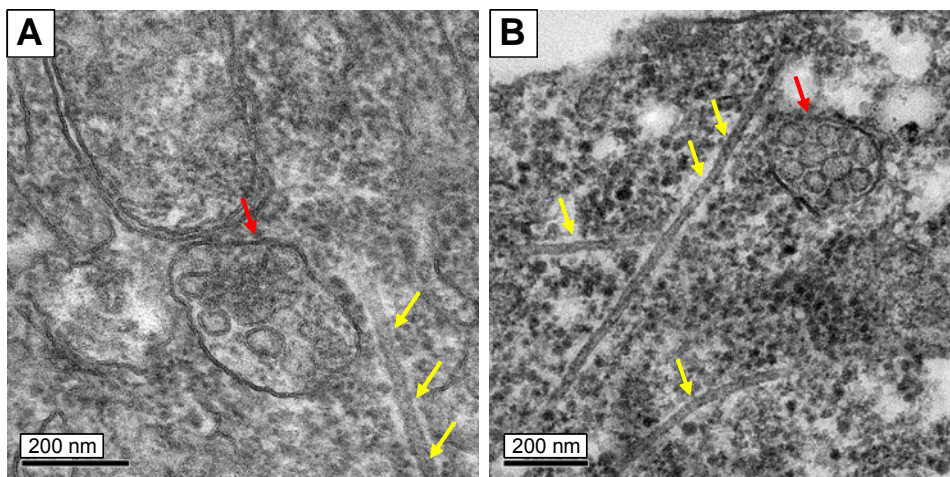


Fig. 71. VCVs were found in close proximity to microtubules as seen by TEM. A and B show VCVs (arrows) located near MTs (arrows). The bars indicate the size.

Actin filaments are not required for DHBV secretion

To test whether actin filaments are involved in DHBV transport and secretion, congenitally DHBV-infected PDHs were treated over night with the actin depolymerising agent Cytochalasin D, mock treated cells were included as controls. To control the activity of the drug, the cells were stained with phalloidin-TRITC to visualize the actin filaments.

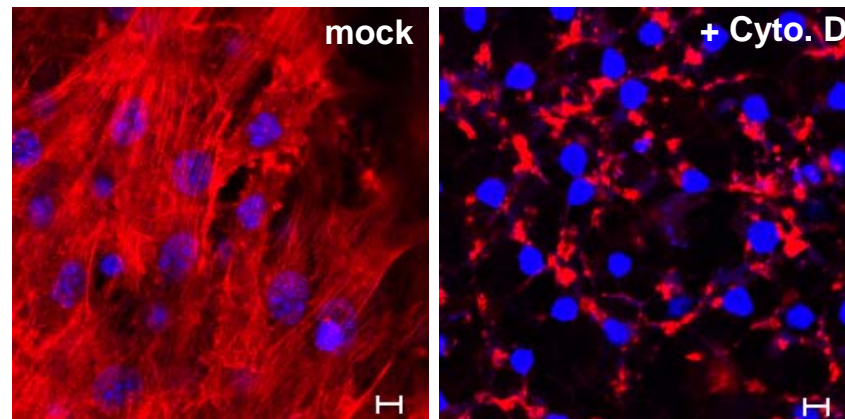


Fig. 72. Actin filaments are efficiently depolymerised by Cytochalasin D. Congenitally DHBV-infected PDHs were treated over night with Cytochalasin D (Cyto D). Non-treated cells were included as a control. Next day, cells were fixed with 3.7% paraformaldehyde and actin was visualized by phalloidin-TRITC. Nuclei were counterstained with DRAQ5 (blue signals). Bars correspond to 5 μ m.

Non-treated cells showed typical actin filaments while in treated ones only small fragments were seen indicating an efficient depolymerization by Cytochalasin D (Fig. 72). Then the cytotoxicity of the substance was tested by trypan blue and FDA stain which showed a similar viability of treated and non-treated cells (Fig. 73)

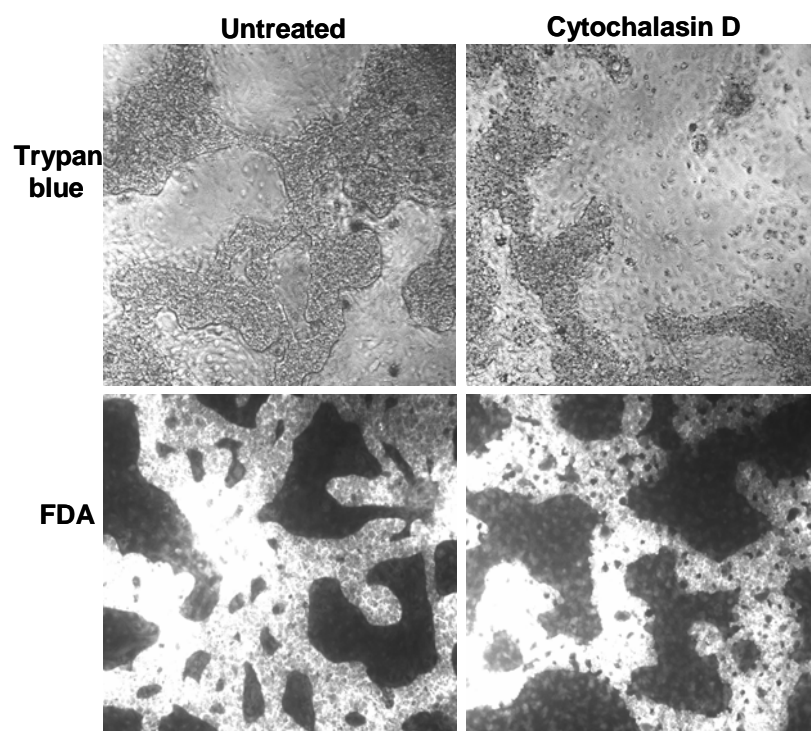


Fig. 73. Cytochalasin D is not toxic for PDHs. To test whether Cytochalasin D was toxic on PDHs, cells were treated or not over night with Cytochalasin D. Next day, a viability test with trypan blue and FDA was performed.

After showing that Cytochalasin D efficiently depolymerizes actin filaments without overt cytotoxic effects, the effect of this treatment on viral secretion was analysed. Treatment of congenitally-DHBV infected PDHs with Cytochalasin D over night did not inhibit viral secretion, in contrast the secretion of both SVPs and virions was slightly enhanced (Fig. 74).

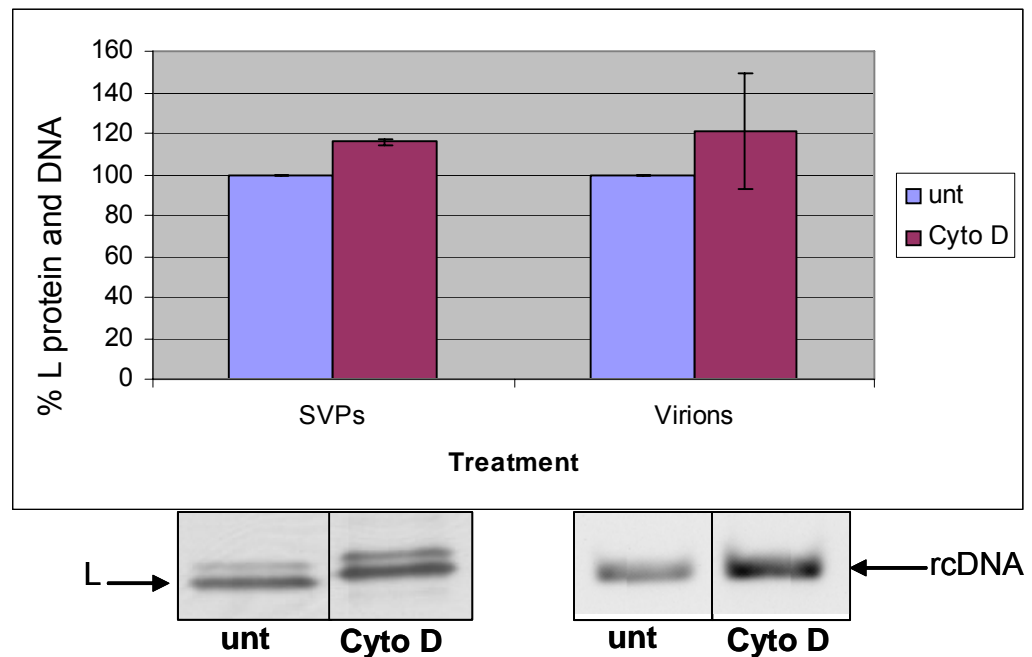


Fig. 74. Depolymerization of actin filaments by Cytochalasin D facilitates viral secretion. Congenitally DHBV-infected PDHs were treated over night with Cytochalasin D. As controls non-treated cells were included. Next day, supernatants were collected and analysed by immunoblotting and PCR for the detection of viral surface protein L and rcDNA, respectively. The signals were quantified by bioimaging. The graph represents 3 independent experiments. Bars indicate the standards deviations.

The fact that viral secretion was promoted after depolymerisation of actin filaments indicates that the filaments form a physical obstacle that normally poses a barrier for intracellular transport or secretion of DHBV. To investigate whether this is really true, the localization of VCVs in respect to the actin cytoskeleton in DHBV-infected PDHs was analysed by CLSM. Z-stacks were acquired and are shown in figure 75.

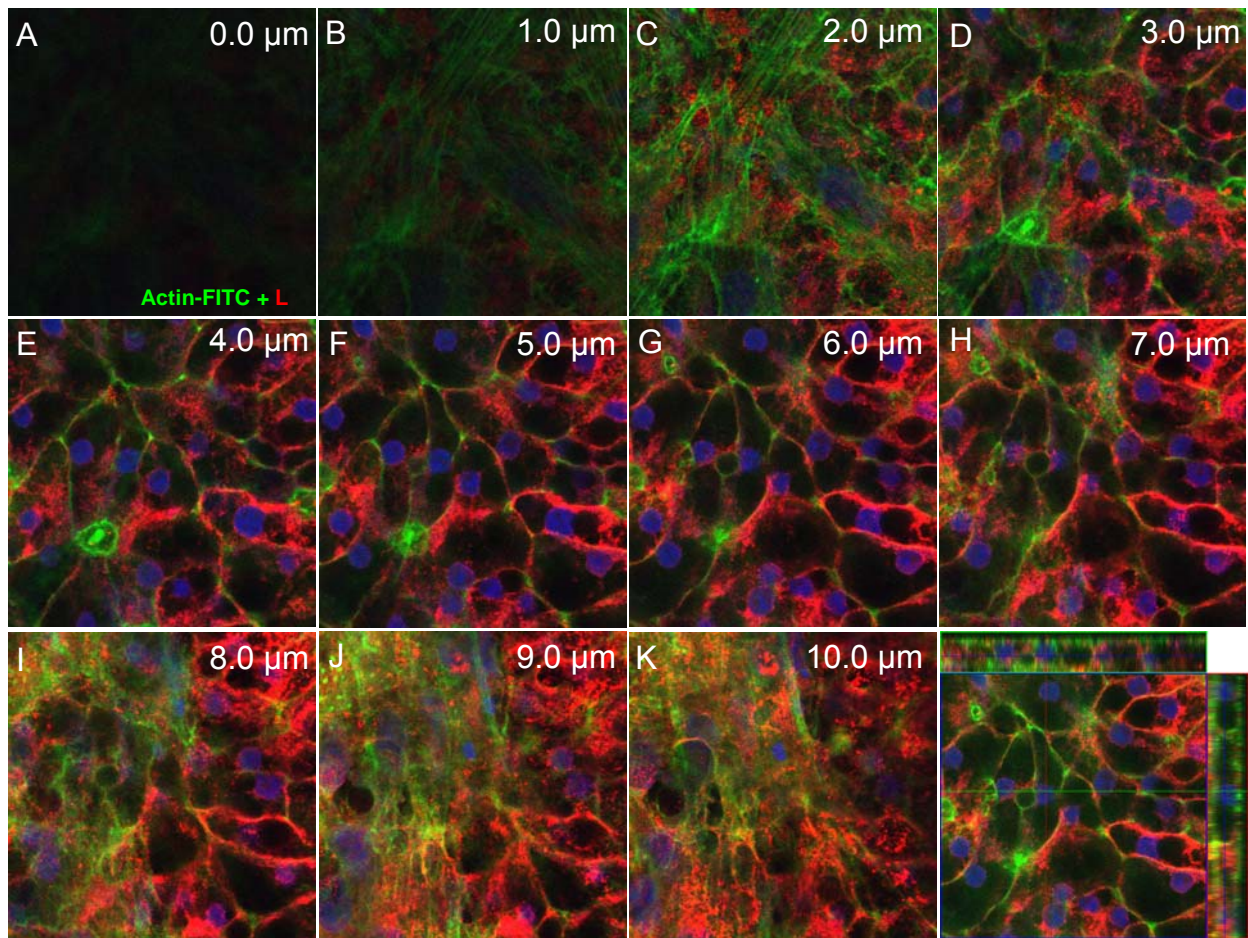


Fig. 75. Actin filaments form a physical barrier for VCVs. Congenitally DHBV-infected PDHs were stained for the surface protein L (red signals) and for FITC-phalloidin to visualize the actin filaments. The merge z-stacks gallery (A-K) shows slices from the bottom (0,0 μm) to the top (10 μm) of the cells. The last panel shows x, y optical section through the center of the cells as well as x, z and y, z projections (right and upside) of this confocal image.

These z-stacks show the strong subcortical organization of actin filaments within the cells and the relative localization of VCVs (Fig. 75, panels A-K). The x, z and y, z projections (last panel) clearly show the presence of VCVs within the actin cortex, indicating that these VCVs must pass through the cortex to reach the PM. Thus, the destruction of actin filaments presumably facilitates the transport of the VCVs to the cell surface and as a consequence, the secretion of viral particles is enhanced.

III.3.3. Role of cholesterol and sphingolipids in DHBV morphogenesis

The envelope of hepadnaviruses has a specific lipid composition. HBsAg particles from serum for example, are composed of 60% phosphatidylcholine and 30% cholesterol.

This lipid composition differs from that of the ER where the virus buds indicating that during the assembly and budding process a selection of specific lipid species and/or the exclusion of others must occur to generate such a specific and unique composition. Cholesterol together with sphingolipids are essential components of the so called lipid rafts which are tightly packed, dynamic lipid assemblies (136, 137). The rafts were shown to be involved in many processes: (i) they function as selective concentration devices for protein-protein complexes and provide platforms for specifically regulated protein-protein interactions (136); (ii) they regulate exocytosis (138); and (iii) are involved in the assembly of enveloped viruses at the PM. To test if lipid rafts play any role in the formation and secretion of DHBV, cholesterol and sphingolipids as critical and essential elements for the formation and stability of lipid rafts were depleted from cells and their effect on both entry and egress of DHBV was analysed.

Depletion of intracellular cholesterol is not critical for viral formation but for viral infectivity

To test whether cholesterol is critical for the formation and secretion of progeny virus, mevillin, a chemical inhibitor of hydroxymethylglutaryl-coenzyme A reductase, a key enzyme in cholesterol biosynthesis (139), was used.

To investigate if reduced levels of cellular cholesterol have any effects on viral formation and secretion, congenitally DHBV-infected PDHs were treated for 48 h with mevillin. A viability test was performed to exclude that cholesterol depletion interferes with the cell viability (Fig. 76).

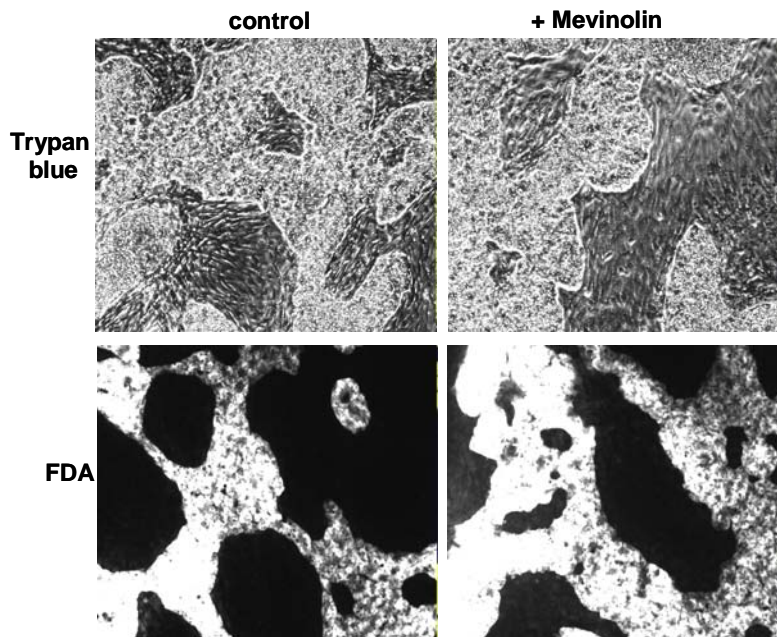


Fig. 76. Mevinolin has no cytotoxic effects on PDHs. Congenitally DHBV-infected PDHs were treated for 24 h with mevinolin. Subsequently, the viability test with trypan blue and FDA was performed.

Then, supernatants and cell lysates of mevinolin treated and non treated cells were analysed for viral protein-L and DNA. As shown in Figure 77, the secretion of DHBV in mevinolin treated cultures was comparable to that of the control cells and the intracellular levels of L protein and DNA were also similar. This indicates that a reduced cholesterol level does not interfere with the formation and secretion of progeny viruses. Unfortunately, the effect of mevinolin treatment on cellular cholesterol was not yet determined, nevertheless, under the experimental conditions used, the secreted viruses from mevinolin-treated cells were altered in their infectivity (Funk et al., manuscript in preparation).

These findings indicate that cholesterol is not required for viral formation, but is essential for the entry during *de novo* infection.

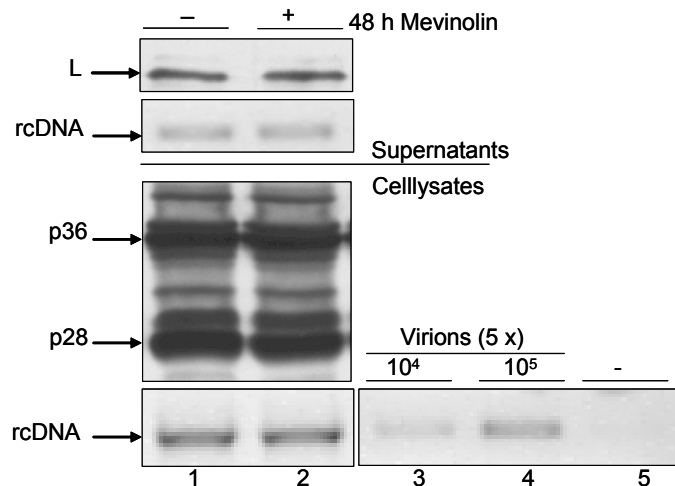


Fig. 77. Cholesterol depletion by mevinolin does not alter DHBV secretion. Congenitally DHBV-infected PDHs were treated for 24 h with 10 μ M mevinolin. Supernatants and cells were harvested and subjected to immunoblot and PCR analysis for viral L protein and rcDNA, respectively.

Depletion of cholesterol from the PM is not critical for viral secretion

Lipid rafts are enriched on the surface of many cells, where they are exploited as platforms for virus assembly by influenza virus and HIV-1 (140-143). It has been shown that the transport of the influenza virus surface protein hemagglutinin (HA) from the Golgi to the PM was slowed in cells treated with methyl- β -cyclodextrine (M β CD) which depletes cholesterol (144). This indicates an essential role for lipid rafts in the transport and thus secretion of virus proteins. To test whether cholesterol and thus lipid rafts are involved in the transport of DHBV, congenitally DHBV-infected PDHs were treated with M β CD, which efficiently binds to cholesterol and extracts it from the cell surface (145). Cells were treated for 12 and 60 h with M β CD. The concentration used were previously shown to reduce the cholesterol level to 56,2% if treated for 1 h (146). Under these conditions, M β CD had no cytotoxic effect on the cells (Fig. 78).

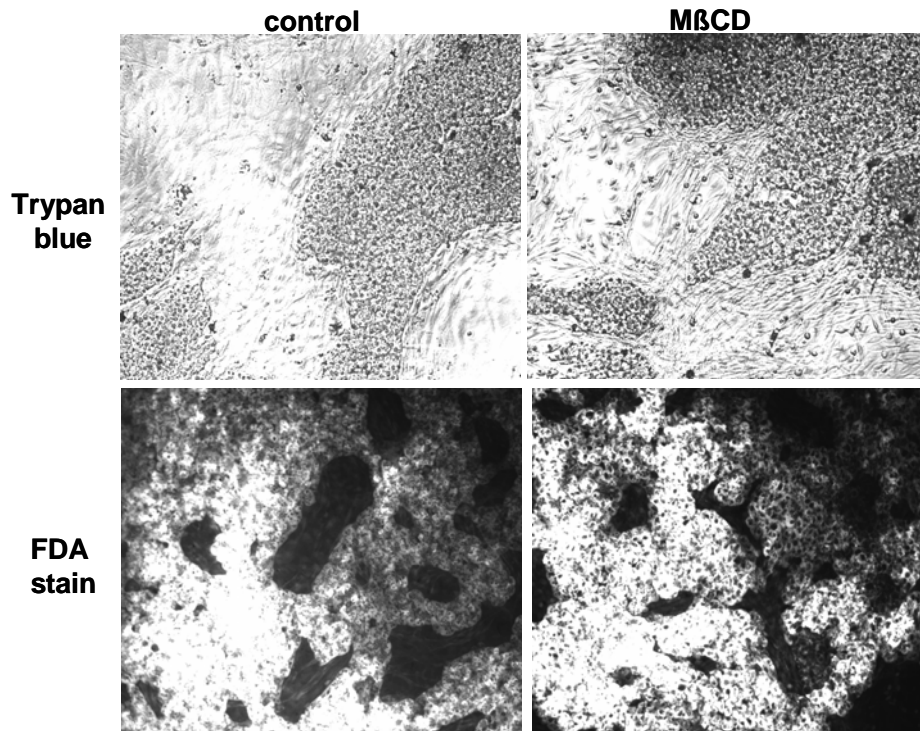


Fig. 78. M β CD has no cytotoxic effects on PDHs. Congenitally DHBV-infected PDHs were treated for 12 h with M β CD and subsequently the viability test with trypan blue and FDA stain was performed

After 12 and 60 h of treatment with M β CD, supernatants and cells were harvested and analysed for viral L proteins and DNA.

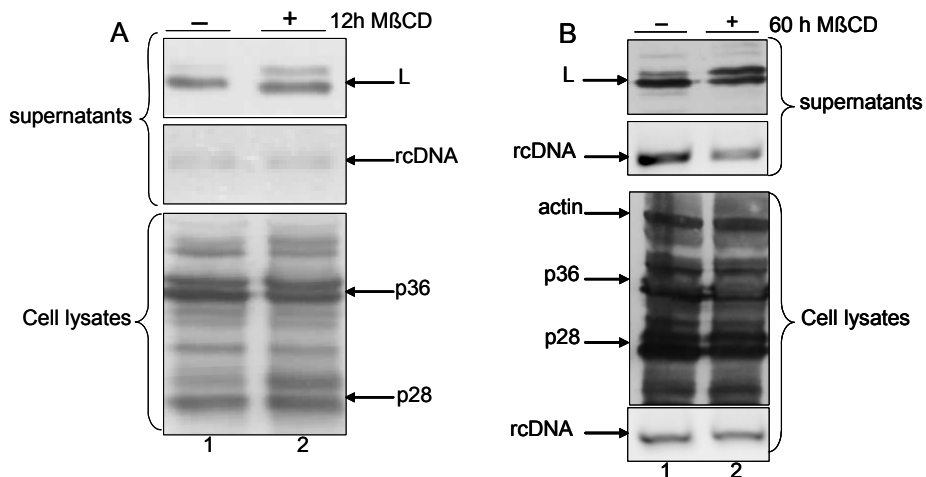


Fig. 79. M β CD does not interfere with secretion of DHBV. Congenitally DHBV-infected PDHs were treated for 12 and 60 h with M β CD. Supernatants and cells were harvested and analysed by immunoblots and PCR for of viral L proteins and rcDNA, respectively.

The secretion of DHBV was not altered by M β CD treatment as shown by both immunoblot and PCR analyses in figure 79A, while in figure 79B, a slight reduction of virions in the supernatant was observed. However, this was due to a reduced level of intracellular DNA in the treated cells in comparison to the control cells. One remarkable feature was that after M β CD treatment, the L protein pattern in the supernatants was changed. In the control cells, the hypophosphorylated L species is the abundant form of L (lower band), while only a minor band of hyperphosphorylated L was present (upper band). In the M β CD-treated cells, the hyperphosphorylated form becomes more abundant in comparison to the control cells. This indicated that M β CD treatment induces a hyperphosphorylation of L-protein in secreted viral particles. This could be the result of the activation of a specific kinase resulting in the hyperphosphorylation of L or to the inactivation of a phosphatase which is normally responsible for the dephosphorylation of L proteins.

It has previously been reported that L is specifically phosphorylated at serine 118 by ERK-type mitogen-activated protein kinases (MAP kinases) in response to extracellular stimuli such as exposure to low temperature, UV-irradiation, and mitogenic phorbol ester (TPA) (52). To test whether MAP kinases were activated following M β CD treatment and thus responsible for the phosphorylation of L, the cell lysates from the above experiment were blotted for active MAP kinase as shown in figure 80.

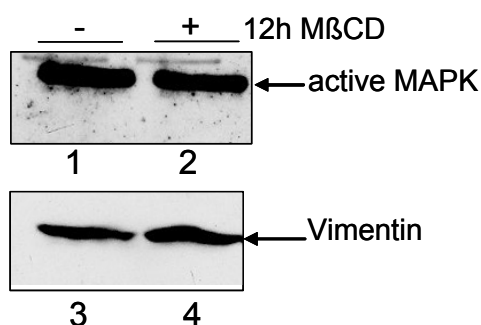


Fig. 80. Hyperphosphorylation of L protein after M β CD treatment does not correlate with activation of MAP kinases. The same cell lysates as in figure 79 were blotted for active MAP kinase (MAPK) (upper panel) to test whether this might be responsible for the hyperphosphorylation of L following M β CD treatment. As a loading control, the same membrane was incubated with anti-vimentin (lower panel).

The immunoblot shown above indicates that the hyperphosphorylation of L proteins following M β CD does not correlate with activation of MAP kinases which are known to phosphorylate L proteins. Thus MAPK could be excluded as the responsible kinase for the observed effects. These results indicate that presumably other kinases are involved in L phosphorylation or that the observed effect was the result of the inactivation of phosphatases which normally dephosphorylate L proteins.

In conclusion, cholesterol depletion either with mevinolin or with M β CD has no effect on the assembly, budding, and secretion of progeny virus. However, cholesterol seems to be required for the infectivity of the virus.

Depletion of sphingolipids does not interfere with DHBV secretion

To further investigate the role of lipid rafts in DHBV morphogenesis, sphingolipids, essential components for the formation of lipid rafts, were depleted from PDHs using 2 independent chemical inhibitors Fumonisin B1 (FB1) and Myriocin (Myr). FB1 is a reported specific inhibitor of ceramide biosynthesis, a precursor lipid for all sphingolipids (147), while Myr inhibits the serine palmitoyltransferase, the key rate-limiting enzyme in sphingolipid biosynthesis (148). Treatment of PDHs for 3 days with 50 μ M FB1 reduces the level of glucosylceramides and ceramids by 84 and 42%, respectively, while treatment with 10 μ M Myr reduces these lipids by 40 and 11%, respectively (unpublished data, kindly provided by Dr. Funk, from the HPI, Hamburg and Dr. Brügger from the Biocenter Klein Flottbeck, Hamburg)

To test whether sphingolipids are required for DHBV morphogenesis, congenitally DHBV-infected PDHs were treated for 60 h with FB1 or Myr to assure an effective depletion of sphingolipids. Fresh medium containing the substances was added every 24 h to permit the secretion of viral particles that had been formed before the depletion had occurred. To show that these long period-treatments (60 h) were not toxic for the cells, a viability test was performed showing no differences between control and treated cells (Fig. 81).

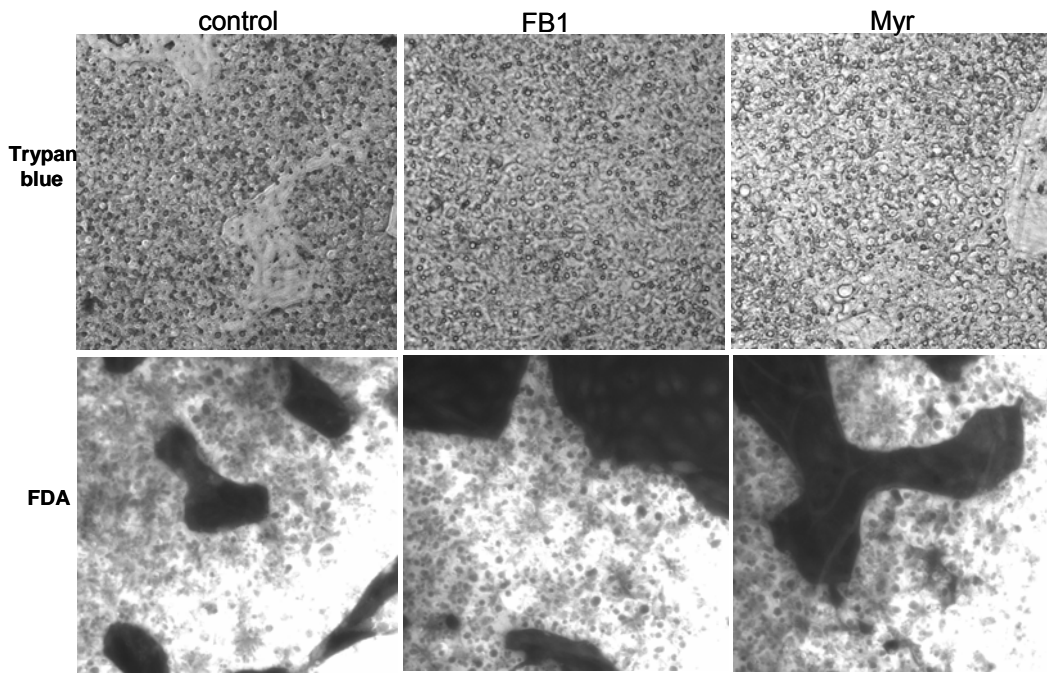


Fig. 81. Spingolipid depletion for 60 h is not toxic. Congenitally DHBV-infected PDHs were treated with FB1 and Myr for 60 h. To test whether these treatments are cytotoxic for the cells, a viability test was performed.

Next, supernatants and cell lysates were analysed by both immunoblot and PCR for the detection of viral L proteins and DNA, respectively. Secretion of DHBV was not altered by spingolipid depletion and the intracellular levels of viral L protein and DNA was also comparable between treated cells and control ones. This indicates that spingolipids depletion and thus lipid rafts are not involved in the morphogenesis of DHBV.

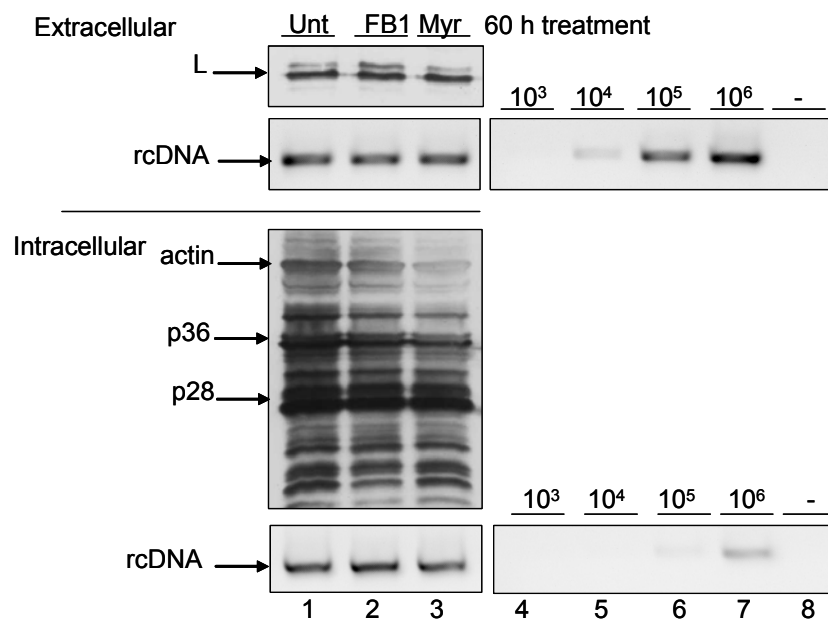


Fig. 82. Sphingolipid depletion does not alter DHBV secretion. Congenitally DHBV-infected PDHs were treated with FB1 and Myr for 60 h. Supernatants and cells were harvested and analysed for viral L protein and rcDNA.

Taken together, the results of this study indicate that cholesterol and sphingolipids are not required for DHBV morphogenesis and that lipid rafts seems to not be involved in the formation, transport, and exocytosis of DHBV. However, cholesterol is required for the infectivity of the virus.

IV. Discussion

IV.1. Assembly and budding of DHBV

The morphogenesis of DHBV and related viruses is largely unknown. Using a combination of biochemical, cell biological, and ultrastructural approaches, it was shown that the formation of viral progeny has unique aspects that distinguish DHBV from all other known animal viruses. Noteworthy and probably unique for hepadnaviral morphogenesis is the peculiar mixture of strategies and elements, which are not only characteristic for DNA viruses, but also for RNA viruses (83, 149).

The ultrastructural analysis of DHBV-infected hepatocytes *in vitro* and *in vivo* shows membrane-surrounded structures containing DHBV particles occupying large regions of the cytoplasm. This finding is consistent with seminal observations reported both for DHBV and HBV in previous ultrastructural studies. Consistent with this study, DHBV SVPs as well as virions were identified by McCaul et al (78) in hypertrophied cisternae of the ER. Visualization of the different stages of the budding process as demonstrated for the first time in the current study strongly corroborates this interpretation. The same may apply for HBV since the different virus particle types were found within ER cisternae (77, 150, 151). Furthermore, in agreement with and similar to this study, naked core particles were observed both free in the cytosol and close to or at cisternal ER membranes. Unlike in my thesis, the identity of the particles was not confirmed by immuno-electron microscopy in previous reports.

Taken together, previous and the current study strongly suggest that DHBV assembles at and buds into ER-derived vesicles. The comparison of DHBV-infected hepatocytes and non-infected ones revealed that these virus-particle containing vesicles (VCVs) are generated during viral replication. Non-infected cells showed a predominant reticular rER network in the cytoplasm. In DHBV-infected cells, instead of such an impressive network, VCVs of different size were the predominant structures throughout the cytoplasm. These findings are strongly suggestive for a reorganization of endomembranes resulting in the generation of VCVs. Indeed, ultrastructural analysis provides evidence for such a scenario since VCVs segregate from ER membranes. The excessive formation of this novel cellular compartment during the course of a DHBV infection is a strong evidence for a virus-induced

process. In line with this notion is that the ectopic expression of the HBV envelope protein L alone induces extensive reorganisation of the hepatocellular endomembranes in transgenic mice, retention and accumulation of subviral particles (SVPs), and cytotoxic demise of hepatocytes leading to formation of hepatocellular carcinoma (152). Thus, reorganization of cellular endomembranes is mediated by L protein and presumably involves both membrane remodelling and/or neogenesis. The upregulation of cellular genes governing lipid biosynthesis which are expected to be altered by viral replication in the liver of HBV transgenic mice supports the membrane neogenesis hypothesis (153).

Both ultrastructural and confocal analysis of L-stained infected hepatocytes showed that the hepadnaviral morphogenetic “centers” are vesicular structures heterogenous in size and morphology. The appearance of VCVs is characterized by an impressive disorganisation of the rER network and formation of virus-filled vesicles as well as small tubules during virus replication. As evident from figure 18, the membrane of some vesicles was decorated with ribosomes indicating that they are derived from the rER. The decoration of VCV membranes with ribosomes should allow the biosynthesis of both cellular and viral proteins at those specific sites. However, the majority of vesicles showed a smooth cytosolic membrane surface which either hints to a different origin of these vesicles or the loss of their ribosome decoration during viral morphogenesis. In agreement with the idea that these VCVs could have another origin than the rER, it was demonstrated that viral particles were present in the perinuclear space. Single or few particles were often seen in this space and the outer nuclear membrane was dilated to different extents at the sites where viral particles were observed. Sometimes, VCVs were observed to segregate from those membranes indicating that the nuclear membrane is also a site for both viral assembly and budding. This observation is consistent with a recent publication (154). The large heterogeneity in the size of vesicles was impressive and could be the result of the pinch-off of variable membrane sacks from the outer nuclear membrane or rER. Alternatively, one could assume that the vesicles grow in size over time. However, this growth would require an increased *de novo* membrane synthesis. Since such a membrane growth is likely to be limited, it can only account, in the best case, for part of the vesicular growth. Alternatively, but not exclusively, the bigger vesicles could be formed through homo- and/or heterotypic fusion. Ultrastructurally, advanced stages of both homotypic fusion and/or fission between intermediate vesicles were observed.

However, it was not possible to distinguish between fusion and fission using EM analyses since under steady state conditions the obtained images could reflect the one or the other process. To gain more insights into the dynamics of the VCVs, live cell imaging using the GFP-tagged-small surface protein S as reporter for the VCVs was performed. This approach revealed that VCVs are dynamic structures undergoing both homotypic fusion and fission with other VCVs to form bigger or smaller ones, respectively. Furthermore and in favour of the heterotypic fusion hypothesis, dual immunofluorescence analyses and subcellular fractionation showed that DHBV-associated vesicles contained the endosomal marker protein Rab5B. This is consistent with a heterotypic fusion between DHBV-associated and endocytic vesicles.

The ultrastructural analysis of VCVs showed that they were filled with spherical particles of rather homogenous appearance. In some vesicles, 2 types of viral particles were observed: empty particles of 40-60 nm in diameter corresponding to SVPs, and filled particles with a diameter of 45-65 nm which are virions. The coincidence of both viral particle entities shows that virions and SVPs exploit a common morphogenetic pathway. Virions were numerically much less than SVPs in both the smaller as well as larger vesicles. Moreover, the majority of VCVs contained only SVPs. This result shows for the first time that the excessive formation of SVPs, a unique feature of hepatitis B viruses, is already determined at the assembly and budding stage. Although shown here for DHBV, this may apply to all other hepadnaviruses as well.

Viral particles were exclusively found in the vesicular lumen, but not free in the cytosol. This result was corroborated by the biochemical analysis of subcellular fractions from infected PDHs, which showed that viral structural proteins L and core as well as viral DNA were only present in fractions containing membrane-surrounded cellular compartments.

Since the viral envelope proteins are cotranslationally inserted into ER membranes (120, 155) it can be anticipated that the VCV membranes contain not yet particulated envelope proteins. A strong argument for this hypothesis comes from the immunoprecipitation experiment in which intact VCVs were immunocaptured using an anti-L antibody. This indicates that the surface protein L was present on the membranes of these vesicles and thus permitted their immuno-isolation.

For the first time, ultrastructural analyses showing different stages of the budding process of SVPs were provided in this study. The membrane of the VCVs showed different degrees of inward membrane invaginations toward the lumen of the vesicles corresponding to early, intermediate, and late steps of the budding process. Compatible with the notion that VCVs are assembly and budding platforms is the presence of ribosomes at the membranes of certain VCVs which would imply a continuous protein synthesis as a prerequisite for virus assembly and budding.

Unlike SVPs, the formation of virions requires interaction of preformed mature nucleocapsids with the surface proteins since the large envelope protein L is essential for formation of both virions and SVPs (156).

Nucleocapsids of presumably different maturation states as indicated by their different electron density could be observed free in the cytosol in contrast to complete virions. The EM pictures showed in addition that only the presumably mature, electron dense nucleocapsids tethered to the membrane of VCVs. This is consistent with previously published floating experiments, which showed that only mature nucleocapsids have the intrinsic affinity and ability to interact with intracellular membranes (43). I have provided ultrastructural evidence showing that electron dense nucleocapsids tether to the membrane of VCVs, leading to its deformation in the sense of an intrusion into the vesicle lumen. This finding was interpreted as the early budding process of virions. Unfortunately, the last phase of the budding, the pinch-off and release of newly enveloped virions could not be pictured.

Since virions and SVPs are formed through the same morphogenetic pathway, the question arises why the intracellular formation of SVPs exceeds the formation of virions. A plausible answer would be that the formation kinetics of SVPs is significantly faster than that of virions. The formation of virions requires the coordinated sequence of the following events: synthesis of core protein, association with the viral pgRNA and polymerase, RNA packaging, formation of immature nucleocapsids, and finally their maturation through reverse transcription of the viral genome. This process depends on a precise regulation and is controlled, among others, by the phosphorylation status of the core protein (120). Obviously, nucleocapsids are strongly selected prior to their envelopment or re-infection of the cell nucleus (42). Only after this molecular selection, nucleocapsids can interact with the viral envelope proteins at the membrane of VCVs to form virions. Indeed, the decoration of VCV membranes with nucleocapsids was very low. This indicates that

the availability of mature nucleocapsids is an important and possibly rate-limiting step in virion formation. In contrast, the formation of SVPs is independent of all the aforementioned steps. Furthermore, the surface proteins have an autonomous and very efficient budding activity. In the absence of nucleocapsids, the spontaneous assembly and budding of empty spheroid particles takes place and SVPs are formed. Thus, formation of SVPs requires fewer steps and is primarily determined by the amount and ratio of viral the envelope proteins S and L as well as the availability of cellular membranes. The autonomous budding activity of the surface proteins combined with the complexity of nucleocapsid formation provide reasonable explanations for the excessive formation of SVPs.

Biochemical analysis of subcellular fractions from DHBV-infected liver showed that the structural virus components L and core proteins as well as the viral DNA were mainly co-incident in fractions containing marker proteins for the ER confirming the ultrastructural data. In addition, the virus components were found to partially co-fractionate with the IC. However, they were mainly excluded from fractions containing Golgi membranes. This finding is further supported by immunofluorescence analyses showing that the intracellular distribution of viral L protein and a cotransfected YFP-reporter protein for the Golgi compartment have only a very minor overlap while the distribution of gamma-2-adaptin, a Golgi protein, was completely distinct from that of VCVs. Moreover, these data indicate that assembly and budding of DHBV rather take place in pre-Golgi compartments, namely the ER and IC. This is in agreement with a study which proposed that HBV surface proteins assemble and bud in a post-ER and pre-Golgi compartment (80). The association of VCVs with the rER suggests that VCVs are not only morphogenetic centres but also sites for translation of structural proteins prior to their assembly and budding. Since the reorganisation of the ER network is accompanied by the emergence of VCVs, one would expect a divergent distribution of cellular compartments, especially the ER, between non-infected and DHBV-infected cells following subcellular fractionation by density gradient ultracentrifugation. However, this was not the case since the ER markers in fractions from infected and non-infected cells were similarly distributed within the gradient. A possible explanation for these unexpected results is that the ER of non-infected cells was fragmented during dounce homogenization of the liver, generating vesicles of different size instead of the large network of membranes cisternae seen by EM and thus these vesicles fractionated to the same densities as the ER-derived VCVs.

In addition to the ER marker proteins calnexin, PDI, and MTP, a number of host-cell proteins like Rab5B and CD63 were identified as components of VCVs. Rab5B and CD63 are marker proteins for early endosomes and MVBs, respectively. Their association with VCVs is strongly suggestive for their recruitment to the VCV membranes. A further argument for this theory is that a second early endosomes marker, EEA1, was not found to colocalize and associate with VCVs as shown by immunofluorescence and IP experiments.

In contrast to CD63, Tsg101, the entry component of the ESCRT-1 complex for endosomal membranes, was largely absent from L-positive VCVs. This indicated that budding requirements for DHBV appear to be distinct from the ones of HIV, which depends on the ESCRT-1 complex for budding into MVBs (100, 157, 158). Overall, these data implicate that assembly and budding of DHBV involves the formation of novel organelles, which have mixed properties of ER, endosomes, and IC as well as MVBs. These findings may also apply to other hepatitis B viruses as recently reported for HBV (159).

The observed drastic reorganization of the host cell endomembranes is known for non-enveloped positive-sense RNA viruses such as poliovirus. Early in replication of the virus, membraneous vesicles appear in the cytoplasm, located early near the nucleus and later spread throughout the entire cytoplasm. Ultrastructural and inhibitor studies initially suggested that the virus-induced vesicles were derived from the host cell secretory pathway. BFA treatment blocked their formation and virus replication (160, 161). Later it was shown that these membranes were generated from ER-derived vesicles and disassembly of the Golgi complex induced by the poliovirus protein 3A (162). It was hypothesized that 3A interferes with the assembly of COPII vesicles so that newly synthesized membranes and those recycled from the Golgi accumulate in the ER. It would be possible that hepatitis B viruses as pararetroviruses follow a similar strategy for their assembly and budding and that the surface proteins L and/or S, like poliovirus protein 3A, could induce such reorganization of host endomembranes and the induction of new compartments with mixed properties of the ER, IC, and endosomes, as was shown in this study. In line with this idea is that the ectopic expression of the HBV envelope protein L alone induces extensive reorganisation of the hepatocellular endomembranes in transgenic mice (152).

Why do some viruses bud into endosome-like vesicles? The endosomal system

clearly plays a significant role in the assembly of many retroviruses (157). Preformed HIV particles from late endosomes are infectious (100). Viruses might also be able to hide in these late endosomes, sequestered away and protected from the entry route and degradative environment, respectively.

As depicted in the model, VCVs seem to be morphogenetic centres for DHBV. It is tempting to assume that VCVs are multifunctional platforms at which the different steps of viral morphogenesis are efficiently executed and coordinated: (i) protein biosynthesis and cotranslational insertion of the surface proteins into the membrane, (ii) recruitment of cellular adaptors and formation of special membrane microdomains, (iii) assembly, (iv) membrane deformation, and (v) finally viral budding.

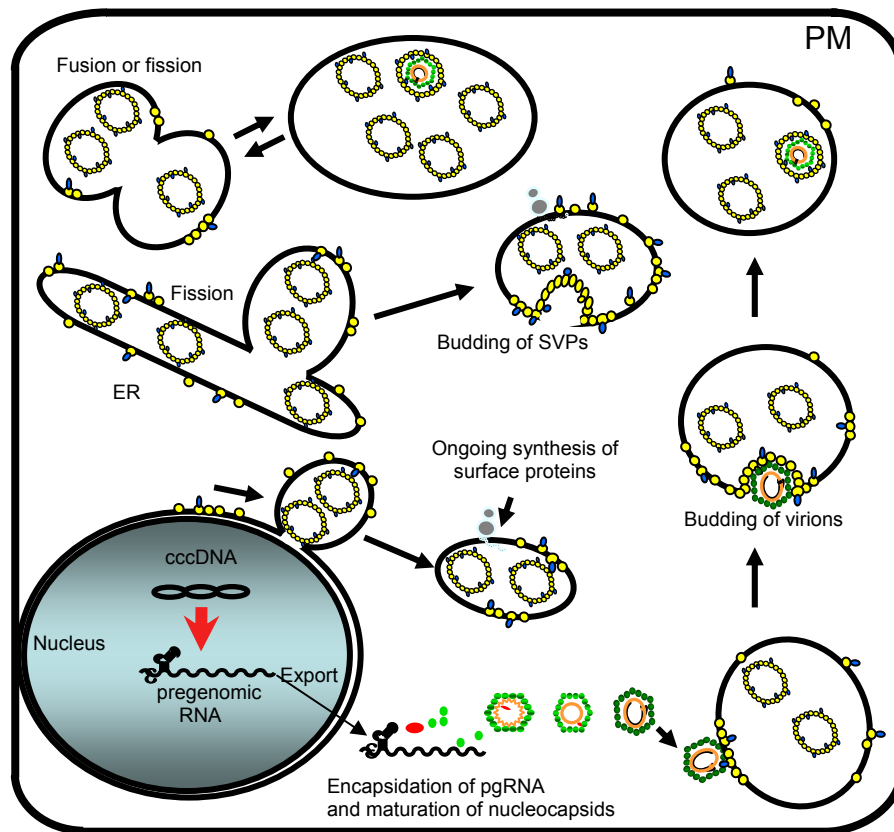


Fig. 83. Assembly and budding model for DHBV. The different aspects of DHBV morphogenesis discussed so far are summarized in this model.

VCVs can also have a maturation and storage function. Molecular elucidation of signals, factors, and mechanisms that are involved in the generation of DHB virus-induced vesicles require further studies to identify which viral and cellular factors play a key role.

IV. 2. Secretion of DHBV

After assembly and budding, it is assumed that HBV is secreted via Golgi-derived secretory vesicles (31). The assumption of the passage of HBV viral particles through the Golgi was based on the fact that surface proteins of secreted viral particles contain complex oligosaccharide polypeptides which are endoglycosidase-H resistant and known to be processed in the Golgi (163). However, there is no experimental evidence for this assumption. Besides the existence of ultrastructural studies showing the presence of HBV particles within dilated ER cisternae (154, 164), none of them showed HBV particles within the Golgi. This was attributed to the fact that the transport of HBsAg particles through the Golgi is very fast. Arguing against the Golgi involvement is that virtually all the intracellular glycosylated HBsAg was found in the endo-H sensitive form and therefore has not been processed in the Golgi, but glycosylation presumably occurs immediately prior to secretion (164).

In the current study, the analysis of subcellular fractions from DHBV-infected hepatocytes showed that the structural virus components L and core protein are mainly excluded from fractions containing Golgi membranes. This finding was further supported by the morphological observation that the intracellular distribution of viral L protein was distinct from that of 2 independent Golgi markers used in this study. Only a very minor overlap between L and the ectopically expressed YFP- β -galactosidase, a reporter protein for the trans-Golgi, at the periphery of the Golgi structure was observed. In line with this notion is the ultrastructural evidence showing that Golgi membranes and stacks were devoid of any viral particles and that no VCVs were seen budding from the Golgi. Since all transport steps along the secretory pathway are mediated by vesicular carriers, one could expect to visualize the fusion or fission of VCVs with or from the Golgi. The lack of such events at the Golgi could not be attributed to experimental limitations or to the rarity of these processes since VCVs were often seen segregating from the ER and the outer nuclear membrane as well as fusing and/or segregating from each other. However, it is not possible to completely exclude that a minor subpopulation of VCVs is transported to and through the Golgi since VCVs were observed in close proximity. It would be possible that after assembly and budding into the ER, a minor fraction of DHB viral particles would be carried along the secretory pathway by bulk fluid-phase transport. The presented

data do not formally exclude, but make a direct involvement of Golgi in DHBV assembly, budding, and secretion highly unlikely.

The intracellular transport and secretion of both cellular and viral secretory and membrane proteins have been extensively studied. There are specific low-temperature-sensitive steps along the secretory pathway. Exocytosis for example is inhibited at temperatures below 20°C and transport of secretory proteins and viral membrane glycoproteins from the trans Golgi to the cell surface is arrested at this temperature (132). Incubation of DHBV-infected hepatocytes at 20°C resulted only a slight reduction in the amount of secreted SVPs and virions while the secretion of the 2 cellular proteins albumin and apolipoprotein A-I in the medium was strongly reduced indicating that DHBV secretion is not temperature sensitive. As expected, VSV-G accumulated in the Golgi/TGN at 20°C, in contrast no similar effects were seen for the L protein. Moreover, the subcellular distribution of L-positive vesicles was unchanged at 20°C as compared to that in control cells incubated at 37°C indicating that the cellular distribution and transport of VCVs is temperature-independent. These data strongly suggest that DHBV progeny virus does not exploit the constitutive secretory pathway to exit the host cell. How can the slight reduction of secreted viral particles at 20°C be interpreted? One possible explanation is that the secretion of DHBV requires cellular proteins and factors that are transported via the constitutive secretory pathway to the cell surface where they may play important roles during exocytosis. Thus, inhibiting the delivery of such proteins to the PM could negatively influence the efficacy of viral secretion. An alternative explanation is that the observed slight reduction could reflect the subpopulation of viral particles which are presumably transported to and through the Golgi and thus are sensitive towards low temperature. The proof of one or the other interpretation requires additional experiments. Ultrastructural analysis of DHBV-infected cells incubated at 20°C would provide evidences for or against the proposed hypothesis.

Overall these data strongly suggest that the majority of viral particles follow an alternative secretory pathway rather than the constitutive one. It can be assumed that the mode of DHBV secretion involves an exocytic process. First, VCVs are directed to the proximity of the PM, presumably by an anterograde transport mechanism, where they dock to and finally fuse with the PM. Docking and fusion should then lead to the release of the vesicle content by fusion of both membranes. This model is supported by the following independent findings: EM analysis and life cell imaging

clearly demonstrated the topological proximity of VCVs to the PM. Morphologically, the observed subcortical VCVs were similar to those seen in the interior of the cells. However, it is not possible to exclude that they were biochemically different from those observed closer to the nucleus. It would be conceivable that these VCVs undergo maturation on their way to the cell surface by acquiring new adaptor proteins or losing others in order to coordinate and fulfil their different functions. These subcortical VCVs were variable in size and shape and occasionally in contact with the PM. Their distribution was polarized showing an accumulation at the basolateral membranes of hepatocytes. During the exocytic trafficking, they were occasionally observed undergoing putative fission and fusion, suggesting that these processes are highly dynamic. Moreover, and for the first time, a direct ultrastructural picture provided strong evidence for an exocytic process.

When DHBV-infected hepatocytes were stained for L, a clear labelling of the PM was seen since the contour of the cells was easily recognisable. This L-associated cell surface staining was confirmed by co-staining the PM with either CTB that binds to its receptor, the ganglioside M1 at the cell surface, or with ectopically expressed CD63-RFP, a tetraspanin localizing to MVBs and the PM. The data revealed that both markers stain the same membrane as the anti-L antibody indicating that L was indeed present at the PM. Moreover, biotinylation of cell surface proteins using membrane-impermeant, non-cleavable biotin (sulfo-NHS-biotin) revealed in 2 independent, but complementary assays that a fraction of non-particulated surface protein L was indeed located at the cell surface. These L proteins are presumably transferred to the PM through fusion of the VCV membrane containing not yet particulated L proteins with the PM. This would confirm previous studies describing HBsAg at the PM in HBV-infected liver tissues (165-168). One could speculate that the observed L-staining of the PM results from binding of secreted viral particles to the cell surface. However, the EM analysis revealed no evidence for such binding. Extracellular viral particles were seen without being in direct contact with the PM at least in the examined sections making such an explanation unlikely. The incorporation of the surface protein L into the PM might have important implications for the understanding of the well known but unclear superinfection resistance of infected hepatocytes. Recently, it was shown that the superinfection exclusion in DHBV infection is mediated by the L protein (63).

In agreement with exocytic release is the kinetics of virus release showing that about 40-80 virions and 46,000 SVPs are secreted per hour and per hepatocyte. These numbers clearly suggest a bulk secretion of viral particles rather than single particle release. In contrast to the release of huge amounts of virus particles, the exocytic process was rarely observed. This was mainly due to the fact that secretion is a very dynamic and fast event. To capture such processes by live cell imaging, high time resolution microscopes have to be used. Second, considering that about 10 viral particles are liberated during one exocytic event, it would implicate that only 1.2 exocytic events will occur per second in the whole cell. To screen the entire hepatocyte about 200 sections (of 50 nm thickness) are required and thus the chance to see such an event by EM is very unlikely.

For viruses that spread via extracellular progeny, as DHBV, one last hurdle after assembly and budding is to avoid the binding to the receptor in the producer cell. Different strategies have been evolved by viruses to overcome this problem. Some viruses like paramyxoviruses incorporate a receptor-destroying enzyme to inactivate the receptor during transit through the secretory pathway. Others, like retroviruses overcome this problem by expressing accessory proteins that bind the receptor and induce its degradation. Hepadnaviruses seem to have evolved other mechanisms to overcome this problem. First, the generation of vesicular platforms where all morphogenetic steps assembly, budding, intracellular transport, and secretion are concentrated would avoid the contact with the receptor that could be present along the secretory pathway. Second, the formation of large excess of SVPs that has an identical envelope as virions (at least in the case of DHBV) would also be a strategy to bind the receptor, if encountered, preventing the trapping of DHB virions.

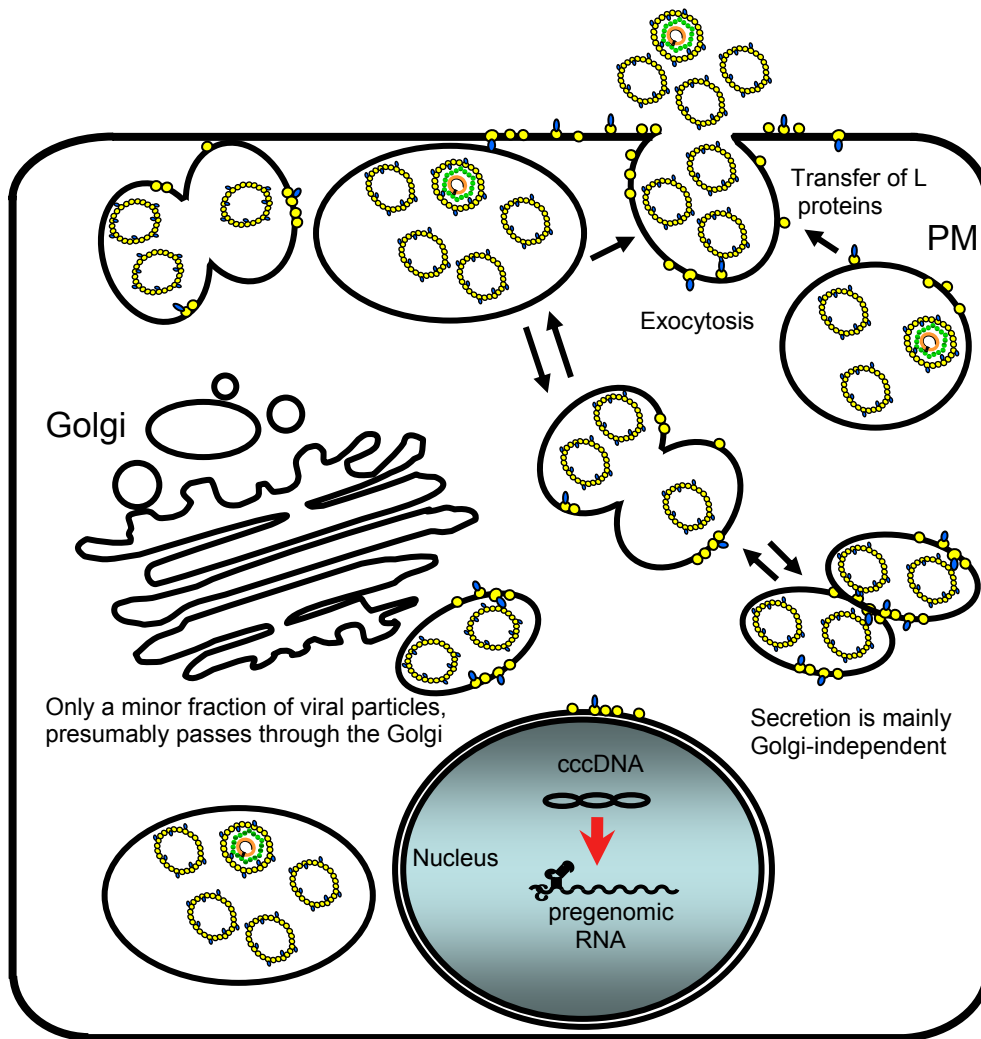


Fig. 84. Secretion model for DHBV. The different aspects of DHBV secretion discussed so far are summarized in this model. The secretion of DHBV is largely Golgi independent. However, a small fraction of viral particles could be transported through the constitutive secretory pathway. Liberation of progeny virus occurs via exocytosis leading to the transfer of non-particulated L protein to the PM.

To extend and complete the data shown above, dual life cell imaging for VCVs and the Golgi complex would be helpful to gain further insights into the role of the Golgi in DHBV morphogenesis.

IV.3. Cellular requirements for DHBV intracellular transport and secretion

IV.3.1. BFA strongly inhibits viral secretion

BFA dramatically inhibited secretion of both SVPs and virions while the intracellular levels of viral structural proteins L and core as well as rcDNA were not altered indicating that the secretion inhibition was not due to a deficit in viral components. Furthermore, the assembly and budding of viral particles was not affected by BFA since viral particles were found within large membrane vesicles and tubes in the cytoplasm of treated cells. Remarkably, the size of these vesicles reached 3-4 μm in diameter and thus were 4 to 5 times as big as those seen in the control cells. Two types of VCVs were observed upon BFA treatment, large dilated membrane tubules around the nucleus which were interconnected forming a network and large vesicles without connections to other membranes. I have not yet studied the composition of these large VCVs, so that I can only speculate about their nature. One possibility would be that new VCVs fail to segregate from the donor membranes, notably the ER. In non-treated cells, one characteristic feature of DHBV morphogenesis is the fragmentation of the ER network by segregation of VCVs from ER cisternae as shown in this study. BFA could have an inhibitory effect on the fission event leading to the formation of these large VCVs. Another possibility is that large vesicles could be formed by homotypic fusion between VCVs. In favour of this hypothesis is the absence of the small and intermediate sized VCVs in BFA-treated cells. A third possibility would be that they are formed by heterotypic fusion with other cellular membranes. Consistent with this notion is that upon BFA treatment, the Golgi tubulates into uncoated membranes and rapidly collapses into the ER forming a mixed ER-Golgi system (135). Concomitantly with the fusion of the Golgi with the ER, a nearly complete block of membrane transport out of the mixed ER-Golgi system occurs (169). This could account for the observed dilated ER-tubule structures containing viral particles. Analogous to the mixing of the Golgi with the ER during BFA treatment, the TGN mixes with the recycling endosomal system. This altered system remains functional with normal cycling of proteins between PM and endosomes. However, no random mixing between ER-Golgi and endosomes-TGN occurs (105). The observed large VCVs could be the result of the combination of all

above mentioned possibilities resulting in large mixed vesicles. It is even conceivable that VCVs are generated by fusion of VCVs with both the ER-Golgi system and the endosomes-TGN system for the following reasons: (i) the induction of large membrane tubules and huge vesicles was only observed in DHBV-infected but not in non-infected cells, arguing for a specific virus induced phenomenon, (ii) VCVs have mixed properties of the ER, IC, and endosomes, as was shown in this study, and thus could induce the heterotypic fusion of ER-Golgi membranes with endosomes-TGN membrane which normally does not occur (105). To prove such hypothesis further studies providing biochemical evidences are required. Immunoprecipitation of VCVs from BFA-treated cells would indicate whether these vesicles are biochemically different from those of control cells and whether they carry markers specific for Golgi, TGN, and recycling endosomes.

Since BFA neither alters viral protein biosynthesis nor the assembly and budding, one alternative explanation for the strong inhibitory effect would be that the intracellular transport of VCVs to the cell surface is affected. However, this was not the case since large VCVs full of viral particles were seen accumulating beneath the cell surface. Whether the intracellular transport of these VCVs continued in the presence of BFA or whether the observed VCVs were already localized at cell periphery before commencing treatment is not clear. However, this shows that the inhibition of viral secretion was not due to the failure of VCVs to reach the PM. All the above rejected hypotheses strongly suggest that the inhibitory effect of BFA is at the level of exocytosis itself. Arguments in favour of this hypothesis were provided in this study since large VCVs were located beneath the cell surface but no secretion occurred. Second, in BFA-treated cells, the L-associated PM staining disappeared indicating that no transfer of non-particulated L proteins to the PM occurred as a consequence of the inhibited fusion process between VCVs and cell surface. This would implicate that fusion of VCVs with the PM is BFA-sensitive. The primary target of BFA is the small GTPase ADP-ribosylation factor (ARF) 1 which localizes to the Golgi (170-172). BFA stabilized ARF1 in its GDP-bound form enabling the exchange of GDP/GTP (173, 174). Thus, ARF1-GTP is consumed and all cellular processes like membrane recruitment and activation of various proteins involved in vesicular trafficking are blocked (175). However, the targets of BFA in the Golgi differ from those in the peripheral organelles (105). The sensitivity of exocytosis towards BFA would implicate that ARF-1 or other BFA-targets (still unidentified) are implicated

either directly in this process or indirectly by failing to recruit or activate other proteins or factors.

One interesting experiment would be to ultrastructurally investigate the fate of the large VCVs after removal of BFA. Would they fuse as large membrane packets with the PM or would they fragment into smaller vesicles and then fuse? Actually, this experiment was started during the writing of my thesis but could not be completed due to time limitations. This experiment was also performed in the hope to reach a more synchronous secretion of viral particles after removal BFA for visualisation of the different steps during the exocytic release.

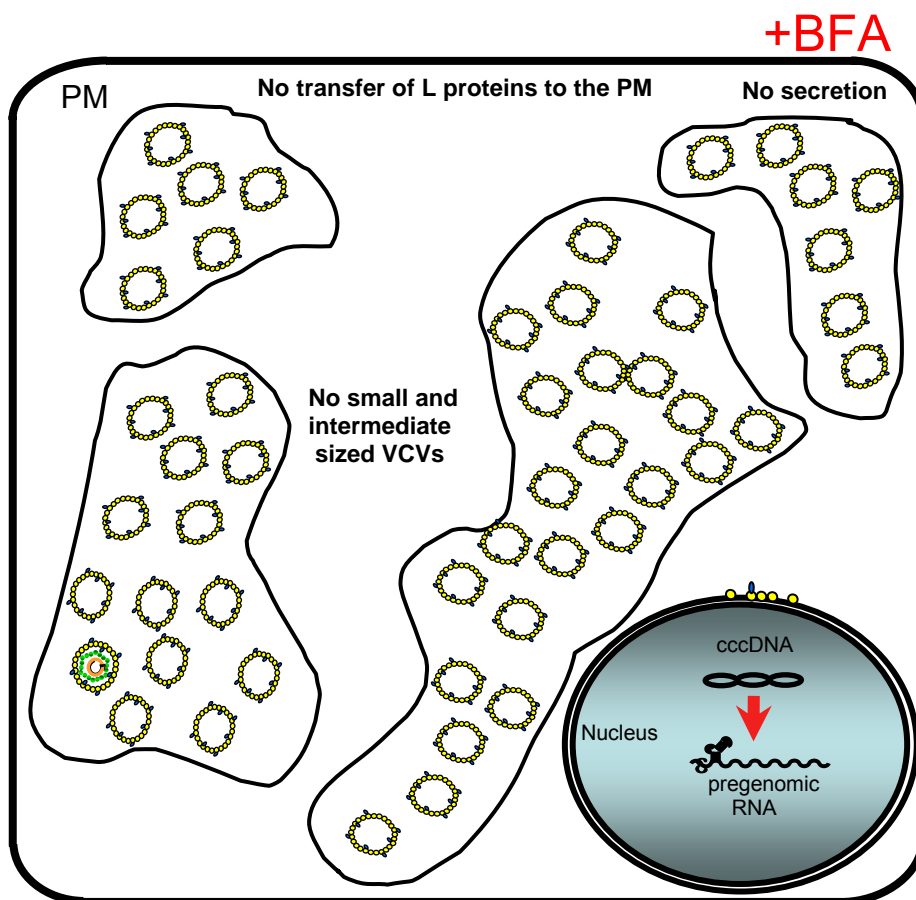


Fig. 85. Effects of BFA on DHBV morphogenesis. The different effects of BFA discussed so far are summarized in this model. Upon BFA treatment, DHBV particles accumulated in large membrane tubules and vesicles. The small and intermediate sized VCVs disappeared. Large vesicles were located beneath the PM. However, secretion was inhibited and as a consequence, no transfer of L protein to the PM occurred.

IV.3.2. Role of the cytoskeleton in DHBV transport and secretion

Following assembly and budding of DHBV particles, VCVs were transported to the PM where they fuse and liberate progeny virus. As shown before, the transport likely does not occur via the constitutive secretory pathway. The question remains how the VCVs are directed to the cell surface? One possibility would be that they freely diffuse to the PM, however such diffusion is restricted by the cytoplasm that poses a substantial barrier due to its high protein concentration and to the presence of cellular organelles and cytoskeleton. The second possibility would be to exploit the cellular cytoskeleton. Using pharmacological inhibitors for both microtubules (MTs) and actin, the data obtained showed that intact but not dynamic MTs are required for the intracellular transport of VCVs while actin filaments were dispensable. Nocodazole treatment, which depolymerizes MTs, inhibited viral secretion by about 1 log₁₀. This incomplete block could be interpreted as a consequence of incomplete depolymerization of MTs under the experimental conditions implicating that some residual MTs are still able to accomplish the transport of the majority of VCVs. Alternatively, depolymerization of MTs that normally contribute to the molecular crowding of the cytoplasm, now permitted a partially free diffusion and thus the remaining secretion is due to the passive diffusion of these VCVs to the cell surface. Remarkably, the effects of MTs depolymerization were slightly more pronounced on virion secretion than on that of SVPs. It could be assumed that MTs are not only required for the transport of VCVs to the cell surface for viral secretion but also for the transport of nucleocapsids to the assembly and budding site. Nucleocapsids aligned along MT as shown by EM support this hypothesis. Therefore, the secretion of virions would be more affected than that of SVPs since their formation and secretion required more MTs-dependent steps. Secretion inhibition by Nocodazole was completely reversible only 48 h after removal of the substance. This relatively long time period for complete re-establishment of viral secretion could argue for a dramatic effect of Nocodazole on MTs and other cellular organelles due to the relatively long treatment period (about 16 h).

When the dynamic turnover of MTs was inhibited by Paclitaxel, only the secretion of virions was affected. This argues for a role of dynamic MTs in the morphogenesis of virions probably during the assembly and/or budding. Moreover, these findings indicate that stable MTs are sufficient for the transport of VCVs to the cell surface. In

contrast to the egress of DHBV, the entry of DHBV requires both intact and dynamic MTs (69).

Actin filament depolymerization showed no negative effect on viral secretion, in contrast, the secretion of both viral entities was slightly promoted. Confocal z-sections showed no interaction of VCVs with actin arguing for an actin-independent transport. Notably, cortical actin is believed to act as a physical barrier that must be overcome during exocytosis. When the cortex is depolymerised, secretory vesicles could better reach and fuse with the PM (110). In contrast to DHBV, other viruses exploit actin for their morphogenesis, intact actin microfilaments are required for the maturation of measles virus for example. In the presence of the actin disrupting agent Cytochalasin D, the release of this virus was drastically decreased (111). Furthermore, the retroviral Gag proteins were shown to interact with actin filaments. When actin was stabilized by phalloidin, the production of virions was reduced, however when actin was depolymerised briefly, virion secretion was enhanced (112). this argues again for the physical barrier imposed by actin.

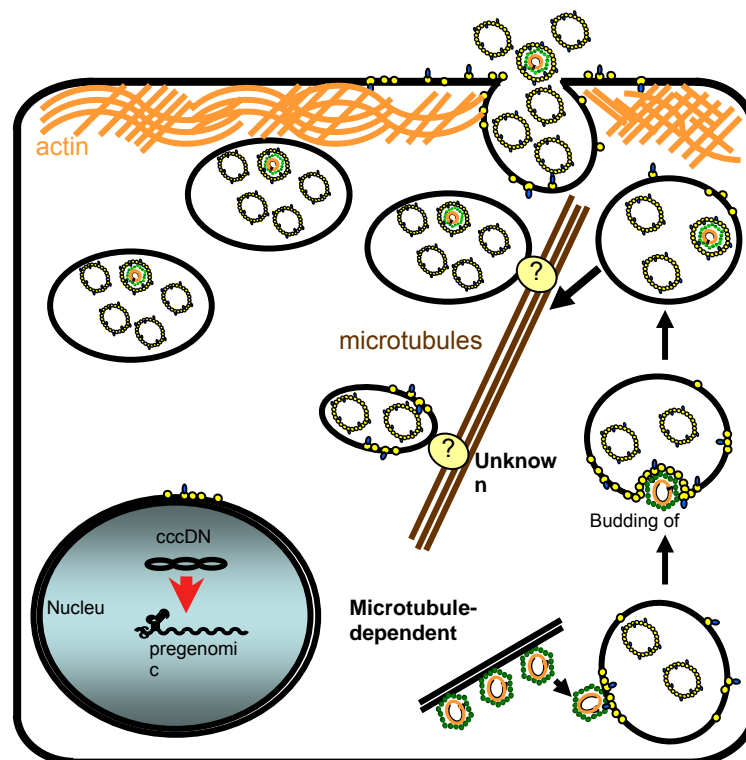


Fig. 86. Intracellular transport of DHBV. The different aspects of DHBV transport discussed so far are summarized in this model. Intact but not dynamic microtubules are required for the transport of VCVs. Formation of virions required MT-dependent steps presumably also for the transport of nucleocapsids to the envelopment site. This step presumably relies on both intact and dynamic MTs. The actin filaments are dispensable for viral secretion; moreover, they form a kind of barrier that must be breached during secretion.

IV.3.3. Role of cholesterol and sphingolipids in DHBV morphogenesis

The envelope of HBsAg from serum contains high levels of cholesterol (30% of all lipids), this could reflect a specific role for this lipid in the viral life cycle either in viral morphogenesis or during infection. Moreover, cholesterol and sphingolipids are essential components of lipid rafts which have been implicated in the assembly and release of many enveloped viruses such as HIV, Ebola, Marburg, influenza, and measles viruses (176, 177) as well as in intracellular trafficking (178, 179).

To explore whether cholesterol is necessary for the assembly and budding process of DHBV, endogenous cholesterol levels were decreased using mevillin, a specific inhibitor of cholesterol biosynthesis (139). Release of viral particles from mevillin-treated cells was not affected, however, the produced viruses were less infectious (Funk et al., 2007, manuscript in preparation). Accordingly, the concentration of cholesterol in DHBV membrane appears to be important for maintaining viral infectivity, but is not critical for viral assembly and budding. Although cholesterol does not play a critical role in the formation of progeny viruses, cholesterol and lipid rafts may be involved in the intracellular transport and release of DHBV. To examine such a role, the lipid rafts were disrupted by the use M β CD which extracts cholesterol from cellular membranes (145) and by either Fumonisin B1 or Myriocin, two specific inhibitors of sphingolipid biosynthesis (147).

Previous reports showed that M β CD induces cholesterol depletion in different cell types resulting in the reorganization of PM lipids and coalescence of remaining liquid-ordered domains (180). Moreover, cholesterol extraction resulted in reorganization of the actin cytoskeleton resulting in a restriction of the lateral mobility of PM proteins (181). Release of virus particle from cholesterol-depleted and sphingolipid-reduced cells was not inhibited. This would implicate that the intracellular trafficking of VCVs towards the cell surface does not involve lipid rafts and that exocytosis of VCVs does not occur at these lipid domains known to provide platforms for protein-protein interaction.

In some experiments a slight stimulation of viral secretion upon M β CD treatment was observed and could either indicate that disruption of lipid raft domains at the cell surface facilitates the exocytosis or that the disorganization of cortical actin is responsible for these effects. This would be in line with the results of Cytochalasin D treatment discussed above, which also enhanced viral secretion. Remarkably, M β CD

treatment affected the phosphorylation pattern of secreted viral L protein. The treatment induced the hyperphosphorylation of L protein which is known to be phosphorylated by active MAP kinases in response to extracellular stimuli such as exposure to low temperature, UV-irradiation, and mitogenic phorbol ester (TPA) (52). However, MAP kinase was presumably not responsible for the observed effect arguing for other possible kinases that could be involved or for the inhibition of phosphatases that normally dephosphorylate the L protein. The effect of such hyperphosphorylation of the surface protein L on viral infectivity was not yet tested. Although lipid rafts are not essential for DHBV formation, cholesterol seems to be indispensable for viral infectivity. Thus, the understanding of the molecular organization of lipid rafts and the interaction of viral proteins with these raft domains and specifically with cholesterol could contribute to the development of new antiviral therapies. Small molecules that interfere with the interaction of viral proteins with cholesterol for example, could provide a means for the production of disordered non-infectious viral particles.

V. MATERIALS & METHODS

V.1. MATERIAL

V.1.1. Chemicals and reagents

All chemicals and reagents were purchased from Merck (Darmstadt), Roche (Mannheim), Roth (Karlsruhe), Serva (Heidelberg), and Sigma (Steinheim) if not otherwise mentioned.

Enzymes

Alkaline phosphatase	Biolabs, Frankfurt am Main
Kollagenase	Biochrome, Berlin
Proteinase K (PCR grade)	Roche Diagnostics, Mannheim
Restriction endonucleases	Biolabs, Frankfurt am Main
<i>Taq</i> -Polymerase	Biolabs, Frankfurt am Main
T4 DNA ligase	Roche, Mannheim

Kits

ECL Western Blotting Reagent	Pierce, USA
Qiaquick Gel Extraction Kit	Qiagen, Hilden
Plasmid Mini/Midi/Maxi Kit	Qiagen, Hilden
Readyprime II Random Prime Labeling System	Amersham, Heidelberg

Other Chemical substances and inhibitors

Table 1. The working concentrations were determined either by dose escalation studies or adapted from the literature, all substance were stored at -20°C except for CTB-FITC (4°C).

Name	Working concentration	Dissolved in	Manufacturer
Brefeldin A (BFA)	10 µg/ml	DMSO	Sigma, Deisenhofen
Cholera toxin subunit B (CTB)-FITC	5 µg/ml	H ₂ O	Sigma, Deisenhofen
Cytochalasin D	20 µM	DMSO	Sigma, Deisenhofen
Fumonisin B1	50 µM	DMSO	Sigma, Deisenhofen
Fluorescein-diacetate	ca. 1 µg/ml	DMSO	Sigma, Deisenhofen
Methyl-β-cyclodextrin	10 mM	H ₂ O	Sigma, Deisenhofen
Mevinolin	10 µM	DMSO	Sigma, Deisenhofen
Myriocin	20 µM	DMSO	Biomol, Hamburg
Nocodazole	20 µM	DMSO	Sigma, Deisenhofen
Paclitaxel	20 µM	DMSO	Sigma, Deisenhofen
Phalloidin-FITC/TRITC	4 µg/ml	H ₂ O	Molecular Probes, UK

V.1.2. Bacterial strains

Top 10	<i>F. mcrA</i> Δ(<i>mrr-hsdRMS-mcrBC</i>) Φ80 <i>lacZ</i> ΔM15 Δ <i>lacX74 recA1 araD139</i> Δ(<i>araleu</i>) 7697 <i>galJ galK rpsL</i> (Str ^R) <i>endA1 nupG</i> (Invitrogen, Karlsruhe)
DH5α	<i>F</i> - φ80 <i>lacZ</i> ΔM15 Δ(<i>lacZYA-argF</i>)U169 <i>recA1 endA1 hsdR17</i> (r _k ⁻ , m _k ⁺) <i>phoA supE44 thi-1 gyrA96 relA1 tonA</i> (Gibco BRL, Eggenstein)

V.1.3. Cell culture

Cell lines and primary cells

LMH	Chicken hepatoma cell line
D2	LMH cells stably transfected with DHBV-genome, kindly provided by J. Summers and W. Mason, USA
PDHs	Primary duck hepatocytes isolated from Pekin duck foetuses
Liver biopsies	from adult Pekin ducks

Reagents for cell culture

Cells were cultured at 37°C with 5% CO₂.

All cell culture reagents were purchased from Gibco BRL (USA), Sigma (Mannheim), or Biochrom (Berlin). The media were supplemented as follows:

Dulbeco's Modified Eagle's Medium (DMEM) for LMH and D2 cells

10%	Heat inactivated FCS
100 U/ml	Penicillin
100 µg/ml	Streptomycin
1mM	Sodium pyruvat
1%	Non essential amino acids

Williams' medium E for PDHs

2 mM	L-glutamine
15 mM	HEPES, pH 7.2
1.5%	DMSO
10 µM	Hydrocortisone
1 nM	Insulin
100 U/ml	Penicillin
100 µg/ml	Streptomycin

For temperature block experiments, cells were cultured in a CO₂-independent medium (Invitrogen, Karlsruhe) supplemented as described for DMEM medium for D2 cells or for Williams' medium E for PDHs.

Trypsin solution

0.25%	Trypsin
1 mM	EDTA

Tissue culture lab ware

All cell culture plastic ware was purchased from Greiner (Solingen), and Sarstedt (Nuembrecht).

V.1.4. Antibodies

Primary antibodies

Name	Species	Dilution for WB/IF	origin
anti-actin	mouse	WB 1:10000	Sigma, Deisenhofen
anti-albumin	rabbit	WB 1:5000	Nordic immunology, Offenbach
anti- α -tubulin	mouse	WB 1:10000 IF 1:1000	Sigma, Deisenhofen
anti-apolipo- protein A-I	rabbit	WB 1:5000	M. Hermann, Vienna
anti-calnexin	rabbit	WB 1:5000 IF 1:200	Stressgen, Canada
anti-core	rabbit	WB 1:10000 IF 1:400	L. Cova, Lyon, France
anti-EEA1	rabbit	WB 1:2500 IF 1:200	Stressgen, Canada
anti-gamma- adaptin	rabbit	WB 1:2000 IF 1:200	R. Prange, Mainz
anti-GFP	rabbit	WB 1:5000	Santa-Cruz, California
anti-L 1H1	mouse	IF 1:100	(182)
anti-L Kpnl	rabbit	WB 1:10000 IF 1:800	(183)
anti-membrin	mouse	WB 1:5000 IF 1:200	Stressgen, Canada
anti-MTP	rabbit	WB 1:5000 IF 1:200	M. Hermann, Vienna
anti-PDI	mouse	WB 1:5000 IF 1:200	Abcam, UK
anti-rab5B	rabbit	WB 1:5000 IF 1:200	Santa-Cruz, California
anti-duck S	rabbit	WB 1:2500 IF 1:100	H. Schaller, Heidelberg

Table 2. Primary antibodies diluted in TBST containing 3% blocking milk. Abbreviations WB: western blot; IF: immunofluorescence.

Secondary antibodies

Name	Species	Dilution	Manufacturer
anti-rabbit-HRPO	goat	WB 1:10000	Dianova, Hamburg
anti-mouse-HRPO	goat	WB 1:10000	Dianova, Hamburg
anti-goat-HRPO	doncky	WB 1:5000	Dianova, Hamburg
anti-rabbit-488 (Alexa 488)	goat	IF 1:800	Molecular Probes, Netherlands
anti-rabbit-594 (Alexa 594)	goat	IF 1:800	Molecular Probes, Netherlands
anti-rabbit-555 (Alexa 555)	goat	IF 1:800	Molecular Probes, Netherlands
anti-mouse-488 (Alexa 488)	goat	IF 1:800	Molecular Probes, Netherlands
anti-mouse-594 (Alexa 594)	goat	IF 1:800	Molecular Probes, Netherlands
anti-mouse-555 (Alexa 555)	goat	IF 1:800	Molecular Probes, Netherlands

Table 3. Secondary antibodies

The secondary antibodies coupled with HRPO were dissolved in sterile 50% glycerol according to the manufacturer instructions and diluted in TBST containing 3% blocking milk.

Antibodies coupled with fluorophores were diluted in 1 x PBS. Abbreviations WB: western blot; IF: immunofluorescence

V.1.5. Primers

Oligonucleotides were purchased from Invitrogen (Karlsruhe) or MWG (Ebersberg).

Analytical primers

Both primers were adapted from (66).

DHBV P1 5'-GCG CTT TCC AAG ATA CTG GAG CCC AA-3'

DHBV P2 5'-CTG GAT GGG CCG TCA GCA GGA TTA TA-3'

Primers for cloning

Construct	Primer name	Restriction site	Sequence 5'-3'
EGFP-S	Forward EGFP-S	<i>Bgl</i> II	GCG AGA TCT ATG TCT GGT ACC TTC GGG GGA
	Reverse EGFP-S	<i>Sac</i> II	GCG CCG CGG CTA ACT CTT GTA AAA AAG AGC AGA
S-EGFP	Forward S-EGFP	<i>Eco</i> RI	GCG GAA TTC ATG TCT GGT ACC TTC GGG GGA
	Reverse S-EGFP	<i>Sac</i> II	GCG CCG CGG ACT CTT GTA AAA AAG AGC

V.1.6. Plasmids**Commercially available plasmids**

pcDNA 3.1 (-)	Invitrogen, Karlsruhe
pEGFP-N1	BD Biosciences/Clontech, USA
pEGFP-C1	BD Biosciences/Clontech, USA
YFP- β -galactosidase	BD Biosciences/Clontech, USA

Provided plasmids

RFP-CD63, RFP-CD82, YFP-Rab11, YFP-Rab7, and Tsg101-YFP were generously provided by W. Mothes, New Haven, USA (157).

VSV-G-GFP: encodes the glycoprotein G of the vesicular stomatitis virus (VSV) within the pEGFP-N1 vector (H. Sirma, HPI, Hamburg).

DHBV wt: encodes a 1.2-fold genome of DHBV, pDHBV16/1.1 (184).

DHBV 16t-27: encodes the DHBV 16 genome in tandem (185).

Generated plasmids

Name	Vector	Insert	Resistance	Origin/Reference
EGFP-S	pEGFP-C1	Duck S sequence amplified by PCR, cloned via <i>Bgl</i> II and <i>Sac</i> II	Kanamycin	L. Lin. and H. Sirma HPI, Hamburg
pDuck-S	pcDNA 3.1	Duck S (generated by the transfer of the S coding region from SEGFP into pcDNA3 via <i>Bam</i> HI and <i>Apa</i> I)	Ampicillin	M. Mhamdi, HPI, Hamburg
pGEM-D1OG (Expression vector for duck preS/S)	pGEM13 zf (+)	D1OG (DHBV full length monomere), cloned via <i>Eco</i> RI	Ampicillin	N. Lohrengel, HPI, Hamburg
SEGFP	pEGFP-N1	Duck S sequence amplified by PCR, cloned via <i>Eco</i> RI and <i>Sac</i> II	Kanamycin	M. Mhamdi, HPI, Hamburg

V.1.7. Devices**Centrifuges**

Mini ultracentrifuge, Sorvall Discovery M120	Hitachi, Japan
RC-5B refrigerated super speed centrifuge with the rotors GSA, SS-34	Sorvall, Bad Homburg
Table Centrifuge 5415 R (refrigerated)	Eppendorf, Hamburg
Table Centrifuge 5415 C	Eppendorf, Hamburg
Ultracentrifuge Optima LE-80K with the SW-41 rotor	Beckman, USA
Centrifugation tubes for SW 41, 14 ml	Beckman, USA

Microscopes

Light microscope	Leica, Bensheim
Fluorescence microscope	Zeiss, Jena
CLSM LSM 510	Zeiss, Jena
Electron microscope	Siemens, Germany

Other devices

Film developer Curix 60 Agfa,	PMA Bode, Hamburg
Fluor-S multi-imager	Bio-Rad, USA
Fraction recovery system	Beckman, USA
Gel documentation system	Decon, Hohengandern
Homogenisator	GlasCol, USA
Image-sacnner	Epson, Meerbuch
Incubator (for cells)	Thermo, Berlin
Incubator shaker	New Brunswick scientific, USA
pH meter	Inolab, Germany
Phosphoimager Fujix Bas	Raytest, Straubenhardt
Photometer Ultraspec 3000 pro	Pharmacia, Freiburg
RoboCycler Gradient 40/96	Stratagene, Netherland
Semi-Dry-System Trans blot SD	Bio-Rad, USA
SDS-PAGE device	Bio-Rad, USA
Shaker	IKA, Staufen
Sterile bench	Thermo, Berlin
Thermomixer compact	Eppendorf, Hamburg
UV-Stratalinker	Stratagene, Netherland
Water bath	Milian, France

V.2. METHODS

V.2.1. Cell culture and Treatments

V.2.1.1. Preparation of primary duck hepatocytes

To obtain primary duck hepatocytes (PDHs), eggs from congenitally DHBV-infected ducks were incubated for 21 days at 37°C in a saturated water atmosphere. Eggs were opened, the embryos were removed and the liver was isolated. The liver was cut into small pieces and transferred to a tube containing 3 ml of 0.5% sterile collagenase solution. The liver pieces were digested for 45 min at 37°C in a water bath and the suspension was shaken every 10 min. Cells were then pelleted by centrifugation for 5 min at 800 rpm. The supernatant was aspirated and washed with 5 ml medium (without additives). The wash steps were repeated 3 times. The final pellet was resuspended in Williams' Medium E (with all additives) and plated in 12-well plates at a density of about 5×10^5 cells per well. For immunofluorescence analysis, cells were cultured on glass coverslips (Roth, Karlsruhe) in a 24-well plate with a density of about 10^5 cells.

About 4 to 5 h post plating (when the cells were attached to the plastic), medium was changed. New medium was given everyday, and the experiments were performed at day 4 to 7 post plating if not otherwise indicated.

The obtained PDHs culture was a mixture of hepatocytes and non-parenchymal cells (186).

V.2.1.2. Cultivation of cell lines

LMH and D2 cells were grown in DMEM complete medium. Cells were cultivated in 75 cm² cell culture flasks at 37°C, 5% CO₂ and >90% humidity. The maintenance culture was passaged by trypsinization every 3-4 days.

V.2.1.3. Treatment of cells

Congenitally DHBV-infected PDHs were cultured in 12-well plates. 3-4 days post plating cells were washed once with sterile 1 x PBS and 1 ml fresh medium was added. Cells were treated with different substances over night (16 h) or for the indicated time points (12, 24, 48 or 60 h), untreated cells were used as control cells. If treatments were longer than 24 h, fresh medium and new substances were added every 24 h. Next day, supernatants were collected, cleared by centrifugation for 5 min at 6.000 rpm at 4°C, transferred to a new tube and stored at -20°C. Cells were harvested for immunoblot and PCR analysis. For each treatment, 3 independent experiments were performed.

10 x PBS, pH 7.4

140 mM	NaCl
8 mM	Na ₂ HPO ₄
2 mM	KH ₂ PO ₄
3 mM	KCl

BFA washout

To determine the time point of reversibility of BFA, cells were treated over night as described above. Next day, cells were washed twice with PBS and further incubated in fresh medium without the drug for the indicated time points. Supernatants and cells were harvested as indicated above.

Temperature block

The transport of protein from the Golgi and TGN to the cell surface can efficiently be inhibited at 20°C. To investigate whether DHBV secretion depends on the Golgi complex, congenitally DHBV-infected PDHs as well as D2 cells transfected with VSV-G-GFP (at day 2 post-transfection) were incubated over night either at 37°C or at 20°C in a CO₂-independent incubator. Cells were washed twice with PBS and fresh medium (CO₂-independent) was added. Next day, supernatants were harvested and

cleared by centrifugation as described above and D2 cells were fixed directly in 3.7% paraformaldehyde (PF) for immunofluorescence analysis.

Viability test

Congenitally DHBV-infected PDHs were treated over night or for the indicated time points with the indicated substances. Next day, cells were washed twice with PBS and 0.4% trypan blue (Gibco BRL, USA) in PBS was added to the cells for 3 min. Cells were washed again, monitored under the microscope and pictures were acquired. If the used substances were cytotoxic, cells would die and the plasma membrane would become leaky allowing the diffusion of trypan blue into the cytoplasm which will be stained. The same cells were further used for the second test with fluorescein diacetate (FDA). Cells were washed once with PBS, fresh medium was added. Cells were incubated with 5 μ l FDA (about 2 mg dissolved in 1 ml DMSO) for 5 min at 37°C, medium was changed and cells were analysed under a fluorescence microscope. Only hepatocytes possess a specific lipase required for the conversion of FDA to fluorescein and thus only living hepatocytes are stained green.

V.2.1.4. Transient transfections

PDHs

Congenitally DHBV-infected PDHs were grown on coverslips in 24 well tissue culture plates. One day post plating, cells were transfected with 3 μ g DNA/well of the indicated plasmids using 6 μ l JetPEI (Polyplus transfection, France) according to the manufacturer's instructions. Next day, medium was changed and transfection efficiency was estimated by epifluorescence microscopy. Cells were cultivated for further 24 h to 48 h prior to fixation.

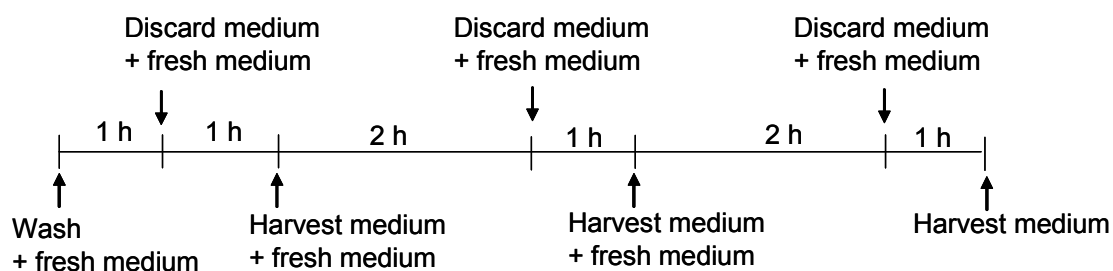
D2 cells

D2 cells were seeded at a density of 1×10^4 or 5×10^4 on coverslips. Next day, cells were transfected using FuGene6 (Roche, Germany) according to the manufacture's instructions. Briefly, 90 μ l medium without any supplements, 1 μ g plasmid DNA, and 3 μ l FuGene6 were mixed and incubated for 15 min at RT. The mixture was added to

the cells and incubated over night at 37°C. Next day, the transfection solution was removed, fresh DMEM medium was added, and cells were further cultivated for 24-48h.

V.2.1.5. Secretion kinetic and its quantification

To determine the secretion kinetics of DHBV and the ratio between virions and SVPs, congenitally DHBV-infected PDHs in 12-well plate were used and the supernatants were collected according to the following scheme:



The quantification of secreted virions as measured by viral DNA was performed by DNA-dot blot analysis.

For the quantification of SVPs, serial dilutions of recombinant preS protein (kindly provided by S. Urban, Heidelberg) with known amount were used as a standard and quantified with a Multimager (Biorad).

V.2.2. Protein biochemistry

V.2.2.1. Subcellular fractionation and iodixanol gradient ultracentrifugation

The protocol was adapted from (187, 188) and modified. Congenitally DHBV-infected fetal livers were cut into small pieces and resuspended in 3 ml homogenization buffer (HB). The suspension was centrifuged for 4 min at 100 g and 4°C, the pellet was then washed twice with HB. Afterwards, the pellet was resuspended in 0.5 ml HB and homogenized in a glass homogeniser with 15 strokes. The homogenate was centrifuged for 10 min at 2.500 g and 4°C. The post-nuclear supernatant (PNS) was transferred into a new tube, the pellet was resuspended in 500 µl HB, re-centrifuged, and both PNS were pooled. For a 0-26% linear iodixanol gradient, a stock solution of

60% (w/v) iodixanol (Optiprep, Axis-shield, Oslo) was initially diluted to 50% by adding 5 volumes optiprep to 1 volume of the diluent solution. Equal volumes of this working solution and HB were mixed to make a 25% iodixanol solution. A 12 ml continuous density gradient was prepared using a two chamber gradient maker by mixing 6 ml 25% iodixanol and 6 ml HB. The PNS was loaded on top of the gradient and centrifuged for 1h 55 min at 41.000 rpm and 4°C in a Beckman SW 41 rotor. Seventeen fractions of 700 µl each were collected from the bottom by tube puncture. Their refractive index was measured and the densities were calculated according to the formula $\rho=3.333\eta-3.442$.

<u>Homogenization buffer (HB)</u>	0.25 M	Sucrose
	1 mM	EDTA
	10 mM	Hepes-NaOH, pH 7.4
	1 tablet Protease-Inhibitor-Cocktail (Roche)	
<u>Diluent solution</u>	0.25 M	Sucrose
	6 mM	EDTA
	60 mM	Hepes-NaOH, pH 7.4

V.2.2.2. Immunoprecipitation of virus particles-containing vesicles

Congenitally DHBV-infected PDHs cultures from a 6 well plate were scraped in PBS and pelleted. The pellet was dissolved in HB and cells were potted 15 times. Half of the homogenate was subjected to immunoprecipitation. For immunoprecipitation from subcellular fractions, 100 µl of fraction 8, 9, 10, and 11 were pooled, diluted to 1.5 ml with PBS and incubated with the antibody-decorated beads over night at 4°C under rotation. For immunoblot analysis, 5% of input, 5% of post-IP supernatant, and 20% of the IP pellet were loaded.

<u>Homogenization buffer (HB)</u>	0.25 M	Sucrose
	1 mM	EDTA
	10mM	Hepes-NaOH, pH 7.4
	1 tablet Protease-Inhibitor-Cocktail (Roche)	

V.2.2.3. Labelling of cell surface proteins with sulfo-NHS-biotin, immunoprecipitation, and detection of biotinylated surface proteins

Non-infected and congenitally DHBV-infected PDHs were cultured in 12 well-plates. Six days post plating, cells from 3 wells were washed 3 times with ice-cold 1x PBS. Cell surface proteins were biotinylated using 100 µg/ml cell-impermeant sulfo-NHS-Biotin (Pierce, USA) in PBS for 1h at 4 °C. Control cells were treated in the same way without being incubated with biotin. Unlinked biotin was quenched and removed by 3 washes with ice-cold PBS supplemented with 10 mM glycine. Cells were either directly harvested in 500 µl PBS, collected by centrifugation at 6,000 rpm and 4°C for 5 min or incubated for 20 sec with 500 µl 0.25% trypsin-EDTA solution. Trypsin was aspirated and cells were further incubated for 2 min at RT. Cells were then harvested in 500 ml serum-containing medium to inactivate trypsin, pelleted and washed once with PBS. Cell pellets were lysed for 30 min at RT in 500 µl lysis buffer and cell lysates were centrifuged at 6.000 rpm and 4°C for 10 min. Supernatants were collected and processed in 2 different ways.

<u>Lysis buffer (189)</u>	50 mM	Tris-HCl, pH 7.5
	150 mM	NaCl
	1%	Triton X-100
	1%	Deoxycholol

Immunoprecipitation of biotinylated surface proteins using streptavidin-coated beads

25 µl streptavidin-coated magnetic microspheres (Bangs laboratories) were added to the samples, incubated for 2 hours under rotation, washed 3 times with PBS and lysed in SDS-loading buffer.

Immunoprecipitation using an L-specific antibody

Half of the above prepared supernatant from cell lysates was used for immunoprecipitation with DHBV-preS specific antiserum, the other half was immunoprecipitated with a control antiserum. Samples were processed as for the streptavidin IP. For immunoblot, 5% input and 20% IP pellet were loaded.

To detect biotinylated surface proteins, membranes were blocked in TBST supplemented with 1% BSA (Sigma) for 1 h at RT, washed twice with TBST and incubated with HRP-conjugated streptavidin (Sigma) (1:10.000) in TBST for 1 h. The membrane was washed 6 times for 5 min with TBST and biotinylated proteins were visualized by indirect chemiluminescence (Pierce, USA). The same membrane was then reprobbed with DHBV-preS specific antiserum after inactivation of the peroxidase with sodium azide for the detection of the viral surface protein L.

V.2.2.4. SDS-PAGE and Immunoblot

Following treatments, cell culture supernatants and cells were harvested for immunoblotting. Briefly, supernatants were harvested, cleared by centrifugation, transferred into a new tube, 15 µl were transferred to a new tube and 5 µl 4 x Laemmli lysis buffer were added.

Cells were washed twice with 1 x PBS, 200 µl 4 x Laemmli buffer per well were added, cells were scraped and transferred into a reaction tube. 20 µl were used for immunoblotting.

For immunoblotting of samples from immunoprecipitation, 5% input, 20% IP pellet, and 5% of post IP supernatant were loaded.

For detection of viral L and core proteins as well as cellular marker proteins within subcellular fractions, 17.5% from each fraction were loaded on a 5-20% gradient gel prepared using a two chamber gradient maker.

SDS-PAGE

Polyacrylamide gel electrophoresis (PAGE) permits the separation of proteins according to their electrophoretic mobility which depends on the molecular weight and post-translational modifications of the proteins. In the presence of the anionic detergent SDS, the secondary and non-disulfide-linked tertiary structures are denatured and the proteins acquire a negative charge proportional to their mass.

Prior to loading on gels, samples were boiled for 5 min at 99°C to permit the reduction of disulfide linkages by the reducing agents within the SDS-loading buffer.

Following electrophoresis, the proteins were transferred to a nitrocellulose membrane (Schleicher and Schuell, Dassel) by electroblotting. Then, the membrane was blocked for 30 min at RT with 3% non-fat-dry milk (Bio-Rad) in TBST (Tris buffered

saline plus 0.1% Tween 20) to reduce unspecific binding of the primary antibodies. The membrane was incubated with primary antibody at the appropriate dilution either for 1 h at RT or over night at 4°C. Subsequently the membrane was washed 3 times for 5 min with TBST and a horseradish peroxidase-linked secondary antibody at the appropriate dilution in TBST was added and incubated for 1 h at RT. The membrane was washed again 3 times for 5 min with TBST and signals were detected using indirect chemiluminescence (Pierce, USA).

<u>Laemmli lysis buffer (190)</u>	100 mM	Tris, pH 6.8
	20%	Glycerol
	2%	SDS
	0.1%	bromophenol blue
	0.2%	β-mercaptoethanol
<u>1 x SDS electrophoresis buffer</u>	250 mM	Tris
	19 mM	Glycine
	0.35 mM	SDS
<u>1 x Semi-dry transfer buffer</u>	48 mM	Tris
	39 mM	Glycine
	20%	Methanol
<u>1x TBST, pH 7.4</u>	10 mM	Tris
	100 mM	NaCl
	0.1%	Tween 20

V.2. 3. Molecular biology techniques

V.2.3.1. Detection of viral rcDNA by PCR analysis

Polymerase chain reaction (PCR) was used to amplify specific DNA sequences by simultaneous primers extensions of complementary strands. DNA accumulates exponentially by cyclic repetitions of 3 steps (i) denaturation (separation of DNA double strands), (ii) annealing (hybridization of the primers to their complementary sequences), and (iii) elongation (synthesis of the complementary strand by the *Taq*-polymerase). The PCR allows the rapid and sensitive detection of low DNA amounts. In this work, PCR was used for the detection of viral rcDNA as a marker for virions either in supernatants from congenitally DHBV-infected cells, within the lysates of these cells or within subcellular fractions of DHBV-infected liver.

Detection of viral rcDNA in cell lysates

For the detection of viral rcDNA in DHBV-infected PDHs after treatments with chemical inhibitors, cells were washed twice with 1 x PBS, 500 µl PCR lysis buffer was added to a well and incubated for 5 min at 37°C. Cell lysates were transferred to a reaction tube. Prior to PCR, the viral rcDNA which is contained in the nucleocapsid and surrounded by the envelope, must be liberated to be accessible for the PCR. Thus, 0.1 mg/ml proteinase K (PK) (Roche) was added to the tube and digested for 2 h at 56°C. To inactivate the enzyme, the tube was further incubated for 10 min at 95°C. For the PCR, 1 µl of the lysate was used.

<u>PCR-lysis buffer (66)</u>	50 mM	KCl
	10 mM	Tris, pH 8.3
	0.45%	Tween 20
	0.45%	Nonidet P-40

Detection of viral rcDNA in supernatants from DHBV-infected PDHs

To analyse the effects of different chemical substances on the transport and secretion of DHBV, the amount of released viral particles was compared to that of the control cells. For that, the viral rcDNA was detected by PCR. Supernatants from DHBV-infected PDHs were harvested after treatments and cleared by centrifugation for 5 min at 6,000 rpm and 4°C to pellet dead cells and transferred to a new tube. 50 µl of these supernatants were transferred to another tube and 150 µl PCR lysis buffer and 0.1 mg/ml PK were added. The digestion was performed as described above. 5 µl of each sample was used for PCR.

Detection of viral rcDNA in subcellular fractions from DHBV-infected liver

After subcellular fractionation of a congenitally DHBV-infected liver, fractions of 700 µl each were obtained. 10 µl of each fraction was transferred to a reaction tube and 190 µl PCR lysis buffer were added. The digestion was performed as described above. 5 µl of each sample was used for PCR analysis.

PCR reaction mix

For the PCR the following mix was used

5 µl	DNA
5 µl	10 x PCR-buffer (supplemented with MgCl ₂)
0.5 µl	dNTP-mix (0.2 mM)
0.5 µl	Primer DHBV P1 (50 pmol)
0.5 µl	Primer DHBV P2 (50 pmol)
0.5 µl	<i>Taq</i> -polymerase (2.5 units)
fill up with ddH ₂ O to a total volume of 50 µl	

To control contaminations, a negative control consisting of water instead of the sample was used. Serial dilutions with known genome equivalents (GE) (5×10^3 , 5×10^4 , 5×10^5 , and 5×10^6) for the semi-quantifications of the PCR signals were included on each run.

All samples were overlaid with mineral oil to avoid the evaporation of the mix during the PCR reaction.

PCR program (25 cycles):

1 min at 94°C	denaturation step
3 min at 72°C	DNA-synthesis step

A specificity of this PCR is the missing annealing step to minimize unspecific annealing of the primers.

At the end of the reaction, 10 µl of each samples were loaded on a 1% agarose gel.

V.2.3.2. Agarose gel electrophoresis

Linear DNA fragments are separated by agarose gel electrophoresis according to their size. Agarose is melted in TAE buffer at the appropriate concentration and ethidium bromide (EtBr) is added. The solution is poured into a horizontal gel chamber containing a comb. After solidification, 10 µl of the PCR product and 2 µl loading buffer are mixed and loaded on the gel. The gel was run in TAE running buffer at 100 V for about 20-30 min. The visualization of the DNA was possible by the means of EtBr, which intercalates between the DNA double helix, under UV light.

<u>TAE buffer</u>	40 mM	Tris-HCl, pH 8.0
	40 mM	Sodium acetate
	1 mM	EDTA

<u>Loading buffer</u>	50 mM	Tris-HCl pH 7.6
	60%	Glycerol
	0.25%	Xylene cyanol
	0.25%	Bromophenol blue

V.2.3.3. Dot blot hybridization assay

The secretion kinetic of DHB virions was determined by DNA-dot blot analysis. 100, 250 or 500 µl of supernatants from congenitally DHBV-infected cells were harvested as described above (section V.2.1.5). Serial dilutions of viremic serum with known genome equivalents (GE) was included as standard.

Briefly, all samples were prepared in 500 µl 1 x PBS, dotted with the dot blot device on a nylon membrane (Hybond N, Amersham, Freiburg). The membrane was air dried and DNA was denaturated 2 times for 1.5 min by incubating the membrane on a whatman paper soaked in Soak I buffer. Between each incubation, the membrane was air dried. Subsequently, the membrane was neutralized by incubating it 4 times on a whatman paper soaked in Soak II buffer. The membrane was dried between every step. Then DNA was fixed on the membrane by UV-crosslinking in a Stratalinker. For prehybridization, the membrane was incubated with 5 ml QuickHyb (Stratagene, USA) for 30 min at 68°C. Then the denatured radioactive probe (see next paragraph) was added and incubated over night. Next day, the membrane was washed with wash 1 solution for 30 min at 68°C followed by a second wash step with wash 2 solution at RT. Finally, the membrane was exposed to a phosphoimager screen and the signals were detected by phosphoimaging and quantified with Tina 2.0 software.

<u>Soak I</u>		<u>Soak II</u>	
0.5 M	NaOH	0.5 M	Tris-HCl, pH 7.4
1 M	NaCl	3 M	NaCl
<u>Wash 1</u>		<u>Wash 2</u>	
10%	20 x SSC	1%	20 x SSC
0.1%	SDS	0.5%	SDS

V.2.3.4. Preparation of a radioactively labelled probe

For the detection of DHBV DNA after dot blot, a DHBV-specific probe was prepared. Therefore, plasmid DNA encoding the DHBV16 genome in tandem was used. 50 ng of this plasmid was added to a 45 µl final volume of TE buffer and incubated for 5 min at 95°C to denature the DNA. Subsequently, the DNA was incubated for 5 min on ice. The denatured DNA was transferred to a tube containing Readyprime II random Prime labelling system (Amersham, Pharmacia, Heidelberg), and 5 µl of ³²P-dCTP (Hartmann analytic, Braunschweig) were added and well mixed by pipetting. The reaction mix was incubated for 30 min at 37°C to allow the synthesis of short radiolabelled DNA fragments which are complementary to the DHBV genome. The reaction was stopped by adding 5 µl of 0.2 M EDTA and further incubation for 5 min at 37°C. To remove non-incorporated nucleotides, the reaction mix was applied to a G25-spin column (Amersham, Heidelberg) and centrifuged for 2 min at 3000 rpm. 100 µl of thymus DNA (Sigma, Deisenhofen) was added to minimize the unspecific binding of the probe to the membrane and the activity of the probe was tested in a scintillation counter.

Before incubating with the membrane, the probe was denaturated by incubation for 5 min at 99°C.

<u>TE-buffer</u>	10 mM	Tris-HCl, pH 8.1
	1 mM	EDTA

V.2.3.5. Cloning

Amplification of the duck S gene by PCR

The S gene was amplified by PCR using DHBV wt plasmid as a template and the primers described above in section V.1.5. The PCR conditions were identical to those for the amplification of rcDNA. The PCR product was loaded on an agarose gel.

Isolation of DNA from agarose gel

The DNA fragment was excised from the gel using a clean scalpel and was extracted from the gel using the QIAquick Gel Extraction Kit (Qiagen) according to the manufacturer's instruction. Briefly, the agarose was solubilized, the released DNA bound to a silica matrix under high salt conditions and eluted under low salt conditions with ddH₂O.

Digestion of DNA with restriction endonucleases

Restriction enzymes recognize short DNA sequences and cut double-stranded DNA at a specific site within or adjacent to the recognition sequence. This results in either sticky or blunt ends depending on the restriction enzyme used. Digestion was performed according to the manufacturer's instructions. 1 µg of DNA was digested with 1 U enzyme for 1 h at the appropriate temperature.

Dephosphorylation of DNA

Linearized vectors that would be used for ligation were dephosphorylated at their 5'-end to avoid religation. This is catalysed by the alkaline phosphatase. Generally, 1 µg of linearized vector was incubated with 1 U of alkaline phosphatase for 30 min at 37°C in the appropriate buffer.

Ligation of DNA

DNA ligase is an enzyme which catalyses the formation of phosphodiester bond between juxtaposed 5'-phosphate and 3'-hydroxyl termini of double-stranded DNA. Prior to ligation, the digested insert and the linearized and dephosphorylated vector were purified by gel extraction as described above. The ligation reaction was performed with 20-50 ng vector and 5-fold molar excess of the insert DNA in the presence of the appropriate amount of T4-ligase and the reaction buffer in a 20 µl reaction volume. The reaction was incubated for 16 h at 16°C. Half of the ligation mix was transformed into bacteria.

V.2.3.6. Amplification and extraction of plasmid DNA

Generation of chemically competent bacteria

In order to generate chemically competent bacteria, 50 µl of competent bacteria were plated on an agar plate without antibiotic and incubated over night at 37°C. Next day, one colony was picked into 3 ml 1 x LB medium to obtain an over night culture.

Next day, 1 ml from the over night culture was transferred into 500 ml 1 x LB medium and grown to an optical density of $OD_{600}=0.6$. Bacteria were incubated for 10 min on ice and pelleted by centrifugation for 5 min at 5.000 rpm and 4°C. The pellet was resuspended in 150 ml sterile and cold TFB I solution and incubated for 20 min on ice. Cells were pelleted as described above and the final cell pellet was resuspended in 20 ml TFB II. The suspension of chemically competent bacteria was aliquoted in 200 µl aliquots, immediately frozen in liquid nitrogen and stored at -80°C. Next day, the competence of the cells was tested using plasmid DNA.

<u>Buffer TFB I</u>	30 mM	Potassium acetate, pH 5.8
	100 mM	RbCl ₂
	50 mM	MnCl ₂
	10 mM	CaCl ₂
	15%	Glycerol
 <u>Buffer TFB II</u>	10 mM	MOPS pH 8
	10 mM	RbCl ₂
	75 mM	CaCl ₂
	15%	Glycerol

Transformation of bacteria

For the amplification of plasmid DNA, 50 µl of competent bacteria was thawed on ice, 1 µg plasmid DNA was added and mixed. The mix was further incubated for 10 min on ice to allow the binding of the DNA to the surface of the bacteria. Next, the mix was incubated for 90 sec at 42°C (heat shock) to allow the uptake of the DNA. Bacteria were then incubated for 2 min on ice to permit closing of the pores within the bacterial membrane. 950 µl 1 x LB-medium was added and incubated for 30 min at 37°C to allow bacteria to recover and to begin to express the antibiotic resistance gene. Bacteria were pelleted by centrifugation at 13,000 rpm for 10 sec, resuspended in 30 µl 1 x LB-medium, plated on selection plates and incubated over night at 37°C. Clones were picked for an over night culture in 3 ml 1 x LB-medium containing the appropriate antibiotic, ampicillin (100 µg/ml) or kanamycin (30 µg/ml), and incubated over night at 37°C.

Mini-preparation of plasmid DNA

For the identification of the positive clones containing the DNA of interest, mini-preparation was performed based on alkaline lysis using the solutions of the “Plasmid Maxi Kit” (Qiagen). 1 ml from the over-night culture was transferred into a tube, pelleted by centrifugation at full speed for 5 min at 4°C and resuspended into 100 µl buffer P1. The lysis was performed with 150 µl buffer P2 by incubation for 5 min at RT. Then, 150 µl buffer P3 was added to neutralize the solution. The lysates were centrifuged for 10 min at full speed and 4°C and supernatants were transferred to a new tube. The DNA was subsequently precipitated with 800 µl ethanol and 40 µl sodium acetate by incubation for 10 min at -80°C. The solution was centrifuged for 15 min at full speed and 4°C, DNA pellet was washed twice with 200 µl 70% ethanol and air dried. The pellet was resuspended in 30 µl ddH₂O.

To identify positive clones, 3 µl of the DNA was analysed by restriction digestion.

Maxi-preparation of plasmid DNA

For the amplification of the positive clones, 1 ml from the over night culture was transferred into 250 ml 1 x LB-medium with the appropriate antibiotic and incubated over night at 37°C under shaking.

Bacteria were pelleted by centrifugation at 6,000 rpm and 4°C for 15 min. The preparation of plasmid DNA was carried out with the “Plasmid Maxi Kit” from Qiagen according to the manufacturer’s protocol based on alkaline lysis. The resulting DNA pellet was resuspended in 200 µl ddH₂O and the concentration was measured by UV-spectrometry.

1 x LB, pH 7	10 g	Bacto-Trypton
	5 g	Bacto-Yeast
	10 g	NaCl

Quantification of nucleic acid

Quantification of DNA was performed by UV-spectrometry. The absorption of DNA in water was measured at wavelengths of 260 nm and 280 nm, which are the absorption maxima of DNA and protein, respectively. At these wavelengths, the extinction of 1.0 corresponds to the concentration of 50 µg/ml of double stranded DNA. The ratio between OD₂₆₀ and OD₂₈₀ indicates the purity of the DNA solution, For pure DNA, the ratio is 1.8.

V.2.3.7. Microscopy

Confocal laser scanning microscopy

PDHs or D2 cells grown on coverslips in 24-well plates were treated or not as indicated above. Cells were washed twice with 1 x PBS and either fixed with ice-cold methanol-acetone (1:1) or with 3.7% paraformaldehyde (PF) for 10 min at RT. PF-fixed cells were permeabilized for 10 min with 0.1% Triton X-100. Cells were incubated with the primary antibodies at the appropriate dilutions for 1 h at RT.

Subsequently, cells were washed 3 times with 1 x PBS and FITC- or TRITC-labelled secondary antibodies were applied for 1 h at RT followed by 3 washes.

For visualization of the PM using cholera toxin B (CTB) (Sigma), cells were incubated with 5 µg/ml CTB at 37°C for 30 min prior to fixation, fixed with 3.7% PF for 10 min at RT and processed as described above. To visualize actin, PF-fixed cells were incubated with TRITC- or FITC-labelled phalloidin (1:500 in PBS). Nuclei were stained with DRAQ5 (Biostatus, UK) diluted 1:500 in PBS for 5 min at RT. The coverslips were mounted and embedded in Mowiol (Calbiochem).

Confocal images were acquired with a Zeiss confocal microscope LSM 510 Meta (x 63/1.4 oil Plan-Apochromat objective) and Zeiss Confocal Microscopy Software, Release 3.2. Z-stacks were acquired from the bottom (coverslip) to the top of the cells. Photomultiplier gain and laser power were identical in each experiment. The pinhole setting in every experiment was ≤ 1 .

Live cell imaging

For live cell microscopy, LMH cells were seeded on glass bottom culture dishes (Mat Tec, USA) at a density of about 10^5 cells, and transfected with FuGene6 according to the manufacturer's instructions. Briefly, 90 µl medium without any supplements, 0.5 µg EGFP-S, 3 µg pGEM-D10G, 0.5 µg CD63-RFP or CD82-RFP and 12 µl FuGene6 were mixed and incubated for 20 min at RT. The mix was added to the cells and incubated over night. Next day, fresh medium was added and cells were further incubated.

36 h later, 20 mM Hepes (pH 7.4) was added to the medium, and the cell dish was mounted on a heated stage and analyzed at 37°C by confocal microscopy using Zeiss confocal microscope LSM 510 Meta (x 63/1.4 oil Plan-Apochromat objective) and Zeiss Confocal Microscopy Software, Release 3.2. Three-dimensional (3D) reconstructions and orthogonal projection were performed with "Imaris v.4.1.3".

Electron microscopy

For thin section analysis of non-infected or congenitally DHBV-infected PDHs, cells were prepared as described above (preparation of PDHs) and transferred into cellulose tubes (capillaries) directly after the wash steps by capillary transfer. Tubes were incubated in medium for 5-7 days. For BFA treatment, the substance was

added to the medium for the indicated time points and cells were subsequently fixed with 2.5% glutaraldehyde in PBS for 20 min. High velocity microbiopsies from DHBV-infected ducks liver were isolated and directly fixed as described above. Subsequently, tubes were washed with 1 x PBS and cells were post-fixed within the tubes for 30 min with 1% OsO₄ in PBS, washed with water, stained for 30 min with 2% uranyl acetate in water and dehydrated in a graded series of ethanol. Capillary tubes were embedded in ERL resin for sectioning. Ultrathin sections were counterstained with 2% uranyl acetate and lead citrate. For immunolabelling, capillary tubes were fixed with 2.5% paraformaldehyde (PF) in PBS for 30 min, washed with PBS. Tubes were embedded in ERL resin for sectioning. Ultrathin sections were blocked with 1% bovine serum albumin (BSA) in PBS and sections were subsequently incubated over night with core- and L-specific antisera (dilutions 1:400 for both) at 4°C. Sections were fixed again with 2.5% PF in PBS for 30 min and washed with PBS. Immune complexes were detected with protein A conjugated to 10 nm gold particles. Electron micrographs were acquired with a Philips CM120 transmission electron microscope at 80 kV using DigitalMicrograph software (Gatan).

VI. REFERENCES

1. Robinson W: Hepatitis B Virus and Hepatitis Delta Virus. In: G. Mandell RGDaJB, ed. Principles and Practice of Infectious Diseases. New York: Churchill Livingstone, 1990; 1204-1230.
2. McCollum RW. The size of serum hepatitis virus. *Proc Soc Exp Biol Med* 1952;81:157-160.
3. Blumberg BS, Gerstley BJ, Hungerford DA, London WT, Sutnick AI. A serum antigen (Australia antigen) in Down's syndrome, leukemia, and hepatitis. *Ann Intern Med* 1967;66:924-931.
4. Prince AM. An antigen detected in the blood during the incubation period of serum hepatitis. *Proc Natl Acad Sci U S A* 1968;60:814-821.
5. Dane DS, Cameron CH, Briggs M. Virus-like particles in serum of patients with Australia-antigen-associated hepatitis. *Lancet* 1970;1:695-698.
6. Shepard CW, Simard EP, Finelli L, Fiore AE, Bell BP. Hepatitis B virus infection: epidemiology and vaccination. *Epidemiol Rev* 2006;28:112-125.
7. Bond WW, Petersen NJ, Favero MS. Viral hepatitis B: aspects of environmental control. *Health Lab Sci* 1977;14:235-252.
8. Krugman S. Incubation period of type B hepatitis. *N Engl J Med* 1979;300:625.
9. Hoofnagle JH, Di Bisceglie AM. Serologic diagnosis of acute and chronic viral hepatitis. *Semin Liver Dis* 1991;11:73-83.
10. McMahan BJ, Alward WL, Hall DB, Heyward WL, Bender TR, Francis DP, Maynard JE. Acute hepatitis B virus infection: relation of age to the clinical expression of disease and subsequent development of the carrier state. *J Infect Dis* 1985;151:599-603.
11. Summers J, Smolec JM, Snyder R. A virus similar to human hepatitis B virus associated with hepatitis and hepatoma in woodchucks. *Proc Natl Acad Sci U S A* 1978;75:4533-4537.
12. Marion PL, Oshiro LS, Regnery DC, Scullard GH, Robinson WS. A virus in Beechey ground squirrels that is related to hepatitis B virus of humans. *Proc Natl Acad Sci U S A* 1980;77:2941-2945.
13. Mason WS, Seal G, Summers J. Virus of Pekin ducks with structural and biological relatedness to human hepatitis B virus. *J Virol* 1980;36:829-836.
14. Sprengel R, Kaleta EF, Will H. Isolation and characterization of a hepatitis B virus endemic in herons. *J Virol* 1988;62:3832-3839.
15. Pult I, Netter HJ, Bruns M, Prassolov A, Sirma H, Hohenberg H, Chang SF, et al. Identification and analysis of a new hepadnavirus in white storks. *Virology* 2001;289:114-128.
16. Summers J, Mason WS. Replication of the genome of a hepatitis B--like virus by reverse transcription of an RNA intermediate. *Cell* 1982;29:403-415.
17. Seeger C, Ganem D, Varmus HE. Biochemical and genetic evidence for the hepatitis B virus replication strategy. *Science* 1986;232:477-484.
18. Will H, Reiser W, Weimer T, Pfaff E, Buscher M, Sprengel R, Cattaneo R, et al. Replication strategy of human hepatitis B virus. *J Virol* 1987;61:904-911.
19. Seeger C, Mason WS. Hepatitis B virus biology. *Microbiol Mol Biol Rev* 2000;64:51-68.
20. Marion PL, Cullen JM, Azcarraga RR, Van Davelaar MJ, Robinson WS. Experimental transmission of duck hepatitis B virus to Pekin ducks and to domestic geese. *Hepatology* 1987;7:724-731.

21. Halpern MS, Egan J, McMahon SB, Ewert DL. Duck hepatitis B virus is tropic for exocrine cells of the pancreas. *Virology* 1985;146:157-161.
22. Jilbert AR, Freiman JS, Gowans EJ, Holmes M, Cossart YE, Burrell CJ. Duck hepatitis B virus DNA in liver, spleen, and pancreas: analysis by in situ and Southern blot hybridization. *Virology* 1987;158:330-338.
23. Hadchouel M, Pasquinelli C, Fournier JG, Hugon RN, Scotto J, Bernard O, Brechot C. Detection of mononuclear cells expressing hepatitis B virus in peripheral blood from HBsAg positive and negative patients by in situ hybridisation. *J Med Virol* 1988;24:27-32.
24. Tuttleman JS, Pourcel C, Summers J. Formation of the pool of covalently closed circular viral DNA in hepadnavirus-infected cells. *Cell* 1986;47:451-460.
25. Klingmuller U, Schaller H. Hepadnavirus infection requires interaction between the viral pre-S domain and a specific hepatocellular receptor. *J Virol* 1993;67:7414-7422.
26. Bruns M, Miska S, Chassot S, Will H. Enhancement of hepatitis B virus infection by noninfectious subviral particles. *J Virol* 1998;72:1462-1468.
27. Gavilanes F, Gonzalez-Ros JM, Peterson DL. Structure of hepatitis B surface antigen. Characterization of the lipid components and their association with the viral proteins. *J Biol Chem* 1982;257:7770-7777.
28. Sonveaux N, Thines D, Ruyschaert JM. Characterization of the HBsAg particle lipid membrane. *Res Virol* 1995;146:43-51.
29. Lien JM, Petcu DJ, Aldrich CE, Mason WS. Initiation and termination of duck hepatitis B virus DNA synthesis during virus maturation. *J Virol* 1987;61:3832-3840.
30. Standring DN, Rall LB, Laub O, Rutter WJ. Hepatitis B virus encodes an RNA polymerase III transcript. *Mol Cell Biol* 1983;3:1774-1782.
31. Ganem D, Schneider C: Hepadnaviridae: The viruses and their replication. In: Knipe DM, Howley PM, eds. *Fields Virology*. Volume 2. Philadelphia: Lippincott, Williams & Wilkins, 2001; 2923-2969.
32. Obert S, Zachmann-Brand B, Deindl E, Tucker W, Bartenschlager R, Schaller H. A splice hepadnavirus RNA that is essential for virus replication. *Embo J* 1996;15:2565-2574.
33. Weber M, Bronsema V, Bartos H, Bosserhoff A, Bartenschlager R, Schaller H. Hepadnavirus P protein utilizes a tyrosine residue in the TP domain to prime reverse transcription. *J Virol* 1994;68:2994-2999.
34. Chang LJ, Hirsch RC, Ganem D, Varmus HE. Effects of insertional and point mutations on the functions of the duck hepatitis B virus polymerase. *J Virol* 1990;64:5553-5558.
35. Radziwill G, Tucker W, Schaller H. Mutational analysis of the hepatitis B virus P gene product: domain structure and RNase H activity. *J Virol* 1990;64:613-620.
36. Habig JW, Loeb DD. Small DNA hairpin negatively regulates in situ priming during duck hepatitis B virus reverse transcription. *J Virol* 2002;76:980-989.
37. von Weizsacker F, Kock J, Wieland S, Beck J, Nassal M, Blum HE. Cis-preferential recruitment of duck hepatitis B virus core protein to the RNA/polymerase preassembly complex. *Hepatology* 2002;35:209-216.
38. Nassal M, Rieger A, Steinau O. Topological analysis of the hepatitis B virus core particle by cysteine-cysteine cross-linking. *J Mol Biol* 1992;225:1013-1025.
39. Mabit H, Breiner KM, Knaust A, Zachmann-Brand B, Schaller H. Signals for bidirectional nucleocytoplasmic transport in the duck hepatitis B virus capsid protein. *J Virol* 2001;75:1968-1977.
40. Yu M, Summers J. Phosphorylation of the duck hepatitis B virus capsid protein associated with conformational changes in the C terminus. *J Virol* 1994;68:2965-2969.

41. Perlman DH, Berg EA, O'Connor P B, Costello CE, Hu J. Reverse transcription-associated dephosphorylation of hepadnavirus nucleocapsids. *Proc Natl Acad Sci U S A* 2005;102:9020-9025.
42. Mabit H, Knaust A, Breiner KM, Schaller H. Nuclear localization of the duck hepatitis B virus capsid protein: detection and functional implications of distinct subnuclear bodies in a compartment associated with RNA synthesis and maturation. *J Virol* 2003;77:2157-2164.
43. Mabit H, Schaller H. Intracellular hepadnavirus nucleocapsids are selected for secretion by envelope protein-independent membrane binding. *J Virol* 2000;74:11472-11478.
44. Kann M, Sodeik B, Vlachou A, Gerlich WH, Helenius A. Phosphorylation-dependent binding of hepatitis B virus core particles to the nuclear pore complex. *J Cell Biol* 1999;145:45-55.
45. Garcia PD, Ou JH, Rutter WJ, Walter P. Targeting of the hepatitis B virus precore protein to the endoplasmic reticulum membrane: after signal peptide cleavage translocation can be aborted and the product released into the cytoplasm. *J Cell Biol* 1988;106:1093-1104.
46. Schneider R, Fernholz D, Wildner G, Will H. Mechanism, kinetics, and role of duck hepatitis B virus e-antigen expression in vivo. *Virology* 1991;182:503-512.
47. Milich D, Liang TJ. Exploring the biological basis of hepatitis B e antigen in hepatitis B virus infection. *Hepatology* 2003;38:1075-1086.
48. Pugh JC, Sninsky JJ, Summers JW, Schaeffer E. Characterization of a pre-S polypeptide on the surfaces of infectious avian hepadnavirus particles. *J Virol* 1987;61:1384-1390.
49. Schlicht HJ, Kuhn C, Guhr B, Mattaliano RJ, Schaller H. Biochemical and immunological characterization of the duck hepatitis B virus envelope proteins. *J Virol* 1987;61:2280-2285.
50. Persing DH, Varmus HE, Ganem D. The preS1 protein of hepatitis B virus is acylated at its amino terminus with myristic acid. *J Virol* 1987;61:1672-1677.
51. Grgacic EV, Anderson DA. The large surface protein of duck hepatitis B virus is phosphorylated in the pre-S domain. *J Virol* 1994;68:7344-7350.
52. Rothmann K, Schnolzer M, Radziwill G, Hildt E, Moelling K, Schaller H. Host cell-virus cross talk: phosphorylation of a hepatitis B virus envelope protein mediates intracellular signaling. *J Virol* 1998;72:10138-10147.
53. Borel C, Sunyach C, Hantz O, Trepo C, Kay A. Phosphorylation of DHBV pre-S: identification of the major site of phosphorylation and effects of mutations on the virus life cycle. *Virology* 1998;242:90-98.
54. Macrae DR, Bruss V, Ganem D. Myristylation of a duck hepatitis B virus envelope protein is essential for infectivity but not for virus assembly. *Virology* 1991;181:359-363.
55. Grgacic EV. Identification of structural determinants of the first transmembrane domain of the small envelope protein of duck hepatitis B virus essential for particle morphogenesis. *J Gen Virol* 2002;83:1635-1644.
56. Gazina EV, Lin B, Gallina A, Milanesi G, Anderson DA. Intracellular retention of duck hepatitis B virus large surface protein is independent of preS topology. *Virology* 1998;242:266-278.
57. Guo JT, Pugh JC. Topology of the large envelope protein of duck hepatitis B virus suggests a mechanism for membrane translocation during particle morphogenesis. *J Virol* 1997;71:1107-1114.

58. Swameye I, Schaller H. Dual topology of the large envelope protein of duck hepatitis B virus: determinants preventing pre-S translocation and glycosylation. *J Virol* 1997;71:9434-9441.
59. Bruss V, Thomssen R. Mapping a region of the large envelope protein required for hepatitis B virion maturation. *J Virol* 1994;68:1643-1650.
60. Le Seyec J, Chouteau P, Cannie I, Guguen-Guillouzo C, Gripon P. Infection process of the hepatitis B virus depends on the presence of a defined sequence in the pre-S1 domain. *J Virol* 1999;73:2052-2057.
61. Summers J, Smith PM, Huang MJ, Yu MS. Morphogenetic and regulatory effects of mutations in the envelope proteins of an avian hepadnavirus. *J Virol* 1991;65:1310-1317.
62. Lenhoff RJ, Summers J. Coordinate regulation of replication and virus assembly by the large envelope protein of an avian hepadnavirus. *J Virol* 1994;68:4565-4571.
63. Walters KA, Joyce MA, Addison WR, Fischer KP, Tyrrell DL. Superinfection exclusion in duck hepatitis B virus infection is mediated by the large surface antigen. *J Virol* 2004;78:7925-7937.
64. Chang SF, Netter HJ, Hildt E, Schuster R, Schaefer S, Hsu YC, Rang A, et al. Duck hepatitis B virus expresses a regulatory HBx-like protein from a hidden open reading frame. *J Virol* 2001;75:161-170.
65. Meier P, Scougall CA, Will H, Burrell CJ, Jilbert AR. A duck hepatitis B virus strain with a knockout mutation in the putative X ORF shows similar infectivity and in vivo growth characteristics to wild-type virus. *Virology* 2003;317:291-298.
66. Kock J, Borst EM, Schlicht HJ. Uptake of duck hepatitis B virus into hepatocytes occurs by endocytosis but does not require passage of the virus through an acidic intracellular compartment. *J Virol* 1996;70:5827-5831.
67. Funk A, Mhamdi M, Hohenberg H, Will H, Sirma H. pH-independent entry and sequential endosomal sorting are major determinants of hepadnaviral infection in primary hepatocytes. *Hepatology* 2006;44:685-693.
68. Stoeckl L, Funk A, Kopitzki A, Brandenburg B, Oess S, Will H, Sirma H, et al. Identification of a structural motif crucial for infectivity of hepatitis B viruses. *Proc Natl Acad Sci U S A* 2006;103:6730-6734.
69. Funk A, Mhamdi M, Lin L, Will H, Sirma H. Itinerary of hepatitis B viruses: delineation of restriction points critical for infectious entry. *J Virol* 2004;78:8289-8300.
70. Hu J, Toft DO, Seeger C. Hepadnavirus assembly and reverse transcription require a multi-component chaperone complex which is incorporated into nucleocapsids. *Embo J* 1997;16:59-68.
71. Pollack JR, Ganem D. Site-specific RNA binding by a hepatitis B virus reverse transcriptase initiates two distinct reactions: RNA packaging and DNA synthesis. *J Virol* 1994;68:5579-5587.
72. Wang GH, Seeger C. Novel mechanism for reverse transcription in hepatitis B viruses. *J Virol* 1993;67:6507-6512.
73. Gazina EV, Fielding JE, Lin B, Anderson DA. Core protein phosphorylation modulates pregenomic RNA encapsidation to different extents in human and duck hepatitis B viruses. *J Virol* 2000;74:4721-4728.
74. Almeida JD, Waterson AP. Hepatitis B antigen - an incomplete history. *Am J Med Sci* 1975;270:105-114.
75. Deutsch GF, Spence L. Virus-like particles in the liver and their relationship to Australia antigen. *Lancet* 1972;1:447.
76. Huang SN, Neurath AR. Immunohistologic demonstration of hepatitis B viral antigens in liver with reference to its significance in liver injury. *Lab Invest* 1979;40:1-17.

77. Gerber MA, Hadziyannis S, Vissoulis C, Schaffner F, Paronetto F, Popper H. Electron microscopy and immunoelectronmicroscopy of cytoplasmic hepatitis B antigen in hepatocytes. *Am J Pathol* 1974;75:489-502.
78. McCaul TF, Tsiquaye KN, Zuckerman AJ. Studies by electron microscopy on the assembly of duck hepatitis B virus in the liver. *J Med Virol* 1985;16:77-87.
79. Patzer EJ, Nakamura GR, Simonsen CC, Levinson AD, Brands R. Intracellular assembly and packaging of hepatitis B surface antigen particles occur in the endoplasmic reticulum. *J Virol* 1986;58:884-892.
80. Huovila AP, Eder AM, Fuller SD. Hepatitis B surface antigen assembles in a post-ER, pre-Golgi compartment. *J Cell Biol* 1992;118:1305-1320.
81. Nowak MA, Bonhoeffer S, Hill AM, Boehme R, Thomas HC, McDade H. Viral dynamics in hepatitis B virus infection. *Proc Natl Acad Sci U S A* 1996;93:4398-4402.
82. Funk A, Hohenberg H, Mhamdi M, Will H, Sirma H. Spread of hepatitis B viruses in vitro requires extracellular progeny and may be codetermined by polarized egress. *J Virol* 2004;78:3977-3983.
83. Novoa RR, Calderita G, Arranz R, Fontana J, Granzow H, Risco C. Virus factories: associations of cell organelles for viral replication and morphogenesis. *Biol Cell* 2005;97:147-172.
84. Ishak R, Tovey DG, Howard CR. Morphogenesis of yellow fever virus 17D in infected cell cultures. *J Gen Virol* 1988;69 (Pt 2):325-335.
85. Wang JJ, Liao CL, Chiou YW, Chiou CT, Huang YL, Chen LK. Ultrastructure and localization of E proteins in cultured neuron cells infected with Japanese encephalitis virus. *Virology* 1997;238:30-39.
86. Mackenzie JM, Westaway EG. Assembly and maturation of the flavivirus Kunjin virus appear to occur in the rough endoplasmic reticulum and along the secretory pathway, respectively. *J Virol* 2001;75:10787-10799.
87. Patton JT, Silvestri LS, Tortorici MA, Vasquez-Del Carpio R, Taraporewala ZF. Rotavirus genome replication and morphogenesis: role of the viroplasm. *Curr Top Microbiol Immunol* 2006;309:169-187.
88. Klumperman J, Locker JK, Meijer A, Horzinek MC, Geuze HJ, Rottier PJ. Coronavirus M proteins accumulate in the Golgi complex beyond the site of virion budding. *J Virol* 1994;68:6523-6534.
89. Stertz S, Reichelt M, Spiegel M, Kuri T, Martinez-Sobrido L, Garcia-Sastre A, Weber F, et al. The intracellular sites of early replication and budding of SARS-coronavirus. *Virology* 2007;361:304-315.
90. Matsuoka Y, Chen SY, Compans RW. A signal for Golgi retention in the bunyavirus G1 glycoprotein. *J Biol Chem* 1994;269:22565-22573.
91. Griffiths G, Rottier P. Cell biology of viruses that assemble along the biosynthetic pathway. *Semin Cell Biol* 1992;3:367-381.
92. Hobman TC, Woodward L, Farquhar MG. The rubella virus E2 and E1 spike glycoproteins are targeted to the Golgi complex. *J Cell Biol* 1993;121:269-281.
93. Ganem D, Varmus HE. The molecular biology of the hepatitis B viruses. *Annu Rev Biochem* 1987;56:651-693.
94. Turcotte S, Letellier J, Lippe R. Herpes simplex virus type 1 capsids transit by the trans-Golgi network, where viral glycoproteins accumulate independently of capsid egress. *J Virol* 2005;79:8847-8860.
95. Garoff H, Sjoberg M, Cheng RH. Budding of alphaviruses. *Virus Res* 2004;106:103-116.
96. Nayak DP, Hui EK, Barman S. Assembly and budding of influenza virus. *Virus Res* 2004;106:147-165.

97. Takimoto T, Portner A. Molecular mechanism of paramyxovirus budding. *Virus Res* 2004;106:133-145.
98. Freed EO, Mouland AJ. The cell biology of HIV-1 and other retroviruses. *Retrovirology* 2006;3:77.
99. Jayakar HR, Jeetendra E, Whitt MA. Rhabdovirus assembly and budding. *Virus Res* 2004;106:117-132.
100. Pelchen-Matthews A, Kramer B, Marsh M. Infectious HIV-1 assembles in late endosomes in primary macrophages. *J Cell Biol* 2003;162:443-455.
101. Magliano D, Marshall JA, Bowden DS, Vardaxis N, Meanger J, Lee JY. Rubella virus replication complexes are virus-modified lysosomes. *Virology* 1998;240:57-63.
102. Bienz K, Egger D, Troxler M, Pasamontes L. Structural organization of poliovirus RNA replication is mediated by viral proteins of the P2 genomic region. *J Virol* 1990;64:1156-1163.
103. Ng ML, Pedersen JS, Toh BH, Westaway EG. Immunofluorescent sites in vero cells infected with the flavivirus Kunjin. *Arch Virol* 1983;78:177-190.
104. Lippincott-Schwartz J, Yuan LC, Bonifacino JS, Klausner RD. Rapid redistribution of Golgi proteins into the ER in cells treated with brefeldin A: evidence for membrane cycling from Golgi to ER. *Cell* 1989;56:801-813.
105. Lippincott-Schwartz J, Yuan L, Tipper C, Amherdt M, Orci L, Klausner RD. Brefeldin A's effects on endosomes, lysosomes, and the TGN suggest a general mechanism for regulating organelle structure and membrane traffic. *Cell* 1991;67:601-616.
106. Griffiths G, Pfeiffer S, Simons K, Matlin K. Exit of newly synthesized membrane proteins from the trans cisterna of the Golgi complex to the plasma membrane. *J Cell Biol* 1985;101:949-964.
107. Lang T, Wacker I, Wunderlich I, Rohrbach A, Giese G, Soldati T, Almers W. Role of actin cortex in the subplasmalemmal transport of secretory granules in PC-12 cells. *Biophys J* 2000;78:2863-2877.
108. Rudolf R, Salm T, Rustom A, Gerdes HH. Dynamics of immature secretory granules: role of cytoskeletal elements during transport, cortical restriction, and F-actin-dependent tethering. *Mol Biol Cell* 2001;12:1353-1365.
109. Ryan TA. Inhibitors of myosin light chain kinase block synaptic vesicle pool mobilization during action potential firing. *J Neurosci* 1999;19:1317-1323.
110. Schmoranz J, Simon SM. Role of microtubules in fusion of post-Golgi vesicles to the plasma membrane. *Mol Biol Cell* 2003;14:1558-1569.
111. Stallcup KC, Raine CS, Fields BN. Cytochalasin B inhibits the maturation of measles virus. *Virology* 1983;124:59-74.
112. Chen C, Weisz OA, Stolz DB, Watkins SC, Montelaro RC. Differential effects of actin cytoskeleton dynamics on equine infectious anemia virus particle production. *J Virol* 2004;78:882-891.
113. Miranda-Saksena M, Armati P, Boadle RA, Holland DJ, Cunningham AL. Anterograde transport of herpes simplex virus type 1 in cultured, dissociated human and rat dorsal root ganglion neurons. *J Virol* 2000;74:1827-1839.
114. Penfold ME, Armati P, Cunningham AL. Axonal transport of herpes simplex virions to epidermal cells: evidence for a specialized mode of virus transport and assembly. *Proc Natl Acad Sci U S A* 1994;91:6529-6533.
115. Sanderson CM, Hollinshead M, Smith GL. The vaccinia virus A27L protein is needed for the microtubule-dependent transport of intracellular mature virus particles. *J Gen Virol* 2000;81:47-58.
116. Ward BM, Moss B. Vaccinia virus intracellular movement is associated with microtubules and independent of actin tails. *J Virol* 2001;75:11651-11663.

117. Hohenberg H, Mannweiler K, Muller M. High-pressure freezing of cell suspensions in cellulose capillary tubes. *J Microsc* 1994;175:34-43.
118. Welker R, Hohenberg H, Tessmer U, Huckhagel C, Krausslich HG. Biochemical and structural analysis of isolated mature cores of human immunodeficiency virus type 1. *J Virol* 2000;74:1168-1177.
119. Muller-Reichert T, Hohenberg H, O'Toole ET, McDonald K. Cryoimmobilization and three-dimensional visualization of *C. elegans* ultrastructure. *J Microsc* 2003;212:71-80.
120. Schultz U, Grgacic E, Nassal M. Duck hepatitis B virus: an invaluable model system for HBV infection. *Adv Virus Res* 2004;63:1-70.
121. Prassolov A, Hohenberg H, Kalinina T, Schneider C, Cova L, Krone O, Frolich K, et al. New hepatitis B virus of cranes that has an unexpected broad host range. *J Virol* 2003;77:1964-1976.
122. Condreay LD, Aldrich CE, Coates L, Mason WS, Wu TT. Efficient duck hepatitis B virus production by an avian liver tumor cell line. *J Virol* 1990;64:3249-3258.
123. Hay JC, Klumperman J, Oorschot V, Steegmaier M, Kuo CS, Scheller RH. Localization, dynamics, and protein interactions reveal distinct roles for ER and Golgi SNAREs. *J Cell Biol* 1998;141:1489-1502.
124. Barbero P, Bittova L, Pfeffer SR. Visualization of Rab9-mediated vesicle transport from endosomes to the trans-Golgi in living cells. *J Cell Biol* 2002;156:511-518.
125. Wilcke M, Johannes L, Galli T, Mayau V, Goud B, Salamero J. Rab11 regulates the compartmentalization of early endosomes required for efficient transport from early endosomes to the trans-golgi network. *J Cell Biol* 2000;151:1207-1220.
126. Fukuda M. Lysosomal membrane glycoproteins. Structure, biosynthesis, and intracellular trafficking. *J Biol Chem* 1991;266:21327-21330.
127. Escola JM, Kleijmeer MJ, Stoorvogel W, Griffith JM, Yoshie O, Geuze HJ. Selective enrichment of tetraspan proteins on the internal vesicles of multivesicular endosomes and on exosomes secreted by human B-lymphocytes. *J Biol Chem* 1998;273:20121-20127.
128. Babst M, Odorizzi G, Estepa EJ, Emr SD. Mammalian tumor susceptibility gene 101 (TSG101) and the yeast homologue, Vps23p, both function in late endosomal trafficking. *Traffic* 2000;1:248-258.
129. Odorizzi G, Babst M, Emr SD. Fab1p PtdIns(3)P 5-kinase function essential for protein sorting in the multivesicular body. *Cell* 1998;95:847-858.
130. Swift LL, Zhu MY, Kakkad B, Jovanovska A, Neely MD, Valyi-Nagy K, Roberts RL, et al. Subcellular localization of microsomal triglyceride transfer protein. *J Lipid Res* 2003;44:1841-1849.
131. Lagunoff D, Wan H. Temperature dependence of mast cell histamine secretion. *J Cell Biol* 1974;61:809-811.
132. Matlin KS, Simons K. Reduced temperature prevents transfer of a membrane glycoprotein to the cell surface but does not prevent terminal glycosylation. *Cell* 1983;34:233-243.
133. Saraste J, Kuismanen E. Pre- and post-Golgi vacuoles operate in the transport of Semliki Forest virus membrane glycoproteins to the cell surface. *Cell* 1984;38:535-549.
134. Wood SA, Park JE, Brown WJ. Brefeldin A causes a microtubule-mediated fusion of the trans-Golgi network and early endosomes. *Cell* 1991;67:591-600.
135. Sciaky N, Presley J, Smith C, Zaal KJ, Cole N, Moreira JE, Terasaki M, et al. Golgi tubule traffic and the effects of brefeldin A visualized in living cells. *J Cell Biol* 1997;139:1137-1155.
136. Simons K, Ikonen E. Functional rafts in cell membranes. *Nature* 1997;387:569-572.

137. Brown DA, London E. Functions of lipid rafts in biological membranes. *Annu Rev Cell Dev Biol* 1998;14:111-136.
138. Salaun C, James DJ, Chamberlain LH. Lipid rafts and the regulation of exocytosis. *Traffic* 2004;5:255-264.
139. Alberts AW, Chen J, Kuron G, Hunt V, Huff J, Hoffman C, Rothrock J, et al. Mevinolin: a highly potent competitive inhibitor of hydroxymethylglutaryl-coenzyme A reductase and a cholesterol-lowering agent. *Proc Natl Acad Sci U S A* 1980;77:3957-3961.
140. Scheiffele P, Roth MG, Simons K. Interaction of influenza virus haemagglutinin with sphingolipid-cholesterol membrane domains via its transmembrane domain. *Embo J* 1997;16:5501-5508.
141. Scheiffele P, Rietveld A, Wilk T, Simons K. Influenza viruses select ordered lipid domains during budding from the plasma membrane. *J Biol Chem* 1999;274:2038-2044.
142. Aloia RC, Tian H, Jensen FC. Lipid composition and fluidity of the human immunodeficiency virus envelope and host cell plasma membranes. *Proc Natl Acad Sci U S A* 1993;90:5181-5185.
143. Nguyen DH, Hildreth JE. Evidence for budding of human immunodeficiency virus type 1 selectively from glycolipid-enriched membrane lipid rafts. *J Virol* 2000;74:3264-3272.
144. Keller P, Simons K. Cholesterol is required for surface transport of influenza virus hemagglutinin. *J Cell Biol* 1998;140:1357-1367.
145. Kilsdonk EP, Yancey PG, Stoudt GW, Bangerter FW, Johnson WJ, Phillips MC, Rothblat GH. Cellular cholesterol efflux mediated by cyclodextrins. *J Biol Chem* 1995;270:17250-17256.
146. Funk A. Identifizierung und funktionelle Modulation essentieller zellulärer Komponenten für die Propagation von Hepatitis B-Viren [PhD Thesis]. Hamburg: TU Darmstadt; 2004.
147. Wang E, Norred WP, Bacon CW, Riley RT, Merrill AH, Jr. Inhibition of sphingolipid biosynthesis by fumonisins. Implications for diseases associated with *Fusarium moniliforme*. *J Biol Chem* 1991;266:14486-14490.
148. Hanada K, Nishijima M, Fujita T, Kobayashi S. Specificity of inhibitors of serine palmitoyltransferase (SPT), a key enzyme in sphingolipid biosynthesis, in intact cells. A novel evaluation system using an SPT-defective mammalian cell mutant. *Biochem Pharmacol* 2000;59:1211-1216.
149. Wileman T. Aggresomes and autophagy generate sites for virus replication. *Science* 2006;312:875-878.
150. Roingeard P, Lu SL, Sureau C, Freschlin M, Arbeille B, Essex M, Romet-Lemonne JL. Immunocytochemical and electron microscopic study of hepatitis B virus antigen and complete particle production in hepatitis B virus DNA transfected HepG2 cells. *Hepatology* 1990;11:277-285.
151. Roingeard P, Sureau C. Ultrastructural analysis of hepatitis B virus in HepG2-transfected cells with special emphasis on subviral filament morphogenesis. *Hepatology* 1998;28:1128-1133.
152. Chisari FV, Klopchin K, Moriyama T, Pasquinelli C, Dunsford HA, Sell S, Pinkert CA, et al. Molecular pathogenesis of hepatocellular carcinoma in hepatitis B virus transgenic mice. *Cell* 1989;59:1145-1156.
153. Hajjou M, Norel R, Carver R, Marion P, Cullen J, Rogler LE, Rogler CE. cDNA microarray analysis of HBV transgenic mouse liver identifies genes in lipid biosynthetic and growth control pathways affected by HBV. *J Med Virol* 2005;77:57-65.

154. Patient R, Hourieux C, Sizaret PY, Trassard S, Sureau C, Roingard P. Hepatitis B virus subviral envelope particle morphogenesis and intracellular trafficking. *J Virol* 2007;81:3842-3851.
155. Bruss V. Envelopment of the hepatitis B virus nucleocapsid. *Virus Res* 2004;106:199-209.
156. Bruss V, Ganem D. The role of envelope proteins in hepatitis B virus assembly. *Proc Natl Acad Sci U S A* 1991;88:1059-1063.
157. Sherer NM, Lehmann MJ, Jimenez-Soto LF, Ingmundson A, Horner SM, Cicchetti G, Allen PG, et al. Visualization of retroviral replication in living cells reveals budding into multivesicular bodies. *Traffic* 2003;4:785-801.
158. von Schwedler UK, Stuchell M, Muller B, Ward DM, Chung HY, Morita E, Wang HE, et al. The protein network of HIV budding. *Cell* 2003;114:701-713.
159. Rost M, Mann S, Lambert C, Doring T, Thome N, Prange R. gamma 2-adaptin, a novel ubiquitin-interacting adaptor, and nedd4 ubiquitin ligase control hepatitis B virus maturation. *J Biol Chem* 2006.
160. Bienz K, Egger D, Pasamontes L. Association of polioviral proteins of the P2 genomic region with the viral replication complex and virus-induced membrane synthesis as visualized by electron microscopic immunocytochemistry and autoradiography. *Virology* 1987;160:220-226.
161. Irurzun A, Perez L, Carrasco L. Involvement of membrane traffic in the replication of poliovirus genomes: effects of brefeldin A. *Virology* 1992;191:166-175.
162. Doedens JR, Giddings TH, Jr., Kirkegaard K. Inhibition of endoplasmic reticulum-to-Golgi traffic by poliovirus protein 3A: genetic and ultrastructural analysis. *J Virol* 1997;71:9054-9064.
163. Griffiths G, Brands R, Burke B, Louvard D, Warren G. Viral membrane proteins acquire galactose in trans Golgi cisternae during intracellular transport. *J Cell Biol* 1982;95:781-792.
164. Patzer EJ, Nakamura GR, Yaffe A. Intracellular transport and secretion of hepatitis B surface antigen in mammalian cells. *J Virol* 1984;51:346-353.
165. Furuta S, Kiyosawa K, Nagata A, Akahane Y, Oda M. Letter: HBsAg on cell membrane in symptom-free carrier. *Lancet* 1975;2:227.
166. Alberti A, Realdi G, Tremolada F, Spina GP. Liver cell surface localization of hepatitis B antigen and of immunoglobulins in acute and chronic hepatitis and in liver cirrhosis. *Clin Exp Immunol* 1976;25:396-402.
167. Yamada G, Feinberg LE, Nakane PK. Hepatitis B. Cytologic localization of virus antigens and the role of the immune response. *Hum Pathol* 1978;9:93-109.
168. Kojima T. Immune electron microscopic study of hepatitis B virus associated antigens in hepatocytes. *Gastroenterol Jpn* 1982;17:559-575.
169. Fujiwara T, Oda K, Yokota S, Takatsuki A, Ikehara Y. Brefeldin A causes disassembly of the Golgi complex and accumulation of secretory proteins in the endoplasmic reticulum. *J Biol Chem* 1988;263:18545-18552.
170. Donaldson JG, Finazzi D, Klausner RD. Brefeldin A inhibits Golgi membrane-catalysed exchange of guanine nucleotide onto ARF protein. *Nature* 1992;360:350-352.
171. Helms JB, Rothman JE. Inhibition by brefeldin A of a Golgi membrane enzyme that catalyses exchange of guanine nucleotide bound to ARF. *Nature* 1992;360:352-354.
172. Roth MG. Snapshots of ARF1: implications for mechanisms of activation and inactivation. *Cell* 1999;97:149-152.
173. Peyroche A, Antony B, Robineau S, Acker J, Cherfils J, Jackson CL. Brefeldin A acts to stabilize an abortive ARF-GDP-Sec7 domain protein complex: involvement of specific residues of the Sec7 domain. *Mol Cell* 1999;3:275-285.

174. Mansour SJ, Skaug J, Zhao XH, Giordano J, Scherer SW, Melancon P. p200 ARF-GEP1: a Golgi-localized guanine nucleotide exchange protein whose Sec7 domain is targeted by the drug brefeldin A. *Proc Natl Acad Sci U S A* 1999;96:7968-7973.
175. Dascher C, Balch WE. Dominant inhibitory mutants of ARF1 block endoplasmic reticulum to Golgi transport and trigger disassembly of the Golgi apparatus. *J Biol Chem* 1994;269:1437-1448.
176. Chazal N, Gerlier D. Virus entry, assembly, budding, and membrane rafts. *Microbiol Mol Biol Rev* 2003;67:226-237, table of contents.
177. Ono A, Freed EO. Role of lipid rafts in virus replication. *Adv Virus Res* 2005;64:311-358.
178. Simons K, Toomre D. Lipid rafts and signal transduction. *Nat Rev Mol Cell Biol* 2000;1:31-39.
179. Ikonen E. Roles of lipid rafts in membrane transport. *Curr Opin Cell Biol* 2001;13:470-477.
180. Hao YH, Chen JW. Influence of cholesterol on the biophysical properties of the sphingomyelin/DOPC binary system. *J Membr Biol* 2001;183:85-92.
181. Kwik J, Boyle S, Fooksman D, Margolis L, Sheetz MP, Edidin M. Membrane cholesterol, lateral mobility, and the phosphatidylinositol 4,5-bisphosphate-dependent organization of cell actin. *Proc Natl Acad Sci U S A* 2003;100:13964-13969.
182. Pugh JC, Di Q, Mason WS, Simmons H. Susceptibility to duck hepatitis B virus infection is associated with the presence of cell surface receptor sites that efficiently bind viral particles. *J Virol* 1995;69:4814-4822.
183. Fernholz D, Wildner G, Will H. Minor envelope proteins of duck hepatitis B virus are initiated at internal pre-S AUG codons but are not essential for infectivity. *Virology* 1993;197:64-73.
184. Sprengel R, Kuhn C, Will H, Schaller H. Comparative sequence analysis of duck and human hepatitis B virus genomes. *J Med Virol* 1985;15:323-333.
185. Sprengel R, Kuhn C, Manso C, Will H. Cloned duck hepatitis B virus DNA is infectious in Pekin ducks. *J Virol* 1984;52:932-937.
186. Franke C. Analyse der Dephosphorylierung des Entenhepatitis B-Virus Nukleokapsidproteins: Einfluss auf Replikation und Infektiosität [PhD Thesis]. Hamburg: University Hamburg; 2006.
187. Yang M, Ellenberg J, Bonifacino JS, Weissman AM. The transmembrane domain of a carboxyl-terminal anchored protein determines localization to the endoplasmic reticulum. *J Biol Chem* 1997;272:1970-1975.
188. Zhang J, Kang DE, Xia W, Okochi M, Mori H, Selkoe DJ, Koo EH. Subcellular distribution and turnover of presenilins in transfected cells. *J Biol Chem* 1998;273:12436-12442.
189. Kuroki K, Cheung R, Marion PL, Ganem D. A cell surface protein that binds avian hepatitis B virus particles. *J Virol* 1994;68:2091-2096.
190. Laemmli UK. Cleavage of structural proteins during the assembly of the head of bacteriophage T4. *Nature* 1970;227:680-685.

VII. ABBREVIATIONS

Aa	amino acid
Arfs	ADP-ribosylation factors
APS	Ammoniumpersulfate
ATP	Adenosine triphosphate
Bp	Base pair
β-ME	β-Mercaptoethanol
BSA	Bovine serum albumin
ccc	Covalently closed circular
CLSM	Confocal Laser Scanning Microscope
CTB	Cholera-Toxin subunit B
Da	Dalton
DHBc	Core-protein of DHBV
DHBe	E-Antigen, <i>early antigen</i> , preC
DHBV	Duck hepatitis B virus
DMEM	DULBECCOs Modified EAGLE Medium
DMSO	Dimethylsulfoxide
DR	Direct repeat
DTT	Dithiothreitol
DNA	Deoxyribonucleic acid
ECL	Enhanced chemoluminescence
EEA1	Early endosomal antigen 1
EDTA	Ethylenediaminetetraacetic acid
ER	Endoplasmatic reticulum
EM	Electron microscope
FB1	Fumonisin B1
FCS	Fetal calf serum
FITC	Fluorescein isothiocyanat
GE	Genome equivalents
GFP	Green fluorescent protein
GTP	Guanosine triphosphate
g	Gravitation

h	Hour
HBsAg	Hepatitis B surface antigen
HBV	Hepatitis B virus
Hepadnaviruses	Hepatitis-DNA-viruses
HIV	Human immunodeficiency virus
HRPO	Horseradish peroxidase
Hsp90	Heat shock protein 90
IC	ER-to-Golgi intermediate compartment
IF	Immunofluorescence
IgG	Immunglobulin G
Kb	Kilo bases, 1000 bp
kDa	Kilodalton, 1.000 Dalton
L	Large surface protein
M β CD	Methyl- β -Cyclodextrin
Min	Minute
MIP	maximum intensity projection
mM	Millimolar, 10^{-3} M
MOI	Multiplicity of infection
mRNA	Messenger ribonucleic acid
MTP	Triglyceride transfer protein
MTs	Microtubules
Myr	Myriocin
NCBs	Nuclear core bodies
NLS	Nuclear localization signal
nm	Nanometer, 10^{-9} m
nM	Nanomolar, 10^{-9} M
NP	Nuclear pore
Nt	Nucleotide(s)
OD	Optical density
ORF	Open reading frame
P	Polymerase
P36, p28...	Protein of 36, 28... kDa
PAGE	Polyacylamide gel electrophoresis
PBS	Phosphate buffered saline

PCR	Polymerase chain reaction
PDHs	Primary duck hepatocytes
PDI	Protein disulfide isomerase
PF	Paraformaldehyde
pgRNA	Pregenomic ribonucleic acid
PK	Protein kinase
PM	Plasma membrane
rcDNA	Relaxed circular DNA,
RFP	Red fluorescent protein
RNA	Ribonucleic acid
Rpm	Rotations per minute
RT	Room temperature
RT	Reverse transcription
S	Small surface protein
SDS	Sodium dodecyl sulphate polyacrylamide
SDS-PAGE	SDS-Polyacrylamid-Gelelectrophoresis
SNARE	Soluble N-ethylmaleimide-sensitive factor attachment protein receptor
SVPs	Subviral particles
TBS	Tris buffered saline
TGN	Trans Golgi network
TLM	Translocation motif
TM	Transmembrane domain
TP	Terminal protein
TRITC	Tetramethyl rhodamine isothiocyanate
U	Unit
µm	Micrometer, 10 ⁻⁶
V	Volt
VCVs	Virus particles-containing vesicles
WHO	World health organization
Wt	Wildtype
YFP	Yellow fluorescent protei

VIII. FIGURE INDEX

Figure 1: Geographic distribution of the prevalence of hepatitis B carriers and annual incidence of primary hepatocellular carcinoma (HCC)	6
Figure 2: Cellular composition of the liver	8
Figure 3: Structure of duck hepatitis B viral particles	10
Figure 4: Genome organization of duck hepatitis B virus	11
Figure 5: Structural organization of the polymerase	13
Figure 6: Structural organization of the envelope proteins S and L	16
Figure 7: Dual topology of the surface protein L	17
Figure 8: Illustration of the viral life cycle	19
Figure 9: Subcellular compartments of the secretory pathway	23
Figure 10: Viral assembly and/or budding at cellular membranes	26
Figure 11: In secretory cells, regulated and constitutive pathways of exocytosis diverge in the TGN	28
Figure 12: Primary duck hepatocytes were cultured in a 3D-cell culture system	33
Figure 13: The principal morphogenetic features are conserved both <i>in vitro</i> and <i>in vivo</i>	34
Figure 14: Transmission electron microscopy of immunogold-labelled congenitally DHBV-infected duck hepatocytes	35
Figure 15: Disorganisation of the rough ER network during DHBV infection	37
Figure 16: VCVs are generated through segregation from the smooth ER and rough ER	38
Figure 17: VCVs segregate from the outer nuclear membrane	39
Figure 18: Different features of VCVs	40
Figure 19: Ultrastructural features of the budding steps of SVPs	42
Figure 20: Ultrastructural features of the budding steps of virions	43
Figure 21: VCVs are absent in non-parenchymal cells	44
Figure 22: VCVs are absent in non-parenchymal cells	45
Figure 23: Ultrastructural features of the chicken hepatoma cells D2	46
Figure 24 I : Intracellular distribution of the viral envelope protein L in correlation to protein markers of organelles in infected PDHs	48
Figure 24 II : Intracellular distribution of the viral envelope protein L in correlation to protein markers of organelles in infected PDHs	49
Figure 24 III: Intracellular distribution of the viral envelope protein L in correlation to protein markers of organelles in infected PDHs	51
Figure 25: Analysis of subcellular fractions from DHBV-infected liver for viral and	

cellular markers	53
Figure 26: Distribution of viral and cellular proteins from a congenitally DHBV-infected liver in a linear 0-26% iodixanol gradient	55
Figure 27: Analysis of subcellular fractions from non-infected liver for cellular markers	56
Figure 28: Ultrastructural analysis of immunoprecipitated VCVs	58
Figure 29: Immunocapture of VCVs	59
Figure 30: VCVs undergo homo- and/or heterotypic fusion as well as fission	61
Figure 31: Schematic representation of S-GFP-fusion constructs	63
Figure 32: The fusion proteins EGFP-S and EGFP-S are both expressed in LMH cells	63
Figure 33: EGFP-S shows a subcellular distribution similar to the wild type S protein	64
Figure 34: A large fraction of EGFP-S colocalizes with VCVs	65
Figure 35: 3D reconstructions of VCVs in live cells	67
Figure 36: VCVs are dynamic structures undergoing homotypic fusion and fission as revealed by live cell imaging	68
Figure 37: Viral particles were absent from the Golgi	70
Figure 38: VCVs were located in close proximity to the Golgi but no viral particles were found within the Golgi	71
Figure 39: The Golgi apparatus seems not to be involved in DHBV morphogenesis	72
Figure 40: DHBV secretion is only moderately affected at 20°C	74
Figure 41: The viral surface protein L and VSV-G-GFP do not colocalize at 37°C	75
Figure 42: The viral surface protein L and VSV-G-GFP do not colocalize at 20°C	76
Figure 43: Only a minor fraction of L was colocalized with VSV-G-GFP	77
Figure 44: VCVs are located in close proximity to the PM	79
Figure 45: VCVs are located beneath the PM of 2 adjacent hepatocytes	80
Figure 46: VCVs were seen in direct contact with the PM	81
Figure 47: Viral particles are found in the extracellular space between two hepatocytes	82
Figure 48: Viral particles are found in the extracellular space between hepatocytes and non-parenchymal cells	83
Figure 49: Viral particles are released via exocytosis	84
Figure 50: The viral surface protein L is localised to the PM	85
Figure 51: Following BFA treatment, the L-associated membrane staining was lost	87
Figure 52: The viral surface protein L is localised to the PM	88
Figure 53: The viral surface protein L is localised to the PM	90
Figure 54: VCVs were located to and interacting with the PM	92
Figure 55: VCVs are located near and interact with the PM	93

Figure 56: About 40-80 virions and 46,000 SVPs are secreted per hepatocyte and per h	95
Figure 57: BFA strongly inhibits the secretion of both SVPs and virions	97-98
Figure 58: Treatment of BFA for 12, 24, and 48h showed no cytotoxic effects	99
Figure 59: The secretion block induced by BFA is reversible	100
Figure 60: Intracellular L, core, and rcDNA were not affected by BFA treatment	101
Figure 61: BFA treatment leads to the formation of large VCVs	102
Figure 62: BFA induces the formation of large membrane sacs only in DHBV-infected but not in the non-infected cells	103
Figure 63: BFA leads to the accumulation of large VCVs beneath the PM	105
Figure 64: L protein disappears from the PM upon BFA treatment	106
Figure 65: L protein is associated with the PM	107
Figure 66: PM-association of L is inhibited by BFA	108
Figure 67: MTs are efficiently depolymerised by Nocodazole treatment	109
Figure 68: Nocodazole and Paclitaxel have no cytotoxic effects on PDHs	110
Figure 69: Intact but not dynamic MTs facilitate DHBV secretion	111
Figure 70: The inhibitory effect of Noco is reversible 48 h after washout	111
Figure 71: VCVs were found in close proximity to microtubules as seen by TEM	112
Figure 72: Actin filaments are efficiently depolymerised by Cytochalasin D	112
Figure 73: Cytochalasin D is not toxic for PDHs	113
Figure 74: Depolymerization of actin filaments by cytochalsin D facilitates viral secretion	114
Figure 75: Actin filaments form a physical barrier for the VCVs	115
Figure 76: Mevinolin has no cytotoxic effects on PDHs	116
Figure 77: Cholesterol depletion by mevinolin does not alter DHBV secretion	118
Figure 78: M β CD has no cytotoxic effects on PDHs	119
Figure 79: M β CD does not interfere with secretion of DHBV	119
Figure 80: Hyperphosphorylation of L protein after M β CD treatment does not correlate with activation of MAP kinases	120
Figure 81: Sphingolipid depletion for 60 h is not toxic	122
Figure 82: Sphingolipid depletion does not alter DHBV secretion	123
Figure 83: Assembly and budding model for DHBV	130
Figure 84: Secretion model for DHBV	135
Figure 85: Effects of BFA on DHBV morphogenesis	138
Figure 86: Intracellular transport of DHBV	140

